Scan-to-BIM for architectural heritage enhancement and preservation. Leading techniques and advanced automation processes

Abstract

The digitisation of Architectural Heritage emerges as a pivotal and groundbreaking practice crucial for the preservation and enhancement of cultural assets.
By cutting-edge technologies within a scenario dominated by Artificial Intelligence, which disrupts established paradigms and approaches, this initiative aims to address the inherent challenges of long-term conservation.
The present thesis, adopts comprehensive and multidisciplinary approaches to delve into diverse themes converging within the realm of architectural survey and drawing for heritage virtualisation.
Through extensive field research conducted in both Italy and Spain, the combined methodologies of various surveying techniques and technologies, including LiDAR and Photogrammetry, are thoroughly examined as foundational elements for the digital acquisition of historical monuments.
The resulting data, presented as point clouds, images, and/or polygonal models, undergo a detailed processing and optimisation phase employing semi-automatic procedures.
These procedures, primarily focusing on the semantic enrichment of architectural and structural components, are geared towards facilitating an in-depth analysis of the conservation status of the monument.
Moving beyond the survey activity, the investigation advances towards Heritage Building Information Modelling (HBIM) through the adoption of a Scan to BIM approach. The latter is seamlessly integrated into a unified protocol, streamlining data processing while ensuring adherence to health and safety regulations for the operator.
This methodology enables a thorough analysis and faithful digitisation of the reproduced case studies, leveraging metric and geometric references guaranteed by the instrumentation used, as well as semantic segmentation and classification of data derived from the automations.
The proposed processes of automation, designed to accelerate processing times, control operational costs, and enhance the precision and accuracy of results, are meticulously crafted.

On the cover:

AI-driven Semantic Point Cloud. The Palace of the Counts of Sástago in Zaragoza (Spain)

DICATECh

2024

Michele Buldo

Scan-to-BIM for Architectural Heritage enhancement and preservation. Leading techniques and advanced automation processes

05

D.R.S.A.T.E.

Doctor in Risk and Environmental, Territorial and Building Development

Coordinator: Prof. Vito Iacobellis

XXXVI CYCLE
Curriculum: ICAR 17 – Drawing

DICATECh
Department of Civil, Environmental, Building Engineering and Chemistry

POLITECNICO DI BARI

05
2024

Michele Buldo

Scan-to-BIM for Architectural Heritage enhancement and preservation. Leading techniques and advanced automation processes

Prof. Cesare Verdoscia – DICATECh, Politecnico di Bari *(Supervisor)*

Prof. Luis Agustín-Hernández – Departamento de Arquitectura, Universidad de Zaragoza *(Supervisor)*

Prof. Elena Cabrera-Revuelta – Departamento de Ingeniería Mecánica y Diseño Industrial, Universidad de Cádiz *(Co-Supervisor)*

Eng. Riccardo Tavolare – DICATECh, Politecnico di Bari *(Co-Supervisor)*

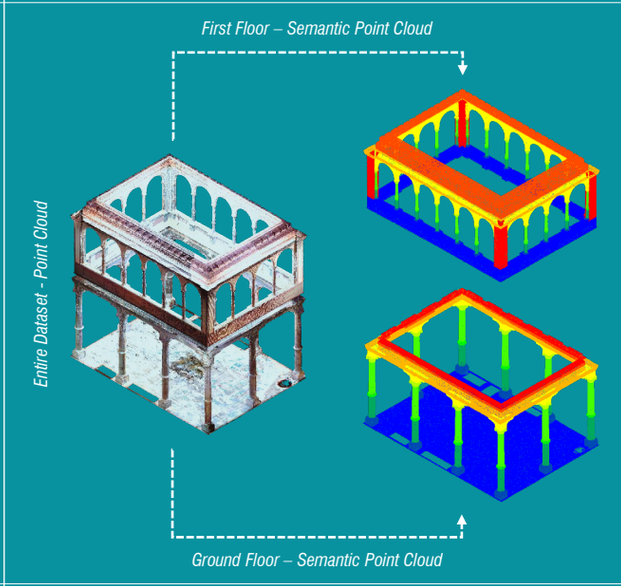

Politecnico di Bari

LIBERATORIA PER L'ARCHIVIAZIONE DELLA TESI DI DOTTORATO

Al Magnifico Rettore
del Politecnico di Bari

Il sottoscritto MICHELE BULDO nato a MELFI (PZ) il 09/08/1989

residente a VENOSA (PZ), in via ZOCCOLANTI 18, e-mail michelebuldomb@gmail.com

iscritto al 3° anno di Corso di Dottorato di Ricerca in Rischio e Sviluppo Ambientale, Territoriale ed Edilizio - ciclo XXXVI

ed essendo stato ammesso a sostenere l'esame finale con la prevista discussione della tesi dal titolo: "Scan-to-BIM for Architectural Heritage enhancement and preservation. Leading techniques and advanced automation processes"

DICHIARA

1) di essere consapevole che, ai sensi del D.P.R. n. 445 del 28.12.2000, le dichiarazioni mendaci, la falsità negli atti e l'uso di atti falsi sono puniti ai sensi del codice penale e delle Leggi speciali in materia, e che nel caso ricorressero dette ipotesi, decade fin dall'inizio e senza necessità di nessuna formalità dai benefici conseguenti al provvedimento emanato sulla base di tali dichiarazioni;

2) di essere iscritto al Corso di Dottorato di ricerca in Rischio e Sviluppo Ambientale, Territoriale ed Edilizio - ciclo XXXVI, corso attivato ai sensi del "*Regolamento dei Corsi di Dottorato di ricerca del Politecnico di Bari"*, emanato con D.R. n.286 del 01.07.2013;

3) di essere pienamente a conoscenza delle disposizioni contenute nel predetto Regolamento in merito alla procedura di deposito, pubblicazione e autoarchiviazione della tesi di dottorato nell'Archivio Istituzionale ad accesso aperto alla letteratura scientifica;

4) di essere consapevole che attraverso l'autoarchiviazione delle tesi nell'Archivio Istituzionale ad accesso aperto alla letteratura scientifica del Politecnico di Bari (IRIS-POLIBA), l'Ateneo archivierà e renderà consultabile in rete (nel rispetto della Policy di Ateneo di cui al D.R. 642 del 13.11.2015) il testo completo della tesi di dottorato, fatta salva la possibilità di sottoscrizione di apposite licenze per le relative condizioni di utilizzo (di cui al sito http://www.creativecommons.it/Licenze), e fatte salve, altresì, le eventuali esigenze di "embargo", legate a strette considerazioni sulla tutelabilità e sfruttamento industriale/commerciale dei contenuti della tesi, da rappresentarsi mediante compilazione e sottoscrizione del modulo in calce (Richiesta di embargo);

5) che la tesi da depositare in IRIS-POLIBA, in formato digitale (PDF/A) sarà del tutto identica a quelle consegnate/inviate/da inviarsi ai componenti della commissione per l'esame finale e a qualsiasi altra copia depositata presso gli Uffici del Politecnico di Bari in forma cartacea o digitale, ovvero a quella da discutere in sede di esame finale, a quella da depositare, a cura dell'Ateneo, presso le Biblioteche Nazionali Centrali di Roma e Firenze e presso tutti gli Uffici competenti per legge al momento del deposito stesso, e che di conseguenza va esclusa qualsiasi responsabilità del Politecnico di Bari per quanto riguarda eventuali errori, imprecisioni o omissioni nei contenuti della tesi;

6) che il contenuto e l'organizzazione della tesi è opera originale realizzata dal sottoscritto e non compromette in alcun modo i diritti di terzi, ivi compresi quelli relativi alla sicurezza dei dati personali; che pertanto il Politecnico di Bari ed i suoi funzionari sono in ogni caso esenti da responsabilità di qualsivoglia natura: civile, amministrativa e penale e saranno dal sottoscritto tenuti indenni da qualsiasi richiesta o rivendicazione da parte di terzi;

7) che il contenuto della tesi non infrange in alcun modo il diritto d'Autore né gli obblighi connessi alla salvaguardia di diritti morali od economici di altri autori o di altri aventi diritto, sia per testi, immagini, foto, tabelle, o altre parti di cui la tesi è composta.

Luogo e data Bari 12/04/2024 Firma 

Il sottoscritto, con l'autoarchiviazione della propria tesi di dottorato nell'Archivio Istituzionale ad accesso aperto del Politecnico di Bari (POLIBA-IRIS), pur mantenendo su di essa tutti i diritti d'autore, morali ed economici, ai sensi della normativa vigente (Legge 633/1941 e ss.mm.ii.),

CONCEDE

- al Politecnico di Bari il permesso di trasferire l'opera su qualsiasi supporto e di convertirla in qualsiasi formato al fine di una corretta conservazione nel tempo. Il Politecnico di Bari garantisce che non verrà effettuata alcuna modifica al contenuto e alla struttura dell'opera.
- al Politecnico di Bari la possibilità di riprodurre l'opera in più di una copia per fini di sicurezza, back-up e conservazione.

Luogo e data Bari 12/04/2024 Firma 

D.R.S.A.T.E.	**POLITECNICO DI BARI**	**05**
Doctor in Risk and Environmental, Territorial and Building Development		**2024**
Coordinator: Prof. Vito Iacobellis		
XXXVI CYCLE Curriculum: ICAR 17 – Drawing		
DICATECh Department of Civil, Environmental, Building Engineering and Chemistry		
	Michele Buldo	
	Scan-to-BIM for Architectural Heritage enhancement and preservation. Leading techniques and advanced automation processes	
	Prof. Cesare Verdoscia – DICATECh, Politecnico di Bari *(Supervisor)* Prof. Luis Agustín-Hernández – Departamento de Arquitectura, Universidad de Zaragoza *(Supervisor)* Prof. Elena Cabrera-Revuelta – Departamento de Ingeniería Mecánica y Diseño Industrial, Universidad de Cádiz *(Co-Supervisor)* Eng. Riccardo Tavolare – DICATECh, Politecnico di Bari *(Co-Supervisor)*	
	La ricerca è stata realizzata con il cofinanziamento dell'Unione europea - POR Puglia FESR FSE 2014-2020 – Asse X - Azione 10.4 "Interventi volti a promuovere la ricerca e per l'istruzione universitaria" - Avviso pubblico n. 2/FSE/2020 "Dottorati di ricerca in Puglia XXXVI Ciclo"	

D.R.S.A.T.E.	**POLITECNICO DI BARI**	**05**
Dottorato di Ricerca in Rischio e Sviluppo Ambientale, Territoriale ed Edilizio		**2024**
Coordinatore: Prof. Vito Iacobellis		
XXXVI CICLO Curriculum: ICAR 17 – Disegno		
DICATECh Dipartimento di Ingegneria Civile, Ambientale, del Territorio, Edile e di Chimica		
	Michele Buldo	
	Il processo Scan-to-BIM per la valorizzazione e la conservazione del Patrimonio Architettonico. Tecniche all'avanguardia e procedure di automazione innovative	
	Prof. Cesare Verdoscia – DICATECh, Politecnico di Bari *(Supervisore)* Prof. Luis Agustín-Hernández – Departamento de Arquitectura, Universidad de Zaragoza *(Supervisore)* Prof.ssa Elena Cabrera-Revuelta – Departamento de Ingeniería Mecánica y Diseño Industrial, Universidad de Cádiz *(Co-Supervisore)* Ing. Riccardo Tavolare – DICATECh, Politecnico di Bari *(Co-Supervisore)*	
	La ricerca è stata realizzata con il cofinanziamento dell'Unione europea - POR Puglia FESR FSE 2014-2020 – Asse X - Azione 10.4 "Interventi volti a promuovere la ricerca e per l'istruzione universitaria" - Avviso pubblico n. 2/FSE/2020 "Dottorati di ricerca in Puglia XXXVI Ciclo"	

EXTENDED ABSTRACT *(eng)*

The digitisation of Architectural Heritage emerges as a pivotal and groundbreaking practice crucial for the preservation and enhancement of cultural assets. This significance becomes particularly pronounced in an era marked by profound transformations and challenges across multiple fields.

By cutting-edge technologies within a scenario dominated by Artificial Intelligence, which disrupts established paradigms and approaches, this initiative aims to address the inherent challenges of long-term conservation. Simultaneously, it aspires to achieve the broader objective of ensuring enhanced access and a more enriched experience of historical monuments for both current and future generations, thereby safeguarding their unique identities.

Heritage's vulnerability must be carefully weighed to strike a delicate balance between accessibility and contemporary interpretation on the one hand, and authenticity and integrity on the other. The hazards of digitisation, including the potential loss of stored information or intentional obsolescence, are closely related to this susceptibility as well as physical material modifications.

The present thesis, born out of these critical considerations, adopts comprehensive and multidisciplinary approaches to delve into diverse themes converging within the realm of architectural survey and drawing for heritage virtualisation.

Through extensive field research conducted in both Italy and Spain, the combined methodologies of various surveying techniques and technologies, including LiDAR and Photogrammetry, are thoroughly examined as foundational elements for the digital acquisition of historical monuments. The resulting data, presented as point clouds, images, and/or polygonal models, undergo a detailed processing and optimisation phase employing semi-automatic procedures.

These procedures, primarily focusing on the semantic enrichment of architectural and structural components, are geared towards facilitating an in-depth analysis of the conservation status of the monument.

This, in turn, translates into improved information management, providing crucial support for subsequent phases involved in constructing the replicated model of the architectural masterpiece.

Moving beyond the survey activity, the investigation advances towards Heritage Building Information Modelling (HBIM) through the adoption of a Scan to BIM approach. The latter is seamlessly integrated into a unified protocol, streamlining data processing while ensuring adherence to health and safety regulations for the operator. This methodology enables a thorough analysis and faithful digitisation of the reproduced case studies, leveraging metric and geometric references guaranteed by the instrumentation used, as well as semantic segmentation and classification of data derived from the automations.

The proposed processes of automation, designed to accelerate processing times, control operational costs, and enhance the precision and accuracy of results, are meticulously crafted. Simultaneously, due consideration is given to the experience and expertise of the operator involved in the activities, ensuring a thoughtful and conscious approach throughout all stages of the process.

keywords: *Cultural Heritage, Architectural Heritage, Digitisation, 3D Survey, Health and Safety, Planning for Scanning, Point Cloud, Mesh, Semantic Enrichment, Segmentation, Classification, Automation, Artificial Intelligence, Machine Learning, Heritage Building Information Modelling, Scan to BIM*

EXTENDED ABSTRACT *(ita)*

Il processo di digitalizzazione del Patrimonio Architettonico si configura come una pratica cruciale e innovativa per la tutela e valorizzazione dello stesso, particolarmente rilevante in un'epoca caratterizzata da profonde trasformazioni e sfide riscontrabili in diversi settori.
La sua realizzazione, facilitata dall'impiego delle tecnologie all'avanguardia e in un contesto in cui l'Intelligenza Artificiale predomina e scardina paradigmi e approcci nel tempo consolidati, mira a fronteggiare le sfide intrinseche alla conservazione a lungo termine, mentre si proietta verso l'obiettivo di garantire un accesso più ampio e una fruizione più ricca dei monumenti storici, da parte delle generazioni presenti e future, per preservarne la loro identità.
La necessità di bilanciare l'autenticità e l'integrità con la reperibilità e l'interpretazione contemporanea richiede una profonda riflessione sulla vulnerabilità del patrimonio, legata sia alle questioni di alterazione fisico-materica cui è soggetto, che ai rischi associati alla digitializzazione, come la perdita di informazioni archiviate o l'obsolescenza programmata.

A partire da tali considerazioni, si inserisce la presente tesi, che con approcci olistici e multidisciplinari si propone di esplorare tematiche diversificate, ma riconducibili ad un unico settore, quello del rilievo e del disegno architettonico per la virtualizzazione del patrimonio.

Attraverso attività di ricerca condotte sul campo, in Italia e in Spagna, vengono esaminate metodologie combinate delle diverse tecniche e tecnologie del rilievo, come i LiDAR e la Fotogrammetria, che costituiscono la base per l'acquisizione digitale dei monumenti storici. I dati ottenuti, presentati come nuvole di punti, immagini e/o modelli poligonali, vengono sottoposti ad un rigoroso processo di elaborazione e ottimizzazione attraverso l'impiego di procedure semi-automatiche. Queste, focalizzate per lo più sull'arricchimento semantico dei componenti architettonici e strutturali, mirano all'analisi approfondita dello stato di conservazione del monumento.

Ciò, a sua volta, si traduce in una gestione informativa migliorata, fornendo un fondamentale supporto per le fasi successive di costruzione del modello replicato dell'opera architettonica.

Dall'attività di rilievo, l'indagine prosegue in direzione dell'Heritage Building Information Modelling (HBIM), mediante l'adozione di un approccio Scan to BIM. Quest'ultimo è integrato all'interno di un protocollo unificato che non solo facilita l'elaborazione dei dati, ma assicura anche il rispetto delle normative di salute e sicurezza per l'operatore. Tale metodologia consente un'analisi approfondita e una fedele digitalizzazione dei casi di studio riprodotti, sfruttando il riferimento metrico e geometrico, garantiti dalla strumentazione utilizzata e altresì dalla segmentazione semantica e dalla classificazione dei dati derivanti dagli automatismi precitati.

I processi di automazione ivi proposti, volti ad accelerare i tempi di elaborazione, contenere i costi operativi e migliorare la precisione e l'accuratezza dei risultati, sono attentamente progettati. Allo stesso tempo, si tengono costantemente in considerazione l'esperienza e le competenze dell'operatore coinvolto nelle attività, garantendo un approccio ponderato e consapevole durante tutte le fasi del processo.

keywords: *Cultural Heritage, Architectural Heritage, Digitisation, 3D Survey, Health and Safety, Planning for Scanning, Point Cloud, Mesh, Semantic Enrichment, Segmentation, Classification, Automation, Artificial Intelligence, Machine Learning, Heritage Building Information Modelling, Scan to BIM*

INDEX

INTRODUCTION

Cultural Heritage (CH), and more especially Architectural Heritage (AH), lie at a crossroads where they can seize both historically unique and exciting opportunities in an era where new technology permeates every part of our society.
A potential innovation catalyst is revealed by the use of digitisation as a critical instrument for heritage enhancement and preservation. Advanced modelling, acquisition, and visualisation techniques are used in this type of process, which is always changing, to provide precise and comprehensive virtual representations of ancient buildings, monuments, and sites. This approach not only facilitates the digital preservation of vulnerable structures over time but also opens the possibility of remotely accessing these historical artifacts, fostering an unprecedented intergenerational dialogue. Simultaneously, it exposes intricate ethical considerations and challenges that necessitate strategic exploration.

To regulate the realm of Cultural Heritage documentation[1] and conservation, a comprehensive framework is shaped and guided by a wealth of international standards, charters, and conventions created to safeguard and sustainably manage historical and architectural treasures globally (RecorDIM, 2007).
Key contributors include esteemed organisations such as the 'International Council on Monuments and Sites' (ICOMOS), the 'United Nations Educational, Scientific and Cultural Organization' (UNESCO), the 'International Committee of Architectural Photogrammetry' also called 'International Committee for Documentation of Cultural Heritage' (CIPA) in collaboration with 'International Society of Photogrammetry and Remote Sensing' (ISPRS) and national bodies, each providing directives that underscore principles for effective heritage conservation.

[1] Heritage Documentation is here defined as 'a continuous process enabling the monitoring, maintenance and understanding needed for conservation by the supply of appropriate and timely information. Documentation is both the product and action of meeting the information needs of heritage management. It makes available a range of tangible and intangible resources, such as metric, narrative, thematic and societal records of Cultural Heritage' (RecorDIM, 2007).

The ‘Venice Charter’ (1964), a foundational document of ICOMOS, serves as a primary guide, outlining principles for the conservation of Cultural Heritage and emphasising the paramount importance of authenticity and site integrity. Complementing this, the ‘Nara Document on Authenticity’ (1994) from ICOMOS specifically focuses on architecture, promoting international standards and consistent conservation approaches. The ‘Burra Charter Guidelines’ (1999), developed by ICOMOS Australia, provide essential principles for the conservation of Architectural Heritage, emphasising adaptability to new uses – a crucial aspect in the evolution of heritage management.

Additionally, the ‘EN 16096 standard’ (2012) offers European-level guidelines for Cultural Heritage conservation, ensuring a cohesive approach on the continent.
To complement these directives, ongoing efforts by ICOMOS are reflected in a series of charters and guidelines, addressing unique challenges posed by 20th-century Architectural Heritage.

Moreover, the ‘London Charter’ (2009) (Brusaporci and Trizio, 2013) establishes fundamental principles for the use of digital visualisation in Cultural Heritage, emphasising intellectual integrity, reliability, documentation, sustainability, and accessibility. It refrains from prescribing specific methods but outlines broad principles for usage across academic, educational, cultural, and commercial contexts, with particular relevance in the entertainment industry related to Cultural Heritage reconstruction.

In Italy, the management of Cultural Heritage is governed by Legislative Decree 42/2004, known as ‘Codice dei Beni Culturali e del Paesaggio’ (Italian Ministry of Culture (MiC), 2004). This legislative framework outlines guidelines for the protection, conservation, and enhancement of cultural and landscape assets in the country.
Covering a wide range of elements, including monuments, artworks, and archaeological sites, the code establishes procedures and responsibilities to ensure compliance with national and international regulations. Its implementation involves various institutions, aiming to preserve Italy's rich historical and artistic heritage for future generations and promote cultural awareness.

Meanwhile, the ‘UNESCO Convention’ of 1972 continues to play a central role in the identification, protection, and preservation of Cultural Heritage worldwide.

In a contemporary context, the continuous updates and revisions of these guidelines, along with the emergence of new standards, reflect the dynamic nature of Cultural Heritage conservation. This dynamism is further accentuated by the integration of emerging technologies and procedures, with notable mentions including point clouds, Digital Twins, Building Information Modelling (BIM) or HBIM (where the H stands for Heritage), and Scan to BIM.

Point clouds, obtained through laser scanning or photogrammetry, provide a detailed set of three-dimensional coordinates, enabling highly accurate representations of architectural objects. These point clouds are invaluable for graphical restitution, enabling the creation of detailed and faithful three-dimensional models.

On the flip side, BIM models emerge as a revolutionary catalyst, reshaping the Architectural, Engineering, and Construction (AEC) landscape by offering a comprehensive and integrated approach to information management across the entire lifecycle of buildings. This transformation is propelled by standards like ISO 19650 (International Organization for Standardization (ISO), 2018), which establish crucial guidelines for effective implementation.
Applied to Cultural Heritage, HBIM offer an integrated view, incorporating not only three-dimensional geometry but also information about the physical and functional properties of objects.

The Digital Twin and Scan to BIM serve as intertwined foundations in the conservation and management of the AH. Scan to BIM, employing advanced techniques for accurate 3D model generation through detailed point cloud analysis, complements the Digital Twin – a dynamic, continually updated digital replica facilitating ongoing monitoring and in-depth analysis. The amalgamation of all these technologies yields a holistic perspective, merging the precision of acquired details with the ever-evolving, seamlessly managed environment facilitated by the Digital Twin.

However, with every innovation, intrinsic risks arise, including the potential loss of authenticity and the introduction of errors during the acquisition process. Risks associated with the intensive use of virtual representations, such as the possible loss of traditional conservation practices and potential disconnection from the physical reality of architectural objects, become apparent. Simultaneously, digital security risks, including breaches and damage to sensitive data of cultural sites, require careful and targeted approaches.

Furthermore, the application of programming languages and Artificial Intelligence (AI) is playing an increasingly advanced role in managing and analysing data derived from the digitisation of heritage assets.
Artificial Intelligence, with its advanced learning and interpretation capabilities, facilitates the interpretation and classification of information, enabling continuous access, exchange, and updating of knowledge related to heritage. In this context, AI techniques are frequently used for segmentation and classification of images and point clouds in order to optimise and significantly speed up these operations, which in turn provides critical support for the in-depth analysis of the structure of digitised architectural objects.
However, the implementation of AI requires an ethical and conscious approach. The risk of misinterpretations or manipulations of information through AI underscores the need for careful ethical and regulatory considerations.

In an attempt to foster further studies and discussions in this field, this doctoral dissertation not only addresses the previously mentioned topics but delves into the intricate details of Architectural Heritage management and preservation. It emphasises innovation while preserving a steadfast commitment to tradition. This dual approach contributes to shaping a comprehensive and balanced vision for the future of safeguarding our rich historical heritage.

GOALS AND THESIS STRUCTURAL OVERVIEW

The thesis explores several tailor-made strategies for the application of advanced technologies in architectural design and surveying, all converging towards the common goal of enhancing the preservation and conservation of Architectural Heritage through digitisation. This involves cutting-edge approaches, particularly in the 3D context, through a unified Scan to BIM protocol that enhances the precision of the representation of Cultural Heritage.
Crucial phases of the process include integrated surveying with point cloud acquisition, advanced point cloud analysis, HBIM, and rigorous testing of data, adhering to international standards for heritage documentation.

The first chapter elucidates state-of-the-art techniques employed in surveying, encompassing the acquisition and recording of point clouds, automated survey planning for scanning, updated specifications and regulations of BIM, Scan to BIM, and optimisation procedures for data management and semantic enrichment. Emphasis is placed on process automation, such as through segmentation and classification.

The second chapter delves into the concept of a unified protocol adopted for the digitisation of Architectural Heritage, elucidating its development and the necessary aspects required for conducting a survey securely, along with guidelines on data delivery.

The third chapter presents initial results from case studies, focusing on the processing of point clouds, the construction of archaeological BIM models linked to relational databases, and other pivotal methodologies aimed at guaranteeing the coherence and efficacy of a BIM project across all developmental and construction stages.

Chapter 4 introduces innovative concepts related to the use of automatisms such as Artificial Intelligence, starting from data acquired through digital surveying to analyse them in contexts such as monitoring the physical-material obsolescence of buildings,

graphic representation of heritage through BIM models, and automated planning of digital surveying.

Semantic segmentation and point cloud classification through open-source algorithms or innovative and increasingly widespread Machine Learning techniques complete the framework of the thesis, along with conclusions and reflections for future developments of the presented work.

1. STATE OF THE ART AND LITERATURE REVIEW

Over the last twenty years, digital documentation associated with cultural, architectural and archaeological artifacts has assumed a prominent role due to its ease of storage, accessibility, and resilience against the threats of material or functional obsolescence and institutional negligence (Puma, 2016; Balzani, Maietti and Mugayar Kühl, 2017).

Particurarly, architectural surveying, as a keystone in spatial representation management, holds a crucial role in the processes of preservation of the heritage, enabling the exploration of architectural morphologies from two-dimensionality to three-dimensionality and viceversa.
Its evolution over time is evident in the widespread adoption of advanced technologies which have gradually replaced or integrated traditional surveying methods (De Fino, Galantucci and Fatiguso, 2023; Junshan Liu *et al.*, 2023). This is because, depending on the level of detail needed and the accessibility of the environment, the varied and contemporary technologies used for data capture allow the heterogeneity and complexity of an object to be taken into consideration, becoming increasingly important.

Significant strides have been made in the fields of Computer Graphics and Computer Vision, particularly within the realms of 'Close-Range Photogrammetry' (CRP) and 'Structure from Motion' (SfM). These advancements include 'reality-based' technqiues, such as 'image-based' methodologies, which reconstruct 3D models from 2D images derived from passive sensors like digital cameras, as well as 'range-based' approaches utilising Light Detection and Ranging (LiDAR) active sensors, recognised for their accuracy and resolution (Remondino, 2011; Aicardi *et al.*, 2018; El-Din Fawzy, 2019; Hassan and Fritsch, 2019; Tan, 2020).

The selection of scanning techniques is influenced by several factors, encompassing precision needs, object dimensions, portability, and project budget. However, both active and passive surveying methods converge in generating a point cloud as their

ultimate output, with a frequent utilisation of a hybrid approach (Beraldin, 2004; Yang, Xu and Huang, 2022; Pierdicca *et al.*, 2023).

This type of combination results in an efficient methodology that rapidly delivers accurate point clouds, spatially located through spatial coordinates and colorimetric characteristics (Beraldin, 2004; Florio, Catuogno and Della Corte, 2019; Aterini and Giuricin, 2020). Such an approach allows for diverse applications, including parametric three-dimensional modelling (Hichri, Stefani, De Luca, Veron, *et al.*, 2013; Verdoscia, Musicco and Tavolare, 2019), graphic representations of archaeological sites (Fiorillo *et al.*, 2015; Monterroso-Checa and Gasparini, 2016; Willis *et al.*, 2016), and multiscalar analysis for documenting changes in historic buildings over time (Russo and Manferdini, 2014).
It is essential to highlight that achieving an accurate integration of data obtained through various acquisition techniques necessitates rigorous control over metric accuracy. This becomes particularly vital since image-based technologies are not inherently intended for capturing the absolute dimensions of objects.

Lately, Neural Radiance Fields (NeRF) technology has introduced a new era in realistic and accurate 3D modelling by using Deep Learning and Computer Vision to reconstruct historical sites and artefacts from 2D photos by exploiting artificial neural networks (ANN), revolutionising the preservation of Cultural Heritage (Croce, Caroti, *et al.*, 2023; Mazzacca *et al.*, 2023).

Moreover, this versatility of the these modern approaches extends to various domains, encompassing historical documentation (Remondino, 2011; Brusaporci and Trizio, 2013; Alshawabkeh, Baik and Miky, 2021), conservation and protection (Akca *et al.*, 2006), monitoring and classification of degradation forms, as well as computerised diagnostics (Lerones *et al.*, 2016; Messaoudi *et al.*, 2018; Bruno *et al.*, 2019; Fatiguso and Buldo, 2020).
It further applies to temporal simulations and analysis (Gonizzi Barsanti, Guidi and De Luca, 2017b; Rodríguez-Gonzálvez *et al.*, 2019) virtual reality and computer graphic

applications (Voinea and Girbacia, 2019), three-dimensional libraries (Andrews, Zaihrayeu and Pane, 2012; Baik, Boehm and Abaikkauedusa, 2017), multimedia museum exhibitions, and remote visualisation and navigation, among other contexts (Osman, Wahab and Ismail, 2009; Amicis *et al.*, 2010; Bonacini, 2015; De Fino, Galantucci and Fatiguso, 2019). This diverse applicability underscores the robustness and utility of these methodologies in addressing various facets of Cultural Heritage and architectural exploration.

Three-dimensional survey data can be included into Building Information Modelling (BIM) information systems, where architectural elements dynamically change their value according to datasets collected in the survey stage and historical records (Pocobelli *et al.*, 2018). Utilising techniques like ODBC (Open DataBase Connectivity), proprietary interfaces (Eastman *et al.*, 2011; Verdoscia *et al.*, 2020), Visual Programming Language (VPL) applications like Dynamo Studio Autodesk® and Graphisoft Grasshopper® (Negendahl, 2015), and real-time monitoring in cloud platforms, platforms integrated into modelling environments facilitate data management and evaluation.

Nevertheless, finding a way to effectively combine heterogeneous information that help assigning a meaning to the 3D data derived from point clouds, meshes and images, is still a very difficult objective to be attained.
Reconstruction of diachronic models (Templin, Brzezinski and Rawa, 2019; Verdoscia *et al.*, 2020), formal analysis, conservation and preservation (Diara and Rinaudo, 2020), structural analysis (Vatan, Selbesoglu and Bayram, 2009), documentation processes, and virtual reality enhancement (Banfi, 2020) are some of the areas where BIM has shown particularly impressive results.

Additionally, devising a method to effectively merge diverse data that assists in providing context for 3D data generated from point clouds, models, and images continues to be an extremely challenging task.

In BIM, the segmentation technique – which aims to assign a semantic class to any point detected – is immensely helpful in defining a structured and ordered set of geometric points that can be used for additional elaborations, like extrapolating generatrices, or erasing the objects that are useless to a specific purpose.

This process uses its automatic modality to identify primitive geometrical elements (i.e., sides, edges, planes, cylinders, etc.) by taking advantage of the properties and spatial relationships that can be assigned to each point in relation to those nearby (Rabbani, van den Heuvel and Vosselman, 2006).

In recent years, a transformative innovation has emerged in the field of Cultural Heritage through the integration of Artificial Intelligence. This paradigm shift has significantly enhanced the segmentation and classification processes of point clouds, revolutionising the analysis and preservation capabilities within the heritage domain. The application of these advanced technologies not only allows for semantic segmentation of point clouds but also optimises and improves processing workflows within the Building Information Modelling (BIM) framework, providing a more efficient and accurate approach to managing 3D spatial data.

Providing that the training dataset is correctly arranged, such techniques allow to obtain an automated segmentation according to the criteria and proprieties chosen *a priori* by the user (Brodu and Lague, 2012). In particular, the use of Machine Learning or Deep Learning (Llamas *et al.*, 2016; Grilli, Menna and Remondino, 2017; Jeevitha *et al.*, 2020; Matrone, Grilli, *et al.*, 2020; Pierdicca *et al.*, 2020; Yang, Hou and Li, 2023) enables to gather data (points, patches) with similar colorimetric and/or geometric features together in homogeneous subsets (Croce, Caroti, Piemonte, *et al.*, 2021; Russo *et al.*, 2021; Buldo *et al.*, 2023) although the areas of investigation are numerous.

Several studies (Nguyen and Le, 2013; Grilli, Menna and Remondino, 2017; Xie, Tian and Zhu, 2020; Zhang *et al.*, 2023) have identified the most popular methodologies for segmenting and classifying point clouds. These methodologies include ‘edge-

based', 'region-based', 'model-based', 'attributes-based', and 'graph-based' approaches, which employ algorithms based on clustering of data features from the point clouds.

The classification of point clouds is a versatile process, tailored to address specific objectives. For example, it can be employed to discretise points related to vegetation elements during the survey phase, facilitating their easy exclusion in subsequent modelling stages and alleviating users from visual hindrances. Additionally, this classification technique allows for the identification and labeling of elements within the surveyed area through the application of metadata.
Furthermore, it enables the automatic recognition of distinct rooms within detected buildings by distinguishing their perimeters, showcasing its applicability in diverse scenarios such as urban planning, heritage documentation, and environmental monitoring (Jung, Stachniss and Kim, 2017).

Given the highly diverse geometries inherent in historical architectural environments, the automated application of these algorithms faces some limitations, particularly due to the challenge of acquiring a uniformly structured training dataset. This automated approach often necessitates human intervention to ensure accurate application and verification, underscoring the need for a nuanced understanding of the complex architectural context.
Moreover, despite the promising outcomes demonstrated in point cloud processing, their seamless integration into HBIM modelling procedures remains constrained, as these operations predominantly rely on manual efforts.

To address this limitation, there is a compelling need to explore a Scan to BIM methodology (Hichri, Stefani, De Luca, Veron, *et al.*, 2013; Verdoscia, Musicco and Tavolare, 2019), that, starting from laser scanner and photogrammetric data in form of point clouds facilitates the creation of 'as-built' BIM models, extracting accurate building parameters, particularly from a geometric standpoint (Anil *et al.*, 2013; Antón *et al.*, 2018; Badenko *et al.*, 2019; Radanovic, Khoshelham and Fraser, 2020).

It establishes a foundation for operational planning, supporting the construction of a comprehensive digital information model capable of integration and utilisation for diverse interdisciplinary purposes.

To achieve this goal, it becomes indispensable to clearly define the essential requirements for both the surveying process and model creation, along with their respective informative properties intended for integration. In the absence of global standardisation, individual countries are independently developing protocols and standards based on Levels of Detail/Development (LOD), resulting in inevitable procedural variations, yet mitigating the potential for misunderstandings between clients and designers.

1.1 Survey Technologies and Techniques

The advent of cutting-edge has engendered a transformative impact on survey recording, facilitating an extremely accurate capture of architectural structures (Remondino, 2011; Battini, 2012).
However, it is imperative to underscore that an effective strategy invariably necessitates the judicious integration of both state-of-the-art technologies and conventional approaches (Haddad, 2011). The synergistic amalgamation holds the potential to yield a more exhaustive and precise representation of heritage.
Whether employing active or passive techniques, both surveying methods provide sophisticated tools for collecting comprehensive three-dimensional data.
While passive methods record the radiation that is reflected off a surface, active methods mark a point in space with directed radiant energy.

Active methods entail sending laser pulses in the direction of the object's surface, such as Light Detection and Ranging (LiDAR) surveys. Very accurate three-dimensional coordinates of places on the object's surface may be acquired by timing how long it takes for the pulses to return to the sensor. This method works especially well for capturing morphological and topographical characteristics in outdoor settings

(Chehata, Guo and Mallet, 2009; Kang *et al.*, 2009; Brodu and Lague, 2012; Risbøl and Gustavsen, 2018; Wang *et al.*, 2020) .

Conversely, passive methods such as terrestrial photogrammetry (Beraldin, 2004; Remondino, 2011; Liang *et al.*, 2018; El-Din Fawzy, 2019; Alshawabkeh *et al.*, 2020; Alshawabkeh, Baik and Miky, 2021; J. Liu *et al.*, 2023) and platforms such as Unmanned Aerial Vehicles (UAVs), collect geometric information from photographic pictures or movies. Accurate 3D models may be built by analysing related points in the photos using complex algorithms. The cost-effectiveness and versatility of photogrammetry make it an ideal choice for digitising objects, whether they are located indoors or outdoors.

Recently, there has been a notable proliferation of mobile vehicles (Mader *et al.*, 2016; Adami *et al.*, 2019; Bakirman *et al.*, 2020), and other ground-based platforms (García-Gago *et al.*, 2014; Palomba *et al.*, 2019; Yang, Xu and Huang, 2022), portable mobile 3D laser mapping systems (Serna *et al.*, 2014; Sevgen and Abdikan, 2023), low-cost spherical cameras (Sun and Zhang, 2019; Herban *et al.*, 2022), and smartphone-mounted LiDAR sensors (Teppati Losè *et al.*, 2022; Mazzacca *et al.*, 2023; Musicco, Rossi and Verdoscia, 2023).
These methods yield remarkably realistic large- and small-scale representations of embellishments and complex surface features, thanks to the remarkable accuracy of the point clouds produced. It facilitates meticulous recordkeeping and enables more targeted restoration strategies and in-depth examinations.

In 1999, Boehler and Heinz attempted to illustrate the implementation range of different 3D registration methods (Boehler and Heinz, 1999), as shown in Fig. 1. In the diagram, the scope of each technique is represented in terms of object size (x-axis) and the number of points per object (y-axis).
Traditional methods, such as manual and tactile measurements, are suitable for small details or objects, especially in museum contexts, while geodetic and tachymetric measurements are limited in long-range registration.

3D documentation of movable and immovable assets can cover dimensions from a few millimeters to a few thousand meters, with no practical limits on the number of points and images acquired. Documentation methods can be further grouped based on those involving light registration (orange areas) and those that do not (yellow areas).

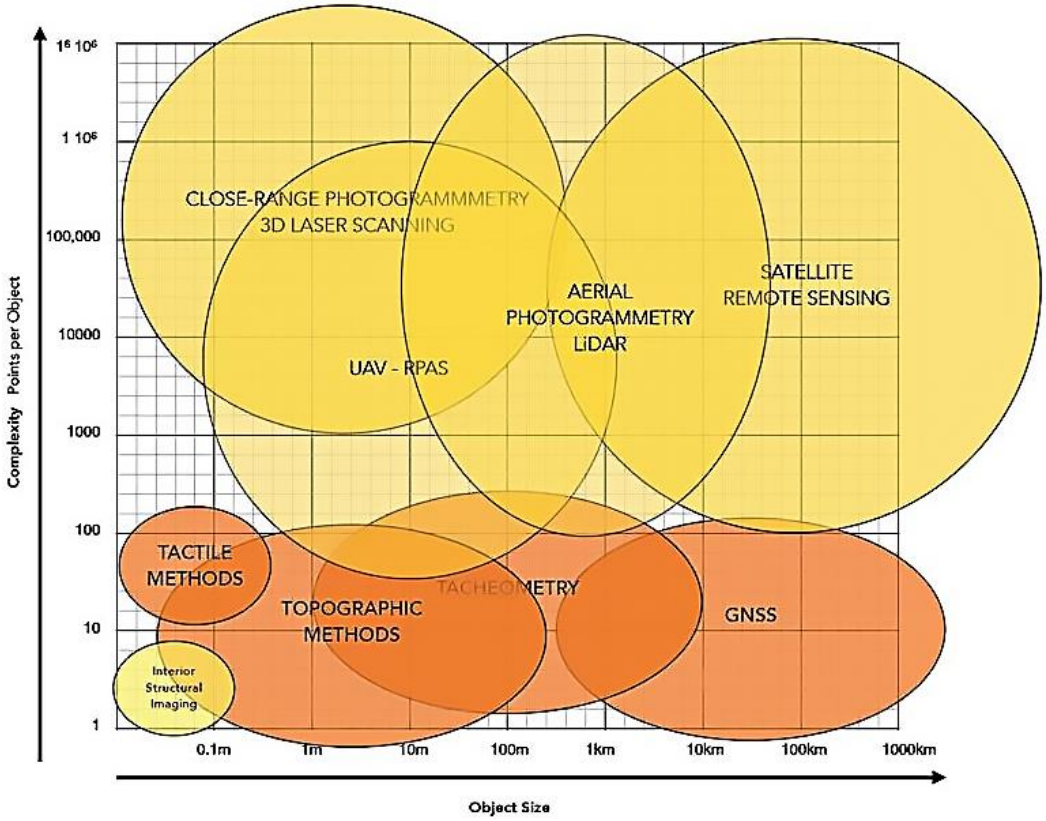

Fig. 1 Survey methods classified by size and object complexity (©UNESCO Chair on Digital Cultural Heritage at CUT (Pritchard *et al.*, 2022), ©adapted from (Boehler and Heinz, 1999)).

Key concepts to bear in mind regarding measurement errors in instruments are undoubtedly ‘precision’ and ‘accuracy’, as they together provide a comprehensive view of the quality and reliability of the employed instruments.

Precision and accuracy (shown in Fig. 2) are often mistakenly considered synonymous.

- 'Precision' refers to the consistency and repeatability of results obtained from a measuring instrument. In practice, a precise instrument will yield similar results on multiple occasions, providing a measure of its reliability and consistency over time.
- 'Accuracy' is linked to how well the measurements made with an instrument coincide with values considered true or accepted. An instrument is deemed accurate if its measurements closely align with reference values. Thus, accuracy assesses how closely the obtained result corresponds to the actual value intended for measurement.

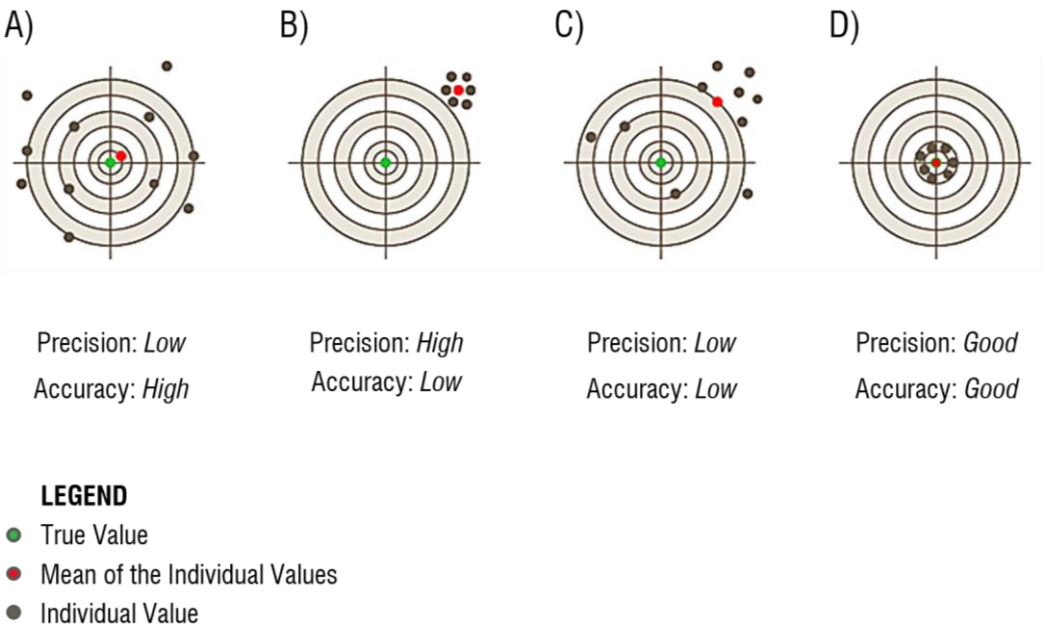

Fig. 2 . Conditions of Precision and Accuracy for measurement errors of the instruments.

1.1.1 Active Recording Systems

While traditional manual measurements through direct surveying may be suitable for relatively small objects, the use of topographic instruments becomes essential for larger objects and the establishment of extensive control networks.

Instrumental surveying, also known as topographic surveying (Luh *et al.*, 2014; Raju and Khandakar, 2022), relies on the visual sighting of points, and it is used as a complement to direct and indirect surveying for precise measurements, extensive planimetric surveys, and points that are inaccessible. It is essential for connecting the surveyed structure to the national topographic network.

In the past, optical-mechanical theodolites were used for geodetic and topographic surveys. Today, these instruments have been replaced by total stations, which differ significantly from traditional optical-mechanical theodolites as they are equipped with an electronic distance meter and a computer for data storage and calculation.

Total Stations can measure angles and distances of a series of points, determining their spatial location relative to a predefined coordinate system. Unlike the Global Navigation Satellite System (GNSS), a total station is an autonomous instrument that does not require satellite presence (Rifandi, Ningtyas and Assagaf, 2013; Altuntas, Karabork and Tusat, 2014). However, it is affected by atmospheric conditions such as humidity and temperature, influencing the refractive index and increasing the average error. Nowadays, the Total Theodolite Station (TST) incorporates Global Positioning System (GPS) technology, which increases the efficiency and accuracy of field surveys with angular and distance measurements. The disadvantages are related to the monotony of the operation and the time-consuming recording of points.

Instead, GNSS measurements exhibit a high level of accuracy, typically on the order of a few centimeters or even better, establishing a robust network of Ground Control Points (GCPs). GNSS is characterised by other its properties of integrity, continuity, and availability.

It is a technology essential for georeferencing, providing precise geographic coordinates to objects, locations, or phenomena on Earth. It relies on a network of satellites like GPS or GLONASS, and GNSS receivers on devices use signals from these satellites to accurately determine their position. This technology is crucial for applications such as navigation, surveying, and remote sensing, enabling precise location-based information across various sectors.

By using laser beams that allow to record information on the position of each point with the intensity of the reflected radiation, active range sensors known as laser scanners, play a central role for high-precision capture of three-dimensional data in the Cultural Heritage field (Edl, Mizerák and Trojan, 2018).

Terrestrial laser scanners (TLS) are commonly employed for medium-range surveys, capturing details such as building surfaces, historical monuments, and archaeological sites. They can also extend their range to 300 meters, allowing for large-scale surveys of terrain and vegetation, similar to the capabilities of airborne laser scanners (ALS). Laser scanners offer high accurate, non-invasive, and swift 3D data acquisition. Their versatility and seamless integration with other technologies make them essential for detailed and efficient documentation (Muralikrishnan, 2021).

A type of scanning instrumentation is the Triangulation Scanner (TS), where an emitter laser directs a point or laser line reflected by a rotating mirror towards the object. This laser beam reflects back and is captured by one or more Charged Coupled Device (CCD) or Complementary Metal Oxide Semiconductor (CMOS) sensors at predefined distances, crucial for spatial geometric definition.

TS includes Single spot, Slit scanner, and Structured Light Scanning (SLS) Systems. Single spot scanners use individual laser points redirected by lenses to record illuminated points on the surface, primarily employed in precision-demanding industrial settings. Slit scanners project the laser as a line, recording the object's profile step by step, suitable for small objects to extract their profile and surface sections. SLS differ

as they do not project a laser but capture shapes, often horizontal and vertical lines, recorded by a camera.

Another commercially available TLS systems include Time of Light (ToFS) and Phase Shift (PSS) scanners (Fig. 3), widely used in architecture and surveying, providing centimeter to millimeter precision at a data collection rate of up to 10,000 points per second. These instruments are compared to Total Stations, using a laser rangefinder oriented by azimuthal and zenithal angles set during the initial setup. ToF scanners consist of a laser emitter, rotating mirrors, and a laser receiver. The distance of the scanned object is determined by calculating the time taken for the laser to travel from emission to return. They are less suitable for detailed surveys.

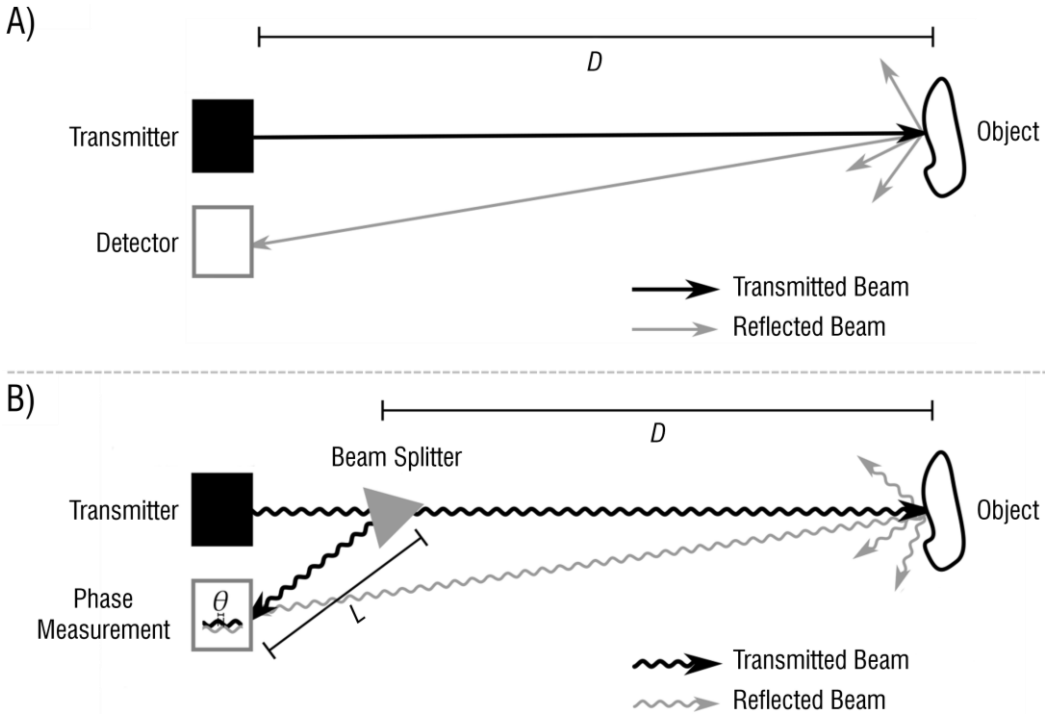

Fig. 3 Operating principles of the laser scanner A) Time of Flight; B) Phase Shift (©adapted from (Frey, 2019).

An alternative method involves the development of a scannerless device, where a single emitter emits divergent light to illuminate the entire targeted scene. The reflected light is subsequently captured on a two-dimensional array of photodetectors, specifically using a ToF depth camera (Horaud *et al.*, 2016). Unlike conventional cameras that gauge the intensity of ambient light, ToF cameras measure the reflected light originating from the camera's dedicated light-source emitter.

Concerning Phase Shift Scanners, the emitted laser reflects off the object's surface with a different wavelength. The phase difference enables the calculation of the object's distance from the scanner's center. When employing a ToFS or PSS, the measurement error increases linearly with the detection distance. Greater distances result in a larger error in data registration. On the contrary, in the case of Triangulation Scanners, accuracy follows a parabolic trend that improves with the scanner-to-object distance. Greater distances lead to higher precision in data recording.

3D Optical Triangulation Scanners (OTS) are examples of hybrid devices that typically include a projector and a camera. These systems, which provide detailed information down to the submillimeter level, are widely used in the automotive and aerospace industries. They work by projecting a known pattern onto the object and using triangulation techniques to digitise the surface, measuring deviations from the original pattern (Schlarp, Csencsics and Schitter, 2020). They do have certain drawbacks, though, such as a small field of view and short scanning distances. Additionally, they frequently exhibit sensitivity to changes in ambient brightness.

An additional type of scanner is the Mobile Laser Scanner (MLS), an advanced three-dimensional sensing system that integrate laser technology and often come equipped with GNSS and an Inertial Measurement Unit (IMU) to enhance precision in positioning and orientation during data acquisition. These devices also incorporate optical cameras and are mounted on mobile platforms such as ground vehicles or aircraft (Di Stefano *et al.*, 2021).

Their operation involves one or more laser scanners installed on a moving vehicle. These scanners emit lasers towards the surrounding surface, recording the return of the light beam for each detected point, along with information on distance and angular orientation. Thanks to the vehicle's speed, it is possible to rapidly acquire data over extensive areas, generating high-density three-dimensional point clouds. MLS are ideal tools for various applications, including topographic surveying, buildings and urban modelling, land management, and infrastructure design (Adán, Quintana and Prieto, 2019).

Smart technologies known as SLAM laser scanners (Keitaanniemi *et al.*, 2021; Camiña *et al.*, 2022) empower robots or autonomous vehicles to navigate unexplored territories by initially determining their location with a laser scanner, which assesses the size and shape of nearby objects as they move. Utilising these data, SLAM algorithms construct and continually update a real-time map of the surroundings, all while continuously estimating the device's position. This ongoing process enables the system to autonomously navigate even in intricate environments. Upon completion of the initial mapping and localization, the system can independently navigate the world using the generated map.

Regarding the success of data registration using laser scanners, it is closely influenced by both the number of scans and the quality of the acquired data. Insufficient data, in terms of both quantity and quality, will compromise the necessary overlap for effective registration, while an excess of scans may result in a significant and unnecessary expenditure of time. Therefore, it is essential to find an optimal balance between the number of scans conducted and the computational efforts employed.

For TLS, two primary phases can be distinguished: coarse and fine registration (Biswas, Bosché and Sun, 2015).
Coarse registration of point clouds involves aligning 3D features using either artificial targets or algorithms capable of extracting discriminative features naturally present in

the scene. Manual insertion of targets may extend scanning time, while automated algorithms reduce this time, still necessitating corresponding features between scans.
On the other hand, fine registration, following coarse registration, represents an optimal solution that utilises more data from scans, often relying on the Iterative Closest Point (ICP) algorithm. This iterative algorithm estimates the rigid transformation by aligning points in one point cloud with the nearest points in the successive scan.

1.1.2 Passive Recording Systems

Passive recording systems are a crucial component in documentation, data acquisition, and three-dimensional reconstruction methodologies, especially in the context of Cultural Heritage. These systems capture light or radiation originating from independent sources, such as the sun or artificial lighting, reflected by objects of interest without the use of active sources like lasers (Russo, Remondino and Guidi, 2011; Del Pozo *et al.*, 2017).
These techniques process optical images to extract metric information about the object, including its geometry and realistic texture. In CH and AH applications, they are often preferred for their efficiency, non-invasiveness, ease of use in both indoor and outdoor environments, and relatively low cost.

A significant challenge is the development of intelligent algorithms in photogrammetric techniques to automate traditional procedures while allowing the use of any type of camera and reducing costs. Therefore, the field of Computer Vision has contributed to automating the process (García-Gago *et al.*, 2014; Aicardi *et al.*, 2018). Image-based techniques can be categorised into single, stereo, or multiple views, depending on the number of images used, even from different sensors, to retrieve metric information in three-dimensional space and generate a point cloud (Tan, 2020).

Algorithms such as Structure from Motion, Multi-View Stereo, or Dense Stereo Matching are used to create a three-dimensional representation of the object (Willis *et*

al., 2016; Wang *et al.*, 2021) The importance of lateral and longitudinal image overlap must be ensured as much as possible (at least 60%-80%).

Aerial photogrammetry typically involves imaging systems on satellites (remote sensing), aircraft, and UAVs, while terrestrial or close-range photogrammetry methods, employing images acquired from a short distance, are used for digitising small objects with sub-millimeter accuracy and resolution (Pierdicca *et al.*, 2023).

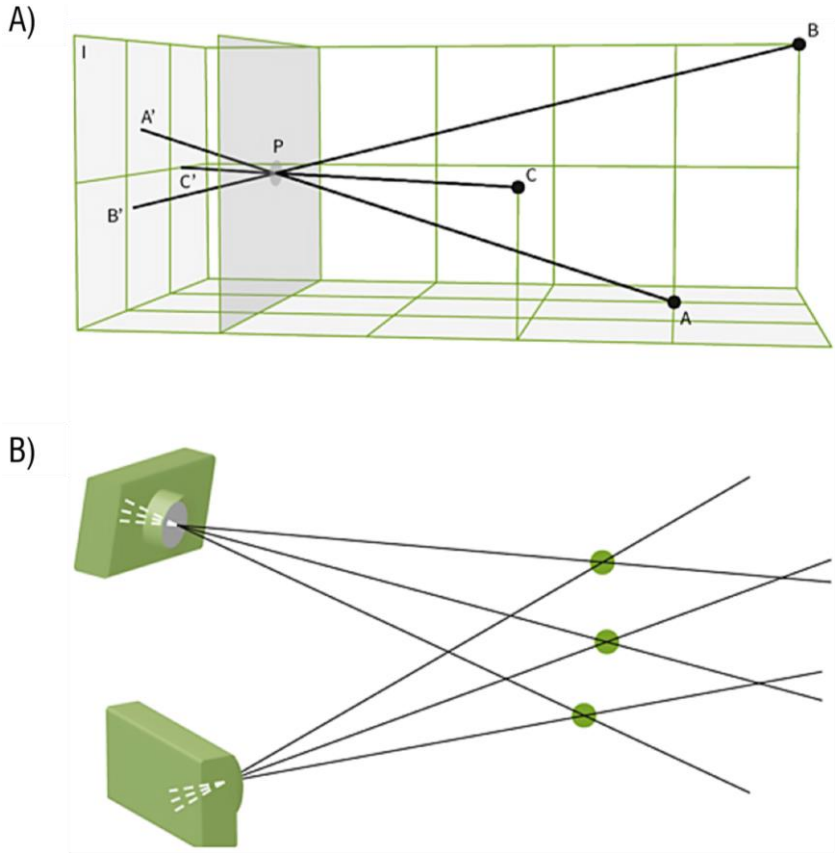

Fig. 4 Collinearity condition: A) Verification of alignment between the projection center, the point on the image, and the point on the object for accurate photogrammetric reconstruction; B) Intersection of rays from two images defining the position of the object in three-dimensional space (©adapted from (Bedford, 2017)).

Photogrammetry relies on converting the two-dimensional image coordinates (2D) into a real 3D coordinate system. This process demands a meticulous verification of collinearity (Fig. 4), ensuring alignment among the projection center, image point, and object point, following the central projection imaging model. The collinearity equations guide the transformation of images, defining the central perspective of a three-dimensional object through nine independent parameters. The three-dimensional coordinates of each point on the object are derived from the images based on the mutual position of the cameras reproducing the same points.

During the capture of an image from a camera, each point on the image represents the convergence of various rays of light. In photogrammetry, the ray of interest is the one theoretically passing in a straight line from the object point through the perspective center and arriving on the image plane at specific positions. The three-dimensional reconstruction of an object requires at least a pair of images providing stereoscopic restitution, and it is crucial to note that parts of the object not visible in at least two images cannot be reconstructed.

Real cameras introduce geometric distortions, and these deviations must be quantified, mathematically described, and compensated for. For this purpose, camera calibration is crucial for metric 3D reconstructions and involves four types of orientation: internal (bundle of rays related to the object in space) and external (position and orientation of the ray bundle relative to the object coordinates in space), which can be relative or absolute.

Internal calibration takes into account the scale factor of a photogrammetric image, defined as the ratio between the distance from the object to the perspective center and the principal distance between the image plane and the perspective center. External orientation parameters describe the geometric model of the camera in terms of spatial position and orientation in the global coordinate system.

Regarding the optical system selection, it is preferable to use fixed focal length lenses to ensure consistent shooting parameters. Lenses with a focal length of 50-60 mm

are ideal for capturing details, while those ranging from 16-20 mm are suitable for general shots. Very long telephoto lenses (80-300 mm) limit the field of view, complicating image overlap, whereas wide-angle lenses (<16 mm) may introduce distortions, especially in cases requiring high detail.

A crucial aspect for photogrammetric application is the required Level of Detail (LOD), determined by the goal of the processing, which may involve accurate two-dimensional representations such as orthophotos and vector plans, or mesh models for use in virtual tours or implementation in BIM models. More data implies longer processing times, often due to data redundancy. Therefore, careful planning of the survey before field execution is essential to facilitate operations.

Oblique imagery, incorporating both horizontal and vertical perspectives, and employing convergent configurations, offers distinct advantages over parallel imaging (Wackrow and Chandler, 2011). This configuration not only mitigates systematic errors resulting from imprecise lens distortion estimation but also enables a complete overlap if needed. This enhances the efficiency of subject coverage and facilitates capturing valuable images in challenging scenarios where conventional stereo photography may be impractical.
In the case of parallel-axis images, the perspective remains similar and parallel, with minimal convergence of optical rays. This implies that the images are captured at a constant angle relative to the object, ensuring significant uniformity in perspective distortion.
This approach is commonly employed for detailed acquisition, primarily focusing on building façades (Fig. 5). In aerial imagery, contemporary photogrammetric software accommodates oblique images from circling flights, markedly enhancing result accuracy when integrated with standard vertical images.

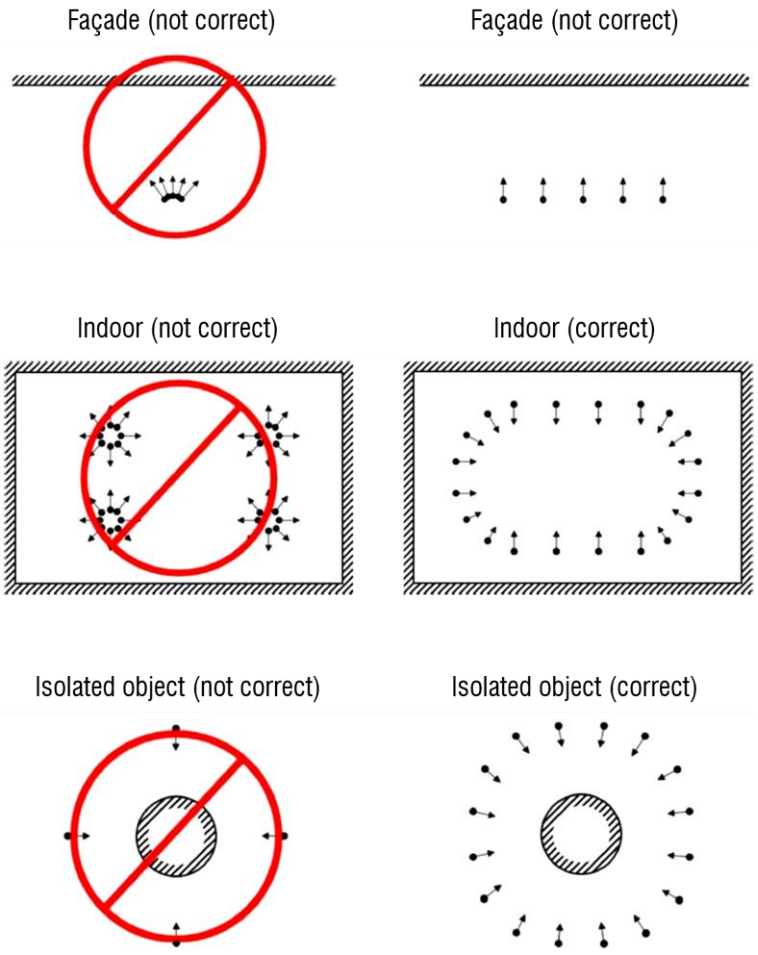

Fig. 5 Photogrammetric survey with parallel and convergent axes (©adapted from (Agisoft, 2020)).

1.2 Some Information on Point Clouds

As previously described, today, amazing details of old buildings may be captured by various technologies, offering a digital perspective that greatly surpasses the constraints of conventional photos or 3D models (Blaise, Florenzano and De Luca, 2004; Yang, Xu and Huang, 2022).

Point clouds are the results of 3D acquisition techniques and represent a significant step towards long-term preservation because it enables the permanent digital archiving of structures, ensuring that their essential characteristics remain intact even in the face of physical damage or alterations. In addition to being useful for research and study, this digital documentation can also prove to be a useful tool for public outreach, giving anybody the ability to digitally visit historical locations from anywhere in the globe.

Undoubtedly, a nuanced complexity underlies this endeavor. The adept management of voluminous datasets, navigation through the intricacies of acquisition technologies, and the mitigation of associated costs present formidable challenges that require judicious attention. Furthermore, the absence of standardisation poses a potential impediment to seamless interoperability among diverse systems and industry professionals (Storeide *et al.*, 2023).

Generic protocols for open and interchangeable point cloud processing formats and digital documentation of CH have been established. For example, the directives stipulated by the 'American Society for Photogrammetry and Remote Sensing' (ASPRS), notably those pertaining to the .LAS open file format for LiDAR data storage and delivery, are an additional and essential resource in ensuring the positional accuracy of digital geospatial data (Samberg, 2007).

ASTM E2807, a pivotal standard from 'American Society for Testing and Materials International' (ASTM International), delineates procedures for data exchange. The .E57 format file, linked to this standard, thoroughly captures 3D point data, attributes including color and intensity, and 2D imagery utilising a hybrid binary and eXtensible Markup Language (XML) format (Huber, 2011).

An additional instance is the revered government agency 'Historic England', which oversees and provides expert advise on metric surveys, thus playing a critical part in the conservation of England's historic heritage. Strict guidelines covering general re-

quirements, performance standards, data formats, and techniques like building surveying, topographic surveying, imaging, terrestrial laser scanning, and building information modelling (BIM) are established, with reference to the metric survey specifications for Cultural Heritage (Bryan *et al.*, 2009).

In a recent review by NASA's ESDIS Standards Coordination Office (ESCO), assessments of point cloud data formats and guidance for cloud-based storage trends were provided, serving as a foundational resource for further research in this field (Khalsa *et al.*, 2022).

The VIGIE 2020/654 study, commissioned by the European Commission, represents a comprehensive exploration of the 3D digitisation landscape for tangible Cultural Heritage (CH) (Pritchard *et al.*, 2022). Conducted by the Digital Heritage Research Lab at Cyprus University of Technology and a team of collaborators, the study is structured into tasks. It encompasses defining and exemplifying the complexity levels of tangible CH for 3D digitisation, identifying, and analysing quality parameters, examining existing formats, standards, benchmarks, methodologies, and guidelines, scrutinising past and ongoing 3D digitisation projects, and mapping the findings to diverse digital purpose.

The inherent limitations in accuracy and comprehensiveness of traditional methods, rooted in manual measurements and paper drawings, propel the standards beyond conventional architectural surveying techniques (Alexander, 1983; Pellegri, 2015). These standards are strategically integrated into avant-garde approaches, demonstrating their pivotal role in advancing the preservation and documentation of heritage.

Concerning the point cloud, as the result of the modern scanning approaches, it is formally represented as a set of three-dimensional coordinates, where each point is characterised by a triplet of Cartesian coordinates *(X, Y, Z).*

Denoting the point cloud as P, a single point p_i in the cloud can be expressed as:

$$p_i = (x_i, y, z_i)$$

[1]

Where:

i = index of the point.

The quality of the representation is largely dependent on the density and spatial distribution of points within the cloud. Density quantifies the number of points within a specific space unit and can be expressed as surface density, measuring points on the surface within a defined area, or volumetric density, measuring points within a specific volume inside the three-dimensional object. The spatial distribution of points on the surface, depends also on the density and encompasses how the points are arranged and the overall pattern they form.

The complexity of a dataset in a point cloud can be enhanced by incorporating additional attributes for each point, extending beyond spatial coordinates. These supplementary attributes may include details such as color, intensity, or other parameters specific to the context of the data (Tatoglu and Pochiraju, 2012).

The extended mathematical representation of a point p_i with these attributes becomes:

$$p_i = (x_i, y, z_i, c_i, I_i, \ldots)$$

[2]

Where:
c_i = colour
I_i = intensity of the point p_i.

These attributes provide details about the visual appearance and radiometric properties associated with each point.

For instance, colour information can capture the surface appearance, and intensity may convey information about the Light Reflectance Value (LRV), i.e. the percentage of light reflected by a surface (Kang *et al.*, 2009).

According to the quality data specifications developed by the U.S. General Service Administration (GSA), there are currently two main criteria by which a point cloud can be evaluated (Akca, 2003, 2010):

- 'Level of Accuracy' (LOA): Tolerance of the positioning accuracy of each individual point in the 3D point cloud data. LOA is typically denoted in millimeters.

- 'Level of Detail' or 'Level of Density' (LOD): Minimum size of the object that can be extracted from the point clouds. LOD refers to the surface sampling, i.e., how close the scanned points are to each other, indicating the density of the point cloud. LOD is typically denoted as a square area (in mm^2) obtained as the product of the vertical and horizontal distance (in millimeters) between nearby scanned points.

While LOD can be assessed using only acquired survey data, evaluating LOA requires additional data obtained from a control network using another sensor with an accuracy that should be an order of magnitude higher (for example, a Total Station).

Tab. 1 shows the four specification levels for LOA and LOD developed by GSA, selected based on the intended use of point clouds or derived 3D models. Typically, for indoor applications (e.g., interior layout) involving small dimensions, a higher LOA/LOD is required. For outdoor applications (e.g., outdoor building components, facades), dealing with larger dimensions, a lower LOA/LOD is desired (Aryan, Bosché and Tang, 2021).

Tab. 1 Standardised data quality requirements by the GSA.

GSA (Level)	**LOA (Tolerance)** (mm / inch)	**LOD (Data Density)** (mm*mm) / (inch*inch)
1	±51 /±2	(152*152) / (6*6)
2	±13 /±1/2	(25*25) / (1*1)
3	±6 /±1/4	(13*13) / (1/2*1/2)
4	±3 /±1/8	(13*13) / (1/2*1/2)

A more recent addition is the parameter 'Level of Surface Completeness' or 'Level of Surface Coverage' (LOC), denoted as the minimum amount of surface of an object of interest that has been scanned, and possibly which parts of this surface need to be acquired (Biswas, Bosché and Sun, 2015).

This criterion is releavant because capturing the entire surface of an object, especially with ground-based stations, can be challenging, but obtaining a sufficient portion of this surface may be adequate for the intended purpose.

1.3 Planning for Scanning (P4S)

The application of terrestrial laser scanning (TLS) in digitising Cultural Heritage necessitates meticulous planning of the architectural survey.
This preliminary phase is crucial to ensuring the comprehensive registration of the target object is accomplished under optimal conditions. Effective planning plays a pivotal role in streamlining the process, thereby reducing the time required and minimising computational expenses associated with complete registration (Aryan, Bosché and Tang, 2021; Huang, Zhang and Hammad, 2021).

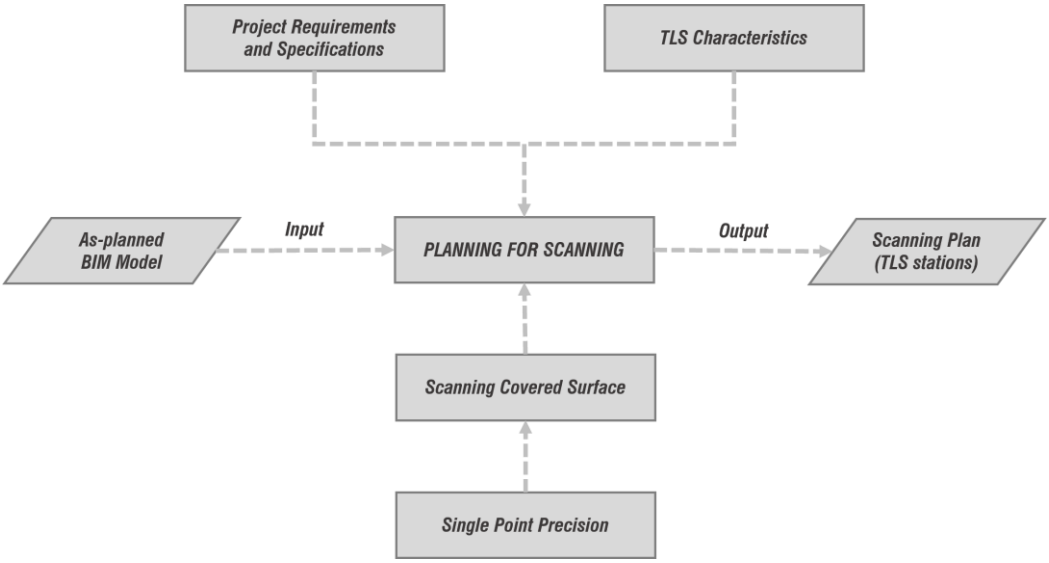

Fig. 6 Planning for Scanning Framework using BIM Models (©adapted from (Aryan, Bosché and Tang, 2021).

This goal can be accomplished through the strategic reduction of laser stations, ensuring the creation of a uniformly distributed dense point cloud while mitigating occlusion from objects within the survey acquisition scene (López *et al.*, 2023). This methodology not only minimises data redundancy *(over-scanning)* but also guarantees no missing pieces *(under-scanning)* and the comprehensive collection of data, thereby enabling a swifter and more efficient post-processing workflow.

However, the decision on where to position the TLS relies on the experience and capabilities of the operator, lacking systematic procedures to optimise the instrument's placement (Cabo, Ordóñez and Argüelles-Fraga, 2017; Huang, Zhang and Hammad, 2021).

The choice of positions is thus subjective, but it can still be appropriately planned by referring to predetermined specifications and requirements, such as Level of Density (LOD), Level of Accuracy (LOA), and Level of Surface Completeness (LOC), as shown in (Fig. 6). This not only enhances efficiency but also ensures the achievement of precise and high-quality results (Biswas, Bosché and Sun, 2015).

Thus, a group of experts has defined, in a systematic review, the Planning for Scanning (P4S) challenge as the task of identifying the minimum number of predefined viewpoints necessary to ensure comprehensive coverage of scanning targets while meeting data quality requirements (Aryan, Bosché and Tang, 2021).

While the need for scanning planning has only recently emerged in the construction industry, it has already been investigated in the manufacturing sector often for different types of 3D laser scanners. Different methods are proposed for the TLS automatic planning with the goal of reducing costs and inspection time (Son, Park and Lee, 2002; Fernández Álvarez *et al.*, 2008; Mahmud *et al.*, 2011; Turkan *et al.*, 2013). These approaches utilise the 3D CAD model of the object to be inspected for planning the scanning operations.

In 2017, a thorough study was conducted on optimisation methods for TLS station placements to enhance architectural survey planning (Cabrera-Revuelta, 2017).This investigation addressed the Art Gallery Problem (AGP) to determine the minimum number of guards required to surveil the internal polygon under consideration in architectural surveying. Additionally, it delved into the Fortress Problem (FP), which focuses on ensuring visibility from the exterior of a polygon (Cabrera-Revuelta, Chávez de Diego and Márquez-Pérez, 2018).
Furthermore, an innovative genetic algorithm (GA), employing a metaheuristic approach, was developed to maximise survey completeness, reduce data redundancies, and minimise point cloud overlaps (Cabrera-Revuelta *et al.*, 2021), as shown in Fig. 7.

In recent years, advancements in scanning technology have prompted the development of novel algorithms aimed at enhancing the precision of data acquisition.
In 2021, a study (Huang, Zhang and Hammad, 2021) focused on optimising the effective scan range by considering neighboring-point distributions on both vertical and horizontal planes.

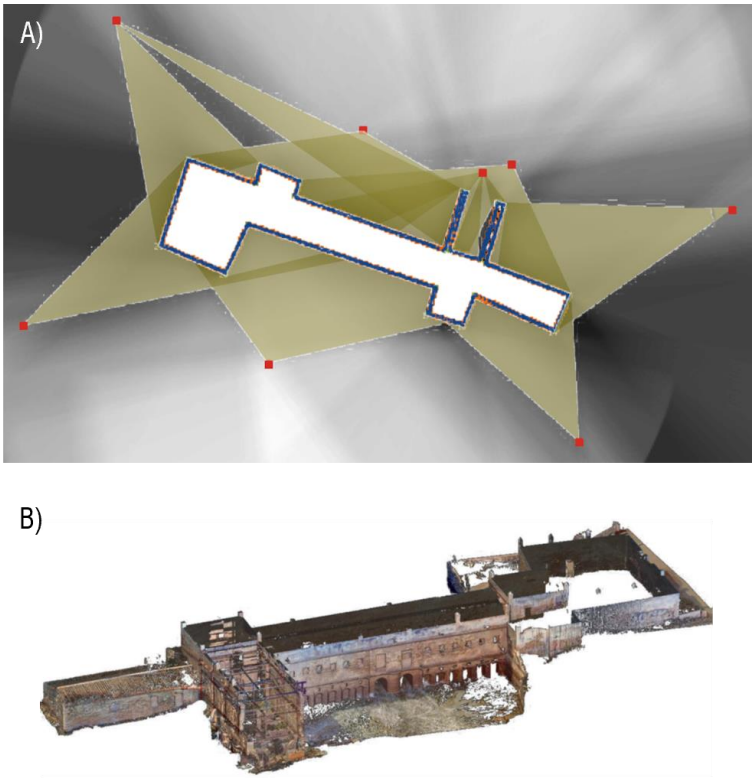

Fig. 7 Automatic TLS survey planning: A) Stations detected with a Genetic Algorithm; B) Point cloud generated by such stations (Cabrera-Revuelta *et al.*, 2021).

Another approach (Dehbi *et al.*, 2021) delved into a comprehensive study, not only addressing the necessity for sufficient bilateral overlap between neighboring stations but also examining the global connectivity of the station network.

Moving into 2022, a paradigm shift was observed in scanning methodologies. While the majority of algorithms were fixated on two-dimensional sketches, a growing recognition of the need for comprehensive three-dimensional data processing led to the development of innovative approaches for planning both static and mobile scans (Frías *et al.*, 2022). During the same year, it was proposed a groundbreaking methodology for optimising the positioning of TLS stations, leveraging a pre-existing three-dimensional triangular mesh model (Rougeron, Garrec and Andriot, 2022).

In 2022, visibility analyser was introduced to enhance optimization processes, constructing a vertical visibility polygon and seamlessly integrating the results into the scanning optimization workflow (Jia and Lichti, 2022).

As the transition to 2023 unfolded, cutting-edge techniques for optimising Terrestrial Laser Scanning (TLS) surveys within three-dimensional environments were explored (López *et al.*, 2023). The employed methodologies, including spatial searches, GA algorithms, and General Purpose Computing on Graphics Processing Unit (GP-GPU), marked a significant milestone, achieving unprecedented efficiency in TLS data acquisition.
In all these advancements, the key aspect lies in determining the optimal position for TLS data acquisition in digital surveying, ensuring meticulous planning for optimal outcomes.

On the other hand, the automation of photogrammetric surveying with predefined flight planners like Pix4D® (Strecha, Küng and Fua, 2012), DJI Flight Planner® (DJI, 2020), Litchi® (Litchi, 2020) or others, has already seen significant development.
While these tools effortlessly generate flight paths, they require prior knowledge of the scene's height to avoid collisions, often necessitating manual interventions by pilots.

Recently, in the field of UAV path mapping, the trend is shifting towards optimisation methods, categorised into ‘model-free’ approaches (for exploring unknown environments) and ‘model-based’ approaches (global optimisation with an approximate model) (Koch, Körner and Fraundorfer, 2019; F. Wang *et al.*, 2022).
'Model-based' strategies are also primarily employed for offline Planning for Scanning (P4S), leveraging pre-existing information about the scanning environment, such as 2D (CAD) floor plans (Scott, 2009; Biegelbauer, Vincze and Wohlkinger, 2010).
Conversely, 'non-model-based' approaches, also kwon as ‘view planning’ or ‘next best view’ (NBV) find application in online planning and are commonly considered within the field of SLAM in robotics (Biegelbauer, Vincze and Wohlkinger, 2010; Potthast and Sukhatme, 2014).

1.4 Building Information Modelling (BIM) and Scan to BIM

In the Architecture, Engineering, and Construction (AEC) field, Building Information Modelling (BIM) stands out as a pioneering methodology, placing the use of intelligent digital models at the core of its approach (Ali, Alhajlah and Kassem, 2022).
It was 1974 when Professor Charles M. Eastman of Carnegie Mellon University in Pittsburgh introduced the theory of a building design process initially called or Building Description System (BDS), later renamed as Building Information Modelling (BIM) (Zhang *et al.*, 2013).
Since then, BIM has undergone significant development, emerging as a pivotal methodology in different fields, such as Cultural Heritage, industrial sectors, infrastructure, real estate, interior design, and more.

This approach is described as a virtual and parametric representation of the structure capable of containing information. The highly detailed models serve as an integrated tool for the design, construction, and management of building structures, providing a comprehensive and three-dimensional view. The paramount goal of BIM is to optimise the life cycle of constructions, fostering greater efficiency in the phases of design, construction, and maintenance (Ali, Alhajlah and Kassem, 2022; Morsi *et al.*, 2022) with implications for effective facility management (Pinti, Codinhoto and Bonelli, 2022).

A natural evolution of BIM applied to the built environment and widely used in the architectural/heritage sector has manifested as 'Historic/Heritage Building Information Modelling' (HBIM), with the term 'Historic' originally coined in 2009 by Professor Maurice Murphy and his colleagues at the School of Surveying and Construction Innovation (Murphy, McGovern and Pavia, 2009).

This specific extension aims to digitally preserve, document, and manage historical buildings and monuments, surpassing mere physical representation of structures (Oreni *et al.*, 2013; Quattrini *et al.*, 2015; Banfi, 2020). HBIM distinguishes itself

through the integration of historical, architectural, and structural data, offering a complete framework of cultural features, *as-built* models, historical information, and conservation interventions (Hichri, Stefani, De Luca and Veron, 2013).

Analysis and simulations constitute another essential component of HBIM, enabling the assessment of potential impacts of restoration interventions or environmental changes on historical buildings. This results in a predictive framework of consequences, supporting informed decision-making. Collaboration is actively encouraged and facilitated through shared access to a digital environment, engaging architects, engineers, conservators, and heritage administrators in a synergistic and cooperative process (Khohar *et al.*, 2021).

The standards for BIM undergo continuous updates and constitute essential documents that establish guidelines, procedures, and technical specifications for the creation, management, and exchange of information based on the digital model of a project.

In the United States, the American Institute of Architects (AIA) has introduced a protocol known as the 'G202-2013 Building Information Modeling' (BIMForum and American Institute of Architects, 2023) This protocol defines Level of Development (LOD) as the level of completeness applicable to an element of the model in five progressively detailed steps, identified by a numeric scale expressed in hundreds, ranging from 100 to 500.
At LOD 100, elements are symbolically represented with information derived from other sources. LOD 200 introduces approximate details, such as quantity and size. LOD 300 refines the design, allowing precise measurements of quantity, size, shape, location, and orientation. LOD 350 extends this by incorporating interfaces with adjacent elements. LOD 400 provides detailed representations suitable for fabrication and installation. Finally, LOD 500 captures existing or as-constructed conditions with a specified level of accuracy, achieved through observation, field verification, or interpolation.

In the United Kingdom, regulations 'NBS 1192:2007' and 'PAS 1192-2:2013' (BSI, 2013) serve as the reference for information exchange in BIM projects. They identify 'Levels of Definition' (ranging from 1 to 7), further subdivided into 'Levels of Detail' (LOD), progressively describing the graphic content of a model, and 'Levels of Information' (LOI), detailing the non-graphic content of a model.

The Italian regulation 'UNI 11337-4:2017' (Ente Italiano di Normazione (UNI), 2017) defines LOD in terms of 'Levels of Development', distinguishing between 'Levels of Geometry' (LOG) for all graphic attributes and 'Levels of Information' (LOI) for all information attributes. It also introduces a LOD scale codified with Latin capital letters (from A to G), including additional intermediate levels that can be defined upon the customer's request (Mirarchi *et al.*, 2020).

In 2018, with the international regulations ISO 19650-1:2018 (International Organization for Standardization (ISO), 2018) on information management in BIM, the definition of 'Level of Information Need' (LOIN) was introduced, aiming to overcome the limitations of a rigid classification based on predetermined classes 1 (Seyis and Cekin, 2020; Godager *et al.*, 2022). Unlike other approaches, LOIN requires a coherent identification of the reading and usability requirements of the model to effectively integrate it into its information processes. A functional classification (based on technology or semantics) gives way to a description illustrating the actual intended use of the object or collected information, thereby explaining the reasons behind certain choices, and avoiding model overload.

BuildingSMART, formerly known as the' International Alliance for Interoperability' (IAI), is an international organisation that seeks to improve information exchange between software applications used in the construction industry. It has developed Industry Foundation Classes (IFCs) as a neutral and open specification for BIM.
This interoperability framework aligns with the broader context of BIM's evolution.

Moreover, the concept of 'Level of Reliability' (Maiezza, 2019) in HBIM finds a relevant application within this framework. This concept goes beyond the formal corre-

spondence between models and point cloud ‘Level of Accuracy’ (LOA) (Antón et al., 2018). Instead, it addresses the broader notion of reliability, encompassing the trustworthiness of information regarding materials, construction processes, and more (Brusaporci, Maiezza and Tata, 2018).

In the broader context of the building project's lifecycle, the various phases or levels of development and implementation of the digital model are referred to as ‘dimensions of BIM’ (Mesároš, Smetanková and Mandičák, 2019; Wang and Jin Liu, 2020).
The 3D dimension, surpassing traditional two-dimensional representation, allows for a comprehensive visualisation of physical elements in a three-dimensional environment. Advancing to the 4D dimension, the temporal element integrates with geometry, enabling the visualisation of project evolution over time. Temporal event sequences, including construction processes, become clear, providing a dynamic and chronological perspective. The addition of the 5D dimension introduces a financial aspect, enabling monitoring and management of project costs across various developmental stages. This establishes a clear foundation for financial management and budget planning.
In the sixth dimension, 6D, sustainability is addressed, incorporating data on energy efficiency, the use of sustainable materials, and other environmental considerations. It is an approach focused on making more sustainable construction decisions throughout the entire building lifecycle. Finally, the 7D dimension focuses on post-construction management and maintenance, providing data on scheduled maintenance, inspections, and overall management. The goal is to optimise operational efficiency and extend the building's lifespan.

As the industry continues to evolve, new dimensions of BIM, such as 8D, 9D, 10D, and 11D may be added to address emerging challenges and opportunities. However, these dimensions are not yet recognised by ISO 19650 (Piaseckienė, 2022).
Specifically, 8D BIM is dedicated to safety during design and construction, integrating risk control and eliminating potential threats before construction begins. The 9D di-

mension of BIM focuses on lean construction, optimising construction processes and reducing waste through the application of lean principles.
The 10D dimension of BIM concentrates on the industrialisation of construction, aiming to increase efficiency and productivity through the use of off-site construction methods and prefabrication. Leveraging a productivity-focused approach and innovative solutions, the conceivable emergence of the 11th dimension of BIM aims to catalyse substantial advancements in energy and systems sectors, enhancing the success and sustainability of client.
Implementing these dimensions allows for a more comprehensive and informed management of construction projects, providing an integrated framework covering physical, temporal, financial, sustainable, and operational aspects.

In the context of Building Information Modelling (BIM), a crucial concept pertains to parameterisation, involving the definition of parameters associated with model elements, encompassing dimensions, shapes, materials, and relationships (De Luca, Veron and Florenzano, 2006; Pocobelli *et al.*, 2018; Croce *et al.*, 2022).

This methodology enables models to be dynamic and adaptable, facilitating advanced analyses and simulations during the design and construction phases. The approach emphasises a comprehensive and interconnected representation of construction elements, further underscored by the concept of 'object-oriented modelling'. It involves representing elements as 'objects' endowed with specific attributes that extend beyond mere geometry (Jeong and Kim, 2016; Li and Xu, 2022).

In practice, the implementation of BIM necessitates the use of specialised software, such as Autodesk Revit®, ArchiCAD®, Bentley®, and more (Wang, Zhu and Wei, 2022). These tools facilitate real-time collaboration among stakeholders (Rocha *et al.*, 2020), promoting greater efficiency and coherence in the design process and the management of the life cycle of constructions (Fig. 8).

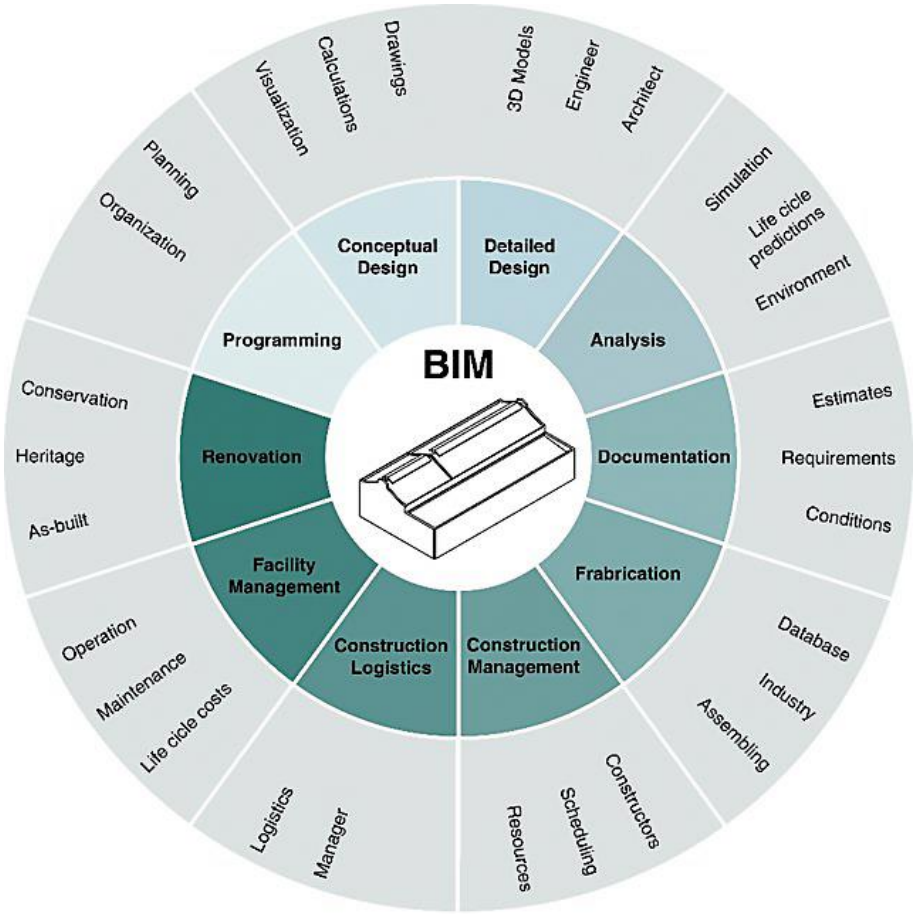

Fig. 8 Diagram of a BIM workflow (©adapted from (Rocha *et al.*, 2020)).

In recent imes, the concept of Scan-to-BIM has gained significant importance as a methodology that leverages data acquired from technological instruments, such as laser scanners or photogrammetry, to obtain accurate metric references during the construction of a BIM model, as faithful as possible to (Dore and Murphy, 2013; Adekunle, Aigbavboa and Ejohwomu, 2022).

Conversely, Scan-vs-BIM highlights the critical examination and validation process involving the comparison of data acquired from laser scans or photogrammetry with an established BIM model (Bosché *et al.*, 2015; Abreu *et al.*, 2023).

This meticulous analysis is geared towards assessing the accuracy and alignment of the BIM model with respect to a point cloud, pinpointing any disparities to refine and enhance the overall congruence between the virtual model and the physical reality.

In Cultural Heritage, several authors explored the creation of models from point clouds for HBIM enrichment (Rocha *et al.*, 2020; Alshawabkeh, Baik and Miky, 2021; Croce, Bevilacqua, *et al.*, 2021; Verdoscia, Buldo, Musicco, *et al.*, 2022b), involving both manual or fast semi-automatic methods (López *et al.*, 2017; Antón *et al.*, 2018), for geometry analysis (Capone and Lanzara, 2019; Qiu *et al.*, 2022).

Applications range from architectural management in BIM e GIS (Saygi and Remondino, 2013), to querying information related to a 3D model for the entire life cycle of a building (Agustín-Hernández, Fernández-Morales and Quintilla-Castán, 2018; Agustín-Hernández and Quintilla-Castán, 2019; Morsi *et al.*, 2022).

Additionally, explorations extend to applications in archaeological contexts (Scianna, Serlorenzi and Gristina, 2015; Battini and Sorge, 2016; Bosco *et al.*, 2019; Capparelli and Camiz, 2019), strategies for BIM modelling education (Agustín-Hernández, Sancho-Mir and Fernández-Morales, 2016), or other fields such as monitoring and diagnostics (Messaoudi *et al.*, 2018; Bruno *et al.*, 2020) or post-disaster built heritage reconstruction process within the digital twin framework (Gros *et al.*, 2023; Nguyen and Adhikari, 2023).

1.5 Semantic Enrichment of Cultural Heritage

Nowadays, climate change, natural disasters, and damages caused by humans present serious difficulties for Cultural Heritage (CH). For this reason, the need to protect and conserve it has become critical. Promising results are being obtained in the areas of documentation and conservation thanks to sophisticated acquisition technologies that get beyond the drawbacks of direct measurements and produce precise morphometric and geometric 3D models.

Nevertheless, even while the volume of data gathered – especially in the form of images and point clouds – represents a significant advancement, problems with disarray and information dispersal remain.

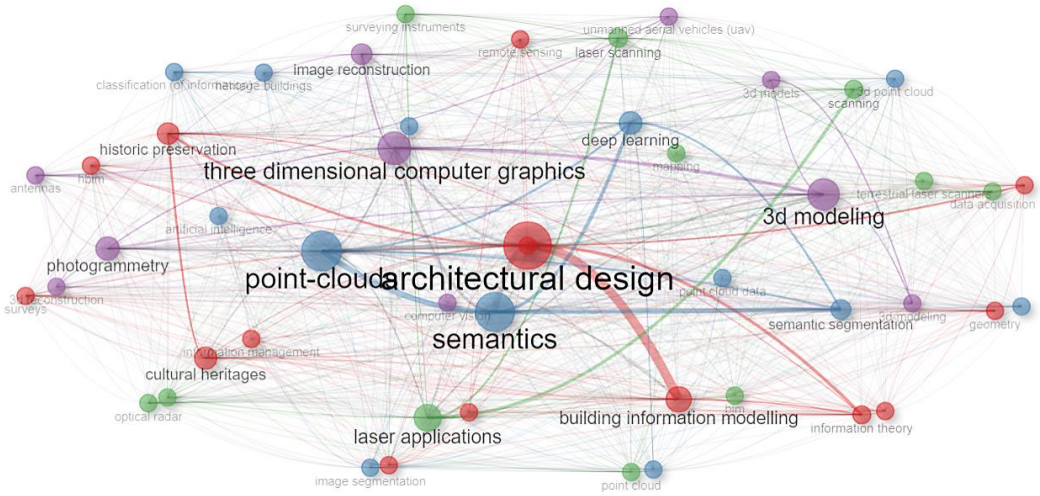

Fig. 9 Network map produced by bibliometric analysis using the the R-tool 'bibliometrix' and the web interface 'biblioshiny'. The graph connects the primary keywords associated with the topic of semantic enrichment using search terms like 'Cultural Heritage', 'Point Cloud', 'Segmentation', and 'BIM'. It is produced from a combination of 470 English-language papers evaluated on Scopus and Web of Science between 2012 and 2024.

The process of semantic enrichment in relation to Cultural Heritage becomes imperative in order to tackle this difficulty (Fig. 9). The objective is to decipher the 3D scene, pinpoint specific elements, and lay the groundwork for generating Heritage Building Information Models (HBIM) via procedures like Scan to BIM, or for preservation, restoration, and monitoring. However, combining heterogeneous information to provide 3D data a semantic meaning is still a difficult requirement that can be satisfied by automated segmentation and classification techniques. The complete comprehension and preservation of CH are made possible by the integration of such approaches, which is crucial for realising the full potential of the collected data.

'Segmentation' is the process of grouping data (points, patches) into subsets (points, homogeneous regions) based on similar features (colorimetric, radiometric, geometric, etc.). Simultaneously, these data are defined and assigned to distinct labelled classes based on various criteria under the term 'Classification'.
Numerous studies are associated with the theme of semantic classification, primarily driven by specific requirements provided by the application field, such as Building Information Modelling (BIM) (Macher, Landes and Grussenmeyer, 2015), Cultural Heritage (Gonizzi Barsanti, Guidi and De Luca, 2017a), Robotics (Maturana and Scherer, 2015), Autonomous Driving (Wang, Zhang and Wang, 2017), Urban Planning (Xu, Vosselman and Oude Elberink, 2014), etc.

The most popular segmentation and classification techniques examined over time, specifically with reference to point clouds, have been compiled in the literature (Yang, Xu and Huang, 2022; Zhao *et al.*, 2023). Therefore, the most recurrent segmentation approaches are grouped into categories such as 'edge-based', 'region-based' (or 'region-growing'), 'attributes-based', 'model-based' (or 'model-fitting'), 'graph-based', 'hybrid', 'Machine Learning' and 'Deep Learning'.

Specifically, *edge-based* segmentation algorithms are divided into two main phases: the first defines edge detection to delineate boundaries of different regions, and the second involves grouping points within boundaries to obtain the final segments

(Rabbani, van den Heuvel and Vosselman, 2006). Edges describe the shape characteristics of objects; therefore, in depth maps, they are defined by points where visible changes in local surface properties (e.g., gradients, normals, principal curvatures, or higher-order derivatives) exceed a certain threshold value (Bhanu *et al.*, 1986; Sappa and Devy, 2001; Wani and Arabnia, 2003).
The quick segmentation process is undoubtedly an advantage of edge-based approaches; nevertheless, accuracy problems relating to noise sensitivity, irregular point cloud density, and the difficult detection of closed segments – which frequently highlight disconnected edges – offset this benefit.

Region-based methods employ 'Neighborhood Information' algorithms capable of combining nearby points with similar properties, thereby obtaining distinct isolated regions. These techniques offer a greater level of noise accuracy as compared to *edge-based* techniques (Liu and Xiong, 2008). However, they have trouble drawing boundaries between regions and may have problems with under- or over-segmentation.

There are two different kinds of approaches in this context, called 'bottom-up' and 'top-down'. Regarding the *bottom-up* approaches, known as *seeded region*, the process commences by seeding a specific number of starting points *(seed points)*. Each region (segment) then develops by adding neighboring points based on data similarity criteria (such as curvature or surface orientation) or compatibility thresholds (Rabbani, van den Heuvel and Vosselman, 2006) (Jagannathan and Miller, 2007).
Therefore, imprecise selection of starting points can impact the segmentation process, leading to under- or over-segmentation problems.
The second class of methods, called *top-down* or *unseeded-region*, starts with all points grouped into an area, and then a single surface is tailored to fit the region. As long as the selected merit figure for adaption is higher than a predetermined threshold, the region subdivision will continue. One of the main challenges for these algorithms is still deciding where and how to divide the region. Another is that they require

a significant amount of prior knowledge (number of regions, object models, etc.), which is typically unknown in complicated scenarios.

Attributes-based methods represent robust approaches centered around the clustering of attributes derived from point clouds. The first step involves computing the attributes of point clouds, followed by grouping them based on the identified attributes into homogeneous regions. While these methods ensure reliability in managing attributes during the segmentation process, they exhibit a limitation on the quality of the attributes themselves, heavily reliant on the precision of calculations crucial for determining the optimal separation process of different classes.
In the literature, various attributes-based methodologies have been proposed. For instance, they have been adopted for clustering surfaces derived from airborne laser scanners (Filin, 2001). Unsupervised approaches, such as fuzzy clustering, have been employed for segmenting point clouds from TLS (Biosca and Lerma, 2008). Additionally, the 'Hough Transformation' (HT) method in 3D form has been utilised for segmenting planar surfaces within irregularly distributed point clouds from laser scanners (Vosselman and Dijkman, 2001).

In *model-based* or *model-fitting* procedures, points with the same mathematical representation are grouped into one area using geometric primitive forms (e.g., sphere, cylinder, cone, or plane). The two most popular algorithms at the forefront of modern methodology are the aforementioned Hough Transformation (HT) and Random Sample Consensus (RANSAC).
RANSAC has been employed to detect mathematical features such as straight lines, circles, etc., for the segmentation and classification of complex point clouds derived from slippery shapes (Gelfand and Guibas, 2004). It has been utilised for the segmentation of data from polygonal meshes and point clouds (Fischler and Bolles, 1981), as well as primitive shapes such as planes and cylinders (Schnabel, Degener and Klein, 2009). RANSAC, being a robust algorithm, demonstrates versatility in segmenting point clouds based on geometric primitives, offering valuable contributions to the field of point cloud analysis.

HT, on the other hand, has been employed to detect arbitrarily complex shapes (Ballard, 1981), identify planes (Vosselman and Dijkman, 2001), cylinders, and spheres (Vosselman and Dijkman, 2001), cilindri e sfere (Rabbani, van den Wildenberg and Vosselman, 2006).
A study comparing approaches for the automatic detection of flat building roofs was carried out, and the findings showed that RANSAC was more effective in terms of execution times and segmentation outcomes, even with the limitations noted in both methods (Tarsha-Kurdi, Landes and Grussenmeyer, 2007). Moreover, it was introduced an altered RANSAC segmentation algorithm that is less susceptible to noise, maintains topological coherence among primitives, and prevents under- or over-segmentation. This was accomplished by applying a region-growing method to separate coplanar primitives using a vector data structure based on irregular triangles and a Triangulated Irregular Network (TIN) (Chen *et al.*, 2014).

'Graph-based' techniques, which treat point clouds as a graph with edges connecting pairs of adjacent points and vertices representing individual points in the data, are becoming more and more popular because to their accuracy and efficiency, particularly in robotic applications. Prominent uses encompass the division of 2D images into designated areas (Meyer and Drummond, 2017), the creation of 3D graphs from point clouds using 'K-Nearest Neighbours' (KNN) algorithms (Golovinskiy and Funkhouser, 2009), and the calculation of normals and colour identification on pictures (Strom, Richardson and Olson, 2010).

These approaches can be coupled to provide 'hybrid-based' techniques for segmenting pictures, polygonal models, and point clouds. This entails figuring out each method's advantages and disadvantages and combining them to improve performance as a whole (Lavoué, Dupont and Baskurt, 2005; Vieira and Shimada, 2005).

The far-reaching influence of 'Machine Learning' (ML) across various sectors within Computer Science and Artificial Intelligence (AI) is notably significant, employing trained algorithms and statistical techniques for accurate predictions and classifications.

Different techniques in the broad field of machine learning propel automatic learning in different directions (Jo, 2021). In 'Supervised Learning', the model learns to generate predictions or classifications by assimilating patterns from labelled data. On the other hand, in 'Unsupervised learning', the model looks for structures in unlabelled data without prior knowledge. Combining aspects of both, 'Semi-Supervised Learning' uses both labelled and unlabelled data for training. 'Reinforcement Learning' involves an algorithm that learns from its interactions with the environment and adjusts its behaviour in response to positive or negative results. Using deep neural networks that can handle complicated data representations makes 'Deep Learning' unique. Multiple model instances are combined in ensemble learning to increase overall performance.

Some example of the most popular unsupervised ML techniques use algorithms like 'K-means Clustering' (KMC), and 'Hierarchical Clustering' (HC), while 'Random Forest' (RF) is a predominat supervised algorithm combining numerous classifiers to enhance a model's performance.

KMC minimises the sum of squared distances between each point and the cluster centre, effectively dividing a set of *n* objects (points) into *k* groups (clusters). Research has focused on developing the technology since MacQueen first developed it in 1967 (MacQueen, 1967), expanding its use to point clouds (Lavoué, Dupont and Baskurt, 2005; Yamauchi *et al.*, 2005; Chen *et al.*, 2014).

HC generates nested sets of clusters by analysing similarities between pairs of points and grouping objects into a hierarchical tree (Ng and Han, 1994). In the last decade, a new HC algorithm has been introduced, capable of grouping data of any dimensionality. It finds application in mobile mapping in the geo-spatial domain and processing point clouds derived from aerial or terrestrial data (Xiao *et al.*, 2013).

RF is an ensemble learning method that creates several *decision trees* during training and combines them to produce predictions that are more reliable and accurate (Fig. 10). Random subsets of the *training data* and *features* are used to build each tree

(Breiman, 2001). The data's randomness and the feature selection process work together to reduce overfitting and improve the model's capacity for generalisation. Random forests can be used for pattern recognition and image segmentation, among other tasks. It is renowned for its robustness and versatiility and excels at managing complicated relationships within the data.

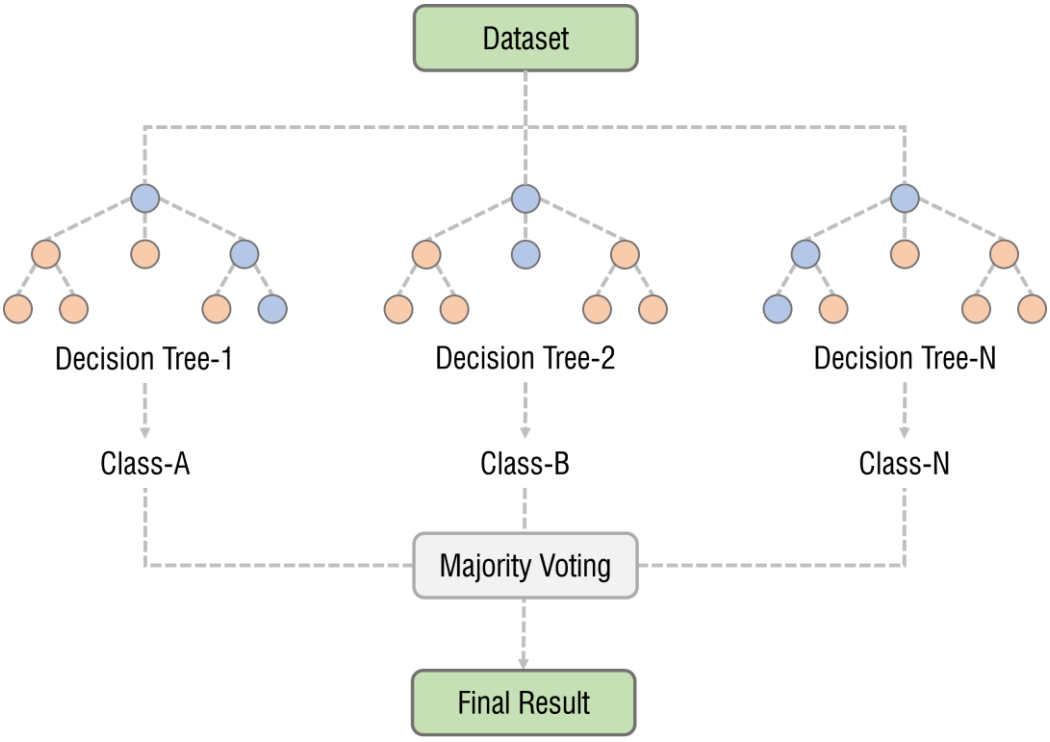

Fig. 10 Random Forest simplified explanation.

Because most work relied on statistical toolboxes applied to tiny datasets that are typically not publicly available, the application of Machine Learning (ML) in the context of Cultural Heritage was limited until a few years ago (Fiorucci *et al.*, 2020). A few classification techniques for 3D models in this field have only recently been defined (Pellis *et al.*, 2022; Kutlu *et al.*, 2023; Yang, Hou and Li, 2023; Zhao *et al.*, 2023):

texture classification from 2D images processed through UV mapping and reprojected onto 3D models, segmentation of ortho-rectified image (Malinverni *et al.*, 2017; Luo, Wang and Tan, 2019; Abgaz *et al.*, 2021; Croce, Caroti and Piemonte, 2021; Vorobel *et al.*, 2021), segmentation of point clouds based on colorimetric and geometric feature extraction (Grilli *et al.*, 2018; Fatiguso and Buldo, 2020; Musicco *et al.*, 2021) (Matrone, Lingua, *et al.*, 2020) (Matrone, Grilli, *et al.*, 2020) and multi-level and multi-resolution classification (Teruggi *et al.*, 2020).

Semantic annotation in HBIM processes has witnessed significant advancements, with dynamic changes driven by the incorporation of Deep Learning techniques (Croce, Caroti, De Luca, *et al.*, 2021; Croce, Caroti, Piemonte, *et al.*, 2021) Notably, methodologies like PointNet, Pointnet++, KNN, and Dynamic Graph Convolutional Neural Network (DGCNN) have been pivotal in segmenting architectural elements like arcs, columns, walls, windows, and more (Malinverni *et al.*, 2019; Pierdicca *et al.*, 2020; Croce, Manuel, *et al.*, 2023; Matrone *et al.*, 2023; Pellis *et al.*, 2023; Battini *et al.*, 2024). These approaches, underscore the dynamic nature of the field, showcasing the continuous evolution in HBIM processes within historic structures.

2. A NOVEL UNIFIED PROTOCOL FOR DIGITISING THE ARCHITECTURAL HERITAGE

In this dissertation, a harmonised methodology was systematically employed across all the case studies, carefully adapted to suit the unique objectives of each investigation. This strategic approach facilitated a seamless and uniform application of the *modus operandi*, ensuring consistency while affording the requisite flexibility to cater to the various contexts and purposes, meeting the specific needs and challenges inherent in each individual research endeavor.

Particularly, incorporating the principle of drawing and descriptive geometry into the architectural survey of the Cultural Heritage proves highly beneficial for computerising building heritage. This is especially crucial for knowledge and preservation, as it leverages modern technologies to investigate morphological and material characteristics in both two-dimensional and three-dimensional environments.
This integration improves the effectiveness of the survey process by providing a comprehensive understanding of architectural elements and facilitating their digital documentation. The use of contemporary technologies further underscores the importance of this approach in capturing intricate details crucial to the preservation and informed management of Cultural Heritage.
Moreover, the implementation of the Scan to BIM methodology amplifies the accuracy and depth of the 3D model, contributing to a more robust and accurate representation of the Cultural Heritage site.

In this context, the adopted approach entails a process of 3D acquisition and elaboration, aiming to deliver digital documentation and reconstruct 3D models of Cultural Heritage through the development of an innovative Scan to BIM methodology. This methodology comprises distinct operational phases:

- Integrated Architectural Survey with Point Cloud Acquisition: Utilising range-based and image-based scanning techniques, along with GNSS for precise

georeferencing, detailed point clouds are captured as foundational data for subsequent stages.

- Point Cloud Analysis and Segmentation: Applying advanced segmentation techniques, acquired point clouds are splitted into meaningful components, enhancing the interpretability of the data.

- Modelling in BIM Environment: Leveraging the segmented point clouds, a meticulous construction of a detailed 3D model within the Building Information Modelling (BIM) environment ensures a comprehensive representation of architectural elements.

- Testing of the Model: Rigorous testing validates the accuracy and reliability of the generated 3D model, aligning with established international standards for the digital documentation of the Architectural Heritage.

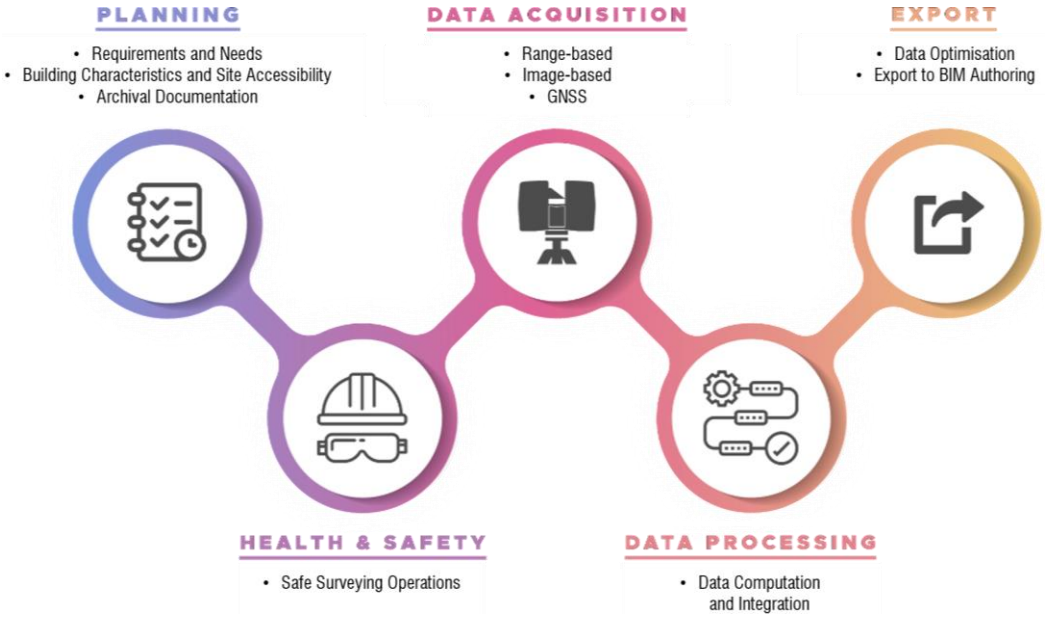

Fig. 11 Scan to BIM Methodology workflow.

According to the procedures for digitisation of Cultural Heritage adopted by international research groups (Bryan *et al.*, 2009; Di Giulio *et al.*, 2017; Stylianidis, 2019; Verdoscia, Buldo, Musicco, *et al.*, 2022b), an operational Workflow of this unified protocol was defined for the integrated three-dimensional architectural survey, briefly summed up as follows (Fig. 11):

i. **Planning**: The initial phase involves identifying project requirements and specific needs to establish an efficient work schedule. Following this, one or more on-site inspections, which may include architectural survey sketches, are organised to examine the building and determine the level of information depth and accuracy of morphometric data in relation to quality indicators.

   These indicators include the LOC (Level of Completeness), representing the minimum surface quantity to be detected (Biswas, Bosché and Sun, 2015). The LOA (Level of Accuracy) indicates the measurement tolerance (expressed in millimeter) applicable to the position of each point in the cloud, and the LOD (Level of Density or Detail), defined as the minimum dimension, denoted in points per unit of surface (specifically points per square millimeter) of the object extractable from the point clouds, essentially denoting the density of the point clouds (Aryan, Bosché and Tang, 2021).

   This planning phase also entails evaluating the architectural characteristics of the building, the site's morphology, weather forecasts, and any restrictions on airspace accessibility. Identification of potential issues such as occlusions, physical obstacles (e.g., electrical cables, pylons), and areas with reduced visibility and accessibility is critical. Additionally, thorough research involves acquiring bibliographic and archival documents detailing the building's history over time. Lastly, the selection of the digital format for accessing and sharing surveys and models aligns with representational needs and is considered an essential aspect of this planning stage.

ii. **Health and Safety**: The acquired information enables the meticulous planning of the survey campaign in adherence to security measures outlined by national technical regulations (Legislative Decree 81/2008, commonly referred to as the 'Testo Unico sulla Salute e Sicurezza sul Lavoro' (Italian Ministry of Labour and Social Policies (MLPS), 2008) and 'Presidential Decree 380/2001' (Italian President of the Republic, 2001)). During this stage, a comprehensive review of certificates of occupancy is imperative, assessing the need for specific security measures on the construction site. Additionally, thorough attention is given to the training and preparation of the professionals involved in the survey to ensure a safe and secure working environment.

iii. **Data Acquisition**: The third phase involves the execution of the survey campaign, utilising a combination of range-based and image-based scan techniques. Additionally, actions to support technological equipment are undertaken, such as conducting photographic surveys, maintaining detailed field notes, strategically placing georeferenced targets and light sources, and employing other complementary methods. This comprehensive approach ensures a rich dataset capturing various aspects of the architectural environment.

iv. **Data Processing**: During this critical phase, diverse datasets, including instrumental data, bibliographical and archival documentation, and photographic surveys, undergo meticulous processing. The objective is to elaborate and integrate all collected data, resulting in a multi-faceted dataset comprising point clouds, meshes, textures, orthophotos, 360° photos, DEM, and more. This integrated database serves as a foundation for subsequent analyses and reconstructions.

The data collected is processed using sophisticated software that harnesses the capabilities of advanced algorithms for image and point cloud processing. This enables the generation of three-dimensional reconstructions from point clouds, showcasing the full potential of these cutting-edge processing techniques.

The processed data undergoes thorough quality checks to ensure accuracy and completeness, establishing a reliable foundation for subsequent stages in the survey and documentation process.

v. **Export**: The final phase involves the optimisation of the processed data, incorporating essential operations such as filtering, decimation, and segmentation. These actions refine the dataset, ensuring it aligns with the desired precision and quality standards. Simultaneously, meticulous graphic configuration of the content takes place, involving choices related to colours, graphic settings, and other visual attributes. This step aims to enhance the overall visual appeal and interpretability of the generated models.

   Furthermore, this phase also includes the conversion of files to the appropriate formats for seamless integration into various applications. This may encompass file formats such as .RCP, .RVT, .FBX, JPEG, and more, catering to specific needs and compatibility requirements. The export stage is crucial for delivering the finalised, optimised, and visually refined outputs, ready for dissemination, analysis, or integration into broader Architectural and Cultural Heritage contexts.

The outlined procedure has been further validated through practical application in the field, with experimentation conducted by the 'Architectural and Urban Modelling Laboratory' (MAULab) of the Politecnico di Bari, with the collaboration of the 'Grupo de Representación Arquitectónica del Patrimonio Histórico y Contemporáneo' (GRAPHyC) of the Universidad de Zaragoza and the 'Graphical Methods, Optimization and Learning Research Group' (GOAL) of the Universidad de Cádiz.
This experimentation involved the examination of several monumental buildings situated in central-southern Italy and abroad, particularly in Spain. Subsequent paragraphs will offer a thorough overview of the procedures employed in these notable case studies, emphasising the key methodologies selected.

3. EXPLORING METHODOLOGIES: BRIDGING 3D SURVEY TO BIM MANAGEMENT

This chapter aims to explore the complex path from three-dimensional surveying, conducted through technologies such as laser scanning and photogrammetry, to the construction of a Building Information Modelling (BIM) model, followed by its management and the critical phase of geometric accuracy validation. This process represents a fundamental step in integrating advanced methodologies for the preservation and management of Architectural Heritage and, in this case, the previously described unified protocol applies.

Throughout this exploration, data acquired through 3D surveying undergoes an integration process, where the combination of information from different sources generates a unified and detailed representation of the architectural object under examination. The subsequent step involves translating this three-dimensional representation into a BIM model using specialised software, enriching elements with essential attributive data. The management of the BIM model then becomes crucial, involving specific methodologies and platforms to ensure its efficiency and continuous updating. The culmination of this journey is represented by the validation of geometric accuracy, wherein the BIM model is compared to the reference data from 3D surveying, utilising advanced techniques such as clash detection and deviation analysis.

Through the analysis of specific case studies, this chapter aims to provide an in-depth perspective on the challenges and solutions in implementing these integrated methodologies. The ultimate goal is to offer a comprehensive knowledge base for those involved in the conservation and management of Architectural Heritage through the practical application of cutting-edge technologies. Namely, in this section various methodologies are introduced, each unique in its approach but united by a common thread. These methodologies are applied across three distinct cases, providing a comprehensive overview of the solutions employed in specific contexts.

Hereafter, brief summaries of the case studies are presented.

- **Church of Saint Mary Veteran in Triggiano (Apulia, Italy):**
  In this project, the primary objective is to validate an integrated survey workflow utilising laser scanning (TLS) and aerial photogrammetry (UAV) data through Iterative Closest Point (ICP) algorithms. The aim is to generate a hybrid point cloud capable of robustly supporting subsequent parametric modelling processes within the Heritage Building Information Modelling (HBIM) environment. The case study revolves around the Church of Saint Mary Veteran, constructed in 1580, exploiting multi-sensor registration for both interior and exterior areas within the point cloud.

- **Baths of Diocletian in Rome (Latium, Italy):**
  This study explores the intricate link between entered data and represented objects, showcasing various methods of managing and computing data within the three-dimensional modelling environment. Techniques include relational databases, open-source middleware, proprietary software, and customisable applications developed through scripts or visual programming languages. Focused on the Baths of Diocletian in Rome, the study illustrates the utility of the A-BIM approach throughout the preservation process, aiding in site survey, archaeological archive compilation, and the development of a detailed three-dimensional model.

- **Former Monastery of the Saint Mary of the Cross in Modugno (Apulia, Italy)**:
  The proposed Scan to BIM approach seamlessly integrates laser scanning, photogrammetry, and parametric modelling for the former Monastery of the Saint Mary of the Cross in Modugno. Geometric accuracy is assessed through Clash Detection and Surface Deviation Analysis, ensuring that the BIM and reference point cloud align within specified tolerances. Clash detection evaluates component positions, identifying clashes, while Surface Devia-

tion Analysis evaluates geometric accuracy and pinpoints modelling errors concerning a model adopted as a ground truth.

The exploration of these methodologies and the analysis of these case studies contribute valuable insights into the holistic process of integrating 3D survey techniques with BIM management for Architectural Heritage. The subsequent sections will delve deeper into each case study, unraveling the nuances and lessons learned in the pursuit of accurate and effective heritage preservation.

3.1 Integrated 3D Survey Techniques

In the realm of Cultural Heritage, achieving precise surveys through 3D acquisition tools has become indispensable to create a digital replica of structures with high metric accuracy. Despite the high costs and limited portability associated with LiDAR technology in certain situations, the photogrammetric technique has gained traction. Each method has its merits and drawbacks, necessitating a careful consideration based on initial documentation needs and specific contextual requirements.

There are three key distinctions between these approaches: i) active systems produce a point cloud directly from the acquisition process, while passive techniques rely on two-dimensional images adhering to photogrammetric principles; ii) the point cloud generated by Terrestrial Laser Scanning (TLS) is considered a metrically accurate reconstruction, in contrast to photogrammetry, which relies on onsite metric references, potentially introducing errors in model capturing and scaling; iii) TLS may encounter challenges in capturing certain parts of a structure, such as rooftops, and may face texture quality issues. To address the limitations inherent in each digital survey technique, the combination of LiDAR and Photogrammetry has become a common practice (Battini and Sorge, 2016; Liang *et al.*, 2018).

The focus of this project is to validate an integrated survey workflow employing laser scanning (TLS) and aerial photogrammetry (UAV) data through Iterative Closest Point (ICP) algorithms. The objective is to generate a hybrid and comprehensive point cloud (Verdoscia, Buldo, Tavolare, *et al.*, 2022) capable of robustly supporting subsequent parametric modelling processes within the Heritage Building Information Modelling (HBIM) environment.
The case study involves the survey of the Church of Saint Mary Veteran, constructed in 1580 atop the ruins of a pre-existing medieval church in Triggiano, Italy.
The survey employed a multi-sensor registration, leveraging range-based data for reconstructing interior and exterior areas within the point cloud.

Simultaneously, image-based data played a crucial role in detecting roofs and filling gaps, particularly where laser scanning from ground stations encountered limitations in capturing the exterior walls.

3.1.1 The Church of Saint Mary Veteran in Triggiano (Italy)

The Church of Saint Mary Veteran (Fig. 12), located a few kilometers from Bari (Apulia), boasts an artistic history spanning from the 1600s to the 1700s, significantly contributing to the artistic life of the region. Built in 1580 on a pre-existing medieval church dedicated to Madonna della Grazia and founded around 1080, the church has undergone various transformations over the centuries to adapt to the demographic and urban growth.

The architectural aspect of the church is remarkable, featuring a tripartite façade in white stone with Ionic pilasters and artistic decorations. Originally facing west, the façade was relocated to the east in 1908-1913, adding a distinctive artistic embellishment. The façade is divided into two levels: a lower one with elements such as Corinthian columns and portals, and an upper pointed one with a precious decorated rose window dating back to 1500. This upper level is surmounted by a sloping tympanum richly adorned. The bell tower from 1580, damaged in 1681, lacks its original pyramidal spire.

Inside, the church follows a basilical layout with three naves and an apse, adorned with decorated pillars and 16th-century round arches. The monumental altar, from the 20th century, is in Byzantine Pugliese style, dedicated to the Virgin and dominated by a painting depicting the Exaltation of the Virgin by Vitantonio De Filippis.

The church houses several side chapels, including the notable ‘Cappellone’ dedicated to Most Holy Mary of Costantinopoli. Artworks inside comprise frescoes, bronze reliefs, and paintings dating from the 16th to the 19th century. The coffered ceiling displays mixed-line paintings portraying the pictorial cycle of the life of the Virgin Mary, though it lost some of its Renaissance character due to the Liberty-style decorations added during the restoration of 1908-1913.

Fig. 12 Exterior and interior view of the Church of Saint Mary Veteran in Triggiano (Italy).

3.1.2 Methodology

The project embraced a data acquisition-and-processing procedure-based approach that combined range-based (terrestrial laser scanner) and image-based (aerial photogrammetry) scanning techniques, in ensuring an integrated and complete survey of the building, to be displayed as a point cloud, thus being useful for subsequent reconstruction in BIM environment.

The segment dedicated to instrumental surveying is integral to a methodological framework aligned with international standards for the digital documentation of Cultural Heritage Culturali (Bryan *et al.*, 2009; Di Giulio *et al.*, 2017; Stylianidis, 2019).

This framework is elucidated through an operational workflow (Fig. 13) delineating the sequential progression across distinct application levels. These encompass the planning phases for the two different techniques, incorporating health and safety operations, data acquisition, and data processing. The latter involves integration with the ICP algorithm and culminates in final decimation and filtering, as detailed below.

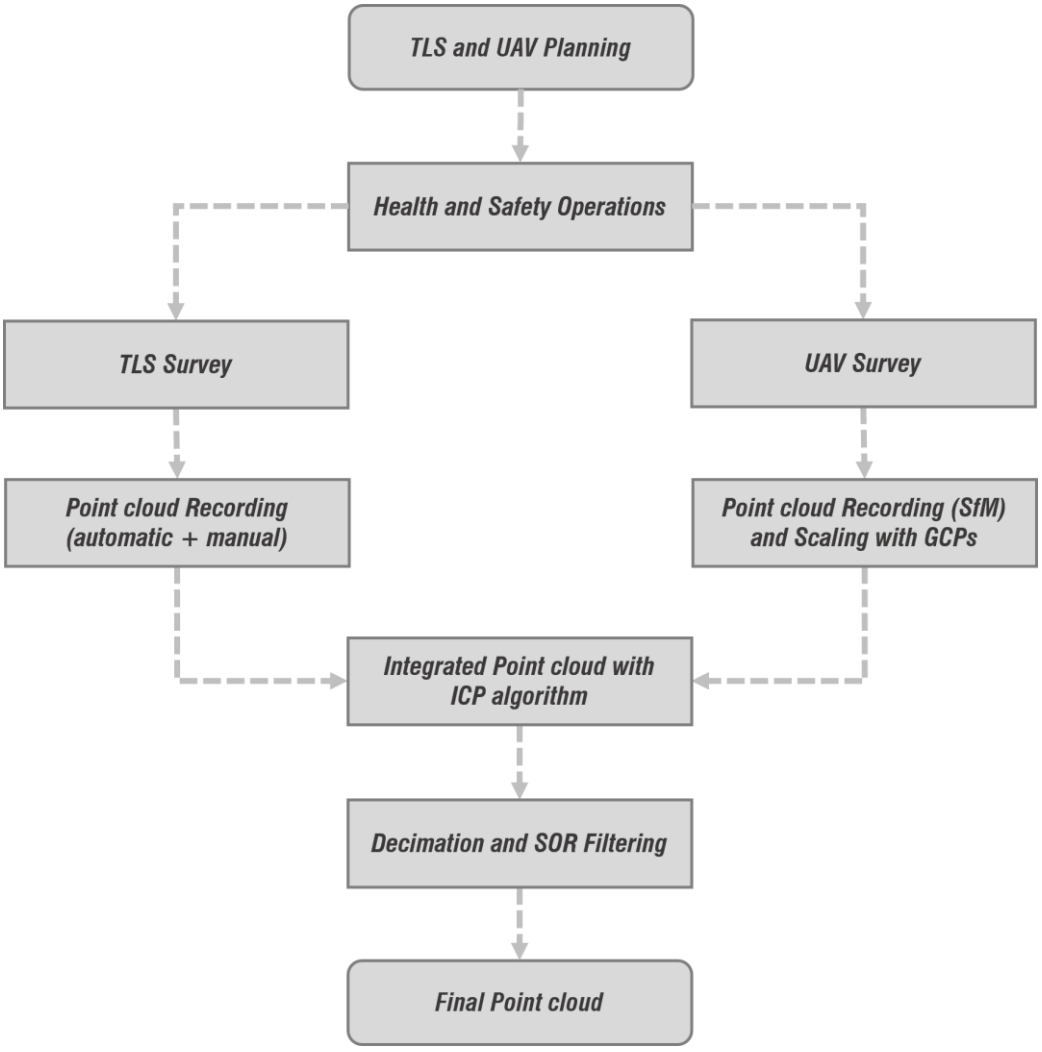

Fig. 13 Operational workflow for the integrated survey of the church.

i. **Planning**

The initial step involvesthe requirements and criteria of the project to ensure an effective activity planning. This includes on-site inspections and the concurrent determination of the depth of information and morphometric accuracy, guided by quality indicators such as the LOC (Level of Completeness), i.e. the minimum quantity of surface detected (Biswas, Bosché and Sun, 2015).

Additionally, the LOA (Level of Accuracy), i.e. the position measurement tolerance (given in mm) of each individual point of the cloud; the LOD (Level of Detail or Density), i.e. the minimum size (given in points per mm^2) of the object that can be extracted from the point clouds, that is the point cloud density (Aryan, Bosché and Tang, 2021).
Furthermore, the assessment encompasses architectural and constructive features of the building, site morphology, anticipated weather conditions, airspace restrictions, potential occlusions, physical obstacles such as power line cables and pylons, and areas with reduced visibility and accessibility.
Selection of the digital format for survey use and sharing, based on graphic requirements, is complemented by the acquisition of archival and bibliographic documentation detailing the building and its time-evolution.

In the case study, covering an area of approximately 34x36 m^2, meticulous planning is undertaken for the range-based survey executed with the CAM2® FARO Focus 3D 120 laser scanner. This involves determining the minimum number and position of shooting points relative to object geometry (concave/convex, closed/open), considering the vertical and horizontal angles (305°/360°) of the instrument's operational coverage. Core criteria include reducing shaded areas and optimising acquisition angles. The objective is to achieve completeness and uniform resolution of the scanned surface in alignment with expected LOC and LOA values (Fig. 14).

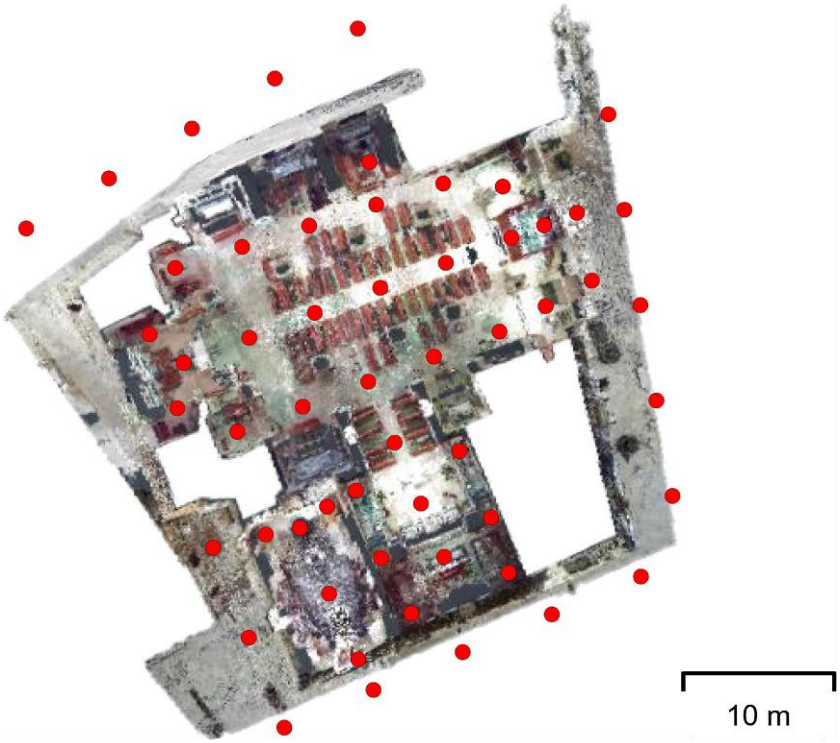

Fig. 14 Laser-scanning survey planning.

In the data acquisition operational phases, the planning of the aerial photogrammetric survey campaign strategically chose the central hours of cloudy days. This decision aimed to mitigate the contrast between light and shadows, ensuring an even illumination of the surfaces.

To achieve the most accurate three-dimensional reconstruction during data processing, a series of manual flight missions (Fig. 15) were executed. These missions employed a double grid and circular type at varying heights, incorporating frontal (0°), oblique (45°), and nadiral (90°) shots.

With respect to LOC, a front and side overlap of 60/80% between contiguous frames was meticulously maintained, along with a Ground Sample Distance (GSD) value of approximately 6 mm/pixel. The dataset comprised a total of 197 shots in JPEG format.

To facilitate alignment and ensure accurate scaling of the survey, Ground Control Points (GCPs)[2] targets were employed. These targets, printed on solid panels sised 80x80 cm, provided essential reference points for the survey.

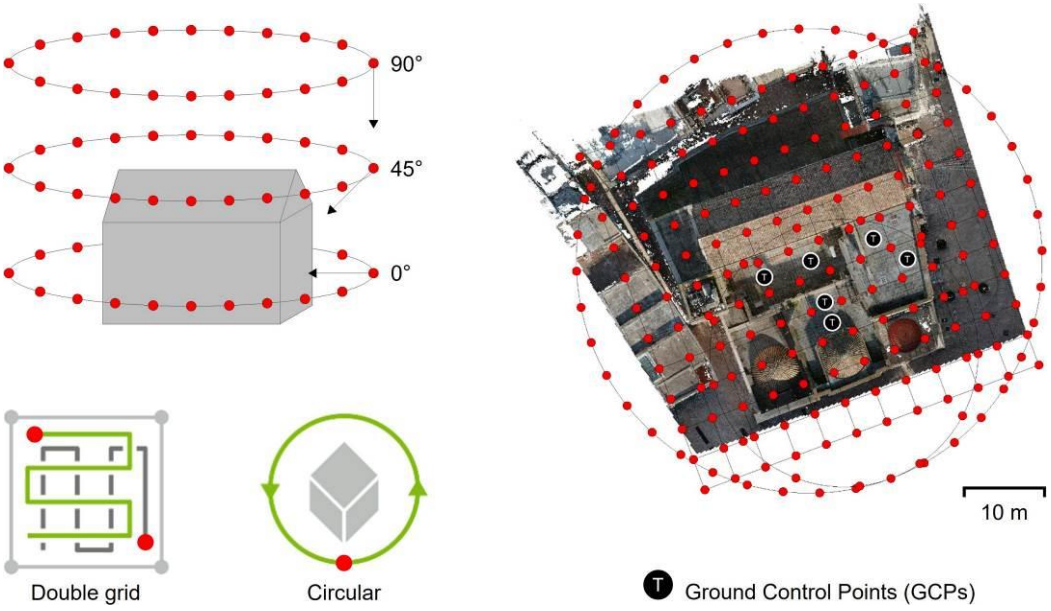

Fig. 15 Aero-photogrammetric survey planning.

ii. **Health and Safety**

National safety regulations (D.Lgs. 81/2008, 'Testo Unico sulla Salute e Sicurezza sul Lavoro', DPR 380/2001) were meticulously considered during the planning phase. This involved educating and briefing all personnel involved in the survey, delineating procedures for the adoption of specific safety measures at the site. This process included a thorough examination of viability and safety certificates necessary for accessing the survey area.

[2] 'Ground Control Points' (GCP) enhance 3D reconstruction accuracy in photogrammetry by providing known reference points for georeferencing. Crucial for applications like cartography and environmental monitoring, GCP strategically correct errors during image processing, ensuring precise alignment with the real-world context.

Furthermore, a preliminary inspection was conducted to assess environmental conditions, identify potential critical issues, and evaluate interferences with urban mobility for both pedestrians and vehicles. Additionally, the survey team scrutinised the presence of construction sites or other activities within the workplace.
In preparation for UAV usage, comprehensive Risk Analysis and Assessment Procedures were adhered to in the days leading up to deployment. This included consulting thematic maps (Fig. 16) and checking for any *Notice To AirMen (NOTAM)* communications.

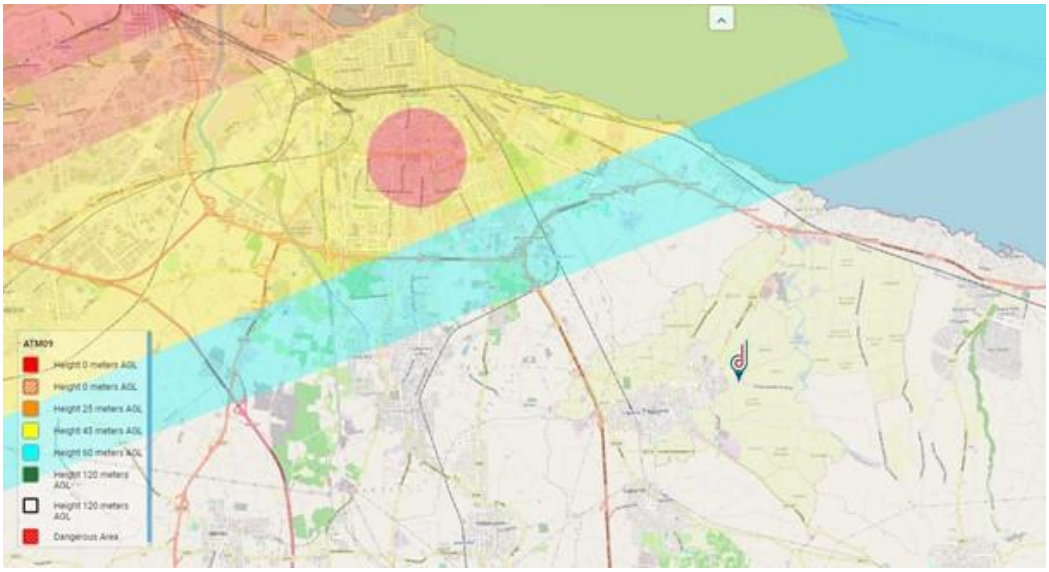

Fig. 16 Thematic map on airspace limitation.

iii. **Data Acquisition**

At this stage, a combination of active and passive scanning methods, along with supporting actions for technological equipment (e.g., photographic survey, in-situ annotations, arrangement of targets, and light sources), is employed.
The outcome includes 19 outdoor scans with a dimensional resolution of 28.2 Megapoints per scan (Mpts) and an acquisition resolution of 7.670 mm/10 m (i.e., the distance between points in a 10 m range). Additionally, 36 indoor scans were conducted

with a dimensional resolution of 11 Mpts and an acquisition resolution of 12.272 mm/10 m.

The initial scan positions, as determined in the planning phase, were adjusted or extended as needed. Notably, unforeseen elements such as chairs, benches, curtains, panels, and chandeliers were minimised to enhance coverage of the main architectural elements. The exposure metering mode was meticulously configured to match the ambient light pattern, using *Horizon Weighted Metering* for indoor areas and *Even Weighted Metering* for outdoor locations.

Throughout the survey operations, any changes in configuration (e.g., brightness variations, opening or closing of doors and windows, transit of persons) were diligently recorded. This documentation facilitated the easy identification and correction of discrepancies during the subsequent data processing phase. To address a specific challenge encountered when merging scans of the nave and those of the wooden choir, connected by a double-winder U-shaped staircase, scans were strategically arranged at varying heights (Fig. 17).

Fig. 17 Laser scanner stationing at different instrumental heights.

iii. **Data Processing**

The alignment of LiDAR and photogrammetric data was performed using specific software tools: Autodesk Recap and CloudCompare for laser scanning (Fig. 18), and Agisoft Metashape Pro® for the outdoor photogrammetric survey.

Fig. 18 Range-based point cloud: internal view.

The registration of the point cloud acquired from the laser scanner was initially carried out through automated procedures within the software. In instances where the software failed to overlay specific pairs of scans, a manual union was performed, involving the identification and connection of three homologous points to maintain model consistency.

Conversely, in generating the aerophotogrammetric 3D model, initially presented as a sparse and subsequently densified point cloud, the Structure from Motion (SfM) software was employed. Following the identification of correspondences among visual

features in overlapping images, the crucial *Bundle Adjustment* process was executed. This step optimised the position and orientation of the cameras used for image acquisition, refining the 3D coordinates of points within the model. It significantly contributed to ensuring a more precise and coherent three-dimensional reconstruction of the scene, mitigating systematic errors, and elevating the overall accuracy of the final model.

This point cloud was subsequently scaled using roof targets as a reference, with distances measured using a tape measure (Fig. 19). The decision was made to dispense with GNSS technology, opting instead for a local reference system with the origin positioned at the entry threshold of the church.

The integration of the obtained point clouds was achieved by selecting homologous points on the main façade of the church – points visible in both point clouds. This process involved fine registration through the *Iterative Closest Point (ICP)* algorithm, minimising distances between clouds of different reference origins.

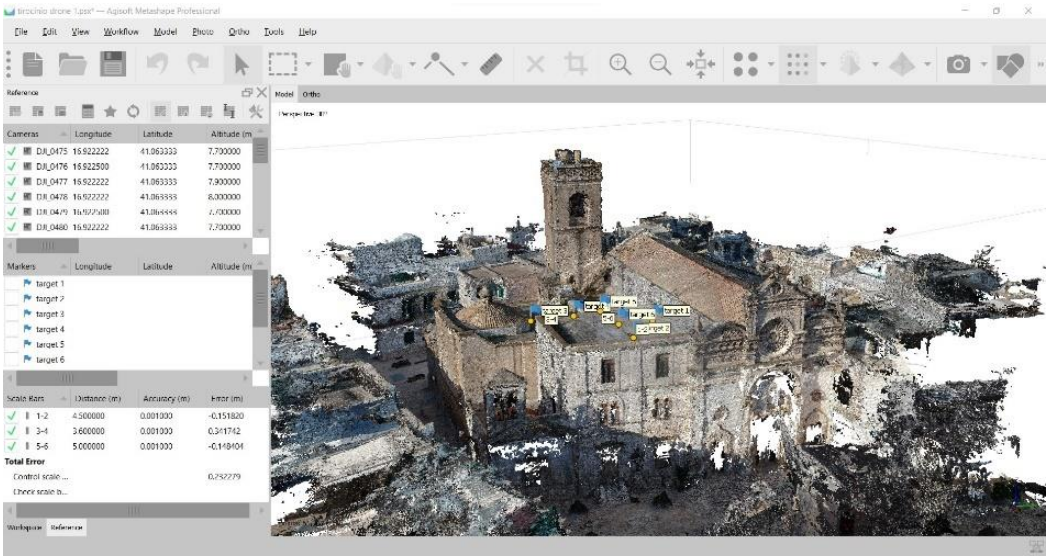

Fig. 19 Image-based point cloud reconstruction and target scaling.

The ICP algorithm introduced by Besl and McKay in 1992 (Besl and McKay, 1992), has been enhanced by various authors, including improvements by Eggert et al. (1998) and Zhang (1994) (Zhang, 1994; Eggert, Fitzgibbon and Fisher, 1998). Another approach involves the method of Least Squares 3D Surface Matching, as demonstrated by Akca in 2010 (Akca, 2010).
ICP involves initialising a transformation, finding the corresponding points, estimating the optimal transformation, applying it to one of the point clouds and verifying convergence. The process is repeated until a satisfactory alignment is achieved. ICP is widely used in applications such as 3D reconstruction and laser scanning registration, but its performance can be sensitive to initial conditions and outliers.

The ICP point-to-point algorithm, as originally described in (Bellekens, Spruyt and Weyn, 2014) establishes point correspondences by finding the nearest neighbour target point *qi* for each source point *pj* in the source point cloud.

The nearest neighbour matching is determined based on the *Euclidean distance metric* [3]:

$$\hat{i} = \arg\min_{i} \|\mathbf{p}_i - \mathbf{q}_j\|^2$$

[3]

Here, $i \in [0, 1, \ldots, N]$, and N denotes the number of points in the targe point cloud. The rotation matrix R and translation vector t parameters are estimated by minimising the squared distance between these corresponding pairs:

$$\hat{R}, \hat{\mathbf{t}} = \arg\min_{R,\mathbf{t}} \sum_{i=1}^{N} \|(R\mathbf{p}_i + \mathbf{t}) - \mathbf{q}_i\|^2$$

[4]

The ICP algorithm iteratively solves equations [3] and [4] to refine the estimates obtained from previous iterations. This iterative refinement process is depicted in Fig. 20, where surface *s* is aligned to surface *t* through multiple *n* ICP iterations.

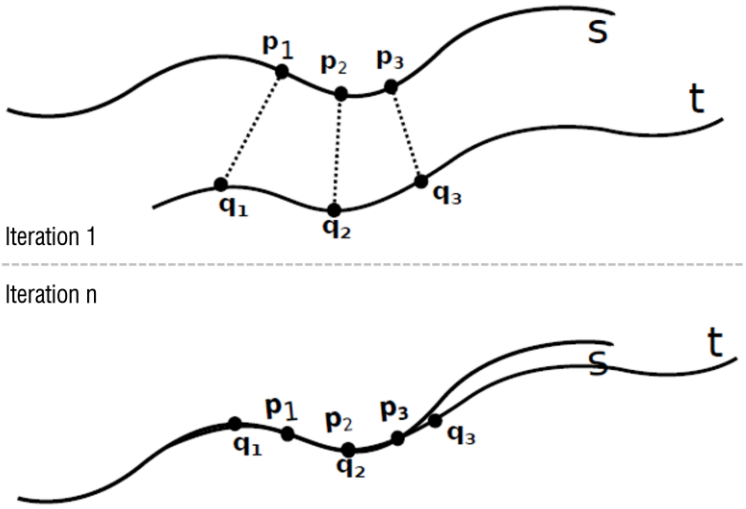

Fig. 20 ICP alignment based on point to point approach (©adapted from (Bellekens, Spruyt and Weyn, 2014)).

Considering the anticipated geometric requirements, and after completing the processing phase, the work underwent additional post-processing, involving the application of 5 mm and subsequently 2 cm decimation algorithms to enhance manageability. To enhance the optimisation of the point cloud, overlaps and interferences were subsequently removed.

An additional decimation, based on statistical criteria, was performed using the *Statistical Outlier Removal (SOR)* algorithm (Fig. 21).
The SOR algorithm has been proposed in different ways in recent, such as work based (Rusu *et al.*, 2008) on calculating the distribution of distances between points

and neighbours in the input data set or removing the radius outlier using the threshold of distance and number of neighbours years (Dung and Lee, 2015).

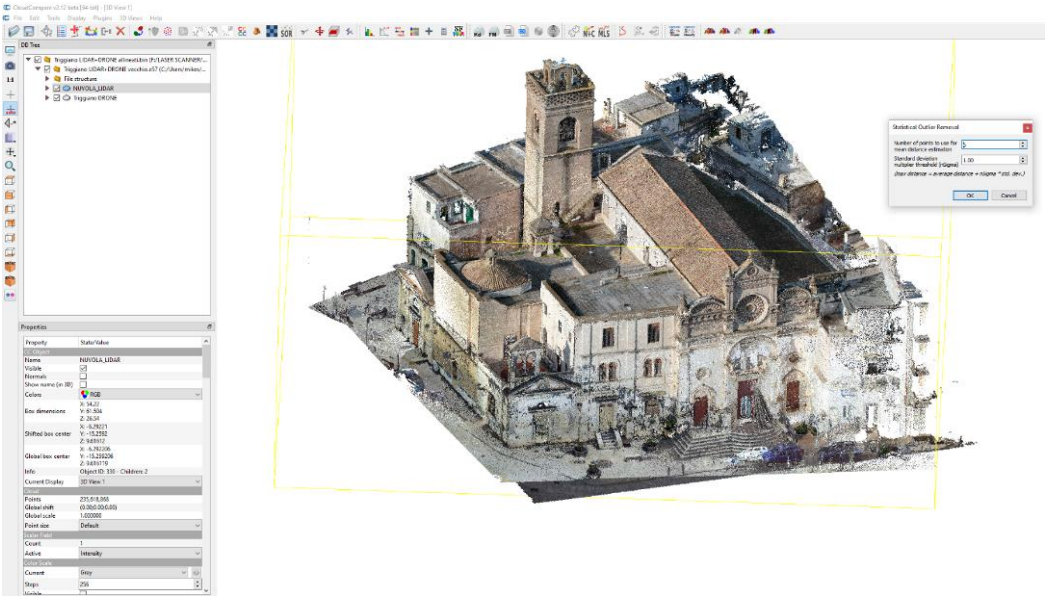

Fig. 21 Integrated point cloud decimation process with the SOR algorithm.

For this purpose, SOR algorithm involved setting the number of points used for *mean distance* estimation to 5 and establishing a *standard deviation multiplier threshold (n_sigma)*, taking into account that the *maximum distance* would be calculated as follows [5].

$$\text{maximum distance} = \text{average distance} + (\text{nsigma} * \text{standard deviation}) \quad \textbf{[5]}$$

3.1.3 Results

The optimisation of the processed data, involving tasks such as decimation and filtering, is intricately connected to rendering settings, including graphic and colour configurations, as well as the choice of file format (.RCP, .RVT, .FBX, OBJ, JPEG).

Fig. 22 Integrated point cloud: internal view (on the top) and external view (on the bottom).

To achieve this goal, the entire process effectively identified and removed isolated points, resulting in a decimated point cloud with 17,145,817 points instead of the initial 260,336,288 points (Fig. 22). This point cloud is not only more geometrically uniform but also spatially coherent.

The SOR filter improved the quality of the point cloud by calculating local statistics for each point, evaluating discrepancies within its neighbouring group, defining a threshold to identify significant deviations, and subsequently removing outliers. The process can be also iterated for further refinement, ensuring a cleaner and more accurate representation.

In the context of a Scan-to-BIM workflow, as three-dimensional models evolve, the extraction of geometric profiles becomes pivotal. These profiles identify generators and directions, crucial for subsequent authoring steps. It is imperative for these operations to align with graphic objectives (such as planimetric and three-dimensional requirements, and scale of representation) and be compatible with the software utilised in the process.

3.1.4 Closing Insights

Conducting an integrated digital survey presents unique challenges, criteria, and critical considerations that may vary based on metric and graphic requirements as well as environmental factors. The effort has resulted in the development of well-defined operational procedures, adhering to a standards-based approach.

This approach incorporates quality and safety parameters, aligning with survey metric and information needs. Consequently, the configuration statistics are harmonised to suit the project's specific use.

The coordinated strategy involves the integration of various technologies and expertise to optimise methods and streamline operational processes. This ensures efficien-

cy in both on-site execution and subsequent data processing by avoiding unnecessary information that could lead to delays. Recognising the significance of planning for information requirements is pivotal for a comprehensive definition of architectural surveys and their graphic representation, making informed methodological choices a key factor in the process.

3.2 Digital Documentation and Archaeological Building Information Modelling

In the archaeological field, the Archaeological Building Information Modelling (ABIM) approach within BIM redefines the semantic aspect of architectural assets. It extends beyond morphometric considerations, incorporating datasets acquired during surveys or archived information (Tomasello, Cascone and Russo, 2018; Bosco *et al.*, 2019).

The entered data are intricately linked to the represented objects and can be managed and computed in platforms integrated with the three-dimensional modelling environment in different ways: i) through relational databases exported/imported with open-source middleware, such as Open Database Connectivity (ODBC) drivers or proprietary software or a proprietary software, such as GDL in ArchiCAD® or MDL in Bentley® (Eastman *et al.*, 2011; Verdoscia *et al.*, 2020); ii) via customisable and flexible applications developed through scripts (add-ins), Application Programming Interface (API), or Visual Programming Language (VPL) (supported for instance by Dynamo Studio Autodesk® and Graphisoft Grasshopper®) (Negendahl, 2015; Alzara *et al.*, 2023); iii) using customisable cloud platforms capable of establishing connections between the three-dimensional model and relational databases for real-time monitoring (Chien *et al.*, 2017).

Focusing on the Baths of Diocletian in Rome, this work illustrates the utility of the A-BIM approach throughout the entire preservation process (Verdoscia, Musicco, Buldo, *et al.*, 2021).
From site survey and archaeological archive compilation to the development of a three-dimensional model with three levels of detail (low, medium, high), the integrated approach aids in both the management and conservation procedures associated with this historical site.

3.2.1 The Baths of Diocletian in Rome (Italy)

The Baths of Diocletian, a monumental complex dedicated to Emperor Diocletian, were constructed between 298 and 306 A.D. Spanning an expansive 13-hectare area between the Quirinal and the Viminal Hills, the design of the baths emulated the architectural patterns of the Trajan and Caracalla thermal complexes. With a capacity to accommodate up to 3000 individuals, the complex comprised three main elements: the Central Building, the quadrangular Outer Settlment, the Large Garden.

This longitudinal structure of the Central Building featured symmetrical rooms flanking the transversal median axis, where various thermal activities occurred. The building (Fig. 23) covered approximately 37,200 square meters and housed entrances, *vestibules*, changing rooms, gyms, heated rooms, such as *laconica* and *sudationes*, the *calidarium*, the *tepidarium*, and the *frigidarium* with a substantial swimming pool. Additionally, it included spaces for body care, massages, eateries (*thermopolia* and *popinae*), and areas for shows. Adjacent to the heated rooms, sizable areas were allocated for technical equipment.

Encompassing an area of about 388x328 meters, the quadrangular space of the Outer Settlment included an exedra with a 150-meter diameter on its south-western part. The exedra housed rooms designated for cultural and recreational activities.

Serving as a scenic buffer, the Large Garden separated the aforementioned spaces and featured green areas adorned with pools and fountains.

Over time, the Baths of Diocletian underwent significant transformations. Following the barbaric invasions in the 6th century, the complex experienced changes in both function and layout. These adaptations included the establishment of a church dedicated to Our Lady of the Angels and Christian martyrs, adorned by Michelangelo in 1562.

Subsequent additions comprised the construction of the annexed Charterhouse in 1754, Gregorio XIII's granaries, and the chapel honoring Saint Isidor, the protector of the harvests, also erected in 1754. In 1889, the thermal complex gained further significance with the establishment of the National Roman Museum (Sanchirico, 2016).

Fig. 23 Room XI of the Baths of Diocletian.

3.2.2 Methodology

This investigation was carried out using a methodology that involved multiple operational phases. First, a large LIDAR point cloud was obtained in the *National Roman Museum*'s rooms VIII, X, and XI using an ABIM (Archaeological Building Information Modelling) technique. The museum is located in the Baths of Diocletian in Rome. A relational data link was subsequently added to this acquisition.

Next, utilising parametric modelling to enable automatic mesh surface extraction from survey outputs, the creation of the three-dimensional geometric model took place. Microsoft Access was used to arrange and classify the data, administrative information, georeferencing, sources, and reference materials that were gathered.
In the end, these components were connected to the BIM model via the ODBC drivers to guarantee excellent connection, providing an efficient and cohesive integration of the whole information system.

i. **The Architectural Survey**

The survey of the building was conducted in conjunction with the exhibition *'Roads of Arabia: Treasures of Saudi Arabia'* jointly promoted by the Ministry of Culture of Saudi Arabia and the Ministry of Cultural Heritage and Activities and Tourism of Italy (MiBACT). The purpose of the work was to support the assessment of proposals presented by the Alda-Fendi-Esperimenti Artistic Direction in collaboration with Klinamen Cloud Srl.

Specifically, the survey focused on rooms X-XI and a portion of room VIII at the National Roman Museum. The initial operational phase involved devising an acquisition plan to optimise the balance between scan quantity, resolution, acquisition time, and appropriate overlap. The laser scanner utilised was the CAM2® FARO Focus 3D 120, known for its specifications providing an accuracy of ± 2 mm, a range from 0.6 m to 120 m, a measurement speed of 976,000 points per second, and a vertical and horizontal plain sight of 305° and 360°, respectively. The laser spot featured a circular pattern with a diameter of 3.00 mm.

Considering the extensive areas of interest, totaling approximately 300 square meters, a decision was made to conduct 45 acquisitions. The resolution varied between 6.0 and 7.5 mm at a distance of 10 m, resulting in approximately 30 million points per scan. This strategy ensured a minimum resolution of 8,248x3,414 pts and a maximum resolution of 10,310x4,268 pts.

ii. **Data Processing**

The data processing phase involved the utilisation of two software tools, Autodesk Recap Pro® and CloudCompare. Each scan's point clouds underwent meticulous scrutiny, and redundant data was eliminated. Subsequently, the scans were aligned and merged to create a unified three-dimensional reconstruction comprising approximately 950 million points. Subsequent to this, the resulting point cloud underwent resampling and decimation, resulting in a reduction to around 550 million points (Fig. 24).

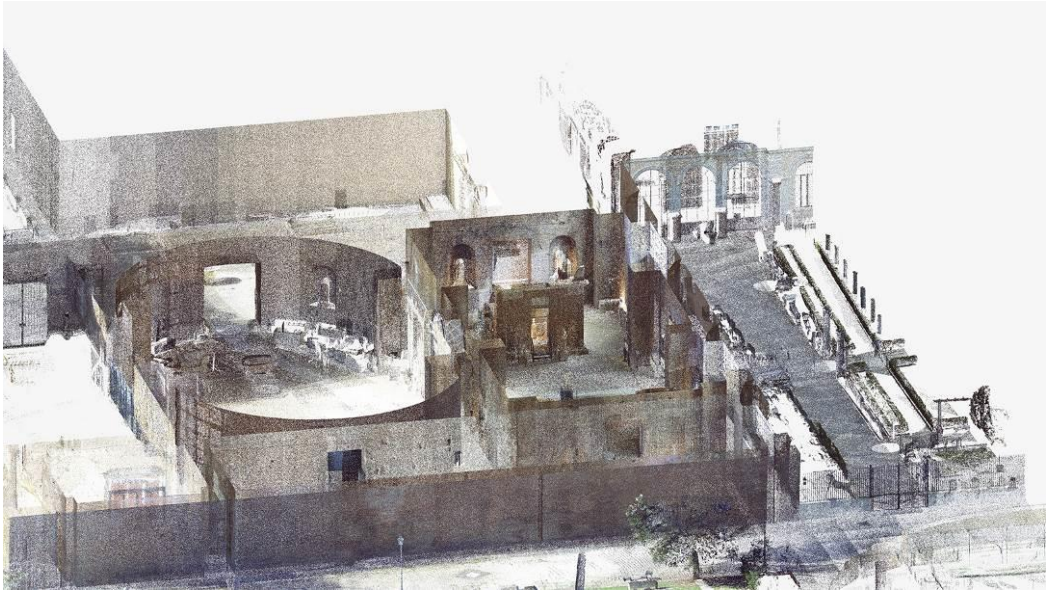

Fig. 24 Point cloud of the entire complex.

Architectural elements, including walls, vaults, columns, and decorations, were extracted with a 10 cm offset, employing a parametric segmentation process that identified 8 coplanar points. This step allowed for the initial identification of elements that would serve as references for modelling parametric families in Autodesk Revit®, ultimately leading to the generation of a three-dimensional mesh (Fig. 25).

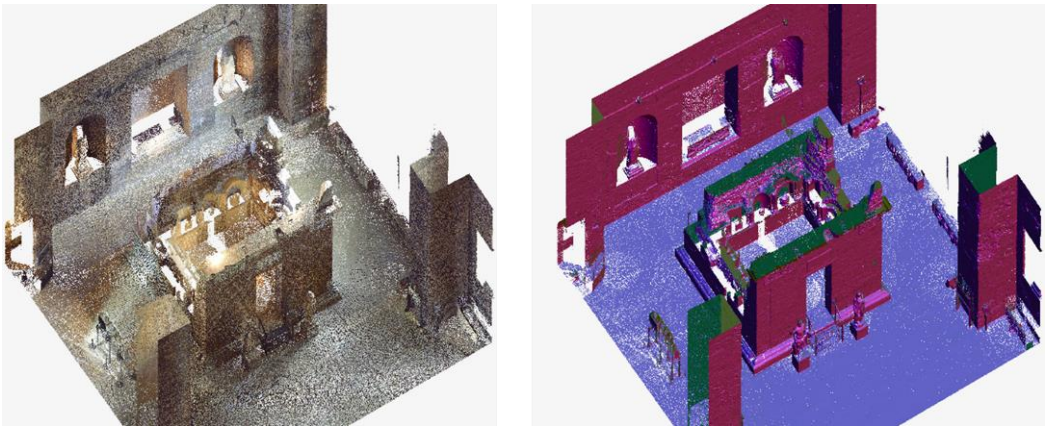

Fig. 25 Tomb of the Platorini decimated point cloud (visualisation in RGB colour scale and normals).

The complex geometric parametrisation of architectural elements presents inherent obstacles when modelling them in BIM. There are no automated tools or programmes that can instantly convert a point cloud into an extensive BIM model, making this procedure exceptionally complicated. To create a BIM model that accurately replicates the actual structure, a suitable Level of Detail (LOD) must be determined using gathered information and operational goals.

In this study, the method was streamlined to reduce errors, guarantee data quality, and maintain important details by building the three-dimensional model from a resampled point cloud. The method preserved the proportional relationships between shapes while closely adhering to architectural requirements. The multi-LOD technique not only allows customisable geometric discretisation, but also gives the freedom to select several display options for object representation based on specific requirements.

Considering the objectives of the A-BIM model, a primarily local modelling approach was adopted, prioritising shapes over information scalability. Specifically, distinct models were created for the *Hercules* and *Achelous* mosaic in the room IX and the Tomb of the Platorini family. For the latter, a relational data scheme was developed to establish an information link.

In addressing the irregular elements comprising the remnants of the barrel vault in room X and the cross vault adjacent to XI, a decision was made to construct a loadable generic model family. This family incorporates a polygonal reconstruction based on a LIDAR point cloud using the Ball-Pivoting algorithm (Bernardini *et al.*, 1999).

This choice preserves the morphological irregularity of the structures (Figs. 26-27).

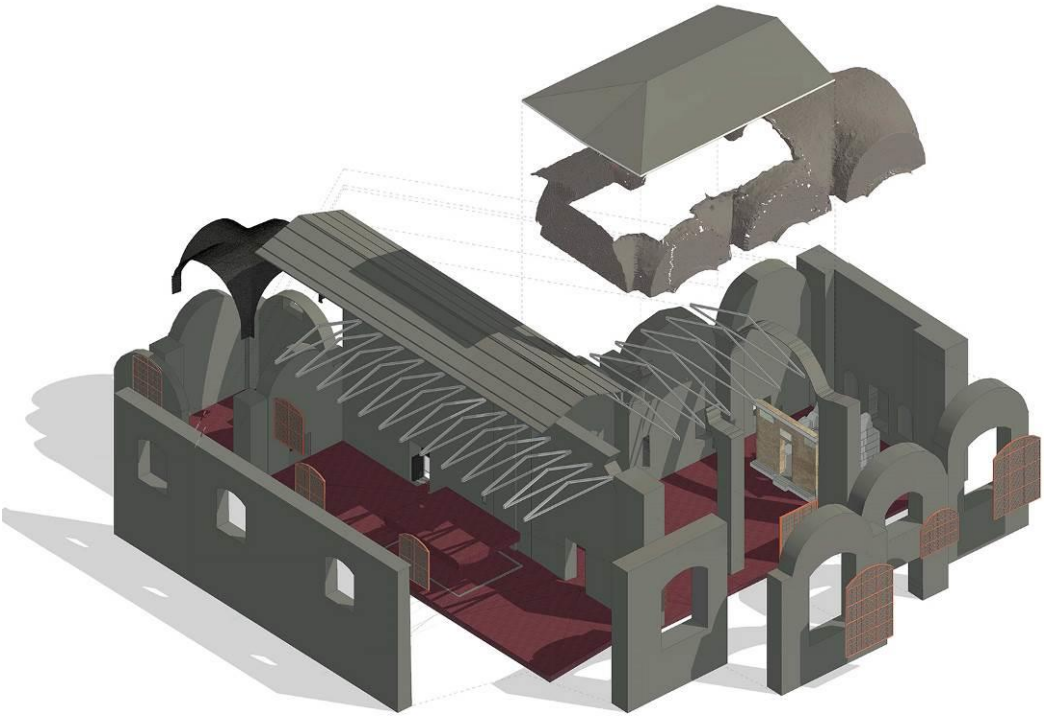

Fig. 26 A-BIM model of the thermal complex.

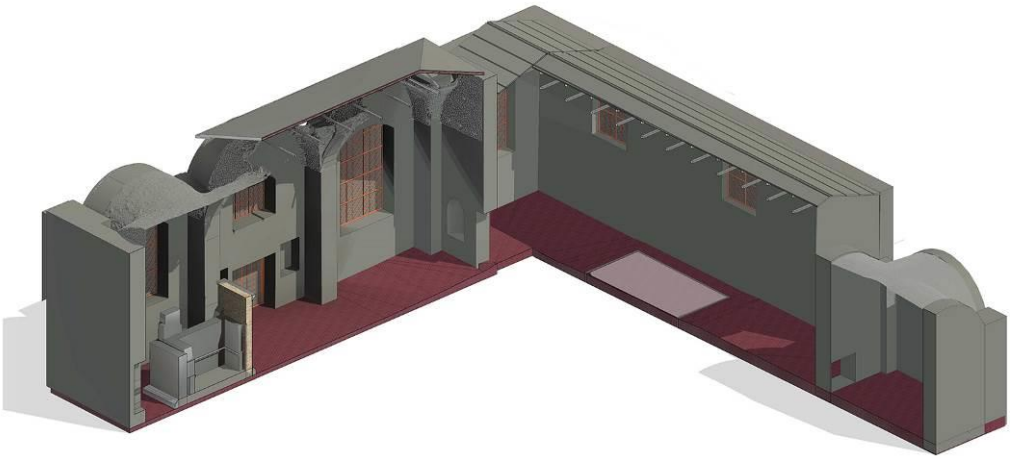

Fig. 27 Axonometric section illustrating the arrangement of 3D meshes and BIM elements in the A-BIM model.

For the Tomb of the Platorini, a loadable family was created to represent the sepulcher, offering three distinct representations with varying levels of detail. The family allows users to activate specific display options within BIM Authoring Autodesk Revit®.

- At a low level of detail, architectural elements were generated from local models using polygonal generators, maintaining a formal separation for potential specific information parameters while achieving high representational simplification.

- With a medium level of detail, the loaded family introduces texture to the outer layers of the volumes. This texture was achieved through RGB mapping derived from the point matrix and optimised using the study of local UV coordinates, preserving material appearance and object style.

- For the high level of detail, the software automatically presents a third version of the Tomb. This version is extrapolated from a polygonal mesh reconstructed from a point cloud through a process of 2 cm decimation and optimisation, carried out using CloudCompare (Fig. 28).

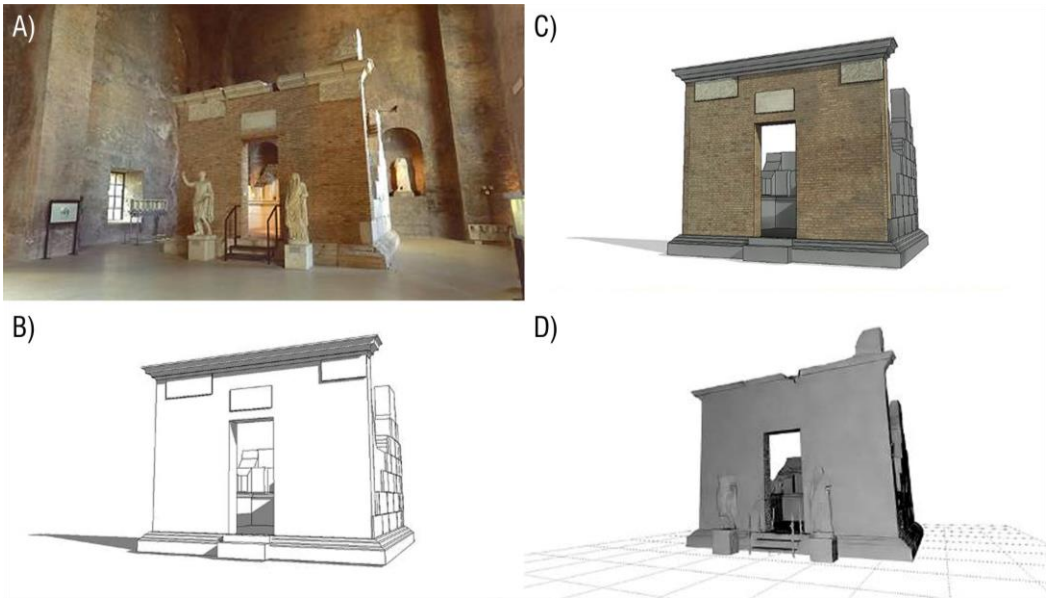

Fig. 28 Representation and compositing of the Revit family for the Tomb of the Platorini, with different levels of detail: A) picture; B) low detail; C) medium detail; D) high detail.

The process of selecting descriptive information to be incorporated into the A-BIM model (Fig. 29) involved a comprehensive approach. Utilising data from the Information Sheets of the General Catalogue of Cultural Heritage served as the foundation, with additional information sourced from the survey, multimedia files, and three-dimensional mesh reconstructions.

This gathered information encompasses a spectrum of details, including the identification of the object with its name, location, type, and function. Administrative geographical aspects, such as the state, region, and address, were meticulously recorded. Georeferencing details, such as the excavation name and period, were also incorporated, providing essential context.

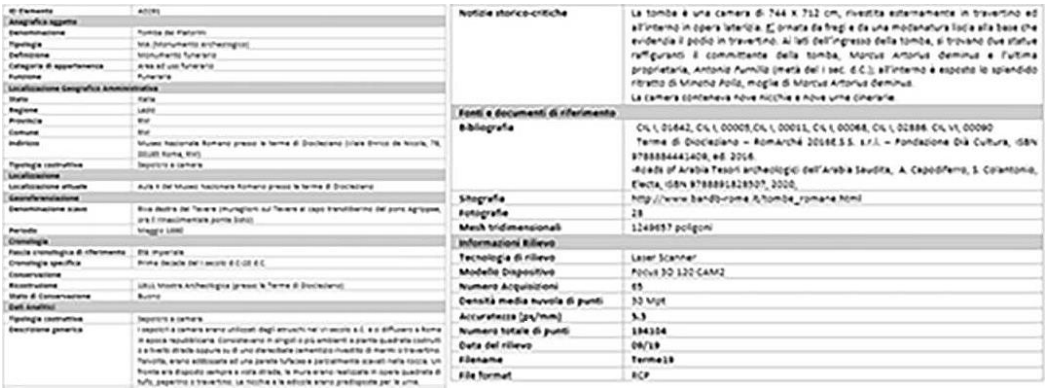

ID Elemento	A0181
Anagrafica oggetto	
Denominazione	Tomba dei Platorini
Tipologia	Tomba (Monumento archeologico)
Definizione	Monumento funerario
Categoria di appartenenza	Area ad uso funerario
Funzione	Funeraria
Localizzazione Geografica Amministrativa	
Stato	Italia
Regione	Lazio
Provincia	Rieti
Comune	Rieti
Indirizzo	Museo Nazionale Romano presso le Terme di Diocleziano (Viale Enrico de Nicola, 78, 00185 Roma, RM)
Tipologia costruttiva	Deposito a camera
Localizzazione	
Localizzazione attuale	Aula II del Museo Nazionale Romano presso le Terme di Diocleziano
Georeferenziazione	
Denominazione scavo	Rive destre del Tevere (muraglioni sul Tevere e capo transtiberino del ponte Agrippa; ora il rinascimentale ponte Sisto)
Periodo	Maggio 1888
Cronologia	
Fascia cronologica di riferimento	Età imperiale
Cronologia specifica	Prima decade del I secolo d.C.(10 d.C.)
Conservazione	
Ricostruzione	Ultici Nicetis Archeologia (presso le Terme di Diocleziano)
Stato di Conservazione	Buono
Dati Analitici	
Tipologia costruttiva	Deposito a camera
Descrizione generica	I depositi a camera erano utilizzati dagli artusti nel I secolo a.C. e si diffusero a Roma in epoca repubblicana. Consistevano in ampi e più ambienti a pianta quadrata costruiti a livello stradale oppure su di una sterrazzata (ampliata rivestita di marmi o travertino. Talvolta, erano addossate ad una parete tufacea e parzialmente scavati nella roccia. Un fronte era disposto sempre a vista stradale, le mura erano realizzate in opera quadrata di tufo, peperino o travertino. Le nicchie e le edicole erano predisposte per le urne.

Notizie storico-critiche	La tomba è una camera di 744 x 712 cm, rivestita esternamente in travertino ed all'interno in opera laterizia, ornata da fregi e da una modanatura lisca alla base che evidenzia il podio in travertino. Ai lati dell'ingresso della tomba, si trovano due statue raffiguranti il committente della tomba, Marcus Antonius dominus e l'ultima proprietaria, Antonia Aumilla (metà del I sec. d.C.); all'interno è esposto lo splendido ritratto di Minonia Polla, moglie di Marcus Antonius dominus. La camera conteneva nove nicchie e nove urne cinerarie.
Fonti e documenti di riferimento	
Bibliografia	CIL I, 01642, CIL I, 00009,CIL I, 00013, CIL I, 00068, CIL I, 02886. CIL VI, 00090 Terme di Diocleziano – Romarché 2016E.S.S. s.r.l. – Fondazione Dià Cultura, ISBN 9788884441408, ed. 2016. -Roads of Arabia Tesori archeologici dell'Arabia Saudita, A. Capodiferro, S. Colantonio, Electa, ISBN 9788891828507, 2020.
Sitografia	http://www.bandb-roma.it/tomba_romana.html
Fotografie	28
Mesh tridimensionali	1249857 poligoni
Informazioni Rilievo	
Tecnologia di rilievo	Laser Scanner
Modello Dispositivo	Focus 3D 120 CAM2
Numero Acquisizioni	69
Densità media nuvola di punti	30 Mpt
Accuratezza [px/mm]	5.3
Numero totale di punti	194104
Data del rilievo	06/19
Filename	Terme19
File format	RCP

Fig. 29 Descriptive information connected to the A-BIM model in the database.

Chronological information played a significant role, covering the chronological context, specific chronology, date of reconstruction, and the current state of conservation. Analytical data, including the type of construction, generic description, and critical-historical insights, enriched the model further.
The inclusion of sources and reference documents involved a thorough bibliography, sitography, and the integration of three-dimensional mesh data. Survey details, such as the technology used, device model, and the number of acquisitions, were also seamlessly integrated.

To establish a robust connection between the model and the database, the Open DataBase Connectivity (ODBC) approach was employed. This ensured application independence from data programming languages. The Autodesk Revit® project was linked to a meticulously structured Microsoft Access® database.
The database itself was organised in charts and relations, employing hierarchical cataloging schemes in the XSD format (Fig. 30).

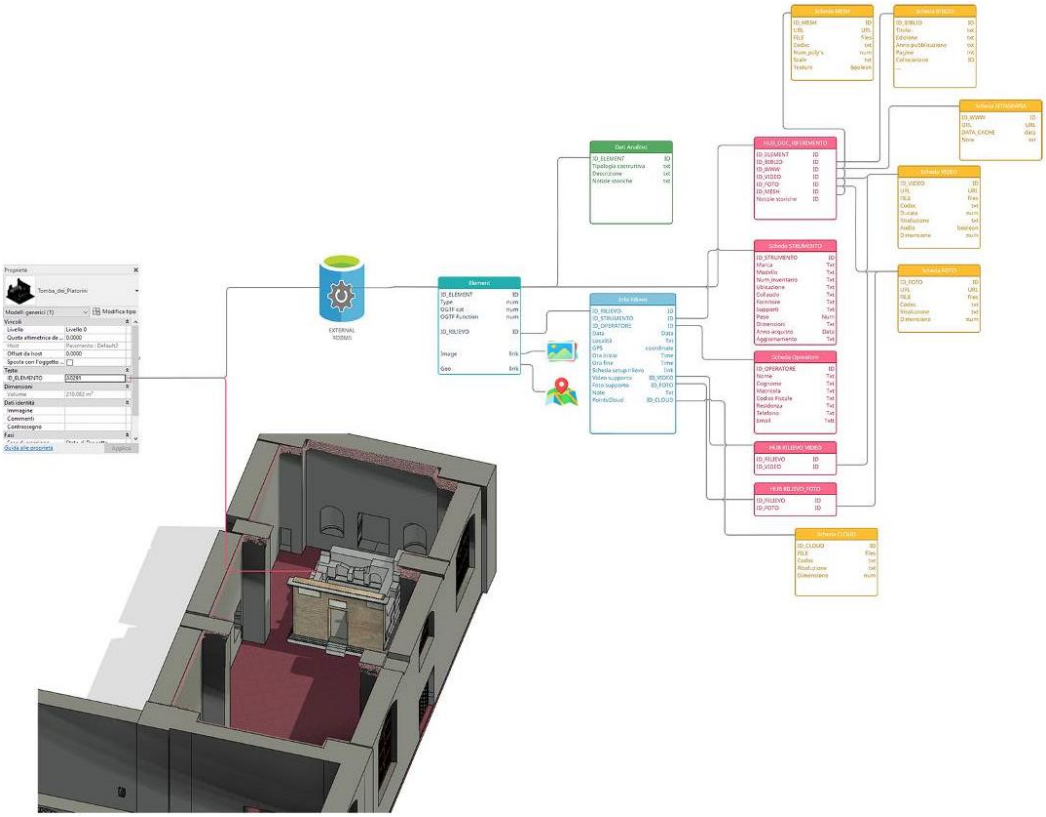

Fig. 30 Microsoft Access format database connection.

3.2.3 Results and Final Remarks

The Baths, distinguished by their irregular and heterogeneous morphology, derive substantial advantages from the dependable A-BIM methodology. This approach harmoniously amalgamates a top-tier model with accurate geometric representation, offering adaptability across varying levels of detail. Moreover, it forges connections with diverse datasets by harnessing a range of relational databases.

This integration between the model and the database facilitated a holistic and information-rich A-BIM model. This methodology, apart from facilitating standardised information organisation, establishes a seamless interface with specific software tools and enables the indexed structuring of textual, graphic, and general information resources.

The linkage between individual elements in the 3D model and their corresponding information base relies on an ID parameter, retrievable via SQL queries. This ensures scalability and customisation in data retrieval.

Essentially, the BIM model serves as a central hub, offering efficient access to and comprehension of all related sources. The hierarchical data organisation enhances storage space management, allowing for file reuse (a single file attributed to multiple model objects) and cross-platform saving options (files can be stored on local hard drives, *network-attached storage (NAS),* or online) (Fig. 31).

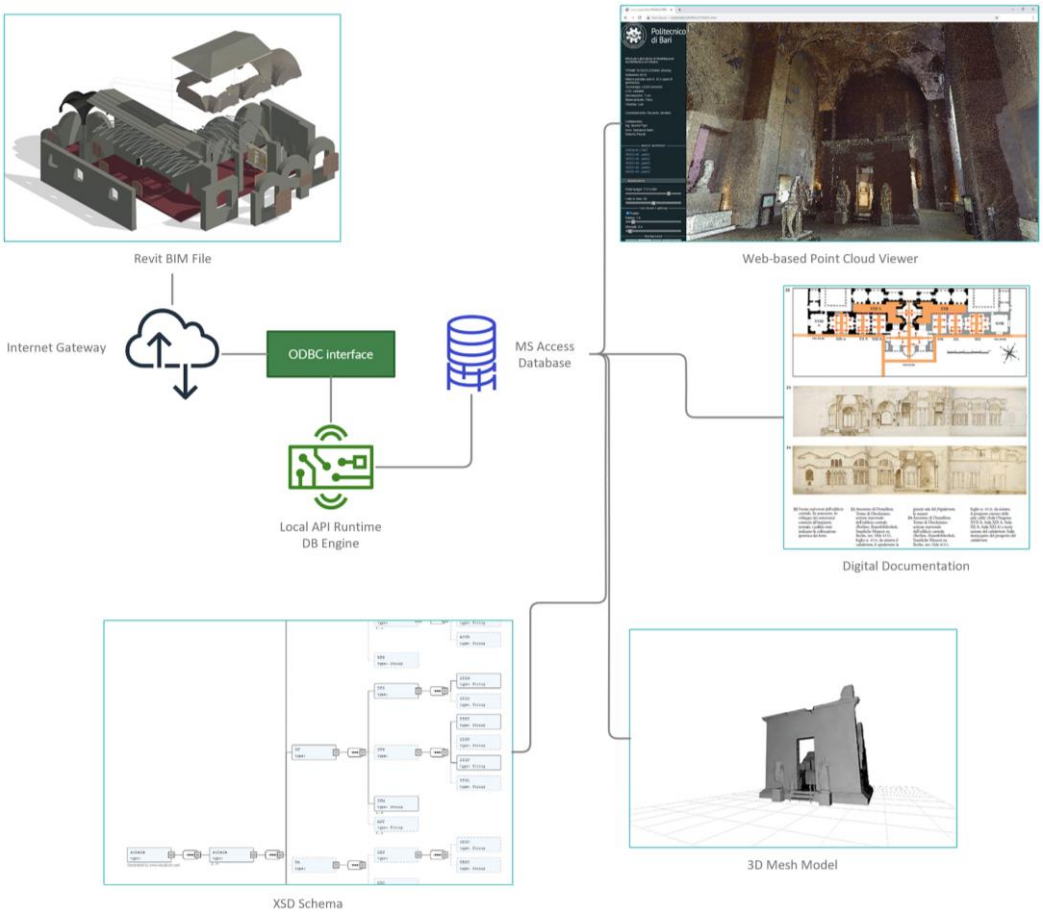

Fig. 31 Cross-platform use of the A-BIM model.

In detail:

- Revit BIM File: This is the model file created in Revit, containing information about the geometry, relationships, and properties of objects within the Baths.

- Internet Gateway: From the Revit modelling environment, the workflow passes through an Internet Gateway, which could be an online link or a platform facilitating connection to external resources or cloud services.

- ODBC Interface: The ODBC (Open Database Connectivity) Interface acts as a bridge between the Revit environment and the MS Access database. This interface enables communication and data transfer between the model and the database.

- Local API Runtime DB Engine: A local API Runtime database engine performs specific functions for accessing and managing data during the workflow. This component can interact with the ODBC Interface to allow access to model data.

- MS Access Database: This is the MS Access database serving as the primary repository for model information. It is divided into various components:

    - XSD Schema: An XSD schema provides a structure for defining and validating data in the database.

    - Web-based Point Cloud Viewer: A web-based viewer for point clouds enables three-dimensional visualisation of specific details of the Baths.

    - Digital Documentation: This part of the database contains documents related to the Baths, providing additional information.

    - 3D Mesh Model: Visualisation of the Tomb of the Platorini as a mesh model (high level of detail).

This organised and interconnected workflow allows for efficient data management, from the modelling environment to linked information resources, enhancing consistency and accessibility of information during the creation, management, and visualisation of the Baths.

3.3 Geometric Reliability Assessment in the Scan-to-BIM Process

In the ever-evolving landscape of Cultural Heritage (CH), a surge of innovative approaches has emerged for the conservation and management of historic buildings. Advancements in laser scanning and photogrammetry have paved the way for the creation of highly precise reality-based models and concurrently, the integration of Heritage Building Information Modelling (HBIM) into the Scan to BIM process has revolutionised the field (Capone and Lanzara, 2019; Adekunle, Aigbavboa and Ejohwomu, 2022). This process seamlessly merges digital survey techniques with HBIM principles, allowing for the systematic translation of point-cloud data collected by laser scanners or photogrammetry into three-dimensional *as-built (as-is)* Building Information Models (BIMs).

However, applying BIM to existing buildings and creating comprehensive as-built models remains challenging. Certain applications, such as visualisation, documentation, or virtual tours, require visual fidelity and high geometric accuracy, while others, like conservation and life-cycle management, demand parametric flexibility and high semantic richness. Despite these advancements, the manual nature of creating as-built BIMs introduces potential errors during data collection, pre-processing, and modelling phases. The intricate irregularities and morphological diversities inherent in ancient buildings pose additional challenges to the geometric parametrisation process.

To this purpose, various methods can evaluate the geometric accuracy of a BIM model (Radanovic, Khoshelham and Fraser, 2020). Visual inspection involves a subjective visual comparison, lacking the ability to provide a quantitative evaluation.
Clash detection, on the other hand, assesses component positions and identifies clashes if they are too close or occupy the same space, using a predefined threshold.

Physical measurement method presents a series of measurements taken from the actual building and their virtual counterparts in BIM. Statistical analysis of these values yields a confidence level, offering an advantage by avoiding errors stemming from point cloud scaling. Nevertheless, it has limitations, as it cannot comprehensively co-

ver all possible measurements, such as those related to ceiling heights or complex morphologies. Additionally, the method struggles to directly identify error sources due to the limited number of measurements, making it a time-consuming process requiring a large dataset.

Surface Deviation Analysis, originating from the manufacturing context, evaluates geometric accuracy and pinpoints modelling errors concerning a model adopted as a ground truth. In the architectural domain, the comparison typically occurs between a 3D model and a reference point cloud. A fundamental assumption is that the BIM and reference point cloud should geometrically align within a specified tolerance (Anil *et al.*, 2013).
Conducting a deviation analysis involves three primary steps. The first entails computing deviations of the point cloud from the BIM model to identify errors. Estimating correspondences between points and the BIM can be achieved through direct or indirect methods, such as i) calculating the minimum Euclidean distance to associate data points with nearby objects; ii) projecting points onto three-dimensional surfaces; iii) tracing rays on surfaces to find correspondences, or eliminating matches based on specific metrics (e.g., normal direction).
The second step involves visualising correspondences through a colour-coded deviation map, colouring each surface according to different distances. Deviation patterns arising from various errors can be analysed to identify their sources, type, and relevance within the point-cloud data or those derived from the as-is BIMs. Several colouring methods, including binary maps, continuous colouring, or unsigned/signed maps (Atasoy *et al.*, 2010), can be employed to enhance understanding.
Finally, the third step entails analysing the deviation maps to identify specific deviation patterns.

The proposed Scan to BIM approach (Verdoscia, Musicco, Tavolare, *et al.*, 2021b, 2021a) seamlessly integrates two three-dimensional survey methods – laser scanning and photogrammetry – along with a parametric modelling approach to develop a comprehensive 3D model for the former Monastery of the Saint Mary of the Cross in

Modugno (Bari, Italy). The investigation into geometric accuracy is conducted through clash detection and deviation analysis.

3.3.1 The Monastery of Saint Mary of the Cross in Modugno (Italy)

The former Monastery of Saint Mary of the Cross, dating back to 1618, is situated in the historic center of Modugno, within the metropolitan city of Bari, Italy. Positioned on Piazza del Popolo square, it stands proudly in front of the Mother Church and adjacent to the Saint Mary of the Cross church, from which it derives its name.

Over the years, the monastery (Fig. 32) has undergone a series of interventions and transformations to accommodate various purposes. In addition to serving as the residence for the Olivetan Benedictine nuns for an extended period, it has also functioned as the location for municipal offices, the district court, the local prison, and an elementary school.

Fig. 32 Internal courtyard of the former Monastery of Saint Mary of the Cross in Modugno (Bari, Italy).

The structure is primarily composed of two bodies surrounding a cloister enclosed by a double order of covered walkways. The ground floor features square pillars with doric capitals, while the first floor showcases columns adorned with phytomorphic decorations.
The covered walkway surrounding the cloister consists of a system of cross vaults on the ground floor, resting on walls that separate internal and external spaces. The internal areas feature a combination of barrel and pillar vaults. The ground floor's smooth tuff façade is clad with ashlar.
During the interventions in the fall of 2018, professionals discovered remnants in a few ground floor rooms that belonged to structures predating the construction of the monastery. These included hypogea with basoli stone paving, walkways, water drainage channels, a cistern, a spiral staircase, stables, as well as copper and bronze objects. Initial expert evaluations suggest these findings date back to the Renaissance period and possibly even earlier periods. Recognised as of notable historic-artistic interest on May 30, 1981, in accordance with Law 1089/39, the monastery stands as a testament to the sacred architecture of the town. Presently serving as the town hall, since 2018, it has also been established as a cultural hub.

3.3.2 Methodology

The monastery was meticulously surveyed using two distinct digital survey techniques. The laser scanner was employed for the comprehensive scanning of the entire building, while photogrammetry was utilised to capture detailed imagery of both the column capitals on the second order, overlooking the internal cloister, and the embellishments adorning the entrance portal.

i. **Laser Scanning and Point Cloud Processing**

For the survey of the entire complex, the CAM2® FARO Focus 3D 120 laser scanner was utilised. This advanced tool boasts technical specifications that deliver a

remarkable measurement accuracy of ± 2 mm, a range spanning from 0.6 to 120 meters, a rapid measurement speed of 976,000 points/second, and expansive vertical and horizontal fields of view at 305° and 360°, respectively.

The selection of scan points was strategically determined through the creation of an acquisition plan, formulated after an initial on-site inspection. This plan served to optimise the balance between the total number of scans and their resolution, the time required for acquisition, and the attainment of adequate overlap. Moreover, it considered the instrument's average distance from the object to ensure uniform precision and minimise shadow areas (Fig. 33).

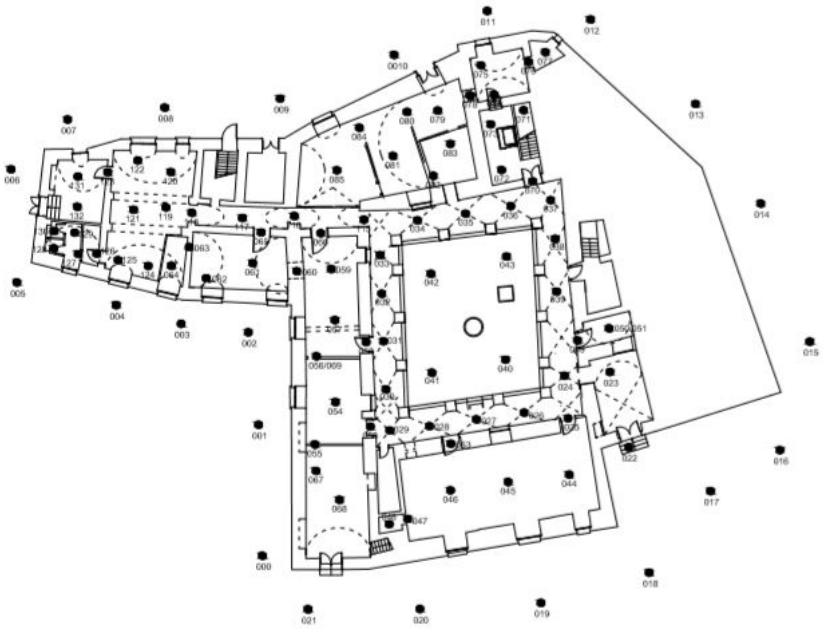

Fig. 33 TLS acquisition for the ground floor.

A thorough analysis of each room was conducted, encompassing the spatial distribution, entrances, wall morphology, ceiling structures, and materials. This detailed examination guided the selection of the most suitable survey method for each specific aspect of the monastery's architecture.

Due to the extensive nature of the complex, a total of 288 scans were conducted at a distance of 10 meters. These scans featured a variable resolution ranging between 6.0 and 7.5 mm, with approximately 30 million points per scan.
This configuration ensured a minimum resolution of 8248x3414 points and a maximum of 10310x4268 points. The processing of the scans was carried out using Autodesk Recap Pro® software. Each point cloud underwent meticulous scrutiny, with a manual alignment process implemented to remove extraneous data and ensure accuracy (Fig. 34).

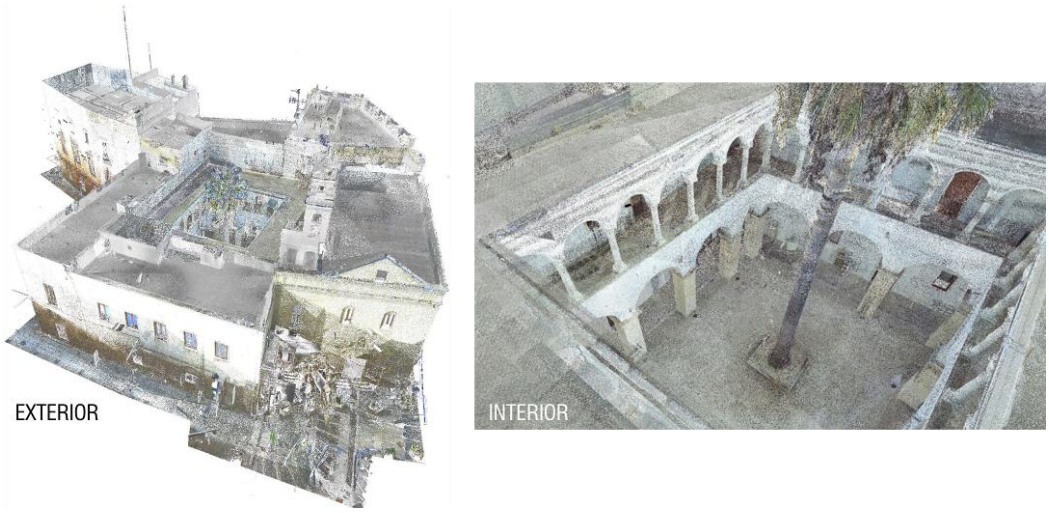

Fig. 34 Point cloud: external view of the entire complex (on the left); internal view of the courtyard (on the right).

ii. **Photogrammetric Survey and 3D Modelling**

The photogrammetric survey utilised a Sony DSC-QX100 digital camera, featuring a 20.2MP sensor resolution, 13.2 mm x 8.8 mm sensor size, CMOS Exmor R® 1' sensor format, and an image resolution of 5472 x 3648 pixels. The camera was mounted on a telescopic rod via a two-axis gimbal. A series of photos were cap-

tured with converging axes at various inclinations to ensure optimal overlap between acquisition points while preventing shadow areas.

Subsequently, all acquired images underwent processing using Agisoft Metashape Pro®, generating a point cloud and a textured polygonal mesh for each element (see Fig. 35). Nevertheless, some refinements were applied to the polygonal mesh, including decimation, removal of outliers, and hole correction.

Fig. 35 Pictures of a portal decoration and a capital (on the left); related polygonal meshes (on the right).

iii. **Construcution of the BIM Model**

The three-dimensional model of the former monastery was generated from the entire point cloud to achieve a superior level of geometric precision while preserving the architectural hierarchies and semantic relationships of the depicted elements.
Autodesk Revit® was employed for the parametric modelling, allowing the consideration of architectural elements as distinct objects from both hierarchical and semantic perspectives, utilising 'Families' endowed with parameters that can be customised and edited to incorporate geometric and informational attributes.

For instance, adaptive families was designed specifically for vaulted structures, based on geometric properties and parametric modelling was employed to create the 3D model of the entrance portal, encompassing details such as moldings, doors, and steps. Additionally, three-dimensional mesh was utilised to capture the intricate phytomorphic decorations and coat of arms, enhancing the overall visual representation of the architectural aesthetics.

Regarding the construction of the parametric families with decorative elements, specific ornamental details were imported as meshes into Revit in .obj format and seamlessly integrated into the design context (Fig. 36).

Fig. 36 Entrance portal of the monastery: picture (on the left); parametric family built on Revit (on the right).

More specifically, an advanced approach was employed for managing meshes within the BIM model context, utilising the Visual Programming Language (VPL) through the Dynamo plugin, and specifically leveraging the Mesh Toolkit package (Fig. 37).

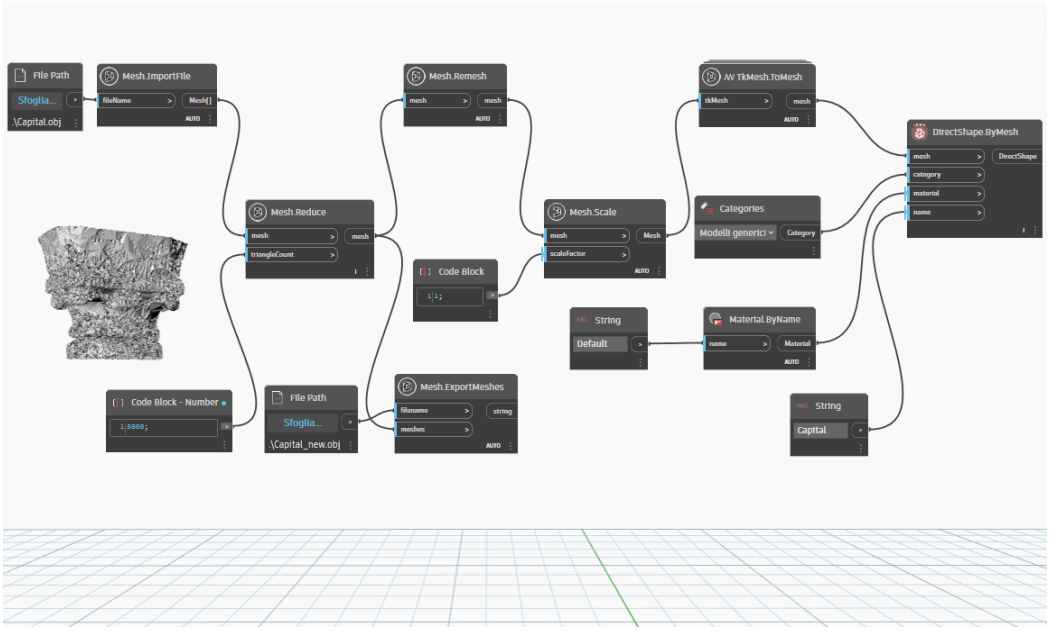

Fig. 37 Application of VPL through Dynamo for the management of meshes within Revit families.

The executed process unfolds in the following manner:

- Mesh Importation: Utilisation of the MeshToolkit.Import.Mesh node or a similar node to import a mesh into the Dynamo project in Revit.
- Level of Detail (LOD) Management: Application of the MeshToolkit.Reduce node to control the level of detail of the mesh by adjusting the number of polygons and optimising performance.
- Uniform Remodelling of Triangles: Use of the MeshToolkit.Remesh node to achieve a uniform remodelling of triangles, thereby improving the structure of the mesh.

- Representation Scaling: Application of the MeshToolkit.Scale node to adapt the dimensions of the mesh to the project specifications.
- Conversion to BIM Object: Utilisation of the DirectShape.ByMesh node in Dynamo to convert the manipulated mesh into a BIM object, seamlessly integrating it into the Revit model.
- Attribution of Parameters and Technical Information: Use of Dynamo nodes to assign specific parameters to the associated BIM family of the mesh. This includes details regarding material and other technical aspects, enriching the model with detailed information.

3.3.3 BIM Evaluation and Results

The support provided by the point cloud has been remarkable, allowing for the approximation of the irregular or curved geometry of the elements with a negligible margin of error and providing real-time geometric dimensions.

The VPL methodology enabled precise control and efficient manipulation of meshes, incorporating stages such as reducing the level of detail, uniformly remodelling triangles, scaling representation, and accurately attributing parameters and technical information. The .obj format facilitated the preservation of the fine details and complex geometries of these elements, offering a high level of fidelity in their representation within the Revit model.

This approach not only contributed to the visual richness of the architectural composition but also provided the design team with the flexibility to tailor and fine-tune these decorative elements to harmonise with the overall design vision. Once completed, the entire model (Fig. 38) serves as the foundation for conducting a series of studies, checks, and simulations, leveraging the concept of interoperability on which the BIM approach to design is founded.

Fig. 38 3D model rendering of the portico on the second floor (on the left) and the inner cloister (on the right).

To this purpose, for validating the precision of the three-dimensional model, we conducted a two-step evaluation. Initially, Clash Detection was executed among the elements of the three-dimensional model. Subsequently, a Surface Deviation Analysis was performed, comparing the point cloud data with the three-dimensional model.

The Clash Detection process was executed using Autodesk Navisworks® software, revealing critical issues resulting from three modelling mistakes (Fig. 39). It identified modelling imprecisions across various elements, leading to a configuration diverging significantly from reality – most notably, an incorrect interpenetration of walls and ceilings.

Additionally, it flagged inferences in certain BIM objects, part of different parametric families constituting the model, exposing interferences between the structural and architectural models, particularly at the beam-masonry interface. This examination also shed light on errors in parameter insertion.
Notably, an interference between a stairway and the lower part of its railing was observed and resolved by implementing an appropriate offset.

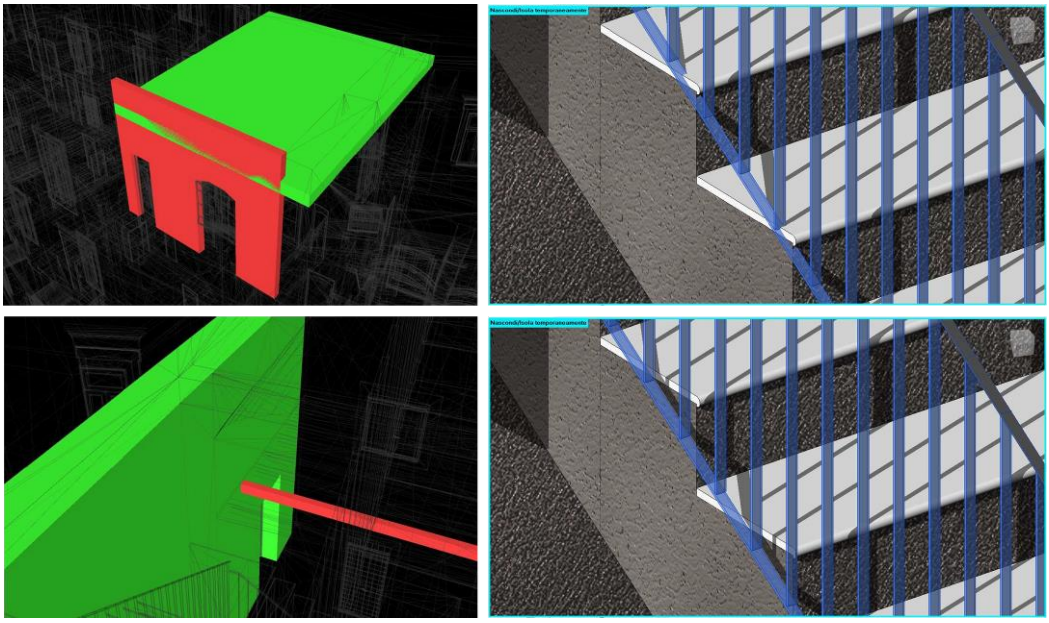

Fig. 39 Identification of interferences among construction elements through Clash Detection (on the left) and recognition of parametric errors (on the right).

The deviation analysis was conducted using the As-built® software developed by FARO Technologies. Specifically, a threshold deviation value was established to compare the minimum Euclidean data-object distance for each modelled architectural component against the point cloud.

Smaller threshold values (20 – 50 mm) proved more effective for visualising detailed deviations, such as local geometric errors, and were therefore applied to elements like frames, vaults, and arched openings. Conversely, larger threshold values (50 – 300 mm) were employed for the walls due to the potential impact of the ashlar on the analysis. The colour scheme ranges from red (indicating the maximum positive value) to green (0 mm, neutral) and blue (the minimum negative value).
Fig. 40 illustrates the consistency between the model and the point cloud. In detail, a negative deviation was identified in the irregular arches supported by the pillars of the first-order cloister, along with a crack not visible in the three-dimensional model.

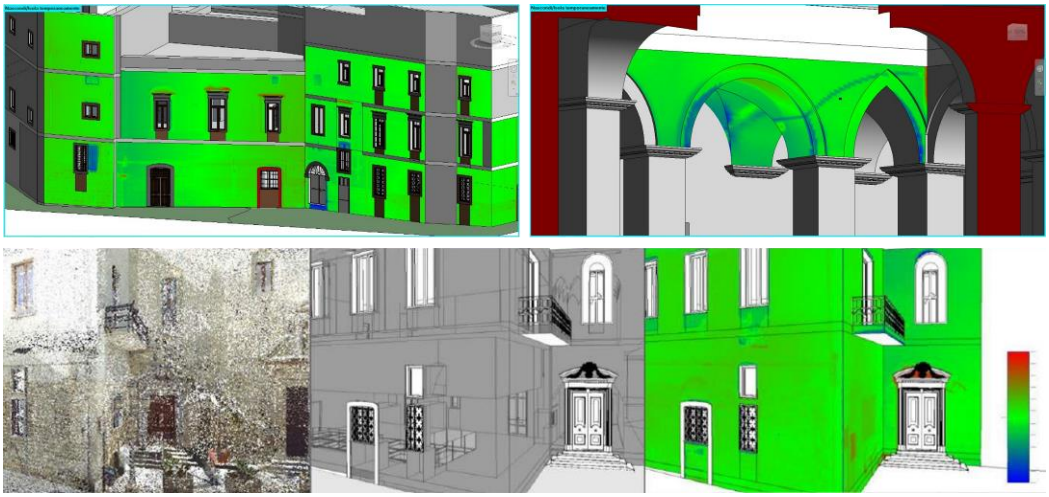

Fig. 40 Surface Deviation Analysis between the point cloud and the BIM model.

After addressing the modelling errors identified through clash detection and deviation analysis, a final BIM model was achieved, characterised by high geometric accuracy. Once the BIM model was obtained, it was exported in the standard Industry Foundation Classes (IFC) format for subsequent import into Unreal Engine®, an optimal environment for crafting virtual reality (VR) experiences (Fig. 41).

Fig. 41 VR Elaboration from the BIM model: Exploring the Monastery of St. Mary of the Holy Cross in the Unreal Engine's environment.

The adoption of the IFC format provided maximum interoperability across diverse software platforms. As an open and neutral format, IFC facilitates seamless data exchange between various applications within the realms of design and construction. Opting for IFC ensured a smooth transition of the BIM model between Revit and Unreal Engine, preserving the integrity of the data and enhancing the overall efficiency of the process.

Within Unreal Engine the model was optimised to ensure smooth real-time visualisation, considering elements such as lighting, materials, and textures. Programming was employed to introduce interactivity into the virtual environment, allowing users to explore the monastery in an engaging manner. This phase included the creation of detailed virtual environments, navigation management, and the implementation of interactive features, such as the ability to open doors or turn on lights within the model.

The distinctive aspect of the project was the use of virtual reality as the mode of experiencing the environment. Thanks to integration with VR devices like Oculus Rift or HTC Vive, users could fully immerse themselves in the virtual environment of the Monastery of St. Mary of the Holy Cross. Virtual reality provides an engaging experience, enabling users to explore every detail of the building realistically and interactively.

3.3.4 Closing Remarks

The innovative approach presented in this study, focusing on scrutinising the geometric accuracy of parametric 3D models derived from point-cloud data, not only demonstrates a robust methodology but also emphasizes the inherent benefits of BIM.

BIM, with its collaborative and data-rich nature, serves as a foundation for comprehensive geometric assessments. The incorporation of VPL, as exemplified through Dynamo, further enhances the efficiency and precision of this process. This

synergy not only contributes to the ongoing evolution of methodologies for geometric accuracy assessment but also reflects the industry's commitment to embracing advanced tools and technologies for more refined and efficient solutions in the domain of 3D building information management.

For evulating the geometric accuracy of the model, two different methods were emplyed: Clash Detection and Surface Deviation Analysis.
The initial method, Clash Detection, served to identify and rectify interferences among the components within the BIM model. Subsequently, a more in-depth analysis unfolded, involving the computation of Surface Deviations between the point cloud and the 3D model. This phase provided a comprehensive assessment, enabling the verification and quantification of errors. The utilisation of a pre-established colour map facilitated the evaluation of the magnitude of inconsistencies, streamlining the identification process within the model.

The seamless integration of these methodologies not only enhances the precision of the 3D models but also contributes to the ongoing evolution of methodologies for geometric accuracy assessment in the realm of architectural and construction projects. As technology continues to advance, the presented approach stands as a testament to the constant quest for refined and efficient solutions in the domain of 3D building information management.

4. ENHANCING SURVEYING AND BIM THROUGH AUTOMATED PROCESSES LEVERAGING MACHINE LEARNING ALGORITHMS AND MORE

This chapter embarks on an exploration of the frontiers of innovation within the realm of architectural surveying and Building Information Modelling (BIM), with a specific focus on advanced automation processes powered by Artificial Intelligence (AI) algorithms.

The segmentation of point clouds emerges as a pivotal element, presenting a dynamic and precise approach to gathering three-dimensional data. Simultaneously, the utilisation of various approaches for geometric modelling contributes to defining a flexible and sophisticated methodology for representing complex structures.

The cornerstone of this innovation lies in the full implementation of machine learning algorithms, introducing a new level of intelligence to the processes. These AI algorithms not only optimise precision and efficiency in digital surveying phases but also play a crucial role in shaping the evolution of BIM operations.

The future outlook of this chapter not only anticipates a revolution in operational practices but also provides insight into a landscape where automation processes converge to redefine how Architectural Heritage is understood, modelled, and preserved.

Here is a brief overview of the analyzed case studies, highlighting their respective adopted methodologies.

- **Venosa's Most Holy Trinity Complex (Basilicata, Italy):** The study aims to create a unified process using diverse architectural surveying techniques, including both range-based and image-based methods, with a focus on the Most Holy Trinity Complex in Venosa. The work explores 360° online virtuali-

sation for architectural surveys, addressing COVID-19 travel restrictions and promoting remote tourism. The methodology involves data extraction, 3D model construction, and an innovative pathology assessment on stone surfaces, utilising advanced techniques such as decay mapping, point cloud analysis, and texture mapping via machine learning algorithms.

- **Disused Industrial Building in Milan (Lombardy, Italy):** The study focuses on the efficient segmentation of point clouds in a disused industrial building near Milan. It employs standards such as UN EN ISO 19650 and UNI 11337, along with denoising, subsampling, semantic classification, and geometric recognition algorithms, such as CANUPO and RANSAC. This thorough and organised process was designed to meet the complicated demands of digital surveying by optimising the point cloud for effective BIM authoring.

- **Nico Palace in Gioia del Colle (Apulia, Italy):** The research concentrates on categorising the intricate staircase within Nico Palace to optimise subsequent modelling steps. The methodology involves voxel downsampling, targeted decimation, and the application of the CANUPO algorithm for classification and the RANSAC method for segmentation. The goal is to extract specific elements from the point cloud dataset, focusing on the geometric quality and completeness of the final 3D model.

- **Vaulted Systems in Various Locations (Italy):** The study assesses an automated iterative process within a scan-to-BIM methodology for various masonry vaulted systems. The process encompasses point cloud segmentation utilising open-source algorithms, initially tested on ideal models and subsequently on real-world models. It involves geometric modelling employing Non-Uniform Rational B-Splines (NURBS) and semi-automated 3D reconstruction. The primary objective is to facilitate 3D parametric/adaptive reconstruction compatible with BIM Authoring, underscoring the complexities introduced by irregular geometries within scanned point clouds.

- **Church of Ognissanti di Cuti in Valenzano (Apulia, Italy):** This case explores two automation techniques for TLS station planning, one based on the 'Art Gallery Problem' and the other utilising a genetic algorithm. The deterministic approach optimises TLS stations, while the genetic algorithm ensures strategic viewpoint additions during on-site surveys. The research aims to improve TLS instrument station layout efficiency, also combining TLS with aerophotogrammetric data and implementing semantic segmentation for parametric modelling in the BIM environment.

- **Palace of the Counts of Sástago in Zaragoza (Aragon, Spain):** The focus is on semantically segmenting the architectural elements of the Palace, utilising a machine learning algorithm in Python. Testing various combinations of geometric features characterising the point cloud, the study aims to classify and break down the point cloud into distinct components. The ultimate goal is to expedite future processes in Historic Building Information Modelling (HBIM).

4.1 Virtualisation of Integrated Survey and Degradation Analysis via Machine Learning algorithms

In the 21st century, the digital documentation of Cultural Heritage has emerged as a crucial ally for preservation and enhancement, serving as a safeguard against institutional neglect and the potential obsolescence of physical materials (Balzani, Maietti and Mugayar Kühl, 2017). The different nature of historic buildings necessitates a broad spectrum of data acquisition techniques capable of delivering comprehensive information, considering factors such as geometric complexity, area accessibility, and the required level of detail.

Managing data obtained from diverse acquisition techniques requires meticulous control of morphometric accuracy and resolution, as image-based technologies alone cannot capture the real dimensions of objects without support from range-based technologies (Remondino, 2011; Aicardi *et al.*, 2018). Their combination (Florio, Catuogno and Della Corte, 2019; Aterini and Giuricin, 2020), yielding point clouds, ensures precise results, optimises data acquisition times, and, through the 'Scan to BIM' process, can be incorporated into various elaboration processes, including parametric three-dimensional modelling (Hichri, Stefani, De Luca, Veron, *et al.*, 2013; Verdoscia, Musicco and Tavolare, 2019), and specific graphic representations through interdisciplinary collaboration (Fiorillo *et al.*, 2015).

This is where the primary objective of this study lies: to develop a unified process using different architectural surveying techniques, including both range-based and image-based methods, illustrated through the case study of Venosa's Most Holy Trinity Complex in Venosa (Potenza, Italy).

Additionally, the work explores the potential of 360° online virtualisation of architectural surveys, contributing to disciplinary knowledge and promoting remote tourism. This addresses travel restrictions imposed by the COVID-19 pandemic, emphasising the need to preserve environmental sustainability. Notably, the concept of tourism applied to Cultural Heritage has evolved worldwide in response to the virus

outbreak, manifesting as innovative virtual travel experiences (Folinas and Metaxas, 2020).

Today, exploring monuments, galleries, and museums closed due to virus prevention measures remains possible (Chirisa, 2020; Deb and Nafi, 2021). This is facilitated through navigation of three-dimensional models, immersive environments based on photographic scanning (De Fino, Galantucci and Fatiguso, 2019), or 360° virtual tours embedded with captions and comprehensive artwork descriptions (Osman, Wahab and Ismail, 2009; Bonacini, 2015). Such experiences are accessible globally, offering ease of access and enjoyment at any time, without the need for advanced planning.

The subsequent segment of this study delves into the application of photorealistic three-dimensional models, presented through coloured point clouds and textured polygonal meshes. These models not only serve as innovative diagnostic tools but also act as comprehensive sources of information regarding morpho-typological and material-conservative characteristics. This digital representation not only facilitates advanced analyses to deepen fundamental knowledge but also opens avenues for automated processes through *image processing* techniques.

3D models enable sophisticated processing, including automated procedures such as segmentation, extrapolation, and classification of specific model portions (Grilli *et al.*, 2018; Grilli and Remondino, 2019). Specifically, for mapping surface alterations on masonry façades, recognition procedures based on colour or texture properties can be implemented (Fatiguso and Buldo, 2020). These methodologies leverage the colour properties of point clouds and the texture of polygonal meshes, allowing for the extraction of detailed information regarding various visible forms of degradation.

Specifically, the study utilises the Most Holy Trinity Complex as a reference case, starting from the extraction of data derived from the previous phases of the 3D model construction. It then proceeds with the subsequent processing of this data aimed at qualifying pathologies observed on stone surfaces.

Point colour selection and Machine Learning algorithms, specifically Fast Random Forest and K-Nearest Neighbours, have been implemented for this purpose.
This approach exemplifies how the integration of photorealistic three-dimensional models and automated analysis processes can provide a detailed and efficient assessment of the structural and conservative conditions of cultural assets.

4.1.1 The Most Holy Trinity Complex in Venosa (Italy)

The Complex of the Most Holy Trinity stands as a significant architectural marvel situated in the ancient Latin colony of Venosa, nestled within the picturesque region of Basilicata in Southern Italy (de Lachenal, 1998). Its historical significance spans from the Roman period (Republican era, III century BC) to the Baroque era (XVII – late XVIII century).

The entire complex (Fig. 42) encompasses various elements: the frontal section leading to the smaller ancient church, characterised by a Paleo-Christian design featuring a central nave, two side aisles, and a distinctive 'corridor crypt'. Adjacent to this is an elegant guesthouse, complementing the ensemble. Behind the primary church stands the imposing 'Unfinished' church, a magnificent structure that, despite its grandeur, was never completed.

The ancient church underwent significant transformations starting from the VII century, influenced by the presence of the Lombards (X century) and later the Normans (XI and XIII century). In 1059, Pope Nicholas II consecrated the abbey, designating it as the familial shrine for the Hauteville family upon the request of Robert Guiscard. By the end of 1297, Pope Boniface VIII entrusted the custody of the complex to the Malta Order. However, the new church's monastic layout was largely ignored and, regrettably, the construction of the complex was never fully realised.

Today, it remains a unique testament to medieval building practices, where the original structure was deliberately left intact until the completion of the new one was feasible (Laviano and Summa, 1999). The Complex of the Most Holy Trinity stands as

a poignant reminder of the intricate historical tapestry woven through the centuries in this captivating corner of Southern Italy.

Fig. 42 The Most Holy Trinity Complex in Venosa (Italy).

4.1.2 Methodology adopted for the 3D Survey

The adopted methodology for documenting the Architectural Heritage (Verdoscia, Buldo, Musicco, *et al.*, 2022a) aims to achieve three key objectives: Digital Documentation, Preservation, and Enhancement (Fig. 43).

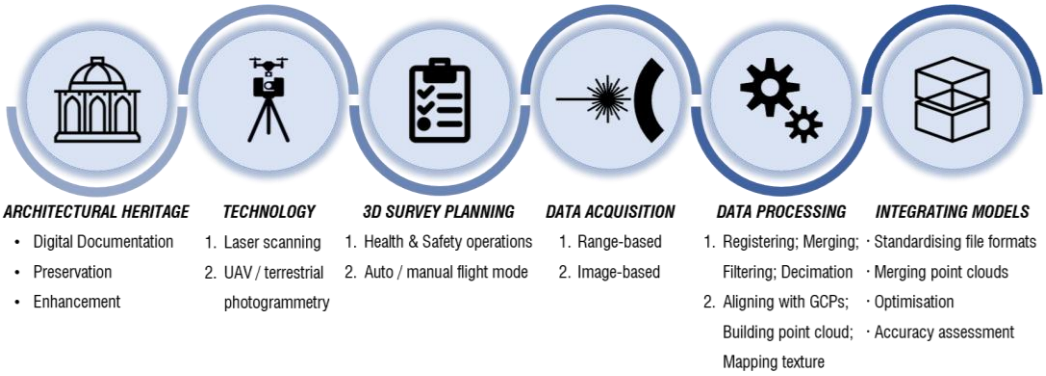

Fig. 43 Methodology workflow.

- Digital Documentation allows for the preservation of every architectural detail in a digital format, facilitating easy access and ensuring long-term conservation. The use of cutting-edge 3D survey techniques provides a unique perspective, contributing to a comprehensive documentation of the entire site.
- Preservation is a central objective, as digital documentation serves as a valuable tool for monitoring the current state of the structure over time, identifying potential damage or changes, and intervening promptly to preserve the heritage's integrity.
- Finally, Enhancement is achieved through the creation of accurate and accessible documentation, enabling scholars, conservators, and the public to virtually explore the abbey. This advanced approach contributes to raising awareness and appreciation for Architectural Heritage, ensuring its historical and cultural continuity.

Utilising advanced tools (see Tab. 2) such as the CAM2® FARO Focus 3D 120 terrestrial laser scanner, the Phantom DJI 3 Professional remote-pilot quadcopter, and the Canon EOS 1200D reflex camera, the goal is to create a detailed and accurate digital representation of the abbey, including the crypt, Roman remains, guesthouse, and the wall structures of the 'Unfinished' church.

For this study, strategic planning of the survey campaign proved essential due to the complex dimensions, considering an area of approximately 150 by 60 square meters.

Tab. 2 Technology parameters.

Technology	Parameters
Terrestrial Laser scanning (CAM2® FARO Focus 3D 120)	Range: 0.6 to 120 m, Capture Speed: up to 976.000 points/sec, Ranging Error: ±2mm at 10m and 25m
UAV Photogrammetry (Phantom DJI 3 Pro)	Lens: FOV 94° 20 mm (35 mm format equivalent), f/2.8 focus at ∞, 12 effective Mpx
Terrestrial Photogrammetry (Canon EOS 1200D)	Lens: 22.3*14.9 mm, 18 effective Mpx and 18.7 total Mpx

i. 3D Survey Planning and Acquisition

The entire survey operations (refer to Fig. 44) were meticulously executed based on a well-structured program. This program accounted for both the number and positioning of shooting points, with the latter determined by considering the geometric characteristics of the objects, including concavity/convexity and openness/closure.

In terms of the laser survey, key criteria were adhered to, ensuring a reduction in shadows caused by occlusions, a decrease in the acquisition angle, and an optimal overlap between scans. Specifically, purpose-built 12-bit targets, measuring 30 by 30 cm with a 20 mm radius, were employed. This choice resulted in scans with consistent resolution, prioritising geometric accuracy, which naturally fluctuated based on variations in the sensor's distance from the object.

A total of 236 scans were conducted, all in colour and averaging a duration of 10 minutes each. These encompassed 153 scans within the abbey, 59 along the outer perimeter, and 24 within the 'Unfinished' church. The scans provided a comprehensive vertical/horizontal Field of View (FOV) coverage of 305°/360°.

This strategic approach ensured a thorough and precise documentation process, capturing the intricacies of the architectural elements both inside and outside the abbey.

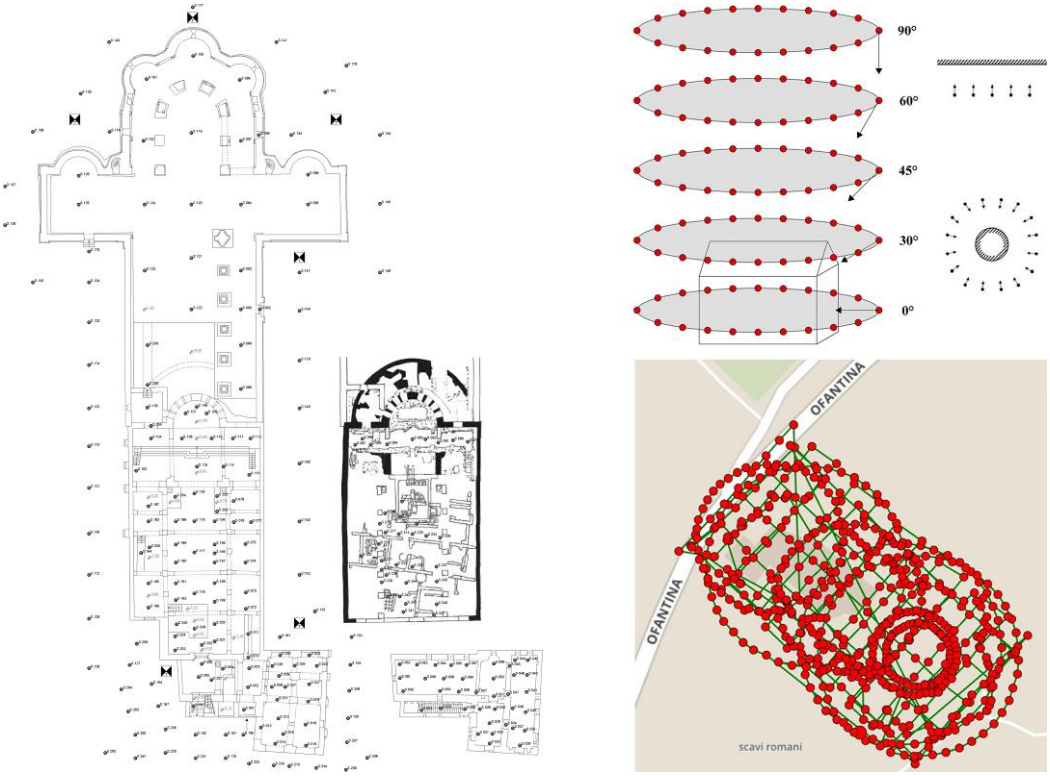

Fig. 44 Range-based (on the left) and image-based (on the right) survey layouts.

The aerial-photogrammetric survey process was preceded by a meticulous series of preparatory steps. This included an assessment of the site's orographic characteristics, a thorough examination of aeronautical charts to navigate airspace coverage constraints, and an evaluation of the building's architectural features to identify areas with reduced visibility. To mitigate the impact of shadows on surfaces during overflights, preference was given to central hours on cloudy days, ensuring greater photogrammetric homogeneity and minimising radiometric errors.

The Pix4Dcapture® application played a crucial role in piloting, facilitating nine flight sessions set in auto-mode, encompassing single, double, and circular grid patterns. Additionally, a manual session was conducted at various heights, incorporating shots at 0°, 30°, 45°, 60°, and 90° angles with rispect the horizontal plane, to aid in the reconstruction of elevation elements. Careful attention was given to maintaining an overlap between contiguous frames, reaching up to 80% in both frontal and lateral shooting directions. This meticulous approach resulted in a total of 618 drone shots, all captured in JPEG format, ensuring the highest manageable resolution for the comprehensive documentation of the surveyed area.

ii. **Data Processing**

For the extraction and processing of laser-scanned point clouds, Autodesk Recap Pro® software was employed. Concurrently, Agisoft Metashape Pro® was utilised for the processing of both aerial and terrestrial photogrammetry frames. To enhance the point cloud's density, a noise reduction filter was applied to the range-based data, coupled with a low decimation grid value (3 mm).

The laser scans underwent a manual registration process, meticulously paired to identify three homologous points in each subsequent scan. This approach, avoiding potential errors inherent in automatic registration – often less effective in large-scale projects – ensured precision and reliability throughout the registration process (refer to Fig. 45).

To streamline the data processing and mitigate potential errors due to overlap among scans, the comprehensive alignment project was strategically divided into three groups. These groups were subsequently merged following a meticulous cleaning of the point clouds to ensure optimal results.

In the realm of photogrammetric processing, aimed at enhancing geometric reconstruction accuracy and overall quality, several crucial operations were executed. These included exposure and contrast optimisation, balancing saturation, whites and

blacks in the images, controlling pixel resolution, and removing extraneous elements, such as people or vehicles.

Fig. 45 Range-based point cloud: A) the ancient church; B) the 'Unfinished' church.

To achieve a high level of accuracy, a specific target was set, defining 1,000,000 Key points (distinct features in a single image) and Tie points (identical features across multiple images) during the alignment phase[3].

The process initiated with the creation of a sparse point cloud, followed by a dense one (Fig. 46) choosing a medium to high level of reconstruction quality. Subsequently, a three-dimensional Mesh was generated, culminating in the processing of textures derived from photographic shots. These textures, sised 8192*8192 pixels, employed a generic mapping mode and a mosaic blending method to achieve a comprehensive and visually compelling representation.

Fig. 46 Image-based point cloud: the abbey complex.

[3] 'Key Points' are distinctive features within each image, characterised by high contrast and good texture. These points of interest, identified by the software, are unique to each individual image and play a crucial role in the alignment process, contributing to the creation of an accurate 3D model. On the other hand, 'Tie Points' are used to establish connections between different images. They represent the matching points between features identified in the Key Points of overlapping images. Essentially, Tie Points link images in pairs, allowing the software to understand their relationships, for constructing a cohesive and three-dimensional model,

Subsequently, using Autodesk Recap Pro® software, the point cloud groups resulting from various scanning techniques were combined, ensuring precise correspondence and uniform dimensional ratios (Fig. 47).
The process of data integration included an initial geometric evaluation of the results, facilitated by Ground Control Points (GCPs). These GCPs were strategically identified using several targets positioned outside the complex, providing a reliable framework for aligning and validating the merged datasets.

Fig. 47 Integrated point cloud of the entire complex.

4.1.3 Results of the 3D Survey

In the context of laser-tech 3D data processing, the device's maximum range – limited tp 120 meters – had no adverse impact on the outcomes. The entire complex was efficiently scanned, maintaining a consistent pace between stations, with the laser beam's maximum range limited to approximately 23 meters at the bell gable coverage highest point.

The point cloud generated from the aerial-photogrammetric survey exhibits a Ground Sample Distance (GSD)[4] of 1.47 cm/px. In contrast, the terrestrial photogrammetric counterpart boasts a finer GSD of 0.661 mm/px, accompanied by a three-dimensional point error of 0.008 meters and a point reprojection error on the image of 0.019 pixels.

To validate the seamless integration of the data, an analysis was conducted within CloudCompare® software. This involved calculating absolute distances between pairs of points originating from different sources – range-based and image-based – utilising the Nearest Neighbour Distance algorithm (as shown in Equations [3] and [4]).

For each point in the image-based cloud, the software identified the nearest point in the reference cloud (range-based) and computed their Euclidean distance (see Fig. 48).

The resulting minimal mean distance (0.01 m) and low standard deviation (0.03 m) unequivocally confirmed the accurate alignment and overlap between the compared point clouds.

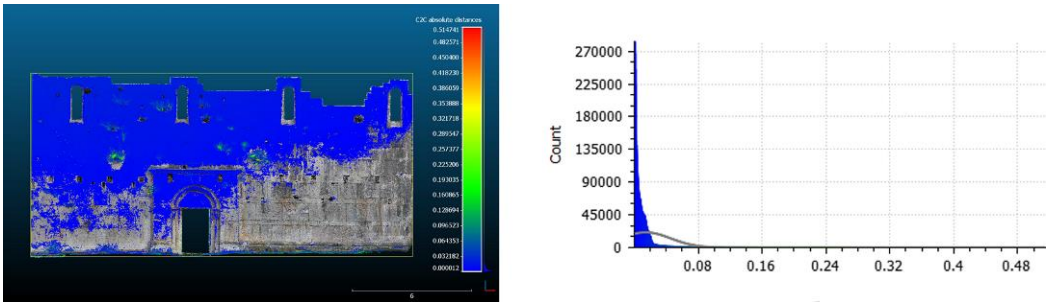

Fig. 48 Graphic visualisation and Gaussian distribution of the absolute distances between range and image-based point clouds.

[4] 'Ground Sample Distance' (GSD) is a critical parameter in aerial photogrammetric surveys, defining the distance between adjacent pixels on the ground or the pixel size relative to real-world dimensions. A smaller GSD indicates higher image detail, with finer pixel representation of the Earth's surface. Influenced by factors like camera focal length, flying height, sensor dimensions, and image size, GSD determines the image's ability to capture detailed information about the terrain.

Furthermore, to assess realistic rendering, two polygonal models, one generated from range-based data and the other from image-based data, were processed for the same wall face. Notably, the entrance portal of the 'Unfinished' church appears more simplified in the range-based meshes compared to the other model. This distinction is primarily attributed to the higher resolution of textures applied in the image-based model, where intricate details are clearly recognisable (see Fig. 49).

Fig. 49 Comparing 3D polygonal models of the 'Unfinished' church portal: A) range-based method; B) image-based method.

4.1.4 Virtual tour during the COVID-19 Era

The current research project also extends its exploration into leveraging architectural survey data for the development of an accessible and sustainable remote tourism experience. The objective is not only to digitally document the acquired reality through advanced techniques but also to conserve and amplify the monument's identity, fostering global sharing. The utilisation of two real-time visualisation software tools enables the online and multimedia consumption of the abbey complex, meticulously captured through diverse scanning techniques and 360° panoramic photos obtained from laser equipment.

The application of Autodesk Recap Pro® software facilitates a virtual tour experience for technically proficient users. It allows seamless navigation within the integrated model, providing customisation options and workflow management. Simple links can be shared without the need for specific software, enhancing accessibility.

For the creation of an authentic virtual tour of the abbey complex from panoramic images, Lapentor® cloud-based software was strategically chosen. The model was enriched by incorporating tags and captions in alignment with the cataloging standards for artworks within the HistAntArtSI web portal database (*HistAntArtSI Site*, 2019). This database is a collaborative project initiated for the preservation, enhancement, and management of Southern Italy's Cultural Heritage, championed by national and international institutional bodies.

Acting as an interactive tourist guide on a per-user basis, the model presented in Fig. 50 aligns with the project's mission to offer a comprehensive and engaging virtual exploration of the abbey complex.

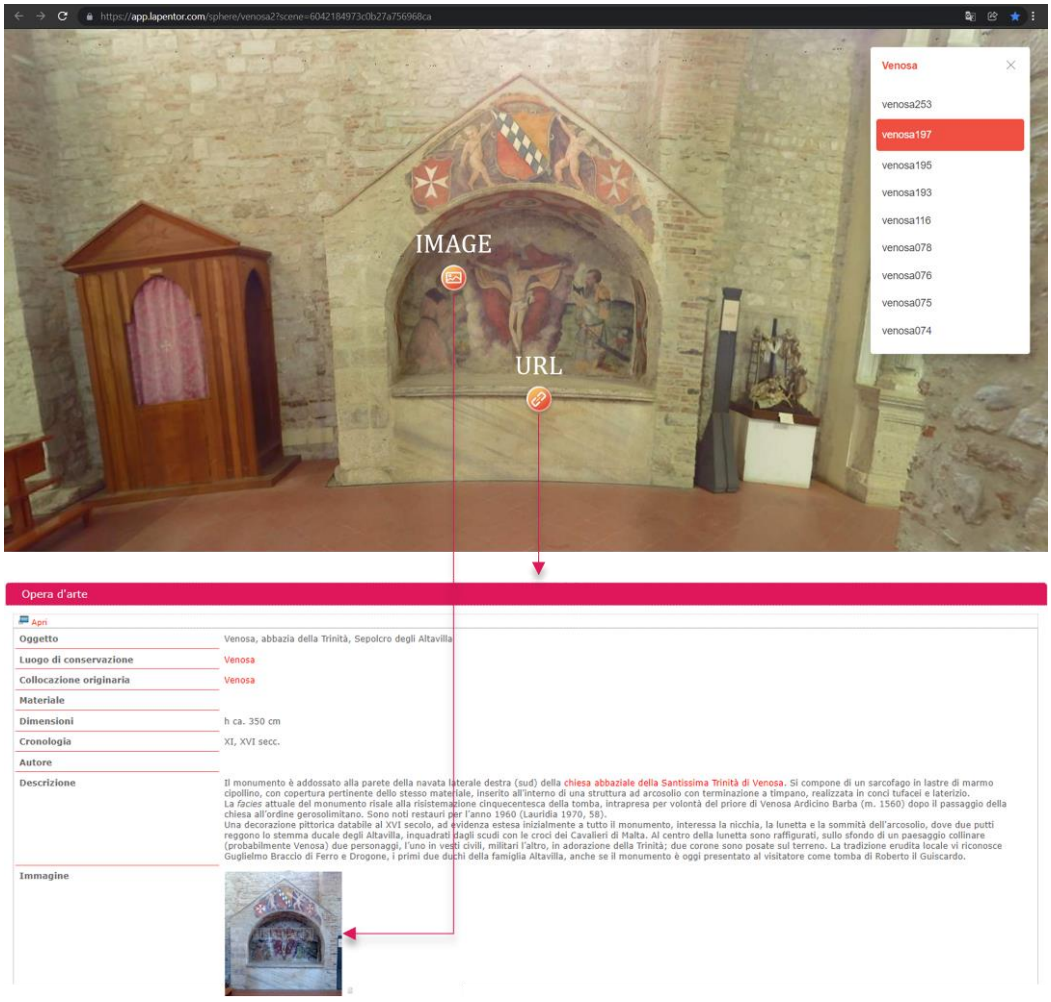

Fig. 50 Virtual tour via Lapentor® linked to the HistAntArtSI web portal.

4.1.5 Methodology for Degradation Mapping

The application of Machine Learning, encompassing both the K-Nearest-Neighbours (K-NN) and the Random Forest (RF) algorithms, plays a pivotal role in image classification within the realm of Architectural Heritage (Janković, 2020). While K-NN classification or regression algorithms encounter challenges stemming from their inherent complexity, particularly in the era of big data, the Random Forest algorithm, Support Vector Machines (SVM) or Deep Learning (DL) present more sophisticated alternatives. These advanced methods provide efficient solutions for accurately identifying architectural styles, historical periods, and specific details in images. In the context where preserving heritage is paramount, the utilisation of learning techniques proves invaluable for safeguarding and intervening early on these significant historical landmarks. Additionally, these approaches contribute significantly to monitoring and assessing the deterioration of historic buildings (Meroño *et al.*, 2015; Fatiguso and Buldo, 2020).

The degradation (or eventually decay) mapping emerges as a crucial process for detecting and analysing any surface alterations present of a building. This comprehensive procedure not only provides a detailed insight into the current conditions of the building surfaces but also serves as a fundamental starting point for implementing preventive or corrective maintenance strategies. This approach significantly aids in preserving the building's structural integrity over time.

In this regard, the decay mapping was conducted on a section of the southwest façade of the Unfinished Church, covering an area of 60 m^2 (Fig. 51).
The initial phase involved an analysis of the point cloud, pinpointing areas linked to diverse surface alterations through the assignment of distinct colours to each region employing conditional statements.
Subsequently, mapping was performed on the texture extracted from the 3D model. Texture analysis was carried out through two distinct approaches: the first approach using proprietary software that employs a machine learning algorithm, specifically the

Fast Random Forest; the second one was developed within the MATLAB® environment using a K-Nearest Neighbours (K-NN) algorithm.

Fig. 51 Southwest façade of the Unfinished Church.

i. **Building the 3D Photogrammetric Model**

To facilitate these processes just mentioned, a high-resolution 3D model was generated. Specifically, photogrammetric techniques were employed using a Canon EOS 1200D digital reflex camera and a Phantom DJI 3 Professional drone, capturing a total of 269 shots for the reconstruction of the model. The shots were taken at a maximum distance of approximately 10 m from the surface, with an overlap of about 80% in both shooting directions between adjacent images. The photographs were pre-processed to optimise exposure, contrast, saturation, sharpness, white balance, and black balance using Adobe Photoshop's Camera Raw plugin.

Subsequently, they were imported into photogrammetric software for digital image processing and the generation of three-dimensional spatial data, specifically using Agisoft Metashape Pro®. The initial alignment of the shots was conducted automatically based on the software's recognition of recurring distinctive points or tie points. However, as not all images were aligned automatically, additional tie points were manually implemented.

Fig. 52 Dense point cloud of the façade.

To verify the correctness of the alignment, both automated and automated/manual procedures were employed, involving the generation of a sparse point cloud, which is computationally and temporally less demanding. Once the alignment was optimised, it was possible to generate the dense point cloud accurately, consisting of almost 64 million points, later reduced to 40 million by eliminating irrelevant portions for analysis purposes (Fig. 52). This point cloud was then scaled to real dimensions based on measurements directly taken on-site.

ii. **Colour-based Classification on the point cloud**

Starting from the dense point cloud reconstruction of the southwest façade of the Unfinished Church, the recognition and extraction of point sets based on homogeneous chromatic characteristics were conducted using Metashape Pro® software, aimed at degradation mapping.

During the experimental phase, four types of surface alterations were identified, as codified by the UNI 11182:2006 standard 'Cultural Heritage - Natural and Artificial Stone - Description of the Alteration - Terminology and Definition' (Ente Italiano di

Normazione (UNI), 2006) and by the Illustrated Glossary on Stone Deterioration Patterns (ICOMOS, 2008):

- Patina: 'Chromatic modification of the material, generally resulting from natural or artificial ageing and not involving in most cases visible surface deterioration'.

- Biological Colonisation (or Biological Patina): 'Colonisation of the stone by plants and micro-organisms such as bacteria, cyanobacteria, algae, fungi and lichen (symbioses of the latter three). Biological colonisation also includes influences by other organisms such as animals nesting on and in stone'.

- Efflorescence: 'Generally whitish, powdery or whisker-like crystals on the surface. Efflorescences are generally poorly cohesive and commonly made of soluble salt crystals'.
- Plant (or Vegetation): 'Vegetal living being, having, when complete, root, stem, and leaves, though consisting sometimes only of a single leafy expansion (e.g. Tree, fern, herb)'.

For each type, the software facilitated the application of a selection procedure for representative points, identifying RGB characteristics to describe unique colours based on the intensity of Red, Green, and Blue.

Subsequently, the application underwent training for segmenting the entire point cloud using an approach where the algorithm employs conditional statements to selectively identify points within the point cloud based on colour criteria. This process enables the algorithm to recognise recurring patterns, thereby facilitating subsequent post-processing or analytical tasks within the Metashape environment.

The following explanation demonstrates how to select the tie points based on RGB colour values and a specified tolerance:

- In detail, the selection method operates on a current document and associated chunk within Metashape. After importing the necessary libraries, including Metashape and sys, the script accesses the active document and its corresponding chunk. The point cloud and track information within this chunk are then obtained for further processing.
- Colour parameters are defined, such as ‘r’, ‘g’, and ‘b’, alongside a tolerance value (‘tolerance’). These values are utilised to establish a range within which points will be selected based on their associated track colours.
- A loop iterates over each point in the point cloud, checking if the colour of the associated track falls within the specified range, considering the defined tolerance. Points meeting this criterion are marked as selected.
- Following the point selection process, the script updates the Metashape user interface to reflect the made selections using ‘Metashape.app.update()’.
- Finally, a message is printed, signaling the completion of the point selection process.

In this case, the manual selection, depicted in (Fig. 53), involved ten groups of representative points in a colour scale for each degradation type. This led to the determination of a tolerance interval for subsequent automated segmentation (Fig. 54) and extraction of thematic point clouds to which semantic classes are associated (Fig. 55).
Finally, starting from these point clouds, polygonal mesh generation was performed for each surface alteration.
These continuous three-dimensional models consist of networks of flat surfaces oriented in space, enabling the implementation of the area calculations of the different forms of degradation (Fig. 56).

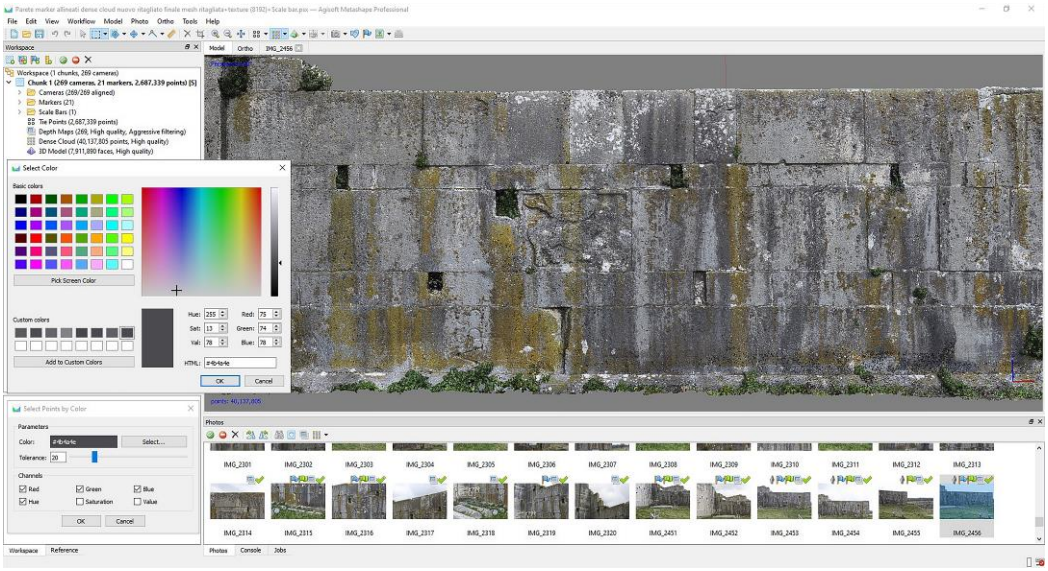

Fig. 53 Manual selection of representative points in RGB scale for different types of degradation.

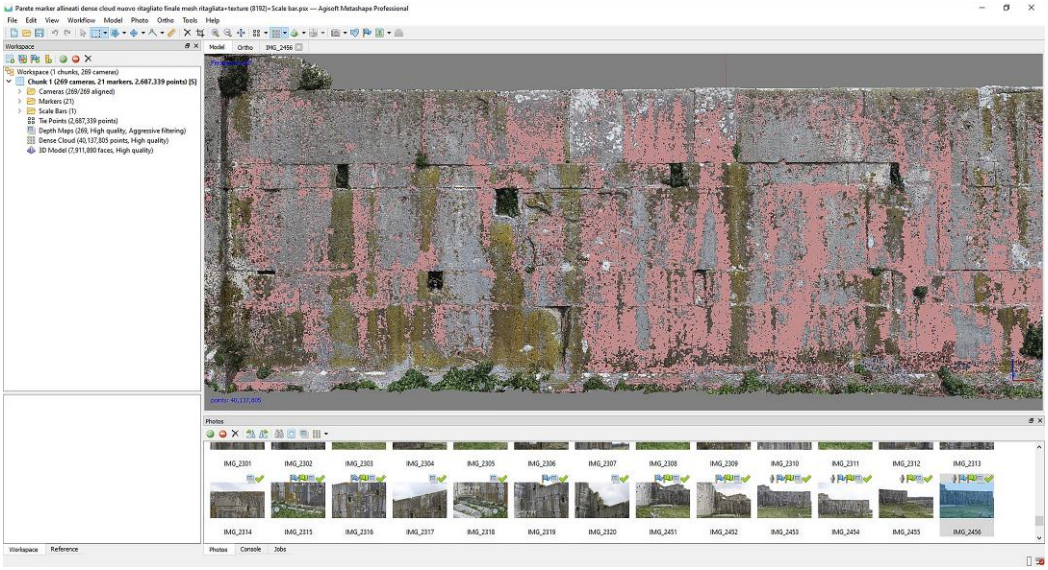

Fig. 54 Example of segmented point cloud: the ‘patina’ class.

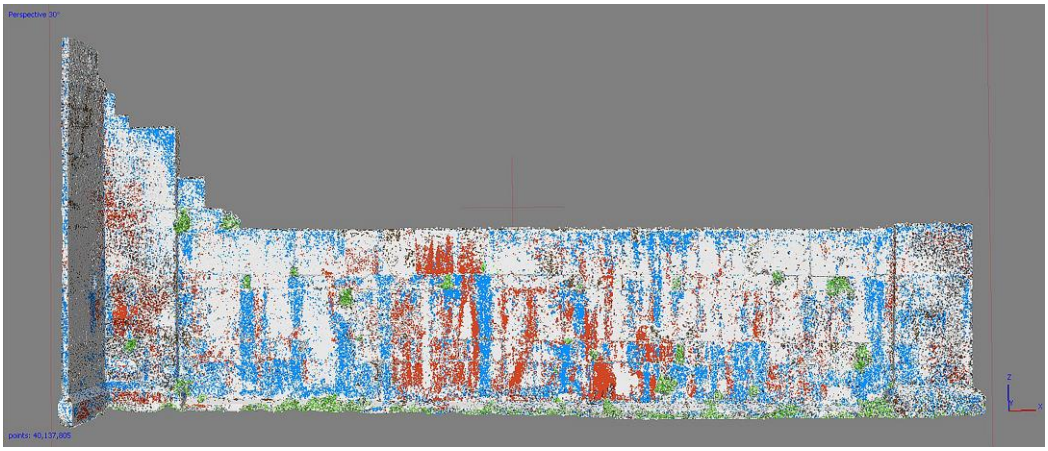

Fig. 55 Semantic point cloud classes: Patina (red); Biological Colonisation (blue), Efflorescence (brown), Plant (green).

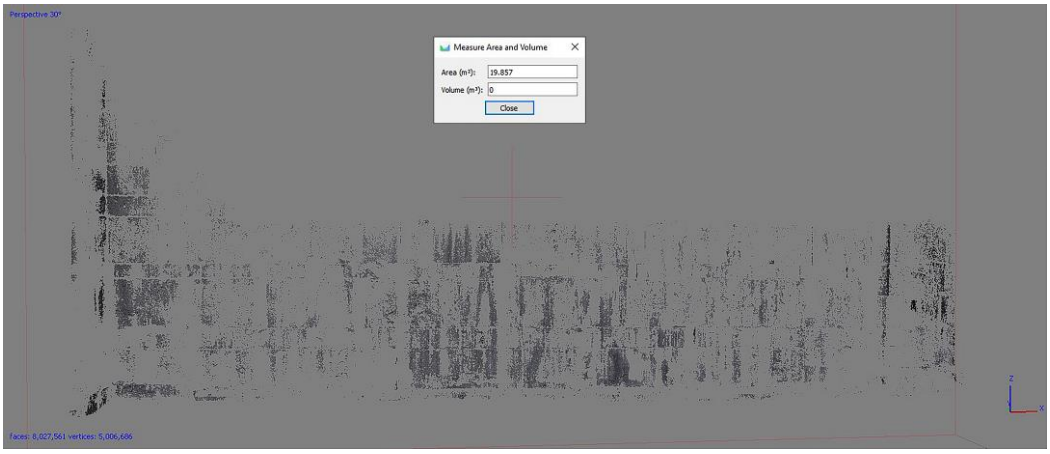

Fig. 56 Example of extracting surface measurements from 'Patina' mesh.

iii. **Texture-based Classification with ML algorithm (Fast Random Forest)**

To evaluate the comparative reliability of various automated approaches for recognising superficial alterations on stone surfaces, image processing procedures were applied to the three-dimensional model of the southwest façade of the

Unfinished Church. These procedures focused on texture characteristics linked to manifestations of degradation.

For this purpose, after generating a textured polygonal mesh of the façade using Metashape Pro® software, a UV mapping was extracted. This mapping involves converting the three-dimensional model, described by points with x-y-z coordinates, into a two-dimensional surface described by points with u-v coordinates.

In practice, the letters U and V indicate the axes of a Cartesian coordinate system, within which the solid model's polygons are arranged to enable subsequent analyses on raster images. In this specific case, the UV mapping of the façade (Fig. 57) was imported into an open-source digital image processing software, such as Open Source FIJI®, based on the Java programming language.

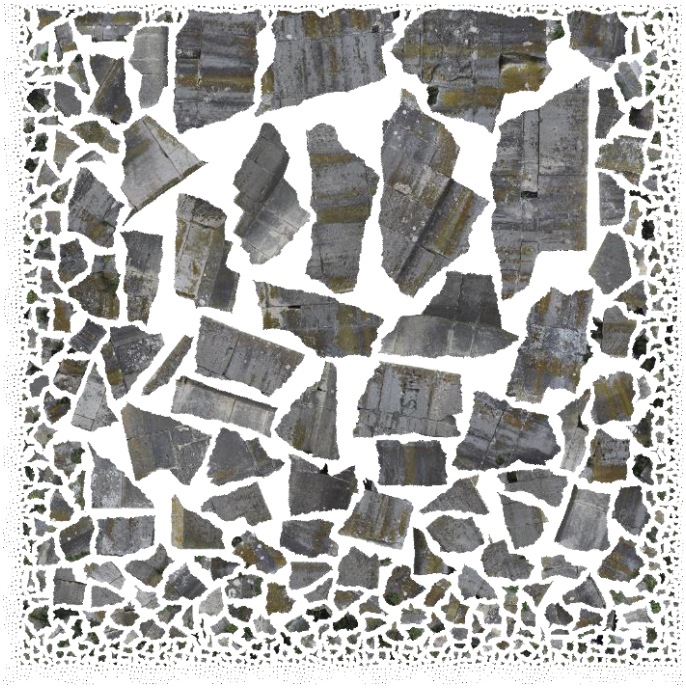

Fig. 57 UV mapping relating to the 3D model of the church.

Before entering the supervised classification phases, a reference scale was established by inputting identical distances measured between targets on the Metashape-processed model. This step is crucial as it establishes a correlation between image pixels and the authentic reference scale of the physical model.
In this case, the software automatically converted the 1024*1024 pixel RGB image into an image with the same radiometric characteristics but in a metric scale of 10.68*10.68 meters.

To perform the texture-based classification, a plugin named Trainable WEKA (Waikato Environment for Knowledge Analysis) Segmentation (Arganda-Carreras *et al.*, 2017) (see Fig. 58) was utilised within the software FIJI (Schindelin *et al.*, 2012), offering a suite of visualisation tools and algorithms for data analysis and predictive modelling. Additionally, it includes user-friendly graphical interfaces for convenient access to these functionalities and supports numerous standard data mining tasks, such as data preprocessing, clustering, classification, regression, visualisation, and feature selection.

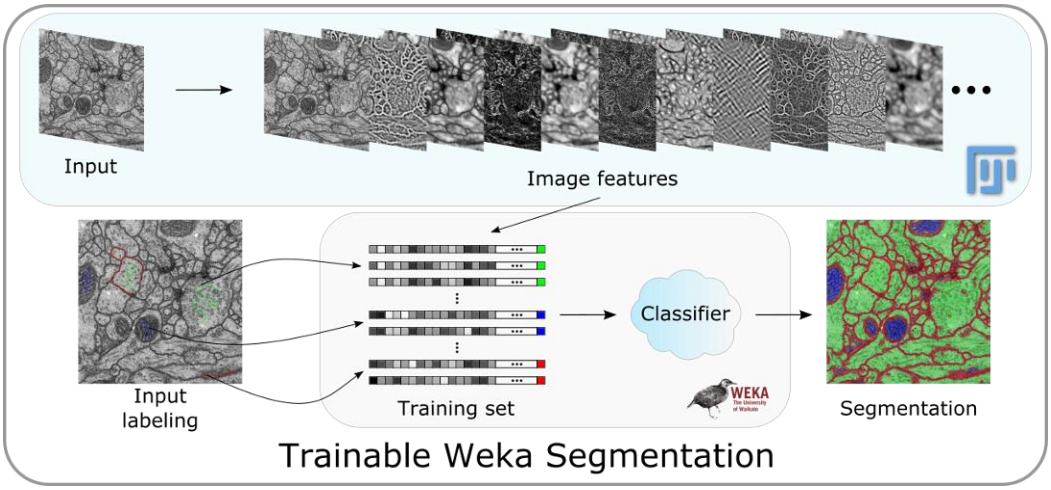

Fig. 58 Trainable WEKA Segmenation Workflow ((Arganda-Carreras et al., 2017).

WEKA's 2D features for training encompass diverse image processing methods, including filters like blur, Sobel, Hessian, and more. These techniques enhance images, highlight differences (e.g., Difference of Gaussians), emphasise membrane-like structures (Membrane Projections), and perform statistical operations.
Filters like Anisotropic Diffusion, Bilateral Filter, Lipschitz Filter, Kuwahara Filter, and Gabor Filter contribute to noise reduction, edge preservation, and texture detection. Additionally, Derivatives, Laplacian, Structure Filter compute high-order derivatives, Laplacian, and structure tensor eigenvalues. Entropy and Neighbours measure image entropy and create features by shifting images. Grayscale images include the original, while colour images consider features like Hue, Saturation, and Brightness.

The default classifier in WEKA is the Fast Random Forest (FRF), a multi-threaded machine learning algorithm based on decision trees that belongs to the Random Forest (RF) family. Random Forest is an ensemble of decision trees, each trained on a random subset of the training data, and its prediction is obtained by aggregating the predictions of the individual trees.
FRF initialised with 200 trees and 2 random features per node is designed to be computationally more efficient than RF, and this implementation aims to reduce training time while maintaining good predictive performance.

However, the exact specifications of the implementation may vary depending on the specific version of WEKA and any modifications made by users or developers.

For this purpose, the tool required the operator to provide training and learning data for each type of texture of interest, identified with a label. This involved manually selecting small image regions of interest (ROI) for training purposes.
Overall, these steps facilitated the execution of a comprehensive analysis aimed at automated recognition and classification of surface alterations based on texture characteristics in the three-dimensional model of the Unfinished Church's southwest façade. The operation was conducted for six types of alterations – Patina, Biological Colonisation, Efflorescence, Plant, No Pathology, Background – each described by ten representative regions (Fig. 59).

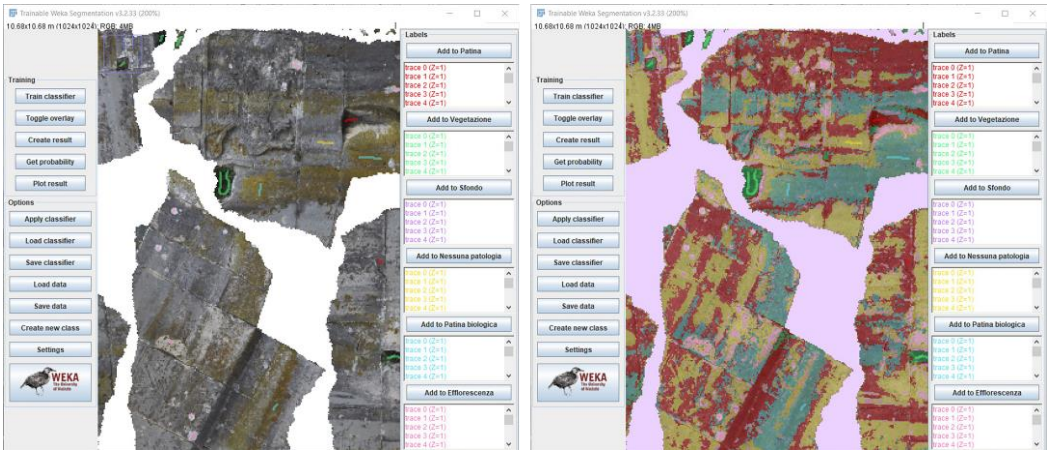

Fig. 59 Attribution (on the left) and processing (on the right) of training data: Patina (red), Biological Colonisation (blue), Efflorescence (pink), Plant (green), No Pathology (yellow), Background (purple).

The 32-bit UV mapping, obtained through subsequent automated classification, can be converted to 8-bit for easier manipulation (Fig. 60).

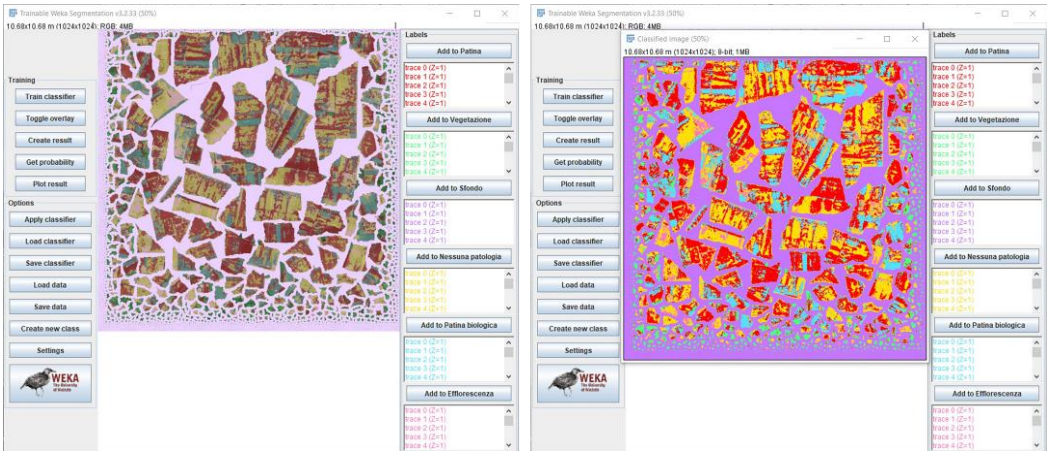

Fig. 60 32-bit pre-classification (on the left) and 8-bit post-classification (on the right) UV mapping.

However, to estimate the surface development of different forms of alteration, probability maps were generated within the software (Fig. 61). These maps highlight, based on thresholds iteratively established by the operator, the portions of the 32-bit UV mapping attributable to each degradation type.

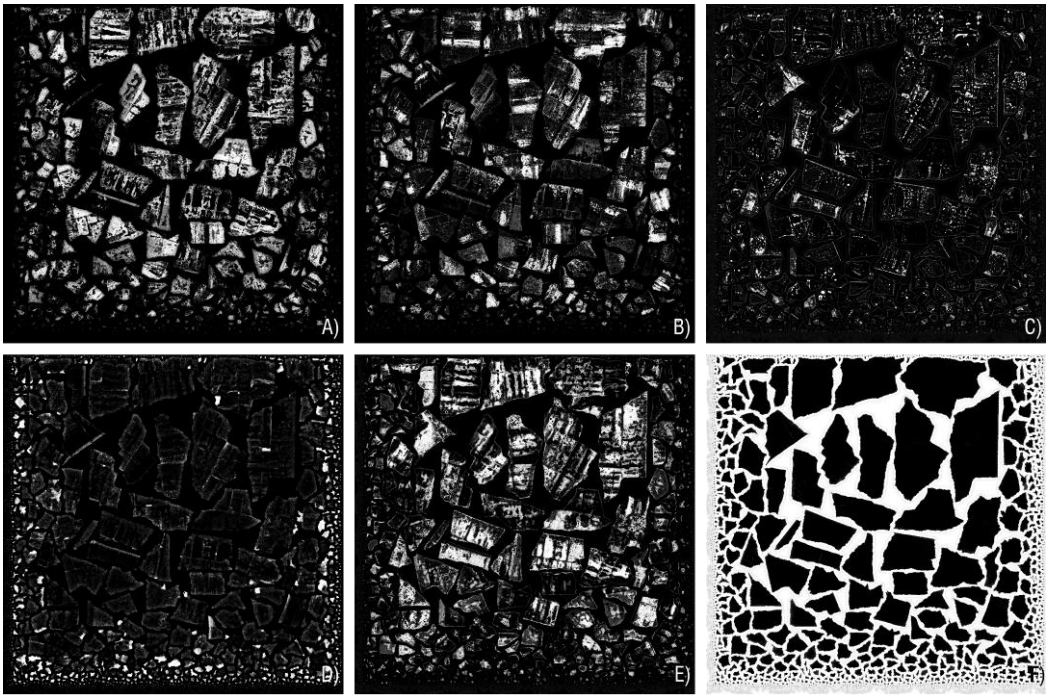

Fig. 61 Probability maps of the segmented classes: A) Patina; B) Biological Colonisation; C) Efflorescence; D) Plant; E) No Pathology; F) Background.

A red colour was employed to highlight selected degradation particles against a black background. Additionally, a method of converting the image into black and white binary was chosen (Convert Stack to Binary) using masks with an inverse Look-Up Table (LUT) (white: 0; black: 255).

The algorithm used to calculate the threshold then separates the image into objects and background based on a trial threshold, computing the mean of pixels above and below the threshold [6]. By incrementally increasing the threshold, the process is repeated until the threshold exceeds the obtained mean.

$$\text{threshold} = \frac{\text{average background} + \text{average objects}}{2} \qquad \textbf{[6]}$$

Subsequently, the surface areas related to every particle of the degradation patterns (Fig. 62) were calculated setting the minimum (0) and maximum (infinity) values of the pixel areas converted to m^2 and excluding unwanted parts of the image by means of circularity values.

Object circularity can be calculated using the formula [7]:

$$\text{circularity} = 4\text{pi}*(\text{area}/\text{perimeter}^2) \qquad [\,7\,]$$

A circularity value of 1.0 signifies a perfect circle, while a decreasing value approaching 0.0 suggests a polygon with increasing elongation.

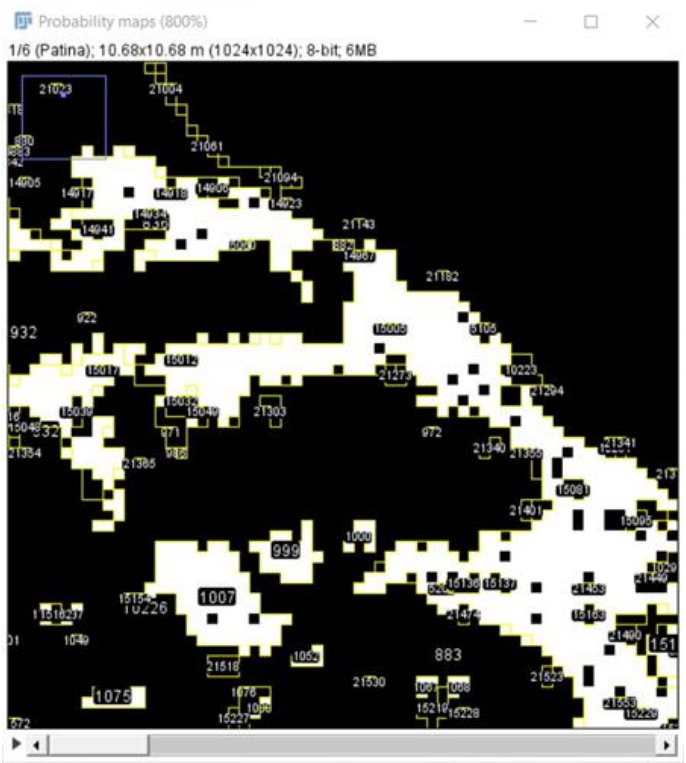

Fig. 62 Example of particle analysis applied to the segmented class ‘Patina’.

iv. **Texture-based Classification with ML algorithm (K-Nearest Neighbours)**

In addition to the Fast Random Forest method, an exploratory work on the study of degradation phenomena was carried out within the MATLAB® work environment. This involved the development of a novel code based on the K-Nearest Neighbours algorithm, specifically crafted for the classification of UV textures extracted from the 3D model of the church.

Specifically, the K-Nearest Neighbours algorithm, which assesses the Euclidean distance in an *n*-dimensional space between the target and elements in the training data. Here, *n* is determined by the number of object attributes employed during classification. This method exhibits greater robustness compared to a traditional nearest-neighbour classifier, as it considers the majority vote of the *k*-nearest distances to determine the target's class.

The K-NN approach proves less susceptible to outliers and noise in the dataset, typically yielding more accurate classification results than traditional nearest-neighbour methods.

In this case, the algorithm is based on the Euclidean distance in the 'ab' colour space and makes use of K-NN with $k=1$ for classification. The coloured representation of the classified image and the scatter plot provide a visualisation of the results.

The methodology used for the code is as follows:

- **Visualisation and definition of the source image size**
    - The script reads and displays the source RGB colour scale image (in red, green, and blue).
    - It also defines the image size in pixels and its corresponding actual size in meters.

The source RGB (red, green, blue) colour scale image is visualised and its pixel dimensions are defined, providing insights into spatial resolution. Additionally, the real-world dimensions in meters are specified, establishing a crucial link for meani ngful interpretations of actual object sizes in the image.

The image discussed is identical to that employed in the previous methodology involving the Fast Random Forest (Fig. 57).

- **Selection of regions of interest (ROI) for each class:**
    - The user selects at least 10 example regions for each class directly from the image.
    - The example regions are stored in 'sample_regions', a cell of logical arrays indicating the positions of the selected regions.

Region of Interest (ROI) designates a specific area within an image chosen for in-depth analysis or processing in contrast to the remainder of the image (Fig. 63).

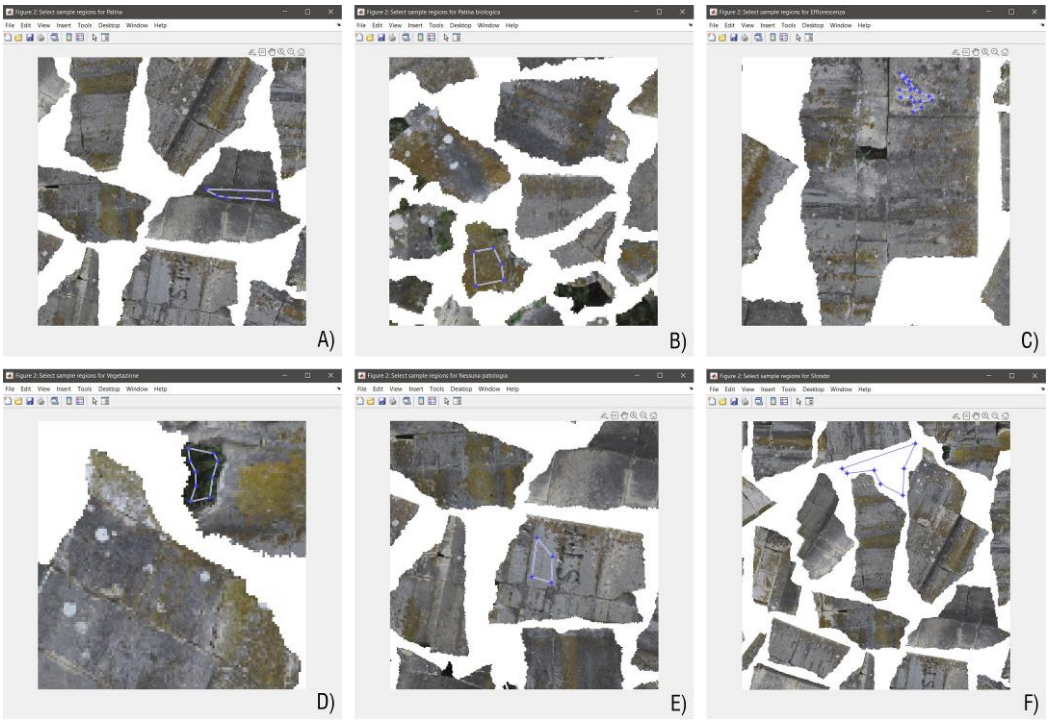

Fig. 63 Examples of region of interest (ROI) for each class: A) Patina; B) Biological Colonisation; C) Efflorescence; D) Plant; E) No Pathology; F) Background.

Allowing the user to manually select example regions enables explicit knowledge acquisition about the nature of different UV texture classes. This is particularly useful when class features are complex or not easily mathematically modeled.

In the code, ten regions of interest (Fig. 64) from an image were manually selected and employed for the k-NN algorithm to characterise each class. This strategy aims to offer a comprehensive representation of class features, particularly beneficial when dealing with intricate classes.

Nonetheless, consideration should be given to the overall dataset size, and performance assessment on a test dataset is essential to optimise the balance between detail and generalisation.

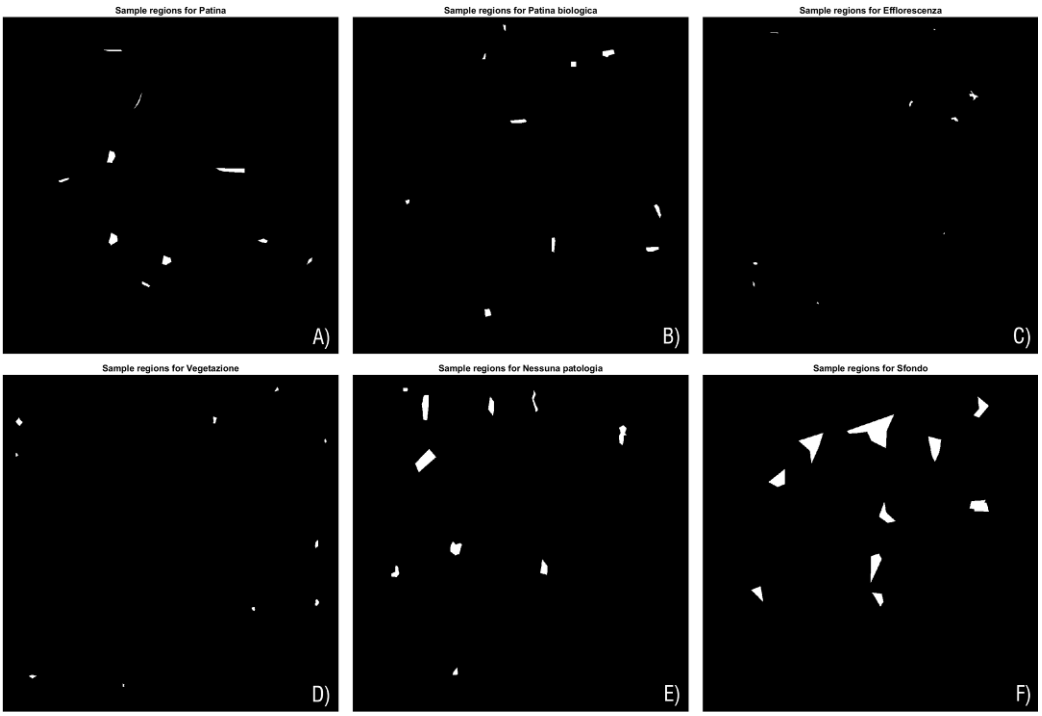

Fig. 64 Sample region for each class: A) Patina; B) Biological Colonisation; C) Efflorescence; D) Plant; E) No Pathology; F) Background.

- **Conversion of the RGB image to the L*a*b* colour space (CIELAB):**
    - The input RGB (Red, Green, Blue) image is converted into an image in the 'Lab' coordinate system.
    - The mean 'a*' and 'b*' values are calculated for each class using the selected example regions

Converting the 'RGB' image to the 'Lab' colour space is chosen to enhance the algorithm's robustness to lighting variations. In the Lab space, the 'L' channel represents brightness, while 'a' and 'b' represent chromatic components. This separation improves the algorithm's ability to capture colour variations by separating colour information from brightness.

- **Pixel classification using K-NN *(k=3)*:**
    - For each pixel in the image, 'a*' and 'b*' coordinates are calculated.
    - The Euclidean distance between the pixel coordinates and the calculated means for each class is computed.
    - The pixel is classified as belonging to the nearest K-NN class *(k=3)*.

When using the k-NN algorithm, a class is assigned to a data point based on the majority class among its 'k' nearest neighbours in the training dataset. Therefore, specifying *k=3* means that during the classification of a given point, the k-NN algorithm considers the labels of the three instances closest to that point and assigns the most common class among these three.

With *k=3* strikes a balance between local sensitivity *(k=1)* and increased robustness against noise *(k>1)*, making the algorithm more suitable for local classification problems where local features are crucial, enhancing the model's ability to discriminate between classes.

- **Visualisation of the classified image:**
    - A coloured image is generated based on the classes assigned to the pixels.

Generating a coloured image in the RGB colour space (Fig. 65) allows for easy visual interpretation of results and facilitates saving. This is useful for quickly inspecting algorithm performance and understanding how classes are assigned in different regions of the image.

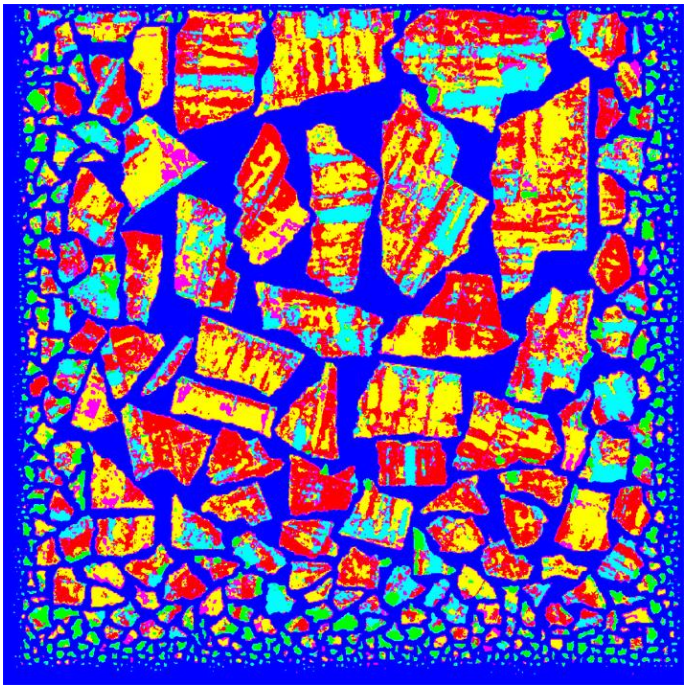

Fig. 65 Classified image in the RGB colour space: Patina (pure red) [255 0 0]; Biological Colonisation (cyan) [0 255 255]; Efflorescence (magenta) [255 0 255]; Plant (pure green) [0 255 0]; No Pathology (yellow) [255 255 0]; Background (pure blue) [0 0 255].

- **Scatter plot in the ‘ab’ colour space:**
    - A scatter plot is created showing the distribution of pixels in the ‘ab’ space with different colours for each class.
    - X-axis (‘a*’ values): Represents the values of the ‘a*’ chromatic component in the Lab colour space.
    - Y-axis (‘b*’ values): Represents the values of the ‘b*’ chromatic component in the Lab colour space.

The scatter plot in the ‘ab’ space (Fig. 66) provides a compact visualisation of pixel distribution for each class, aiding in identifying any overlaps or clear separations between classes in the Lab colour space. The position of the point on the ‘a*’ and ‘b*’ coordinates reflects its location in the Lab colour space, and the colours of the points are determined by the classes assigned during classification.

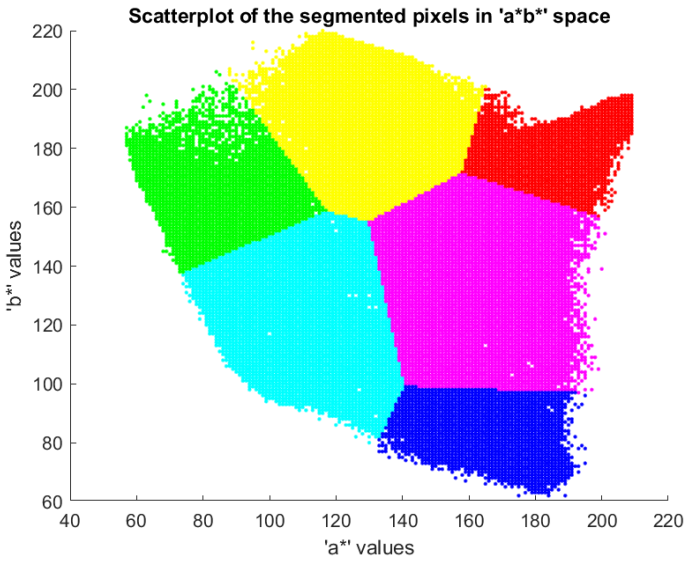

Fig. 66 Scatter plot of the segmented pixels in ‘a*b*’space and visualisation in ‘RGB’ space: Patina (‘r’); Biological Colonisation (‘c’); Efflorescence (‘m’); Plant (‘g’); No Pathology (‘y’); Background (‘b’).

In this context, the interpretation of the scatter plot is as follows: a red point corresponds to a region classified as 'Patina', a cyan point represents 'Biological Colonisation', a magenta point signifies 'Efflorescence', a green point represents 'Plant', a yellow point signifies 'No Pathology', and a blue point stands for 'Background'. These colour assignments are based on the defined colour mapping-

The scatter plot results showcase distinct separations among points representing different classes in the Lab colour space, with negligible overlapping. This observation indicates that the classification algorithm, relying on the 'a*' and 'b*' features, has proven highly effective in discriminating between diverse pathology categories and backgrounds in the image, with minimal instances of overlap.

- **Calculation and visualisation of percentage areas:**
    - The number of pixels and area in square meters are calculated for each class.
    - Percentage areas relative to the total area are displayed on the screen.

Calculating percentage areas provides quantitative information about the spatial distribution of different classes in the image. This information is valuable for assessing the relative prevalence of the various pathologies under consideration.

4.1.6 Results of the Degradation Analysis

Here are the outcomes of the degradation mapping, presented in terms of graphic representation, surface area and percentage relative to the total area. Therefore, data from the three proposed methods are compared: Point Cloud (PC) Colour-based Texture-Based with FRF, and Texture-based with K-NN. Showing the classified point cloud and the polygonal meshes on which the UV textures classified by the two methods were reprojected (Fig. 67 and Fig. 68). To enhance the visualisation of the results, uniform colours were assigned to the classes across all

the three methodologies: ‘Patina’ (pure red), ‘Biological colonisation’ (cyan); ‘Efflorescence’ (magenta); ‘Plant’ (pure green); and ‘No Pathology’ (pure grey).

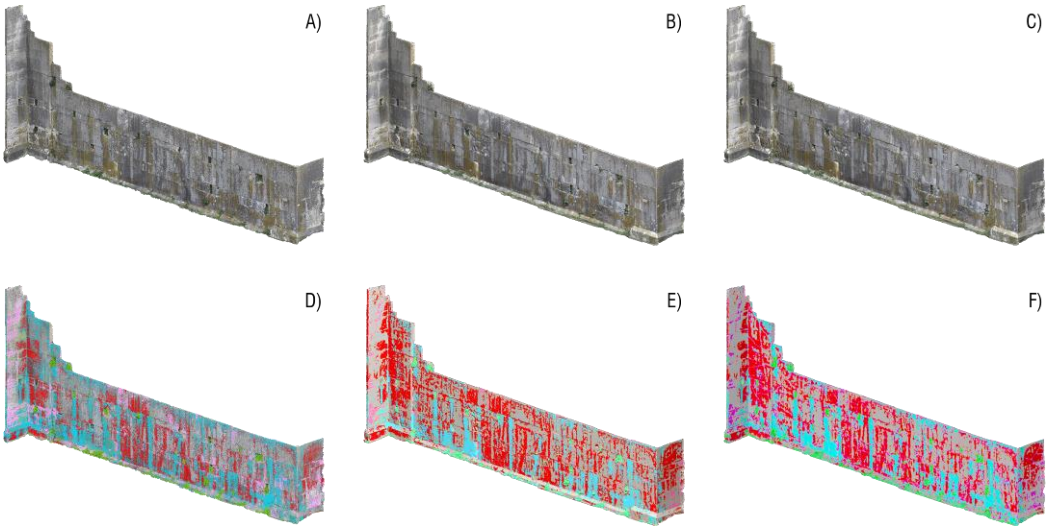

Fig. 67 Visualisation of the starting data (point cloud or mesh) and the final classified data: A) Point cloud; B-C) Poygonal Mesh; D) Classified Point cloud; E) Classified 3D Mesh with FRF; F) Classified 3D Mesh with K-NN.

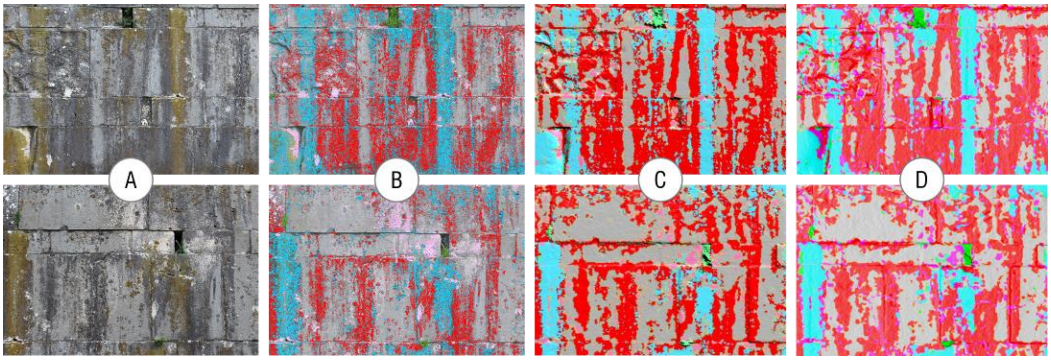

Fig. 68 Displaying details: A) Picture; B) Classified Point cloud; C) Classified 3D Mesh with FRF; Classified 3D Mesh with K-NN.

Significant qualitative strides have been made in recognising patterns corresponding to various degradation phenomena, stemming from the classification derived from the dense point cloud. It's worth noting that the classification, though robust, is never entirely unequivocal. Executing the process with diminished accuracy and a reduced dataset may introduce errors in representing the segmented region across multiple labelled classes.

With the texture-based approach implemented via both FRF and K-NN, the results visually align with the initial approach but face challenges, particularly in accurately identifying the Efflorescence phenomenon. There's a potential for confusion, albeit minimal, with substances of plant origin secreted by lichens within Biological Colonisation. Notably, the Patina and Plant phenomena are more precisely identified, especially with the application of the FRF method.

Comparing the three different mapping approaches shows significant variations in the estimates of the areas occupied by the different types of degradation.

Tab. 3 Results of the degradation mapping with the Point Cloud Colour-based approach.

Type of degradation	Surface area (m^2)	Percentage over total area (%)
Patina	19.86	33.03
Biological Colonisation	10.02	16.67
Efflorescence	5.36	8.92
Plant	5.59	9,30
No pathology	19.29	32.09

Tab. 4 Results of the degradation mapping with the FRF Texture-based approach.

Type of degradation	Surface area (m^2)	Percentage over total area (%)
Patina	20.02	33.33
Biological Colonisation	10.26	17.08
Efflorescence	5.56	9.27
Plant	5.75	9.58
No pathology	18.47	32.75

Tab. 5 Results of the degradation mapping with the K-NN Texture-based approach.

Type of degradation	Surface area (m^2)	Percentage over total area (%)
Patina	18.10	30.15
Biological Colonisation	12.21	20.33
Efflorescence	4.45	7.42
Plant	5.22	8.68
No pathology	20.07	33.42

About the Point cloud colour-based approach (Tab. 3), 'Patina' emerges as the predominant category, occupying 33.03% of the total surface. This percentage is closely followed by 'No Pathology', representing 32.09% of the area. A balanced distribution is observed among various degradation types, with 'Biological Colonisation' and 'Efflorescence' accounting for 16.67% and 8.92% of the surface, respectively. 'Plant' is noteworthy, covering 9.30% of the area.

With the FRF Texture-based Approach (Tab. 4), despite 'Patina' remaining dominant at 33.33%, a significant percentage redistribution is evident compared to the colour-based approach. 'Biological Colonisation' shows a slight increase, reaching 17.08%, while 'Efflorescence' and 'Plant' both see increments to 9.27% and 9.58%, respectively. 'No Pathology' slightly decreases to 32.75%.

The K-NN Texture-based Approach (Tab. 5) introduces considerable variations in surface estimations. 'Biological Colonisation' becomes the dominant category at 20.33%, surpassing 'Patina' (30.15%). 'Efflorescence' undergoes a significant decrease to 7.42%, while 'Plant' and 'No Pathology' maintain their relevance at 8.68% and 33.42%, respectively.

The comparison across the approaches (Fig. 69) reveals the the Point cloud colour-based approach shows a fairly uniform distribution among degradation categories, with 'Patina' and 'No Pathology' in equilibrium.

The FRF approach highlights an increase in the estimation of 'Plant' and a redistribution of other categories compared to the colour-based approach.

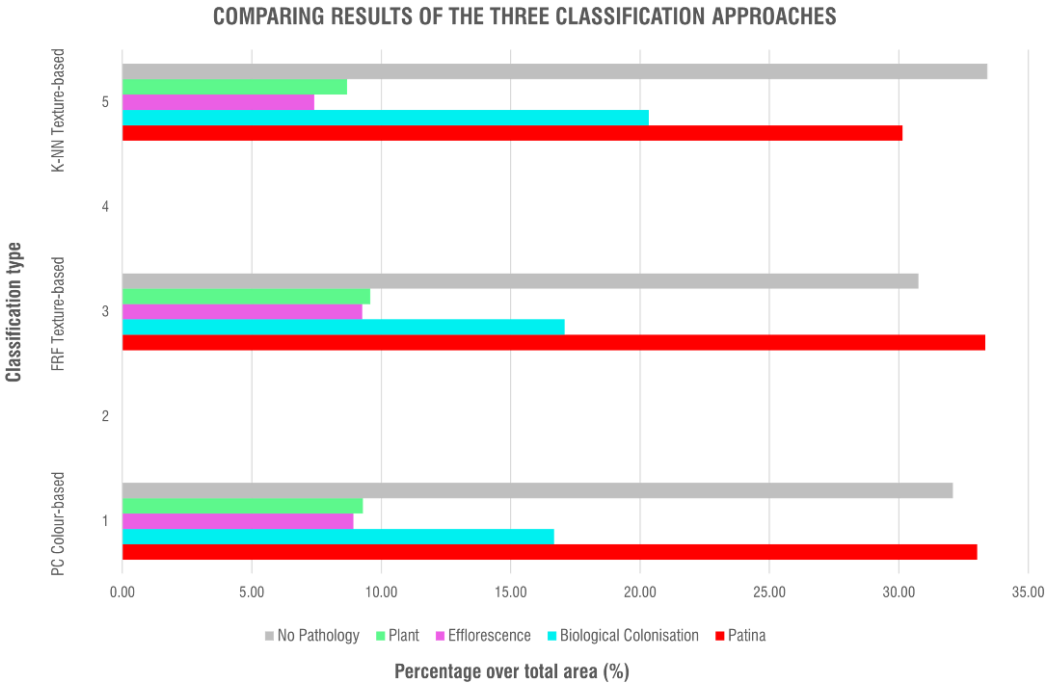

Fig. 69 Comparative analysis of three Classification approaches based on the percentage of occupied area throughout the entire wall.

The K-NN approach presents a surprising variation, with 'Biological Colonisation' emerging as the predominant category and significant shifts in other surface estimations.

Concluding the analysis, a detailed examination of the data highlights how the chosen mapping approach significantly influences surface estimations for different degradation types. Understanding these distinctions is pivotal for precise interpretation, underscoring the importance of selecting an approach tailored to the specific analysis requirements.

4.1.7 Concluding Observations

The research adopted a cognitive approach intricately connected to the mode and acquisition of an extensive array of data in various formats and processing methods. The aim was to develop a standardised protocol for seamlessly integrating architectural surveys. The primary focus of the experimentation was an application closely tied to three-dimensional modelling of the built environment, representing a digital and formal reproduction that serves as a preliminary step for specialised architectural or diagnostic studies. The comparison of the acquired data not only facilitated the evaluation and verification of morphometric accuracy but also considered the merits and drawbacks of diverse acquisition techniques.

The result was a meticulous and reliable 3D survey of the monument, designed not only for technical users but also with the potential of being implemented in digital experiences. This aspect gains particular significance in the current context of the COVID-19 pandemic, enabling tourist visitors to access the benefits of guided virtual tours with just a few clicks.

On the other hand, the implementation of semi-automated procedures for extracting information related to colour properties and texture characteristics from photorealistic three-dimensional representations of architectural surfaces represents a highly valuable and effective tool for semantic classification. This approach is not limited to the classification of degradation forms, as demonstrated in the presented case, but extends to encompass materials, construction techniques, and surface finishes.

However, the operator's oversight remains essential, both in the initial selection of data to establish the knowledge base for subsequent analysis and in validating results through direct comparisons between computer-generated mappings and expert observations from a surveyor.

This preliminary assessment is critical to determining the capacity of colour and/or texture to meaningfully and distinctively describe each category or type of interest compared to others within the same classification. Assuming a positive evaluation, these processing procedures for segmenting coloured point clouds and textured

polygonal meshes can significantly streamline the time and resources required for thematic mapping. Moreover, they have the potential to generate innovative digital formats compatible with further processing tools.

4.2 Automated Processes for Preparing a Point Cloud within the Scan-to-BIM Approach

In the Architecture Engineering Construction (AEC) industry, particularly within the context of *as-built* procedures, the modelling process of Building Information Modelling (BIM) containers introduces challenges in the interpretation of spatial arrangements and building components. These challenges may give rise to difficulties in representation and understanding.

To this end, Scan-to-BIM methods, integrating digital survey phases with subsequent BIM Authoring phases and catering to various expert disciplines, have gained popularity as a solution to these issues. While this integration has expedited the collection and registration of architectural environments, it has also led to the use of increasingly complex and heavy point clouds.

These point clouds often pose challenges due to file sizes and the inclusion of points irrelevant to subsequent modelling phases. Moreover, the demand for producing highly optimised point clouds tailored to specific information needs, which can vary from one project to another, is becoming more prevalent in interdisciplinary modelling.

To effectively employ a point cloud in BIM authoring processes, a range of manual and automatic methods have been researched and implemented. Manual techniques, albeit labor- and resource-intensive, involve visually classifying the building's constituent parts [(Pocobelli *et al.*, 2018; Adekunle, Aigbavboa and Ejohwomu, 2022).

Conversely, labelling and recognition algorithms facilitate the classification of recognised features through various automated procedures, such as identifying primitive geometries, comparing geometric features, and employing semantic segmentation through artificial intelligence (Fiorucci *et al.*, 2020; Pierdicca *et al.*, 2020).

In the context of this study, an evaluation is sought for a workflow aimed at optimising the digital survey for Scan-to-BIM purposes through the implementation of

a mixed manual-semi-automatic segmentation method (Tavolare, Buldo and Verdoscia, 2023).

As a case study, a disused industrial building located on the outskirts of Milan, constructed in the 1960s, featuring a frame structure of reinforced concrete pillars and beams, has been selected (Fig. 70).
Spanning four above-ground floors and a basement, characterised by spacious windows and flat ceilings, the building can be deemed a typical scenario for Scan-to-BIM operations in the engineering field.

Fig. 70 Point cloud perspective view of the façade (Milan).

4.2.1 Methodology

In the initial phase, partitioning criteria were applied following the UN EN ISO 19650 and UNI 11337 standards, utilising the Homogeneous Spatial Scope (ASO) subdivision method. This facilitated the segmentation of the point cloud, enhancing the overall efficiency of the process.

To streamline BIM authoring processes effectively, the methodology continued with a meticulous denoising approach utilising the SOR algorithm, addressing environmental interferences and refining the point cloud. Subsequently, the workflow integrated subsampling through voxelisation to strategically reduce point cloud density, a pivotal step in managing the abundance of surveying data.

Semantic classification, facilitated by the CANUPO algorithm, played a crucial role in distinguishing between windows and walls, enhancing the categorisation of the point cloud. Simultaneously, the RANSAC algorithm contributed to probabilistic geometry recognition, enabling the identification of primitive structures like pillars, floors, ceilings, and walls.
The closing phase involved the customisation of parameters to tailor the export process, ensuring alignment with OpenBIM standards, notably ISO 19650. This comprehensive and structured workflow aimed at optimising the point cloud for efficient BIM authoring purposes, catering to the complexities of digital surveying challenges.

i. **Homogeneous Spatial Scope Segmentation**

In the early stages of the analysis, a comprehensive exploration was conducted into the modelling process of building elements, encompassing entities and classes within the existing OpenBIM coding schemes. Additionally, the investigation extended to more intricate geometries, incorporating advanced Non-Uniform Rational Basis-Splines (NURBS) integration.

For architectural structures of heightened complexity, the strategic application of partitioning criteria within the BIM Management domain, aligned with established standards like UN EN ISO 19650 and UNI 11337, assumed a critical role.

The introduction of a subdivision based on the Homogeneous Spatial Scope (HSS)[5], illustrated in Fig. 71, has proven to be an essential strategy.

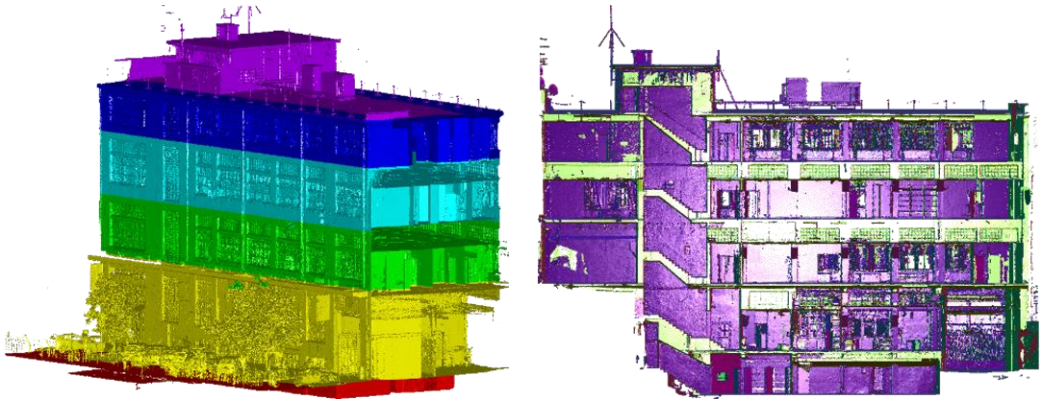

Fig. 71 Height subdivision of the point cloud (on the left) and longitudinal section (on the right).

This method facilitated the systematic segmentation of the point cloud based on reference height levels, offering a structured framework that proved advantageous, particularly in addressing the challenges associated with intricate architectural formations.

[5] The informational structure of space is divided into the following three terms:

'Homogeneous Functional Scope' (HFS), also known as Ambito Funzionale Omogeneo (ASO) in Italian: Represents the spatial delimitation, for both surfaces and volumes, of a natural or built environment. This term refers to a system of homogeneous functional scopes identified based on their common correspondence to a characteristic aggregating function.

'Homogeneous Spatial Scope' (HSS), also known as Ambito Spaziale Omogeneo (ASO) in Italian: Indicates the spatial delimitation, for both surfaces and volumes, of a natural or built environment. In this case, it refers to a set of spaces identified based on their common correspondence to a characteristic aggregator.

'Space': Represents the spatial delimitation, for both surfaces and volumes, of a natural or built environment. This term refers to the common correspondence of that space to its own characteristic function.

This tailored methodology facilitated a nuanced and customised approach in the subsequent stages, aligning the modelling process with the distinct requirements of diverse building elements. It laid the groundwork for the ensuing denoising and subsampling phases, enhancing the overall efficiency of the BIM authoring process.

ii. **Denoising Process with the SOR filter**

Through the emission of an infrared laser beam sensitive to potential interference from environmental factors like temperature and humidity or material conditions, laser measuring activities are conducted during digital surveying.

This behavior can result in the presence of orphan points in close proximity to the measured element, introducing complexity to the geometric interpretation of the element and posing challenges in the registration, alignment, and calculation phases of the point cloud (Mugner and Seube, 2019).

Various algorithms have been developed to automatically detect and eliminate such points, employing diverse approaches. Some methods focus on the identification of geometric descriptors, while others leverage recent advancements in deep learning applications (Hu *et al.*, 2021) and others rely on the triangulation approach of the Ball-Pivoting Algorithm (BPA) (Bernardini *et al.*, 1999).

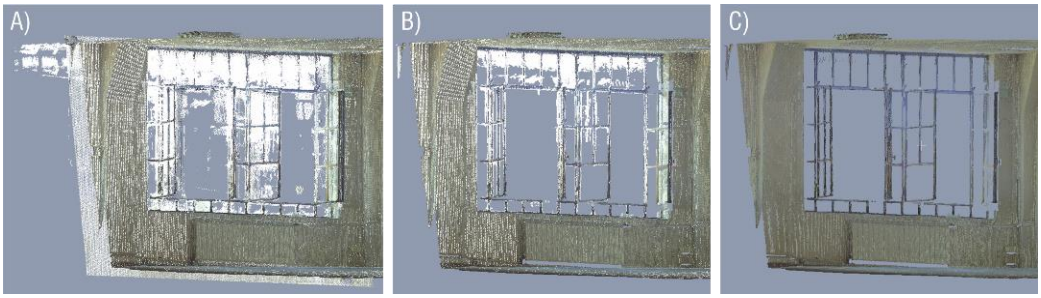

Fig. 72 A) Raw point cloud; B) Cleaned-up point cloud using the SOR filter; C) Optimised point cloud with the RGB colour range filter with 1% variation.

In the quest for a comprehensive approach, the Statistical Outlier Removal (SOR) algorithm, using CloudCompare software, has been chosen for implementation (refer to Fig. 72). This approach is further complemented by the integration of other techniques (Nazeri and Crawford, 2021) (Cheng *et al.*, 2021) to augment its effectiveness.

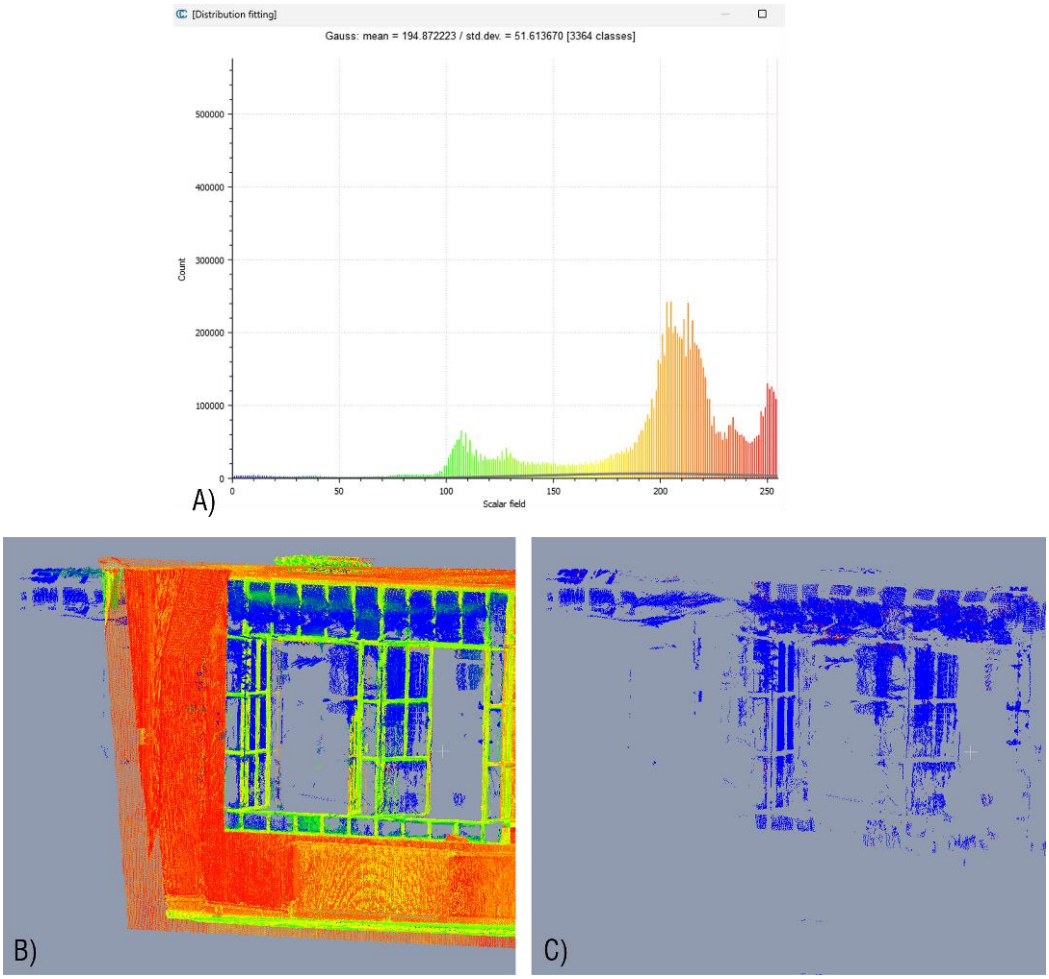

Fig. 73 Gaussian distribution based on scalar reflectance value for analysing point cloud noise generating by the glazing: A) Distribution fitting; B) Point cloud with scalar reflectance; C) Point cloud noise (blue colour).

The average distance between each point and its neighbours is calculated. Points with mean distances falling outside a predefined range are identified, labelled as outliers, and subsequently removed from the dataset, taking into account the resulting Gaussian distribution with a mean and standard deviation.

While more intricate semi-automated methods can be employed to refine the outcomes of this algorithm, they necessitate more complex parameterisation. In this case, an additional filtering method based on the RGB value of the points was implemented, excluding points with a value of 255,255,255 and a variance within 1%, addressing the noise generated in proximity to the windows.

This method is suitable only for environments without objects of the same colour, and the scan must be conducted in the RGB scale. In uncoloured point clouds, a filtering technique based on the scalar reflectance value stored in the file can be utilised.
By examining the distribution of scalar values assigned to the points, it can be inferred that the noise generated by glazing exhibits a sub-threshold reflectance value, falling within the range of blue colours (Fig. 73).

iii. **Sub-sampling Process with Voxelisation**

While capturing a comprehensive and precise point cloud during the surveying process, the abundance of points collected can pose limitations and challenges when utilising modelling tools. To address this, consideration is given to a subsampling (decimation) phase, often relying on mesh- and point-based approaches.

The first method involves polygonal geometric simplification, where three-dimensional meshes are created by interpolating the points within a specific area (Garland and Heckbert, 1997). In contrast, the second method immediately applies simplification techniques to the point cloud. In the latter approach, simplified decimation is commonly employed, utilising a grid with three-dimensional cells to identify points within a certain distance. However, this method may overlook the varying weight, concentration, and importance of different regions within point clouds (Fan and Atkinson, 2019).

A more intricate approach involves resample functions, changing points within each cell to the grid's center of gravity (Sim, Lee and Kim, 2005). While this method alters the spatial positioning of surveyed shapes, it may diminish the elements' recognisability.

For this purpose, after denoising, voxelisation of the point cloud was performed, in Python environment, to reduce the density of the point cloud. This comprehensive voxelisation process (Poux and Billen, 2019) is sub-divided into several sections:

- Grid Structure Initialisation: The inaugural stride involves the creation of a grid structure enveloping the point cloud. This process commences by computing the bounding box, an all-encompassing spatial enclosure for the point cloud. Subsequently, the bounding box metamorphoses into small cubic grids known as voxels. The dimensions of these voxels are determined, either by equating their length, width, and height, or by specifying the desired voxel count along each direction of the bounding box. In this case, a voxel size of 10 cm per side was employed (Fig. 74).

- Voxel Indexing and Point Assignment: Each small voxel undergoes scrutiny to ascertain the presence of one or more data points. Voxels containing data points are preserved, and the indices of the associated points are meticulously documented. The script orchestrates an adept return of designations for each non-empty voxel, employing indices for operational simplicity and efficiency. Unique values rooted in integer indices for each point are identified and subsequently sorted for later linkage with the corresponding voxel index.

- Computation of Voxel Representatives: The conclusive phase involves the meticulous computation of representatives for each voxel. Two contenders vie for this role: the centroid and the point closest to the centroid, discerned through the application of Euclidean distances. An iterative loop navigates

through each non-empty voxel, dutifully updating the voxel_grid dictionary with the catalogue of enclosed points.

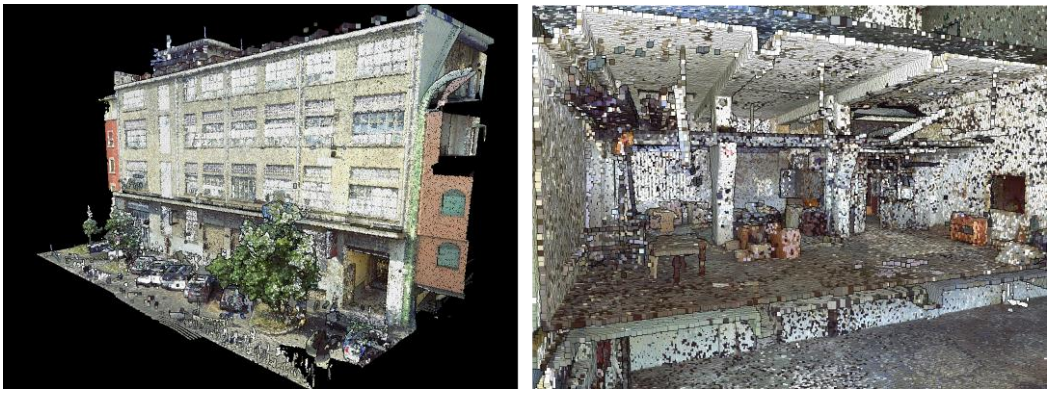

Fig. 74 Voxelisation of the point cloud: external view (on the left) and internal view of the building (on the right).

iv. **Classification with CANUPO and Segmentation with RANSAC**

An alternative to voxelisation, especially when data resolution is crucial for automation in BIM model construction, can be the process of classification or segmentation of point clouds.

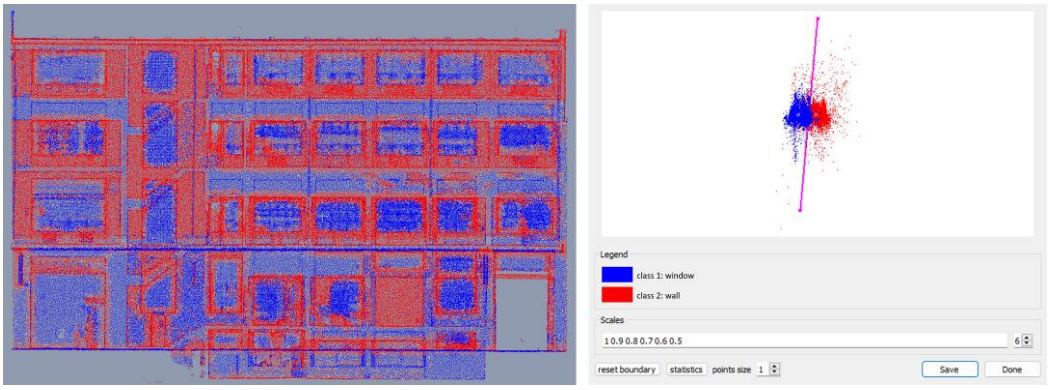

Fig. 75 Use of the CANUPO algorithm for classifying the windows and walls of the point cloud.

In this case, the CAractérisation de NUages de POints (CANUPO), a binary parametric semantic classification algorithm, was applied to segment the point cloud into two subcategories, classifying them as windows or walls (Fig. 75).

This algorithm facilitates point classification by identifying the geometric properties of the space surrounding each point, employing various scales to discern features (Brodu and Lague, 2012). While this approach is limited to the identification of elementary object categories in the scene, it appears to be a simple and initial approach readily available in applications like CloudCompare.

Furthermore, the use of model-fitting algorithms such as RANdom SAmple Consensus (RANSAC) capable of probabilistically finding geometries that interpolate points belonging to primary solids like cylinders, planes, etc., allows for the identification of points associated with primitive geometric structures such as pillars, floors, ceilings, and walls (Fischler and Bolles, 1981; Oh *et al.*, 2021).

The application of this algorithm necessitates the configuration of specific parameters, such as the threshold distance between points and identified surfaces, the maximum number of points that can belong to the surface (a value dependent on surface resolution and extent), and the probabilistic value. These values require the operator to conduct a preliminary analysis based on the point cloud properties and target geometries.

For the case study, the point density distribution within a reference circular surface of 1 m^2 (radius = 0.56 m) was calculated. This value will serve as a starting point for further parameterisation of the model.

Alternatively, Fig. 76 demonstrates that the distribution of points in the environment is non-uniform, exhibiting fluctuations influenced by the orientation of surveyed surfaces and the spatial locations of the stations, while maintaining constant instrumental survey settings.

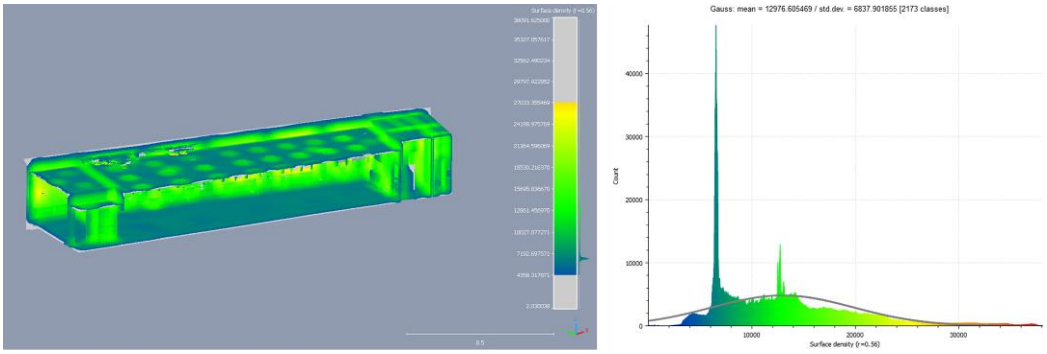

Fig. 76 Distribution of the point density (number of points/m^2).

Given this point density distribution and a typical building floor plan, the geometric recognisability parameters can be aptly configured based on the desired segmentation of elements and their characteristic point densities.

An illustrative configuration is presented in Fig. 77 where the objective is to segment specific building elements (Fig. 78) namely the floor, ceiling, and exterior masonry, while excluding others, such as partitioning.

GEOMETRIC DATA ELEMENTS	RANSAC PARAMETERS
FLOOR • Surface Area : 90 m^2 • Average Density: 13,000 pts/m^2 • Min. Points: 1,170,000	Min support points per primitive: 140000 ☑ Save leftover points into new cloud ☑ Use Least Squares fitting on found shapes ☑ Attempt to simplify shapes ☑ Set Random color for each shape found Primitives: ☑ Plane, ☐ Sphere, ☐ Cylinder, ☐ Cone, ☐ Torus Parameters: max distance to primitive = e = 0.040; sampling resolution = b = 0.020; max normal deviation = a = 25.00°; overlooking probability = 0.010000
PARTITIONING • Surface Area: 13 m^2 • Average Density: 15,000 pts/m^2 • Min. Points: 195,000	
CEILING • Surface Area : 80 m^2 • Average density: 6,000 pts/m^2 • Min. Points: 480,000	

Fig. 77 RANSAC parameters adopted for the segmentation of the geometric data elements.

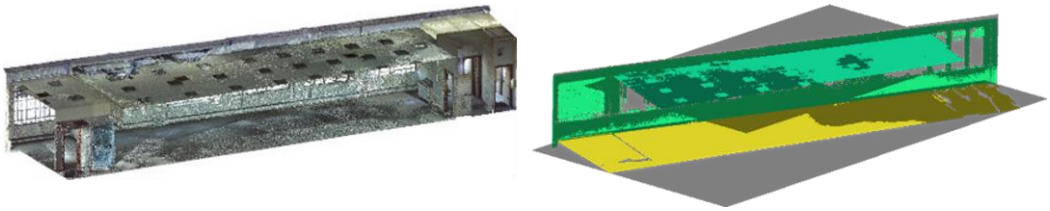

Fig. 78 Section of the point cloud employed in the RANSAC processing (on the left); segmentation result featuring elements exclusively detected through dominant planes (on the right).

Estimations for the minimum points on each element are derived by considering the surface area and average resolution, as shown in the equations [8] and [9]:

$$\text{point density} = \frac{1}{\text{point spacing}^2} \quad [\,8\,]$$

$$\text{min. points} = \text{surface area} * \text{average density} \quad [\,9\,]$$

This information serves as algorithmic input to generate a relevant reference sample for class identification. Furthermore, by defining parameters such as ‘sampling resolution’ and ‘max distance to primitive’, with the latter set at twice the resolution, the average resolution for each element can be ascertained.

4.2.2 Exporting Process and Final Deliberations

In this study, an effort has been made to develop a general workflow consistent with common Scan-to-BIM modelling requirements in the field of building engineering, while highlighting crucial troubles and potential solutions.

Decimation and classification tasks, applied in sequential steps, can improve the preservation of the three-dimensional morphology of the architectural environment's components, providing an opportunity for the designer to choose the level of geometric detailing that he intends to pursue.

Parameter settings, specifically those used with RANSAC, can be changed and customised to subdivide the different pieces of the point cloud, which can then be exported as separate files and employed for the next modelling stage.

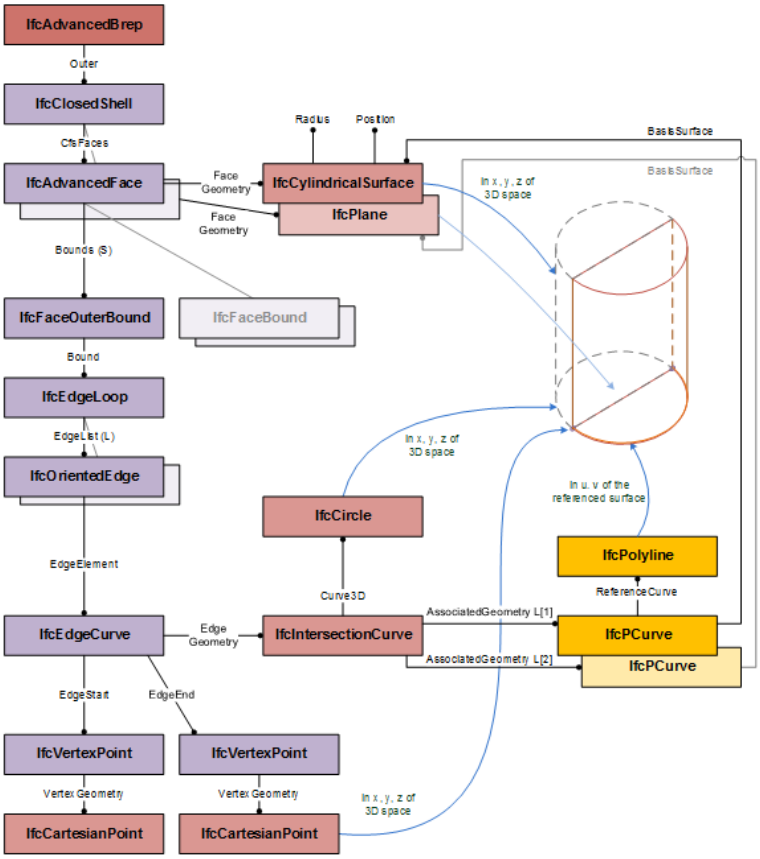

Fig. 79 IfcAdvanceBrep entity definition adapted from advanced_brep_shape_representation defined in standard BuildingSmart and ISO 10303-514.

In this case, the adoption of the Boundary Representation (BRep) modelling could be the best solution, as it aligns with the OpenBIM standards outlined in ISO19650 and complies with the IFC4 and IFC2x3 schema (Fig. 79).

This approach necessitates defining two-dimensional generators and directrices to automate the geometric construction of 3D elements through the extraction of specific building elements within the Scan to BIM process.

To ensure the preservation of the geometric profile of the sectioned element, most algorithms employed for generating such features rely on slicing operations (Daniels *et al.*, 2007; Kyriazis, Fudos and Palios, 2007) or on normal section profiles (Sun, Zhang and Zhang, 2021).

The exporting procedure must be configured to maintain the spatial references of each segmented point cloud, facilitating a proper federation process within BIM Authoring software.

4.3 Optimising Point Clouds for Authoring BIM

The CANUPO multiscale algorithm, mentioned before, has gained increased recognition in the Cultural Heritage (CH) domain, as evidenced by its growing popularity (Moyano *et al.*, 2021). In contrast, the RANSAC model-fitting method is widely adopted, offering the capability to assimilate portions of point clouds into geometric primitives like planes, cylinders, spheres, and cones (Schnabel, Wahl and Klein, 2007).

In the pursuit of streamlining point cloud processing, the research methodology adopts a comprehensive strategy, commencing with the implementation of a minimal Voxel Down-sampling technique (S. Wang *et al.*, 2022). Subsequently, a targeted decimation process is applied, with the specific objective of reducing non-critical points deemed irrelevant for subsequent phases of 3D generation within the BIM Authoring process. Ultimately, the incorporation of the CANUPO algorithm for classification and the application of the RANSAC method for segmentation collectively aim to extract a specific class of elements from the expansive point cloud dataset.

The focus is on meticulously categorising the intricate staircase within Nico Palace, a neoclassical structure in Gioia del Colle, Italy, aiming to optimise the subsequent modelling steps.

4.3.1 Quick Overview of the Nico Palace in Gioia del Colle (Italy)

Nico Palace (Fig. 80), featuring three entrances on Via G. Mazzini, Via Cairoli, and Via G. del Re, provides a unique gateway to its history. Acquired in the 1900s by a relative of Lawyer Nico from Gioia Del Colle (BA), a vast plot of land was obtained, leading to the construction of the magnificent Nico Palace by the architect Cristofaro Pinto.

Fig. 80 Nico Palace in Gioia del Colle (Italy).

Today, the building housed the Nartist Gallery, serving as an innovative platform that goes beyond a physical and virtual space for art exhibition. It fosters collaborative relationships and philanthropic initiatives, expanding art into a daily experience and a channel for solidarity.

From the ground floor, granting access to cellars, the garden, and apartments, a splendid self-supporting staircase ascends, reaching the first floor that houses spacious apartments. The staircase, a distinctive element of the building, presents itself as a geometric masterpiece with two mirrored ramps and a central shared one, totaling three ramps, contributing to the palace a distinct character. The balustrades, neoclassical-style floors, vaults, and other features constitute an architecturally valuable heritage.

The refined interior architecture makes it an exemplary subject for evaluating the effectiveness of advanced computational techniques in classification, laying the foundation for subsequent modelling procedures.

4.3.2 Methodology

The applied methodology in this study encompasses a multi-faceted strategy (Tavolare *et al.*, 2023), primarily emphasising the decimation process through voxel down-sampling of the point cloud. Subsequently, the focus shifts to classification and segmentation phases, leveraging the CANUPO and RANSAC algorithms, respectively. The final stage involves BIM Authoring modelling and model validation (Fig. 81).

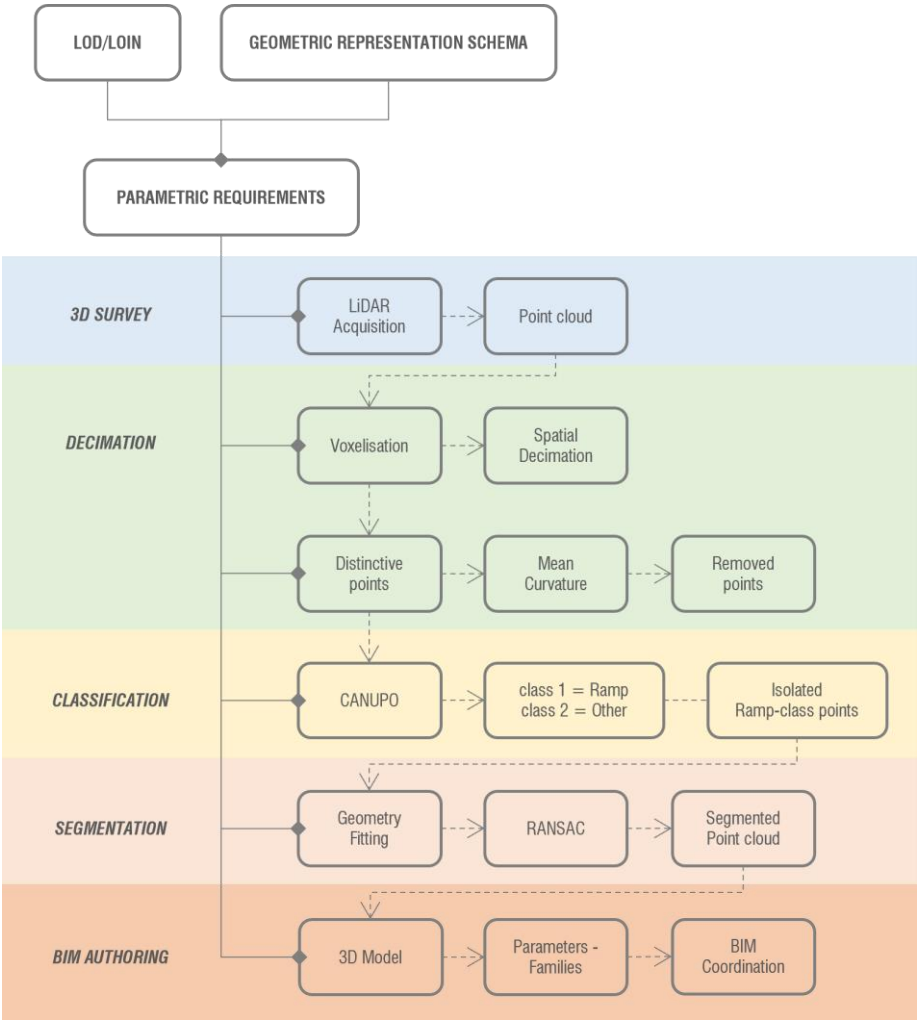

Fig. 81 Workflow for optimising the Scan-to-BIM process.

i. **Point cloud Decimation Process**

The strategy utilised a versatile approach, initiating with a fundamental Voxel Down-sampling and progressing to a decimation process that involved the removal of non-critical points deemed irrelevant for subsequent 3D generation phases.

The choice was made to focus this application specifically on the vertical connection system, comprising five straight ramps per floor, to simplify the parametric analysis of various algorithmic properties. The point cloud, acquired through a TLS survey using the CAM2® FARO Focus 3D 120 laser scanner, comprises 84 million points from 21 scans, detailed in Tab. 6 below:

Tab. 6 Laser scanner technical specification.

Parameters	**Specification**
Resolution	1/5
Nominal Ocular Hazard Distance (NOHD)	10.60/3.30
Quality	4x
Point Resolution	28.2 MPts
Scan Dimension	8248*3414 Pts
Colour	RGB+Scalar

The LiDAR survey product generates a point cloud characterised by non-uniform density (Fig. 82) leading to varying linear resolution in different segments of the cloud. This variability arises from the irregular positioning of the instrument in space and its variable orientation in relation to the building elements.

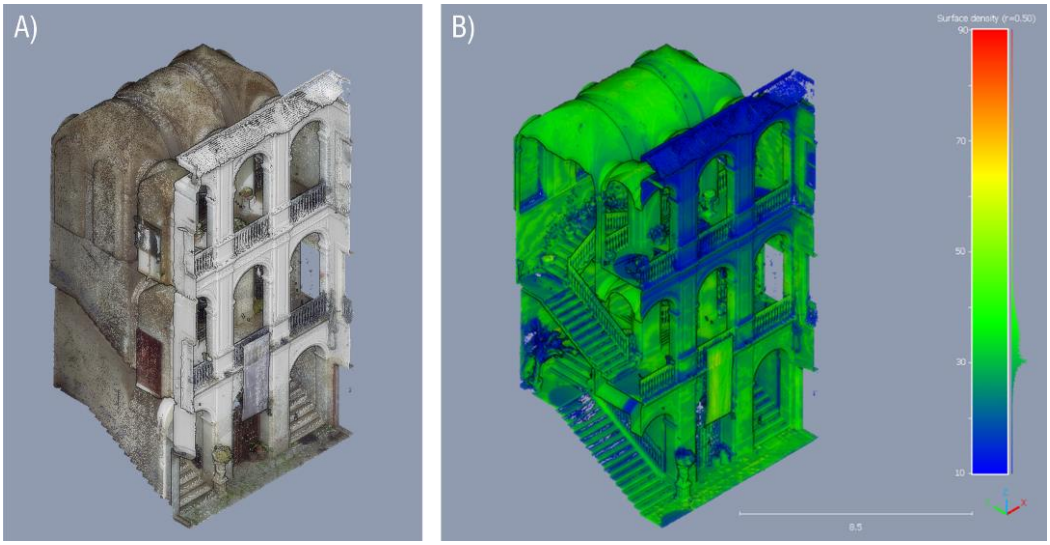

Fig. 82 A) Point cloud of the Nico Palace; B) Point cloud Surface Density (Mpts/m^2).

For this purpose, an initial normalisation process was implemented to standardise the geometric resolution of the points, taking into account the accuracy and Level of Detail (LOD) requirements for the Scan-to-BIM process. This process was carried out within the Python environment, employing a voxel-based spatial decimation method.

While this simplification method is computationally efficient, improper configuration can lead to an overly simplified point cloud, resulting in a loss of detail through the indiscriminate removal of points, including those crucial for maintaining formal recognisability.

The chosen approach involves constructing a three-dimensional voxel grid (Fig. 83), where the distance of each point from the centroid of the individual voxel is calculated. The point closest to the center is retained, while the other points are discarded.

The decimation intensity of the algorithm and, consequently, the preservation of detected details are influenced by the size of the voxel grid. In this scenario, to evaluate the voxel size, a virtual voxelisation of the ramp was conducted, involving a

qualitative analysis of the representability and identifiability of the required details (Fig. 84).

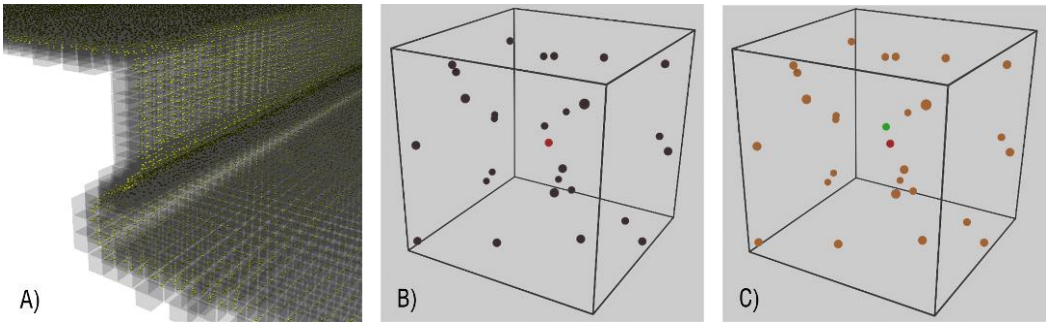

Fig. 83 A) Detail of the voxel grid; B) The red point is the centroid; C) The green one is the nearest point.

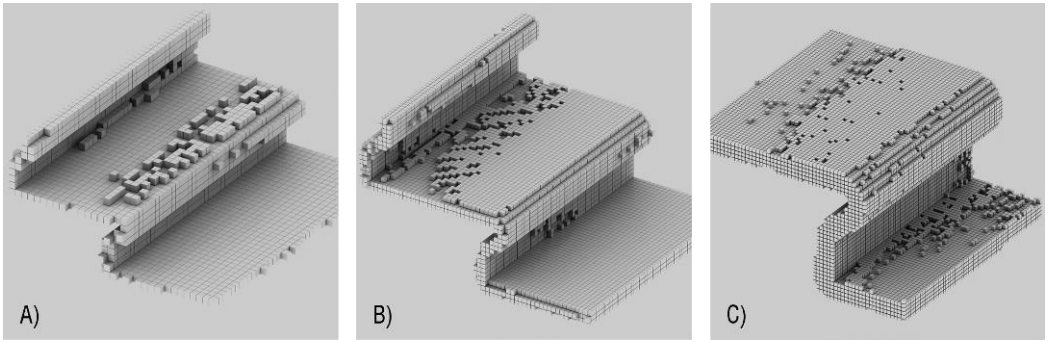

Fig. 84 Voxel size: A) 2 cm; B) 1 cm; C) 0.5 cm.

The visual representation of the geometric voxelisation of the stair steps aids in selecting the minimum resolution necessary for preserving morphological features. Additionally, if the required LOD or geometric precision is known, an analytical evaluation can be conducted to determine the optimal voxel size.

While this initial decimation process can be applied universally across the entire model, it's important to note that conditions for representability often vary depending on the specific area and elements present.

For the second decimation step, it is crucial to pinpoint the defining points – those that encapsulate the key areas of the point cloud indispensable for subsequent 3D generation phases. Typically, these points correspond to the edges of surveyed geometric elements, as exemplified in this case by the profile of the ramp steps.

In the quest to identify these pivotal points, reliance was placed on Mean Curvature Analysis (Yang *et al.*, 2015). This method involves calculating the radius of the segmentation range, defining the circular selection area. This area is determined by comparing the mean curvature value of a selected point to the average mean curvature of the entire point cloud, as shown in the formula below [10]:

$$r_i = \alpha \cdot \frac{\overline{H}}{|H_i|}$$

[10]

Where:

r_i = radius of the segmentation range
α = scale factor of the segmentation range
H = average mean curvature of the entire point cloud
$|H_i|$ = mean curvature of the single i point

The range is narrow in areas with higher curvatures, while it widens in areas with lower curvatures. However, this iterative procedure necessitates a substantial computational effort, potentially causing delays in processing steps. Nonetheless, this approach allows for precise and timely geometric analysis of specific regions within the point cloud.

For this purpose, a simplified computation approach was adopted in this study: specifically, the mean curvature (Har'el, 1995) for each point was calculated concerning the neighbouring points within a radius of 9 cm. This radius was

experimentally evaluated with consideration for the sizes of the elements to be modelled, proving sufficient to highlight critical points on non-planar surfaces.

Points with low mean curvature, potentially indicative of non-critical areas, were treated as redundant and deemed unnecessary for the 3D model representation.

Applying a filter to select points with a mean curvature below a specified threshold enables a parametric simplification of planar points while preserving the recognisability of the features, particularly in the case of the stairway. This process proves valuable for three-dimensional reconstruction within the BIM Authoring environment, as depicted in Fig. 85.

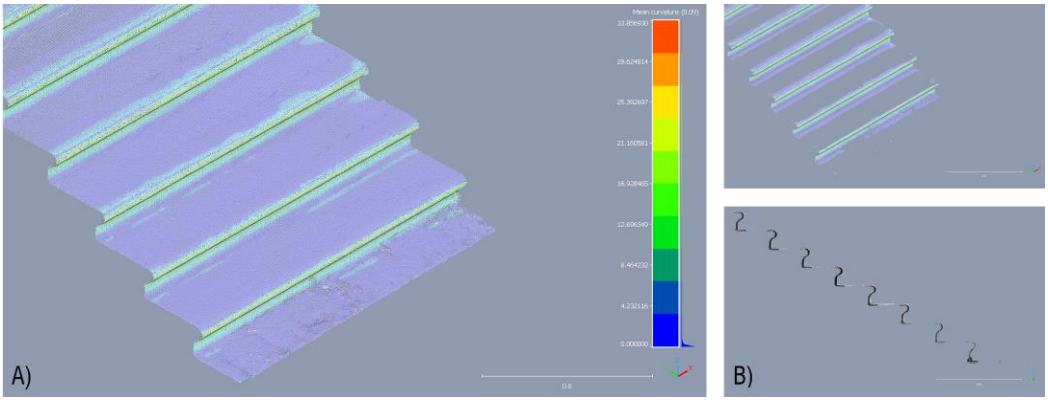

Fig. 85 Point cloud of the staircase ramp with mean curvature visualisation; B) Filtered point cloud with mean curvature > 2 (total points: 229,786).

Indeed, in this simplification stage, it is crucial to trace geometries back to their three-dimensional origin, considering the modelling methods that will be used subsequently. For instance, in the IFC4.1 and IFC4.3 schemes, the ramp is defined through the configuration of specific classes and entities (Fig. 86).

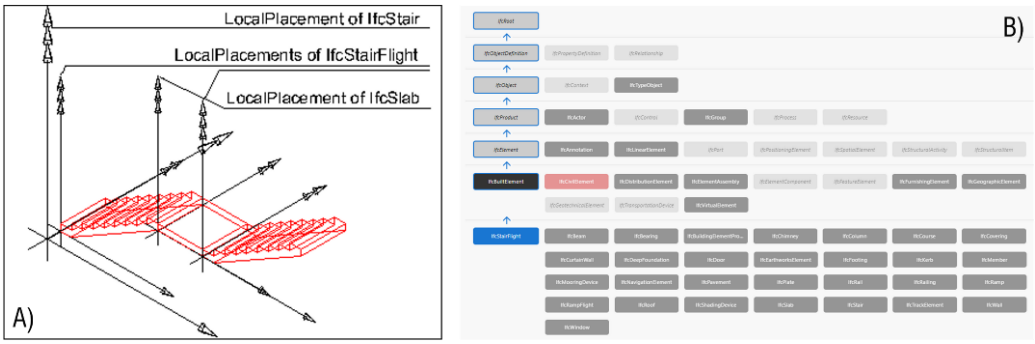

Fig. 86 A) IfcStairType from the IFC 4.1 scheme; B) Entity inheritance from the IFC 4.3 scheme.

The dimensions of the vertical connection, the quantity of risers and treads, and the profiles constituting the step covering serve as parameters for the geometric definition of a ramp in this diagram. All of this information can be inferred from the points that were filtered earlier. The decimation result must undergo validation before being accepted for further processing.

ii. **Classification and Segmentation Processes**

As previously mentioned, the purpose of classification techniques is to 'label' groups of points sharing similar characteristics, categorising architectural elements within the Scan-to-BIM framework in terms of various Levels of Detail (LOD).
This enables the retrieval and individual management of these elements by multidisciplinary teams, allowing them to concurrently work on BIM Authoring procedures. One of the key challenges in these approaches lies in their design complexity and the difficulty of generalising the training process without a reference dataset, essential for achieving satisfactory results.

For this reason, the exploration of utilising the CANUPO algorithm (Brodu and Lague, 2012) has been decided within an optimisation process targeted at extracting points that constitute the profiles of stair ramps. The decision was made to extract a single

section of the ramp and utilise it in the algorithm's training phase, considering the symmetric and modular spatial shape of ramps (Fig. 87).

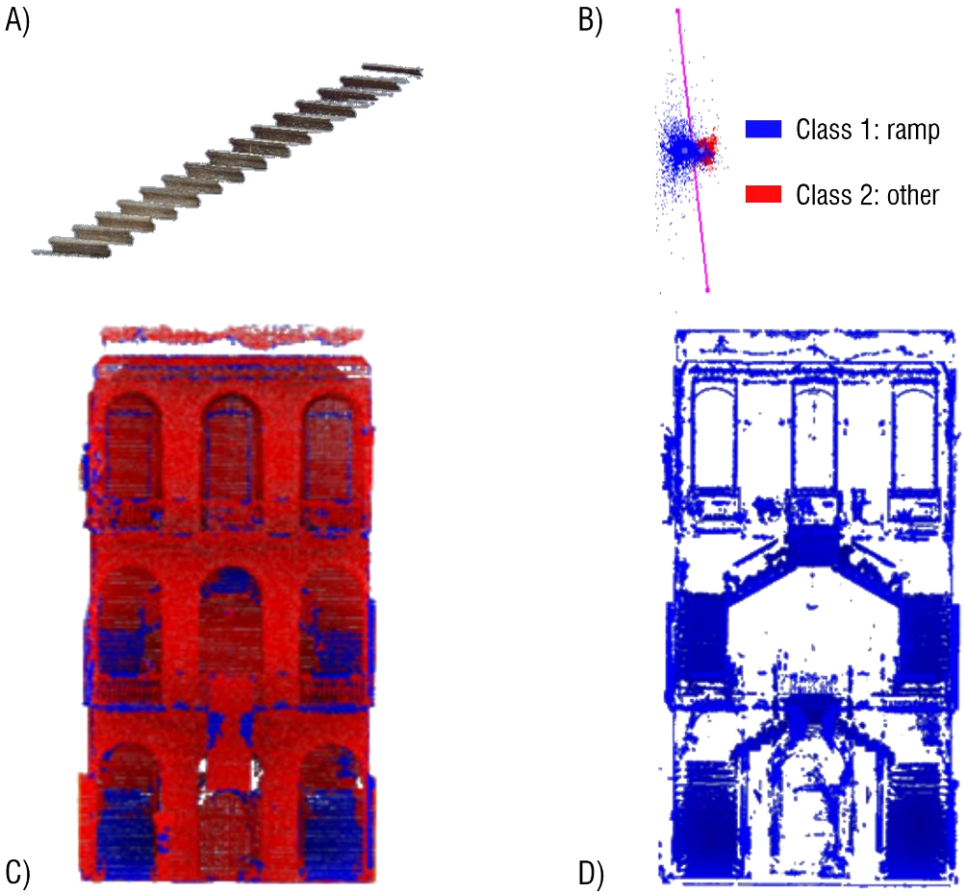

Fig. 87 Training process and binary classification with the CANUPO algorithm: A) Staircase ramp used for the training process; B) Classification distribution for the classe separation; C) Classification result (blue: ramp; red: other); D) Isolation of the ramp-class points.

The algorithm's limitations were shown by the test, which included the classification of flights of stairs while grouping points outside of this category. This was demonstrated by the distribution graph used to represent point classes during training.

The computational simplicity used in the calculation phase and a quick, but unduly basic training strategy limit the method. An additional optimisation method may be explored to enhance the segmentation of staircase ramp points in case the results obtained are not sufficiently satisfactory.

Next, segmentation data were processed by applying the RANSAC algorithm (Fischler and Bolles, 1981; Schnabel, Wahl and Klein, 2007; Oh *et al.*, 2021) to identify the points belonging to the inclined planes denoting the stair ramps.

When the algorithm finds a plane in which to place a group of points, it randomly selects the minimum number of points required to define the model, in this case three non-collinear points. It computes the model utilising the selected points, such as through the least squares approach, and assesses how well these points in the point cloud conform to this model. It then classifies points as ‘inliers’ or ‘outliers’ according to whether or not they are within a given distance threshold. Until a sufficient number of inliers is reached, these stages are iterated a fixed number of times.

This method facilitated the isolation of individual staircase ramps (Fig. 88) from the overall environment, simplifying their integration into BIM procedures and workflows On the point cloud, the segmentation process can also be used as a first step, enabling the extraction of only the geometric elements designated for optimisation.

Following the computation of the average distance between each point and its neighbours, any ‘orphan that are farther away from the average distance plus a specified number of times the standard deviation are eliminated.

To align it with the Autodesk Revit® BIM Authoring software, the resultant point cloud, portraying the assembly of staircase ramps, was exported in .PTS format and transferred into the exclusive Autodesk Recap® processing environment.

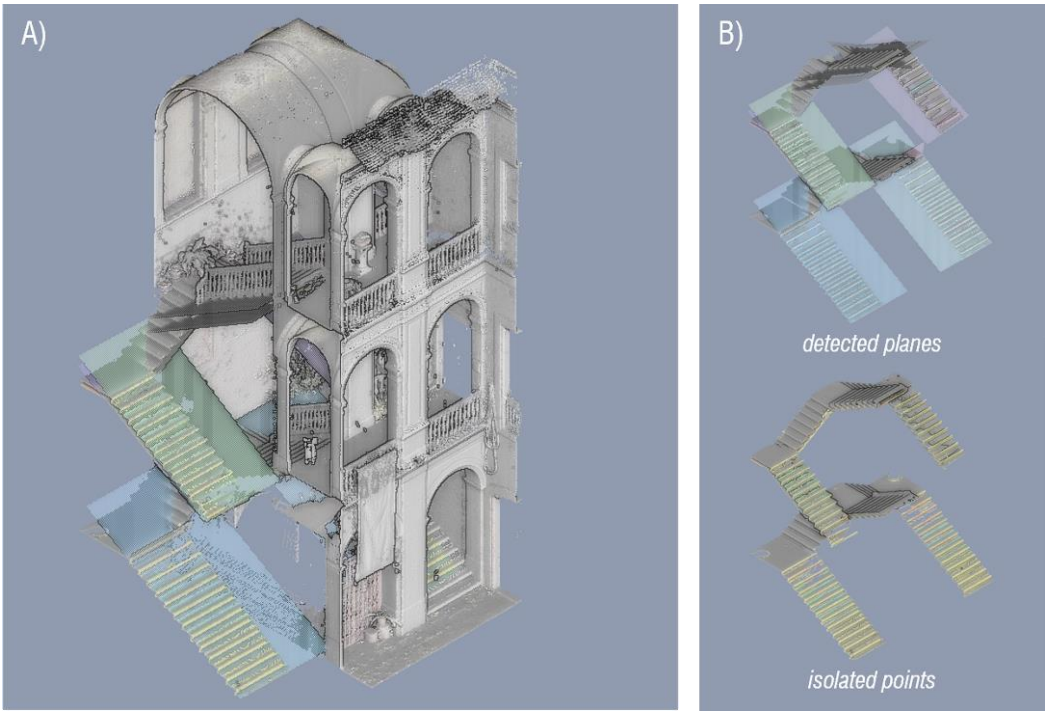

Fig. 88 A) Points grouped by the plans identified in RANSAC for the ramp class 1; B) Detected planes and isolated point.

iii. **BIM Authoring**

Ramp block modelling was done in the BIM Authoring environment in order to verify the geometric quality and completeness of the final product and evaluate the workflow's effectiveness. By applying the previously established automation methods to point clouds it was possible to identify the most distinguishing characteristics of the staircase body, which simplified the operations that followed (Fig. 89).

Step width and slope angle were precisely defined as part of the modelling procedure in order to provide a realistic and useful portrayal of the stair forms within the overall project context (Fig. 90).

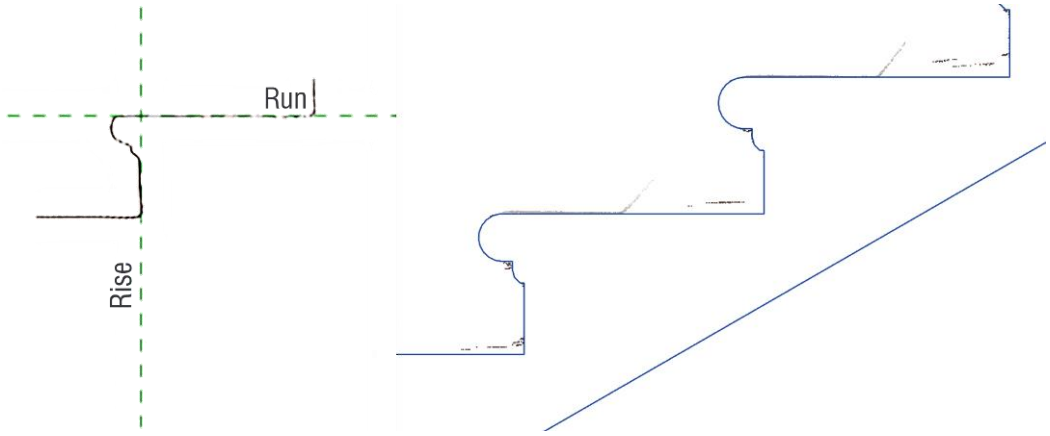

Fig. 89 Modelling the staircase ramp in the BIM Authoring environment using the previously optimised point cloud.

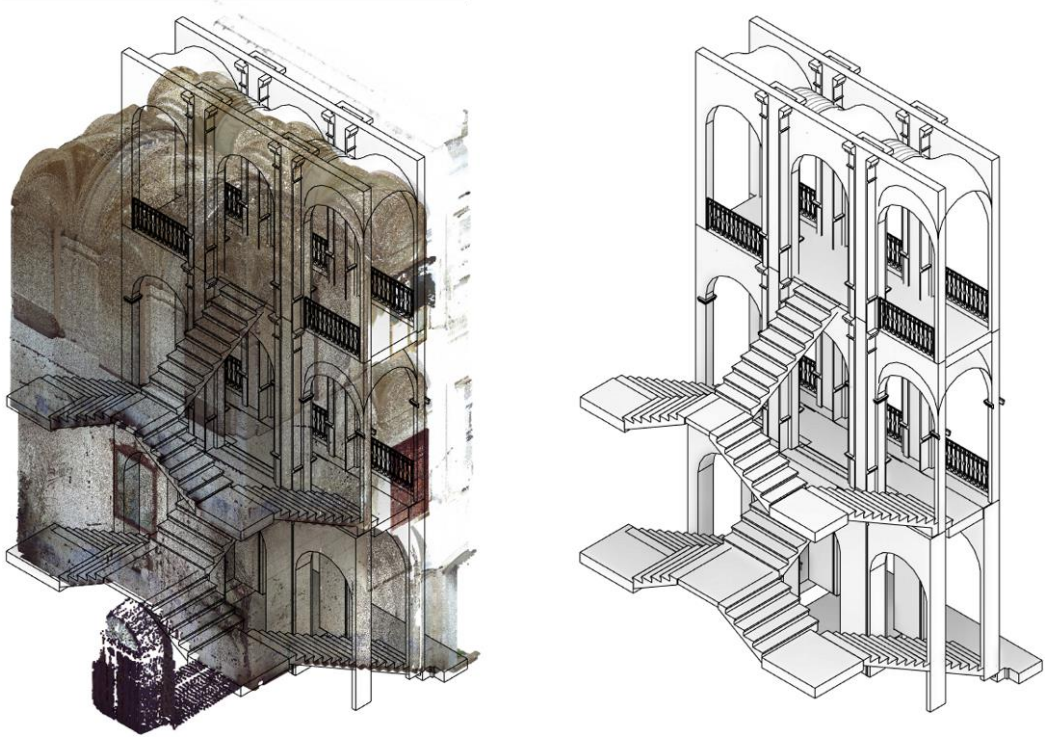

Fig. 90 Final 3D model using Scan to BIM methodology.

The cross vault was another distinctive component used in the model's construction. For this, a unique adaptive parametric family was developed, allowing for the inclusion of offset parameters for the distances at the wall arches, in addition to the heights related to the rises of the groin's generating arches.

4.3.3 Results and Conclusions

Thanks to the methodology employed in optimising point clouds for BIM Authoring, the achieved results can be deemed satisfactory for several pivotal reasons.

First and foremost, the approach demonstrated remarkable precision in maintaining geometric details throughout the entire decimation process. The combination of voxel down-sampling and mean curvature analysis ensured a high level of accuracy, meticulously preserving critical features of the staircase.

The efficiency of the classification and segmentation stages, utilising the CANUPO algorithm and the RANSAC method, respectively, was evident in the consistent isolation of distinctive elements of the staircase. Despite identified limitations during testing, the overall approach successfully captured the desired shapes.

The optimisation of the workflow was a significant outcome, showcasing seamless integration of processes from point cloud preparation to the final modelling in the BIM environment. Consequently, the automated processing of point clouds significantly streamlined subsequent operations, saving both time and resources.

These positive outcomes not only contribute to the accurate modelling of the staircase but also lay a solid foundation for future developments and research in the field of managing point clouds for BIM Authoring.

4.4 Automatic Point Cloud Segmentation and Parametric-Adaptive Modelling of Vaulted Systems

In the context of leverage data derived from digital surveying, the objective of this study is to assess an automated iterative process within a scan-to-BIM methodology. This process commences with automatic point cloud segmentation operations utilising open-source, model-fitting algorithms. The effectiveness of this method is expected to provide substantial support for the concluding phase of 3D parametric/adaptive reconstruction, ensuring compatibility with BIM Authoring.

The work is specifically directed towards various masonry vaulted systems (Buldo *et al.*, 2023). The analysis begins with the examination of these structures using 'ideal models', meticulously discretised and configured by the user. These models serve as a benchmark for validating the parameters of the RANSAC algorithm when applied to point clouds obtained from laser scanners. However, these latter ones exhibit irregular geometries, introducing complexities that pose challenges in terms of comprehension, analysis, and management.

The segmentation of point clouds, whether performed manually or automatically, proves valuable in the analysis of vaulted masonry structures, as highlighted in previous studies (Angjeliu, Cardani and Coronelli, 2019; Lanzara, Samper and Herrera, 2019). This method aims to distinguish and regionalise points associated with the vault from those related to the supports and piers upon which it rests.

Accordingly, this approach yields a precise representation of the structural geometry, significantly enhancing subsequent 3D reconstruction procedures (Santagati, 2005; Capone and Lanzara, 2019). The improvement may include identifying the geometric profiles of the vaults (Agustín-Hernández *et al.*, 2021; Agustín-Hernández, Sancho-Mir and Fernández-Morales, 2023), seamlessly integrating them with advanced algorithmic modelling techniques (Bagnolo, Argiolas and Vanini, 2022), or employing IronPython programming (Angjeliu, Cardani and Coronelli, 2019) and VPL languages (Quattrini *et al.*, 2023).

4.4.1 Methodology

To examine an automated process within a scan-to-BIM workflow, this research initiates with a comprehensive analysis of the geometric genesis related to specific types of vaulted structures represented as point clouds (refer to Fig. 91). The non-deterministic RANSAC algorithm, integrated into the open-source software CloudCompare, was employed to execute an automated segmentation approach.

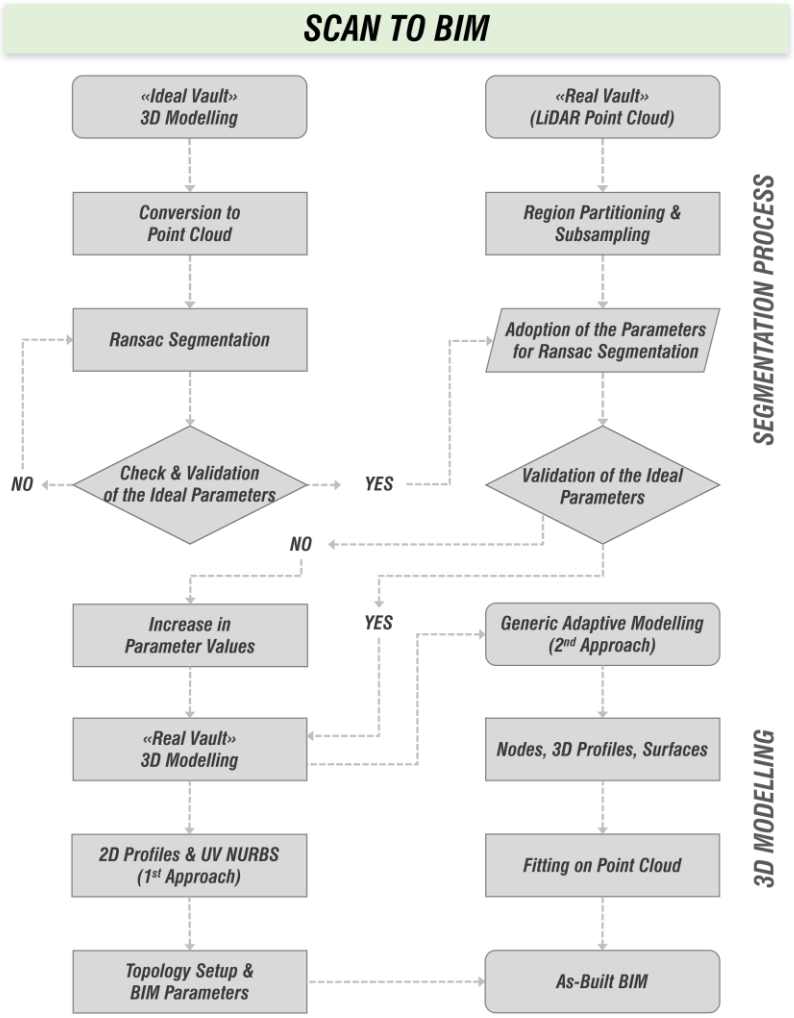

Fig. 91 Scan-to-BIM Workflow adopted for the vaulted systems.

The workflow encompassed the computation of point datasets derived from the discretisation of regular surfaces (plane, spherical, cylindrical) corresponding to vaulting models (Rondelet, 1832; Zaccaria, 1983; Saccardi, 2004), Subsequently, these results were applied to LiDAR point clouds with a comparable geometrical configuration.

The study not only evaluated the validation of the outcomes but also focused on the creation of 3D models utilising open approaches that promote software interoperability. Additionally, the research delved into BIM Authoring, ensuring enhanced consistency and control despite data sharing.

i. **Segmentation Process**

The study investigates seven distinct types of simple and composite masonry vaults, namely the sail, barrel, barrel with lunettes, trought, mirror, groin, and hemispherical dome on a drum and pendentives.

The segmentation process entailed an initial assessment and adjustment of the RANSAC algorithm's parameters on the intrados surface of geometric models classified as 'ideal'. These models are considered ideal due to their perfectly regular and discretized shapes. Generated in the CAD environment, these models were crafted using Boundary Representation (BRep) modelling, subsequently converted into a point cloud with a point spacing of 0.001 m.

The RANSAC algorithm performs a probabilistic and recursive estimation of 'inliers' within a dataset that includes 'outliers' – points not encompassed by the geometric model under consideration. Inliers are collected in predefined subsets ('minimal sets') whose distribution can be linked to a model of available geometric primitives.

Initial testing on these 'ideal' models yielded values for the algorithm variables, subsequently applied to clusters of points derived from LiDAR scans (captured using CAM2® FARO Focus 3D 120, and subsampled at 0.001 m).

Below are the algorithm parameters for the ideal models (Tab. 7) and the real ones (Tab. 8).

- *'Minimum support points per primitive'* represents the number of point samples that govern the density and size of the *'inlier'* clusters for each primitive. This value is inversely correlated with the number of point groups utilised to sample a particular primitive. Through experimental analysis, a threshold value was determined, below which the algorithm struggles to accurately distinguish between different primitive surfaces for the same geometry. This threshold, falling within the range of 0.4% to 2%, is directly proportional to the number of points in the dataset.
- *'ε',* denoting the maximum distance value between points and primitive shapes, was experimentally evaluated within the range of 0.001 to 0.03. This parameter is crucial for discerning the presence of features such as ribs, groins, domes, pendentives, drums, and other typical geometric components. To accommodate the geometric discontinuity in LiDAR point clouds, this value was selectively increased, ensuring a balance that allows the primitives to be adequately fitted to the ideal point cloud while accounting for variations in geometry.
- *'α',* representing the maximum angular deviation between the points' normal and the normal of the primitive surface. This parameter value serves as a threshold, aiding in the identification of points that conform closely to the expected geometric surface *(inliers)* and those that deviate beyond the specified angular threshold *(outliers)*. The threshold, defined here as 25°, is typically determined empirically, taking into consideration the inherent noise present in the point cloud data.
- *'θ',* sampling resolution, which denotes the distance between neighbouring points, is set within an experimental range of 0.060 to 0.100. In cases where the data is irregularly sampled, a lower value for this parameter is often preferred. This adjustment allows for flexibility in handling variations in point

cloud density, ensuring a more adaptable segmentation process that accommodates different data acquisition scenarios.

- The '*overlooking probability' (OP)*, representing the the probability that no better candidate is overlooked during sampling, is kept at a low experimental value of 0.010. By minimising the overlooking probability, the segmentation process strives to meticulously identify suitable *inliers* for each primitive, contributing to the robustness and accuracy of the overall analysis.
- *'r',* which represents the radius size of primitive shapes like sphere and cylinder, is determined based on the dimensions of the generatrices of geometric surfaces. In these specific applications:
    - *sail) 1.* radius of the hemispherical intrados surface (vault);
    - *barrel) 2.* generatrix radius of the semi-cylindrical intrados surface (vault);
    - *lunette) 3.* generatrix radius of the semi-cylindrical intrados surface (lunette) – *4.* generatrix radius of the semi-cylindrical intrados surface (barrel);
    - *trought) 5.* generatrix radius of the semi-cylindrical intrados surface (pavilion) – *6.* generatrix radius of the semi-cylindrical intrados surface (barrel);
    - *mirror) 7.* generatrix radius of the semi-cylindrical intrados surface (pavilion) – 8. generatrix radius of the semi-cylindrical intrados surface (barrel);
    - *groin) 9.* generatrix radius of the semi-cylindrical intrados surface (groin);
    - *dome) 10.* radius of the hemispherical intrados surface (dome) – 11. radius of the hemispherical intrados surface (pendentive) – 12. generatrix radius of the semi-cylindrical surface (drum).

Tab. 7 Algorithm parameters for the 'ideal models'.

IDEAL MODELS

Vault type	***Points***	***Support points***	***Primitive***			***α (°)***	***β (m)***	***ε (m)***	***OP***	***Inliers points***
			Sphere Cylinder Plane	r_{min} *(m)*	r_{max} *(m)*					
SAIL	1,000,000	20,000	s	-	4.24[1]	25	0.060	0.010	0.010	267,476
			c	-	-					
BARREL	1,000,000	20,000	s	-	-	25	0.070	0.010	0.010	390,903
			c	-	3.00[2]					
LUNETTE	1,000,000	5,000	s	-	-	25	0.100	0.010	0.010	999,156
			c	1.40[3]	3.00[4]					
TROUGHT	1,000,000	4,000	s	-	-	25	0.100	0.001	0.010	1,000,000
			c	3.00[5]	3.00[6]					
MIRROR	1,000,000	10,000	s	-	-	25	0.070	0.010	0.010	1,000,000
			c	3.00[7]	3.00[8]					
			p	-	-					
GROIN	1,000,000	5,000	s	-	-	25	0.060	0.001	0.010	423,661
			c	-	3.00[9]					
DOME	1,000,000	20,000	s	5.00[10]	7.08[11]	25	0.100	0.030	0.010	1,000,000
			c	-	5.00[12]					

Tab. 8 Algorithm parameters for the 'real models'.

REAL MODELS

Vault type	***Points***	***Support points***	***Primitive***			***α (°)***	***в (m)***	***ε (m)***	***OP***	***Inliers points***
			Sphere Cylinder Plane	r_{min} *(m)*	r_{max} *(m)*					
SAIL	286,359	5,727	s	-	2.20[1]	25	0.060	0.070	0.010	77,080
			c	-	-					
BARREL	2,936,243	58,724	s	-	-	25	0.070	0.040	0.010	1,285,150
			c		2.60[2]					
LUNETTE	5,767,107	28,836	s	-	-	25	0.100	0.060	0.010	1,841,853
			c	1.20[3]	1.50[4]					
TROUGHT	19,248,518	76,994	s	-	-	25	0.100	0.060	0.010	6,269,093
			c	2.10[5]	2.75[6]					
MIRROR	7,085,760	70,858	s	-	-	25	0.070	0.010	0.010	2,088,021
			c	1.60[7]	2.10[8]					
			p	-	-					
GROIN	5,697,696	28,489	s	-	-	25	0.060	0.030	0.010	1,813,099
			c	-	2.60[9]					
DOME	1,256,367	25,127	s	2.10[10]	3.00[11]	25	0.100	0.030	0.010	1,176,048
			c	-	2.10[12]					

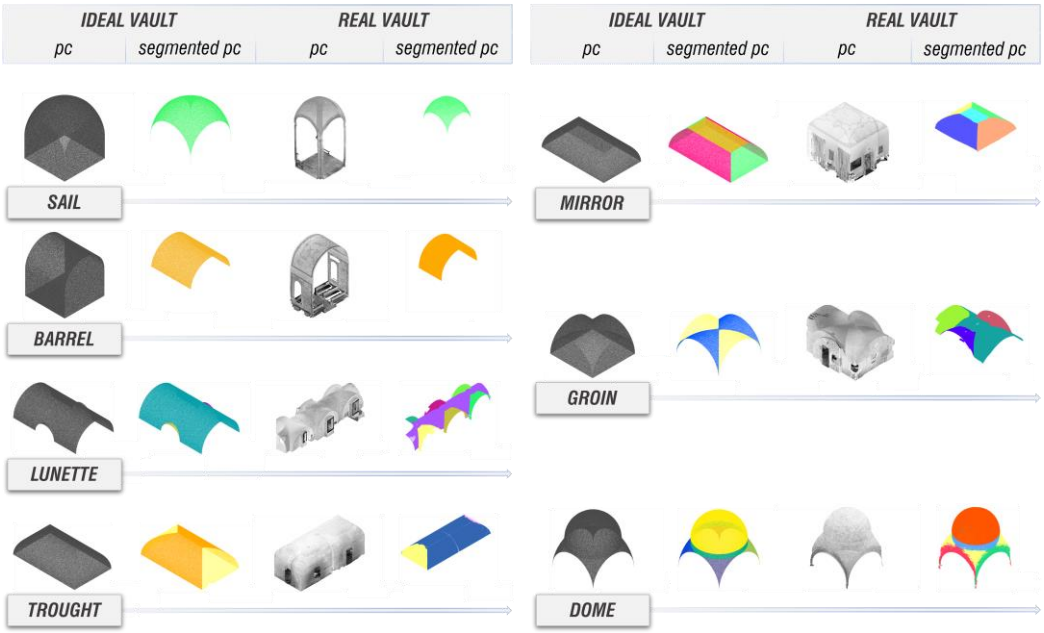

Fig. 92 Point cloud segmentation process, from the ideal models to the real ones.

On both ideal and realistic models, Fig. 92 showcases the outcomes of the segmentation process applied to all types of vaults.

The point clouds acquired by laser scanning are as follows:

- *Sail vault* (Church of St. Mary Magdalene in Sammichele di Bari, Italy);
- *Barrel vault* (Church of St. Mary of the Angels in Barletta, Italy);
- *Lunette vault* (Romanazzi Carducci Museum in Putignano, Italy);
- *Trought vault* (Marquis Palace in Laterza, Italy);
- *Mirror vault* (Romanazzi Carducci Museum in Putignano, Italy);
- *Groin vault* (Romanazzi Carducci Museum in Putignano, Italy);

- *Dome on drum and pendentives* (Abbey of the Most Holy Trinity in Venosa, Italy).

ii. **3D Modelling**

To ensure compatibility between segmentation procedures and their corresponding encodings in open BIM formats, it was imperative to devise an initial approach to geometric modelling.

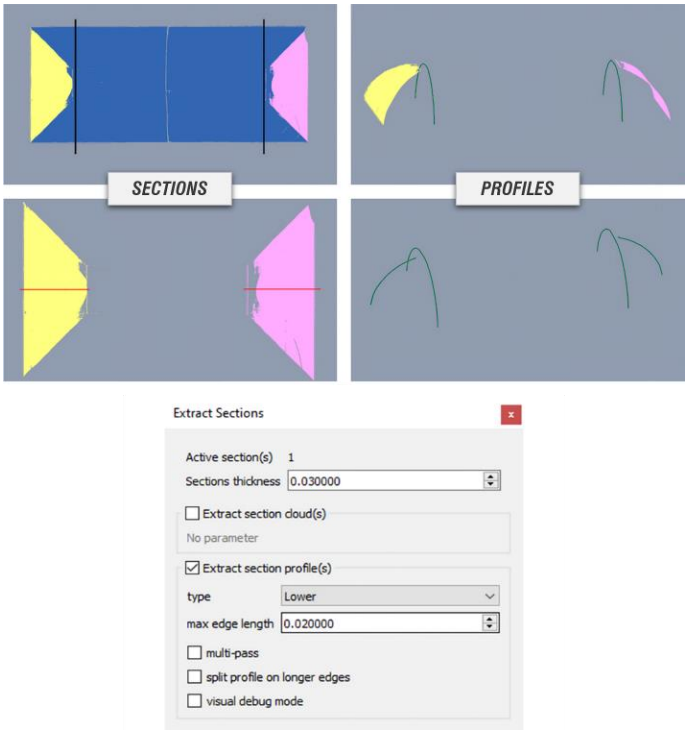

Fig. 93 Utilising the concave hull algorithm to extract profiles of the vaulted structures.

This approach is anchored in the utilisation of Non-Uniform Rational B-Splines (NURBS) generators and polygonal directrices that not only define but also geometrically delimit the analysed surfaces.

The semi-automated 3D reconstruction pinpointed specific section planes within the segmented clusters of the point cloud, intricately linked to the geometric configuration of the vaulted structures.

The interpolation of points situated on these planes was achieved through the CloudCompare software, with meticulous consideration of an offset extension of 0.03 m. Executing this operation involved the application of the 'concave hull' clustering algorithm[6], taking into account both the resolution of the initial point clouds and a grid with a pitch of 0.02 m (see Fig. 93).

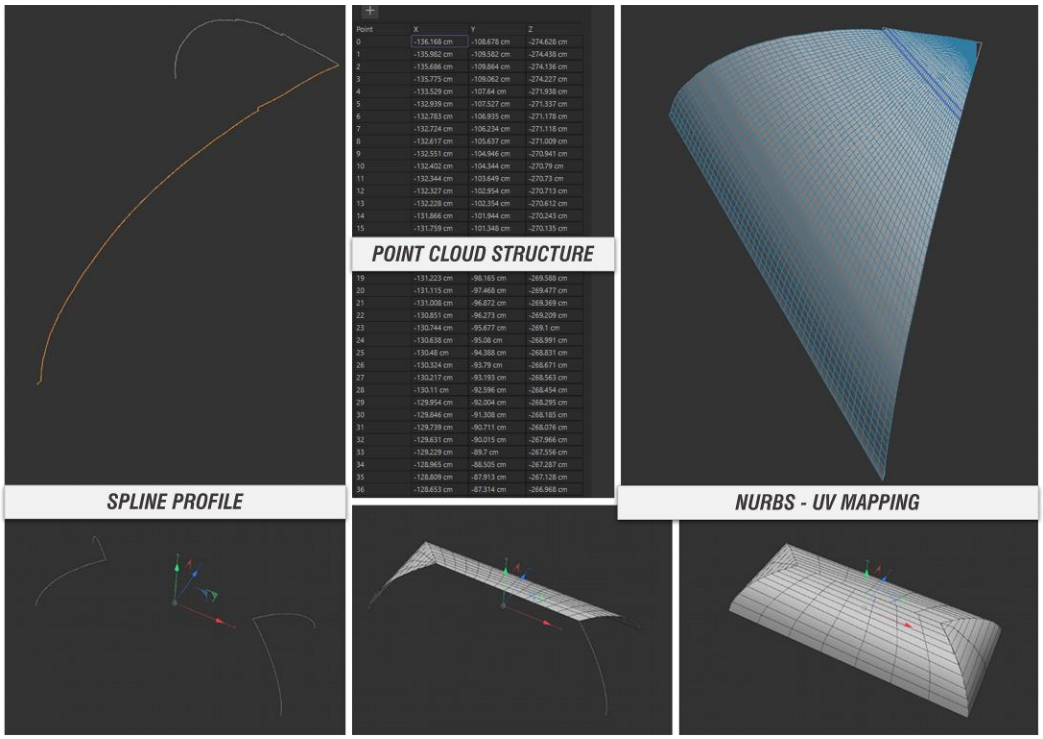

Fig. 94 Topological structure of the the vault using NURBS and UV mapping.

[6] The 'concave hull' algorithm is employed to generate an external envelope that closely conforms to a set of points, adept at capturing intricate details and concavities within the shape. In contrast to the 'convex hull,' which forms a convex outer shell, the concave hull yields a more nuanced and adherent representation, effectively accommodating intricate variations in the surface of the depicted object (Yahya *et al.*, 2017; Yan *et al.*, 2019).

Potential anomalies introduced by noise or interference in the point cloud were mitigated through decimation and vertex segmentation processes applied to the resulting polylines. The profiles were then acquired and seamlessly integrated using multiple NURBS generators in MAXON's CINEMA 4D software, with UV subdivision parameters employed for consistent topological structuring (Fig. 94).

The 3D model underwent a transformation from its fundamental geometry using the BIM authoring tool Autodesk Revit. This facilitated the linking of polygonal surfaces to BIM elements, specifically roofs, and enabled the integration of management data and parameters (see Fig. 95).

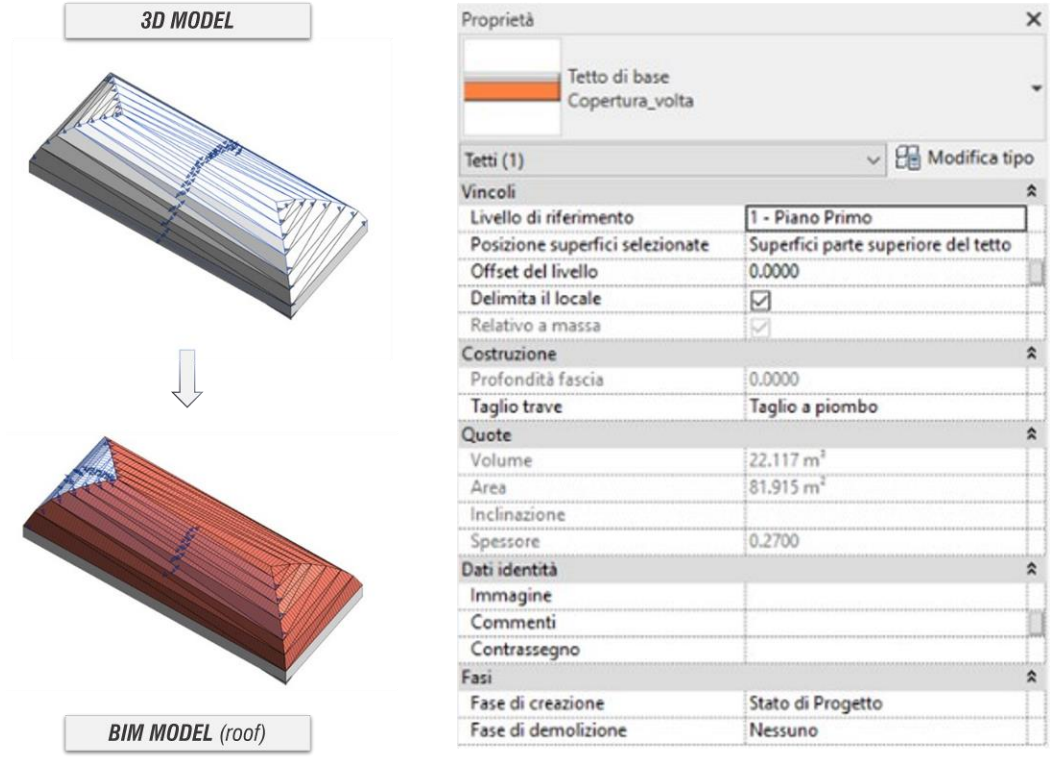

Fig. 95 Association of polygonal surfaces with BIM components.

Exploring an alternative modelling approach, a versatile adaptive metric model (.rfa format family) was created using only Revit for each type of vaulted structure. This model was designed to dynamically adapt to the irregular geometric properties present in the scanned point clouds.

Regarding the flexible components, adaptive shape handle points were generated and interconnected through splines and/or reference lines. This approach was employed to articulate the geometry, whether void or solid, associated with the specific type of vaulted structure, ensuring adaptability to the characteristics of the point cloud (see Fig. 96).

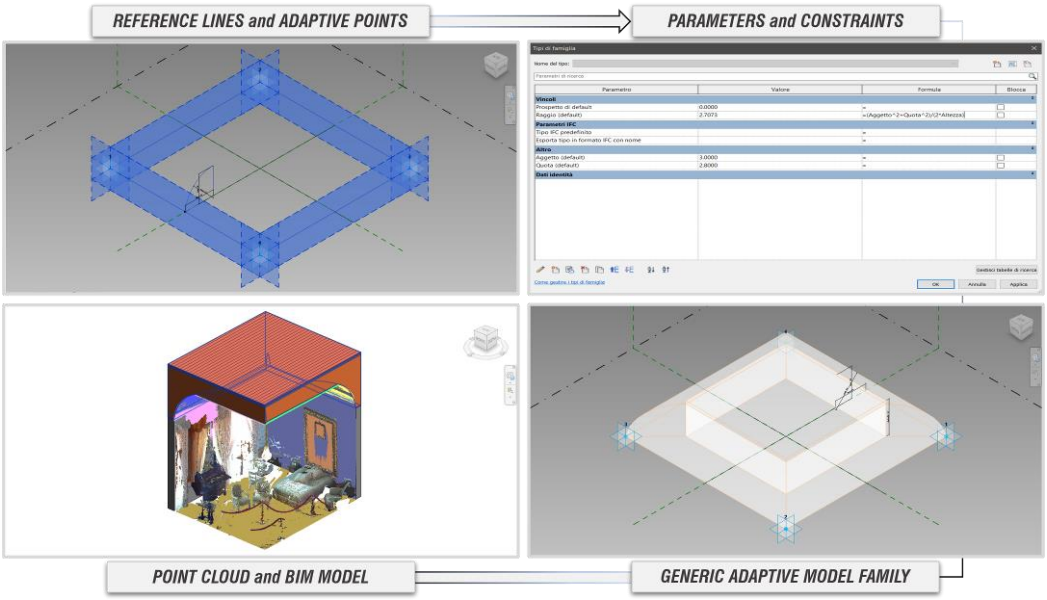

Fig. 96 Parametric modelling workflow: transitioning from adaptive families to the Scan-to-BIM model.

Distance relationships (height and overhang) between points and reference planes, plus the radius of the generating arches were computed using the established parameters and constraints tailored for each model. Providing more details, a parameterisable geometric void, linked to the roof element, allowed the definition of

height parameters for the arch rises and the midpoint of the hemispherical structure associated with the sail vault (see Fig. 98 a).

In the case of the barrel vault (Fig. 98 b), only the heights corresponding to the rises of the two generating arches forming the semi-cylindrical structure were generated.

To construct the lunette vault, additional semi-cylinders were intersected with it, employing smaller yet identically parameterised heights, akin to the individual lunettes Fig. 98 c). Departing from conventional practices, the omission of the horizontal section plane was pivotal in creating the trought vault Fig. 98 d), derived from the mirror vault model (see Fig. 98 e).

Regarding the latter, the radius parameter was linked to the apex height and span parameters, relative to the lowered pavilions, according to the following formula [11] and related to the Fig. 97.

$$\text{radius} = \frac{1}{2} * \frac{\text{apex height}^2 + \text{span}^2}{\text{apex height}} \qquad \textbf{[11]}$$

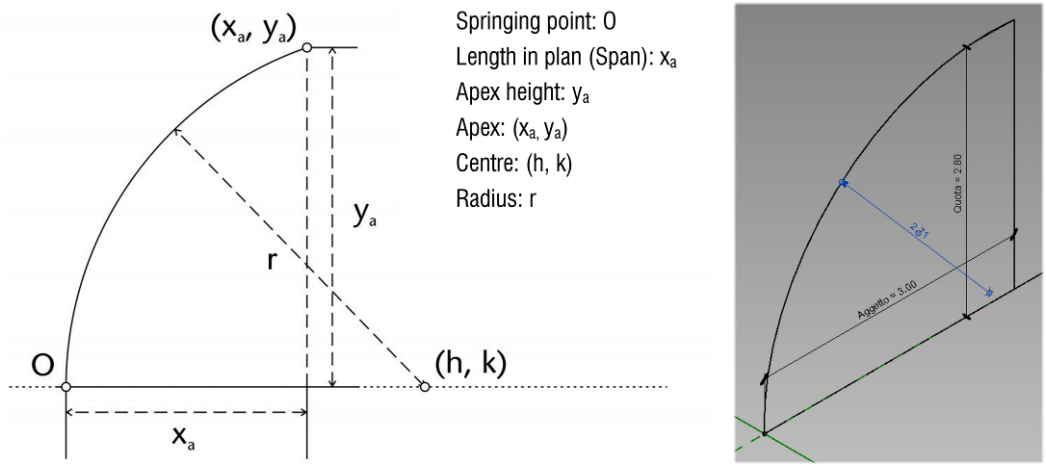

Fig. 97 Geometric properties for the parametric construction of the mirror vault.

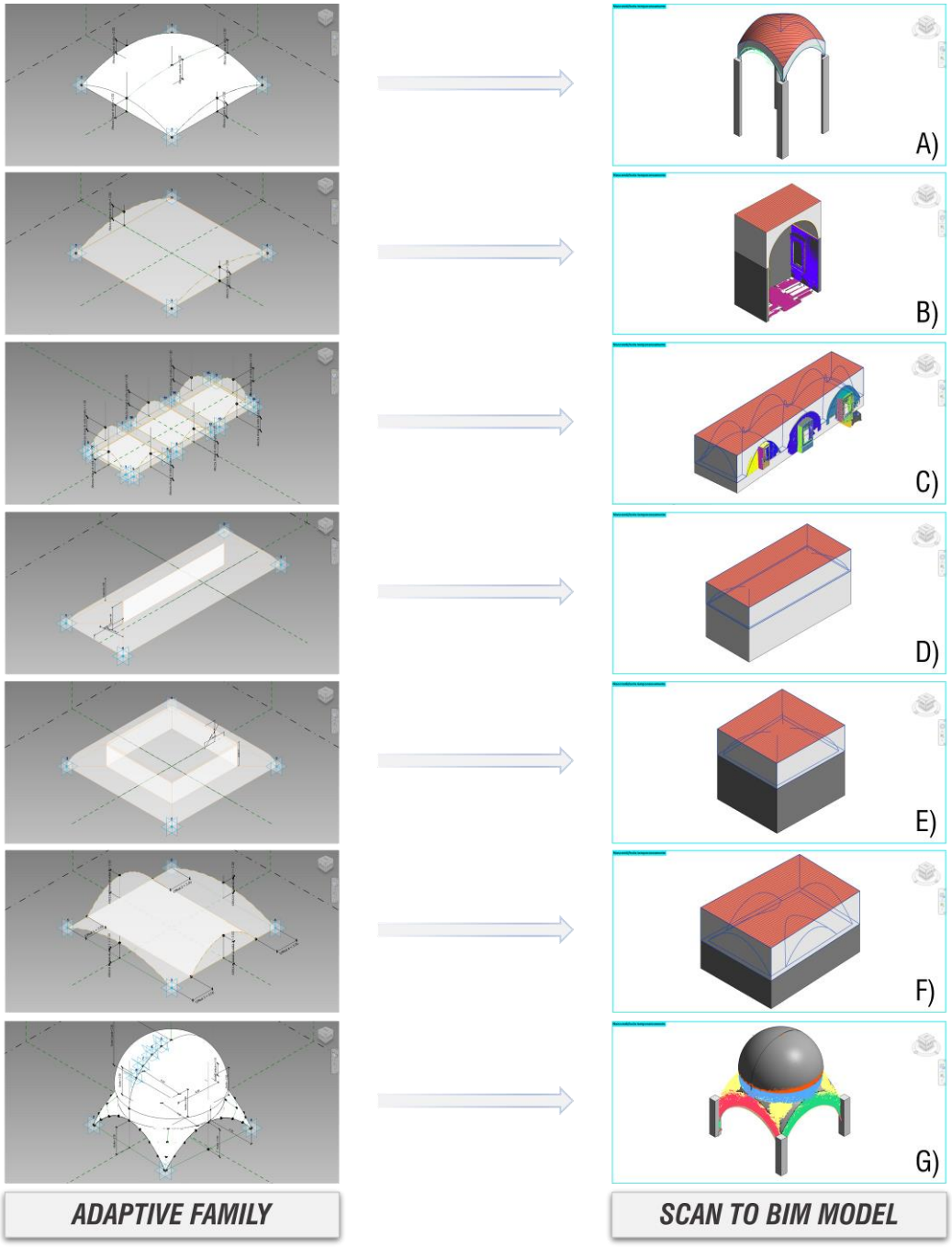

Fig. 98 Parametric adaptive families for the BIM models.

Subsequently, for the groin vault, in addition to the heights associated with the rises of the groins' generating arches, parameters for distance offset at the wall arches were specified (see Fig. 98 f).

In conclusion, for the hemispherical dome, distinct parameters governing the heights of the pendentives, drum, and dome itself were established. Multiple adaptive points were strategically placed to enable the model to adapt to the irregularities of the scanned surface (see Fig. 98 g).

4.4.2 Results

For the ideal models of the vaulted structures, very accurate results were achieved by meticulously choosing the specific value of the algorithm parameters, primitive types, and geometric dimensions. However, when the algorithm was applied to LiDAR point clouds, challenges arose in accurately extracting shapes that deviated from the pre-selected set of primitives.

Consequently, the ε parameter for the real structures was increased to accommodate their geometric irregularities, broadening the range of distances between inliers associated with the primitives. The automatically segmented regions of points representing actual vault components were compared with manually segmented *'ground truths',* considering the number of delected points and the percentage ratio between RANSAC and Ground truth (see Tab. 9). The data were also compared visually (see Fig. 99).

Prominent discrepancies in the real models are evident in the non-spherical and non-uniform nature of the dome pendentives (see Fig. 100), as well as in the barrel vault lunettes, ribs, and groins.

Notably, the cylindrical shape of the barrel vault, the spherical form of the sail vault, and the plane of the mirror vault exhibit better identification owing to their simpler and more complete geometric configurations. Despite these challenges, the obtained results prove valuable for subsequent digital modelling stages.

Tab. 9 Comparing the number of points detected by Ground truth and RANSAC.

Vault type	***GROUND TRUTH***	***RANSAC***
	number of points	***number of points (% RANSAC / GROUND TRUTH)***
SAIL	green: 83,838	green: 77,499 (92.44%)
BARREL	orange: 1,304,199	orange: 1,285,150 (98.54%)
LUNETTE	purple: 988,713; yellow: 195,171; dark-green: 75,236; brown: 188,879; bordeaux: 134,872; green: 182,571; light-green: 129,271	purple: 1,035,354 (104.72%); yellow: 175,170 (89.75%); dark-green: 58,957 (78.36%); brown: 173,385 (91.80%); bordeaux: 120,337 (89.22%); green: 161,220 (88.30%); light-green: 117,430 (90.84%)
TROUGHT	blue: 4,916,063; yellow: 656,343; pink: 696,687	blue: 5,070,519 (103.14%); yellow: 601,256 (91.60%); pink: 597,318 (85.74%)
MIRROR	blue: 580,124; orange: 508,267; green: 533,062; yellow: 463,485; cyan: 193,379	blue: 550,690 (94.93%); orange: 465,861 (91.66%); green: 509,619 (95.60%); yellow: 382,023 (82.42%); cyan: 179,828 (92.99%)
GROIN	dark-green: 660,275; light-green: 562,874; blue: 277,566; bordeaux: 306,677	dark-green: 986,336 (149.38%); light-green: 343,595 (61.04%); blue: 231,113 (83.26%); bordeaux: 252,055 (82.19%)
DOME	orange: 585,629; cyan: 180,365; yellow: 237,693; bordeaux: 39,711; dark-green: 14,992; red: 35,024; light-green: 42,605	orange: 585,292 (99.94%); cyan: 136,201 (75.51%); yellow: 153,206 (64.46%); bordeaux: 78,084 (196.63%); dark-green: 78,443 (523%); red: 69,475 (198,36%); light-green: 75,347 (176,85%)

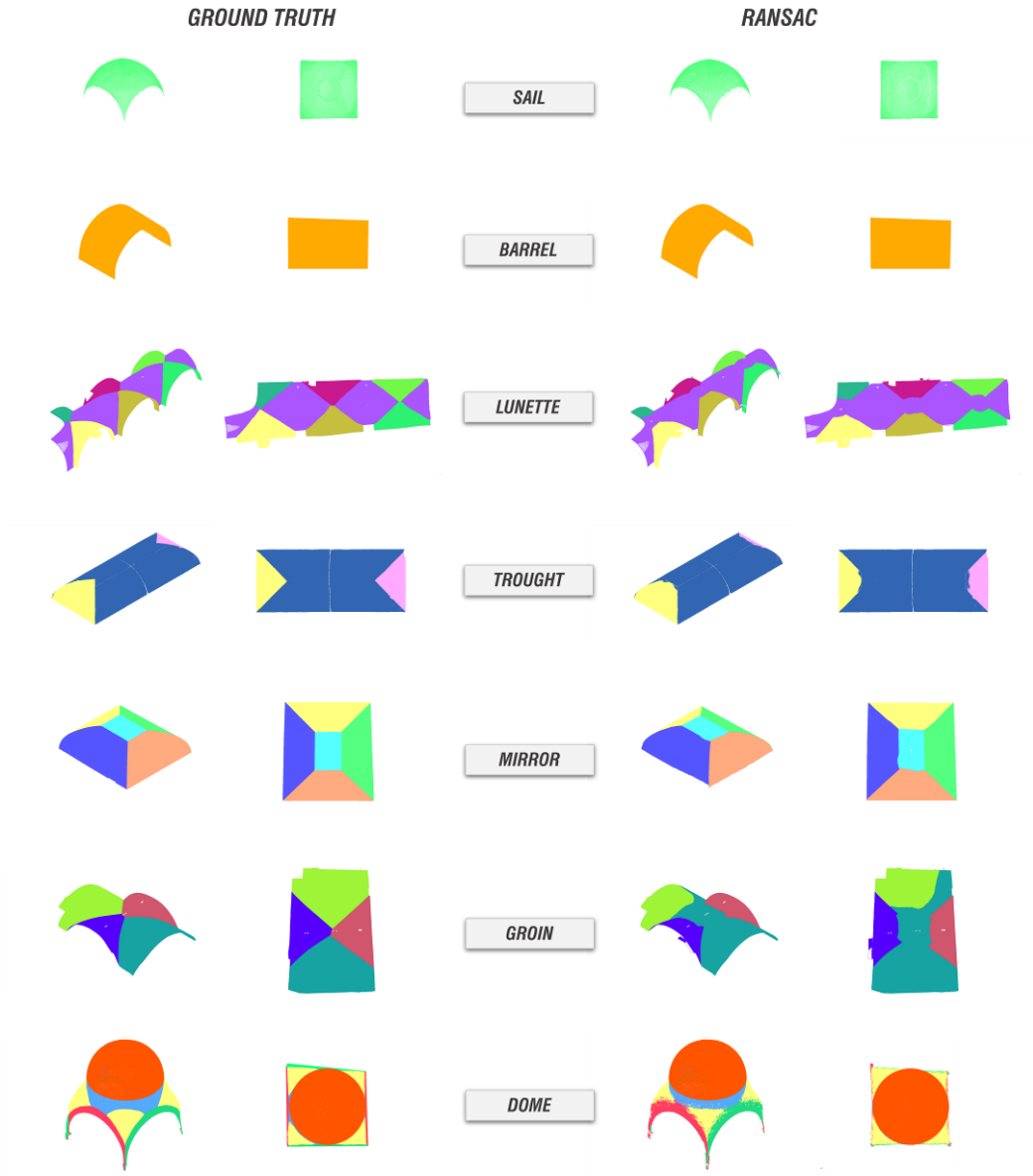

Fig. 99 Comparing Ground truth vs. RANSAC.

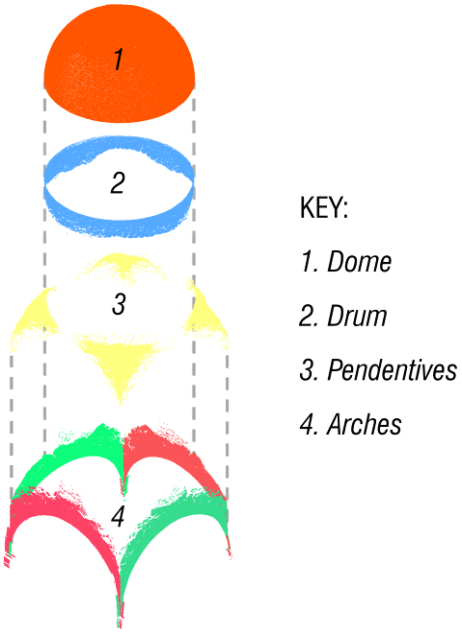

Fig. 100 Example of segmented point cloud: hemispherical dome on drum and pendentives (Abbey of the Most Holy Trinity, Venosa).

The geometric reconstruction process in open-mode particularly excelled in providing robust topological mesh control, facilitating precise UV mapping of surfaces, and allowing customisable polygonal resolution. The translation of the 3D geometry within the BIM authoring software, coupled with the flexibility to choose compatible software tools, facilitated seamless information and management parameter integration.

The adoption of adaptive parametric families in the second modelling approach with BIM authoring enhanced efficiency, enabling the creation of highly tailored architectural elements with greater flexibility than standard system families.

The incorporation of adaptive points, along with meticulous parameter and constraints control, facilitated precise placement of families for diverse structural configurations, resulting in time savings and heightened design efficiency.

An analytical comparison with the point cloud was conducted to verify the geometric coherence of these reconstructions. The analysis revealed minimal discrepancies,

primarily within 0.06 m, attributed to the inherent irregularities in the detected intrados of the real vault. These variations align with the representative limits imposed by the BIM-oriented geometric NURBS regularity (see Fig. 101).

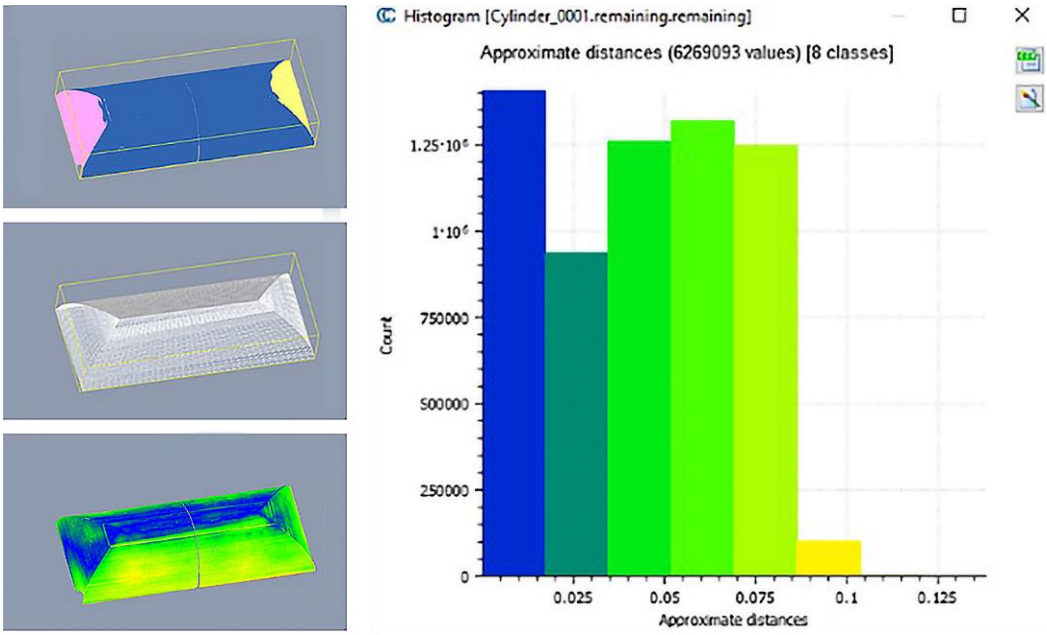

Fig. 101 Deviation analysis between the point cloud and the BIM model (1st approach).

The second modelling approach revealed larger discrepancies for certain vault types, particularly in the case of the trought vault (average distance value of 0.07 m) and the dome, particularly noticeable at the spherical pendentives (average distance value of 0.08 m), as shown in Fig. 102.

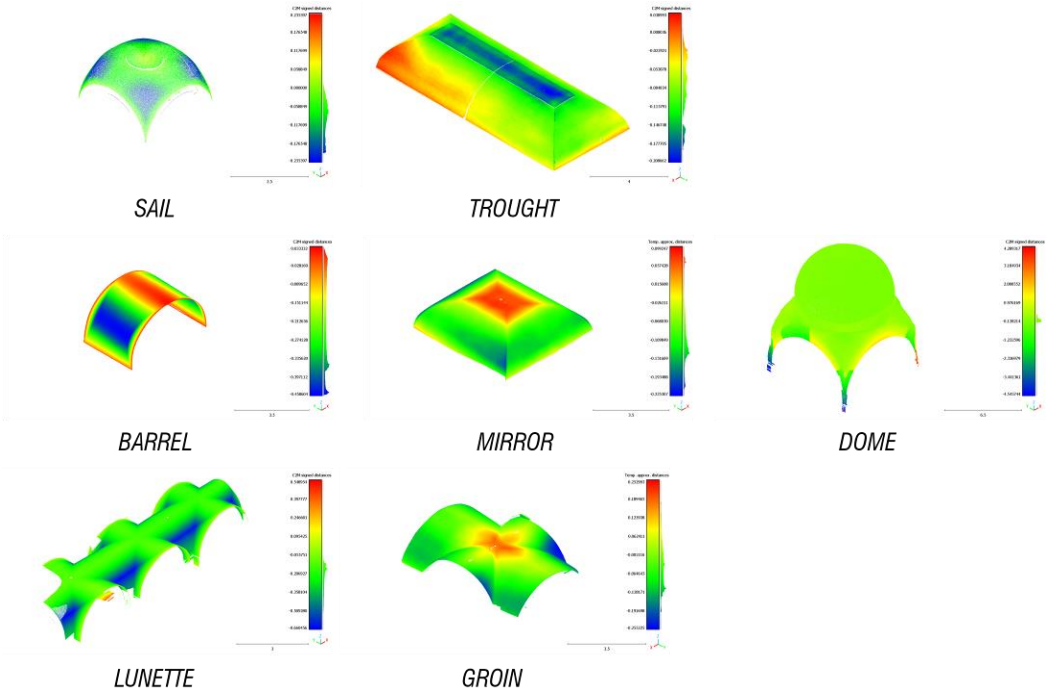

Fig. 102 Deviation analysis between the point cloud and the BIM Authoring model (2nd approach).

4.4.3 Last Remarks

Point cloud segmentation is a useful method for obtaining geometrical and informative data that provides accurate architectural semantization in the domains of AEC (Architecture, Engineering, and Construction) and CH (Cultural Heritage). Through techniques that are easily incorporated into BIM (Building Information Modelling) models, this process is used for 3D reconstruction.

There are numerous benefits to automated segmentation versus manual procedures. Faster processing rates are achieved, particularly when working with large datasets, and accurate repeatability is guaranteed, even for complex shapes that are difficult to segment manually. But for automation to be effective, reliable results from well-calibrated algorithms are necessary.

The RANSAC method has shown to be especially successful in accurately discretising ideal models in the context of this investigation. It dependably provides even when noisy and irregular point clouds are present.

This method's effectiveness can be ascribed to the careful parameter selection that results from a thorough examination of the geometric configuration and graphical representation of the elements that are being analysed.

The main goal of this study is to apply RANSAC to different kinds of vaulted structures, always in cooperation with the relevant BIM models, in order to enhance and broaden the comprehension of the method's suitability in various architectural settings.

4.5 Planning for Scanning using Deterministic and Meta-Heuristic Approaches

The scanning and digitisation of Cultural Heritage have undergone significant strides, particularly propelled by technological advancements and the widespread adoption of Building Information Modelling (BIM) within the Architecture, Engineering, and Construction (AEC) sector.

The utilisation of advanced instrumentation such as LiDAR and photogrammetry has enabled the attainment of high precision and data density. When coupled with meticulous architectural survey planning, these technologies facilitate the comprehensive recording of the object of interest under optimal conditions, ensuring maximum efficiency and data quality. This approach is geared towards minimising both time and costs associated with survey operations.

Often called 'network design', the expression really means 'Planning for Scanning' (P4S), particularly when discussing laser scanner acquisitions (TLS) (Biswas, Bosché and Sun, 2015; Aryan, Bosché and Tang, 2021). As elucidated in the state-of-the-art literature, various algorithms have been developed to identify optimal positions for data acquisition.

In the individual case of the Church of Ognissanti di Cuti in Valenzano (Italy), two distinct automation techniques were applied (Cabrera-Revuelta *et al.*, 2024).
A deterministic approach, based on the 'Art Gallery Problem', was employed for planning TLS stations within the building (Avis and Toussaint, 1981; Chesnokov, 2018). Additionally, a meta-heuristic approach utilising a genetic algorithm (GA) was applied for external acquisitions (Cabrera-Revuelta, 2017; Cabrera-Revuelta *et al.*, 2021).

Verifying the suitability of these techniques for improving TLS instrument station layout is the main goal of this research. This seeks to minimise redundancy and guarantee data completeness in the architectural survey of a heritage asset.

The next steps involved the combination of TLS with aero-photogrammetric data, georeferencing of the resulting point clouds using GNSS, automated procedures employing semantic segmentation using RANSAC, and parametric modelling within the BIM environment, custom-tailored to the specific case under analysis.

4.5.1 The All Saint's Church of Cuti in Valenzano (Italy)

The All Saints' Church of Cuti, situated in the rural expanse of Valenzano (Bari), stands as a relic of a Benedictine monastery with historical, administrative, and religious significance during the development of the Land of Bari (see Fig. 103). With dimensions measuring a mere 18.45 x 12.65 m^2, the church belongs to the category of buildings featuring axis domes, blending Byzantine influences with a distinct Apulian Romanesque design.

Fig. 103 The All Saint's Church of Cuti in Valenzano, Italy.

A detailed analysis of the architectural and structural elements of the edifice reveals a clear dichotomy between the internal arrangement and the external envelope. While external modifications have cast doubt on the validity of chosen solutions, the interior

spatiality – without the tonal fields and frescoes that once adorned the walls – preserves the essence of the original architectural concept.

The church's planimetric layout adheres precisely to pre-existing canons, with a longitudinal axis oriented East-West. The construction is characterised by remnants of a three-arched portico, entrances on different facades, and three naves culminating in apses, where the central apse notably surpasses the two flanking ones in size.

The primary nave is defined by three volumetric modules terminated by domes, while the two side aisles exhibit pilasters and rampant, half-barrel vaults. Beyond the domes, three square-based pyramids, adorned with Apulian stones and roofing slates, grace the exterior. The limestone walls of the church, squared and polished, remain unadorned except for bands flanking the windows.

The choice of this building for the implementation of various optimisation methods is driven by several factors. Firstly, the church stands isolated, offering ample space for TLS placement, free from dense vegetation that might impede visibility. Additionally, its medium height and single-storey structure eliminate the need for scans from elevated viewpoints. Lastly, the regular and symmetric distribution of the interior plan, adorned with domes, facilitates the discretisation of the building as a constant floor plan.

4.5.2 Methodolgy

The primary objective of this study is to conduct a comprehensive quality comparison of data acquired through TLS, employing two distinct methodologies.

- The initial approach employs automated optimisation methods, featuring a predetermined set of viewpoints outlined on the building plan. The internal viewpoints are derived through a deterministic method rooted in the Art Gallery Problem, while the external viewpoints are generated using a meta-heuristic technique based on a genetic algorithm.

- In the second approach, the automatically identified viewpoints form the foundation for introducing additional strategic viewpoints during the on-site architectural survey, guided by the operator's expertise. This ensures an optimal and comprehensive data acquisition process.

Subsequently, two sets of point clouds will be generated: one exclusively featuring the viewpoints automatically surveyed, and another incorporating the supplementary field stationary points.

The comparative analysis of the final point clouds aims to evaluate the overall effectiveness of the methods, emphasising the impact of absent staging points on the comprehensive coverage of the entire survey. Additionally, the study encompasses analyses of working time and the size of generated files.

i. **Planning the Interior Survey**

Reflecting on the Art Gallery Theorem, it asserts that *[n/3]* guards are both occasionally necessary and always sufficient to guard a polygon with *n* vertices (Chvátal, 1975). Avis and Toussaint's Algorithm vividly exemplifies this theorem through three concise steps, as illustrated in Fig. 104:

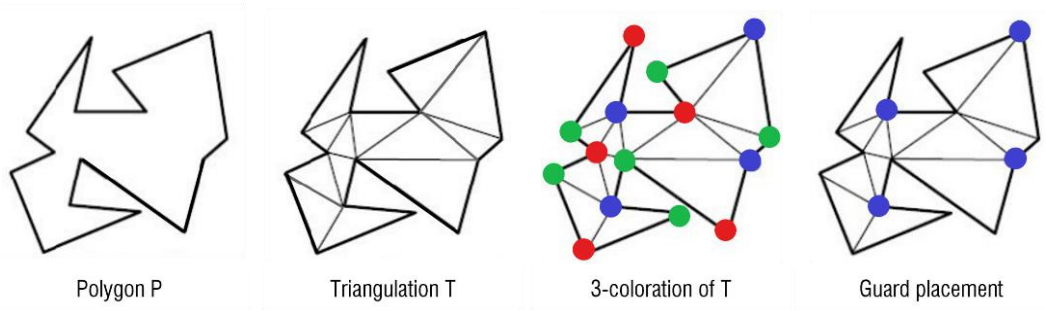

Fig. 104 The Art Gallery Problem (©adapted from (Avis and Toussaint, 1981)).

- Triangulate the polygon P, resulting in the creation of a graph T.
- Apply a three-colouring scheme to the nodes of T.
- Strategically position guards at the nodes assigned the least frequently used colour.

This algorithm computes areas of visibility, outlining regions where a guard can move without losing sight of the designated part of the building they are assigned to protect. The process begins by triangulating the entire interior area of the church.

Subsequently, the vertices of the triangles are colourised with three distinct colours in a manner that ensures no two adjacent vertices share the same colour (Fig. 105), adhering to the principles of the Four-Colour Theorem (Appel, Haken and Koch, 1977).

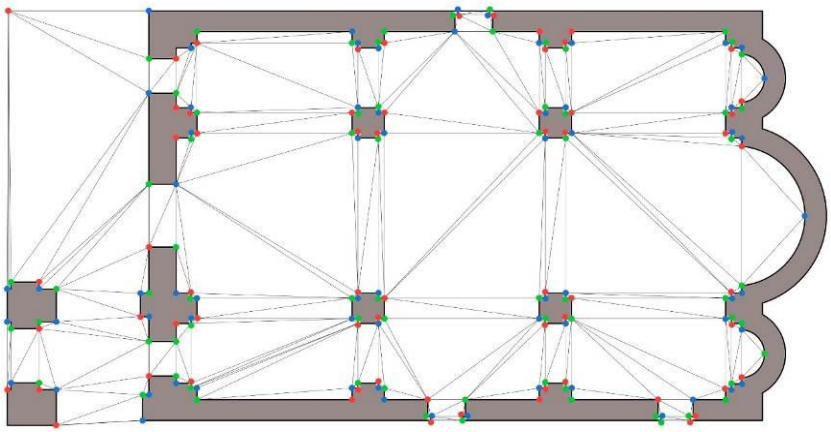

Fig. 105 Triangulation and three-colouring of the church plan.

This colouring approach results in each triangle having one vertex of each colour: blue, green, and red. Consequently, the vertices on the floor of the building are categorised into three sets based on their assigned colour.

The placement of a guard at all points sharing the same colour ensures complete surveillance of the interior enclosure. Following the three-colouring process, the subset of vertices sharing the colour with lower repetitions is selected. In this instance, the least repeated colour is red, occurring a total of 63 times, in contrast to 68 occurrences for both blue and green. Subsequently, the areas of visibility are calculated, outlining regions where the 'guard' (in this context, a TLS instrument tasked with monitoring a specific area) can navigate without losing sight of the assigned part of the perimeter. For each red vertex, the edges of the building floor that the guard must monitor are extended to generate convex areas, delimited by the building walls.

To illustrate the detailed procedure for finding these visibility areas, let's consider a specific part of the building's floor plan. As depicted in Fig. 106a, each red vertex is assigned the surveillance of a section of the building's perimeter based on the triangulation. Taking a specific vertex, Fig. 106b highlights the five edges that the guard must oversee, depicted in red.

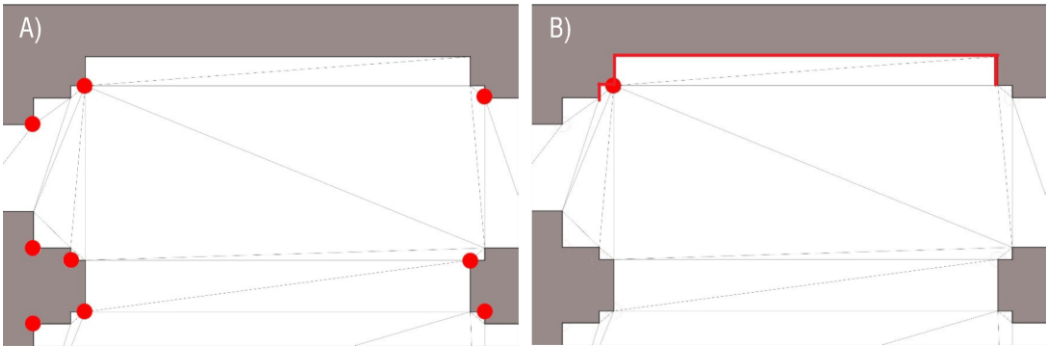

Fig. 106 A) Triangulation of an area of the church plan; B) The selected vertex and the five edges to be guarded by the guard are highlighted in red.

To delineate the area around which the guard can move without losing sight of an edge, the line defining the edge is extended. This extension generates a straight line that divides the space into two parts: one encompassing the walkable area and the

other including obstacles such as pillars and walls. The guard is positioned on the walkable side.

The five edges that the guard monitors are denoted as *a1, ..., a5*, in a clockwise direction. These edges are considered primary, while the others are secondary. Starting with the primary edge *a1*, the visible side is determined as the right side (See Fig. 107a). If an extension of a primary edge intersects with another edge, the operation is iterated for the new edge. This process continues until a convex area is generated, ensuring visibility of the primary edge (see Fig. 107b).

This procedure is repeated for the remaining edges. The next edge area, *a2*, is analyzed in Fig. 107c and it is possible for visibility areas of multiple edges to overlap, as seen with edges *a1* and *a2*. Continuing with the same approach, areas of visibility for edges *a3*, *a4*, and *a5* are shown below (Fig. 107d-e-f).

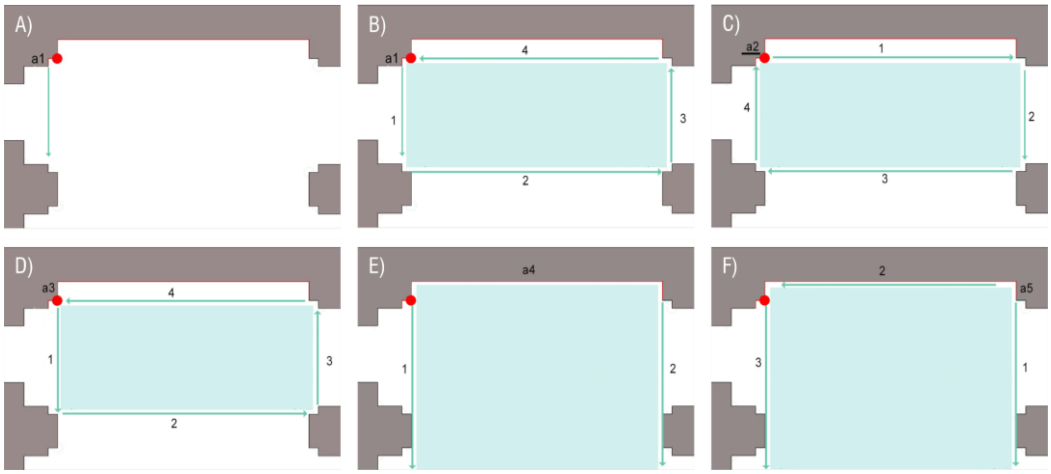

Fig. 107 A) Extension of the primary edge *a1*; B) Extension of the edge *a1* and interesction with the other edges, resulting in convex areas of visibility; C) Visibility area for the edge *a2*; D) Visibility area for the edge *a3*; E) Visibility area for the edge *a4*; F) Visibility area for the edge *a5*.

After calculating the visibility areas for each guard, it becomes essential to overlay them, allowing for the identification of the common area (see Fig. 108a). This composite region represents the total visibility area within which the guard can

maneuver without losing sight of the designated five edges (see Fig. 108b). This comprehensive process is repeated for every vertex, resulting in a total of 63 visibility areas corresponding to the 63 red-coloured vertices. Subsequently, the study of overlapping areas is conducted to minimise the number of positions by considering the coincidences among these regions (see Fig. 108c).

Fig. 108 A) Overlapping of the five visibility areas: B) Common visibility area for the selected vertex; C) Overlapping of calculated visibility areas for the vertices within a section of the church's interior.

In conclusion, a total of 11 visibility areas have been identified to ensure comprehensive surveillance of the building interior. To execute the TLS scanning of the building, the instrument must be positioned in each of these 11 designated areas (see Fig. 109).

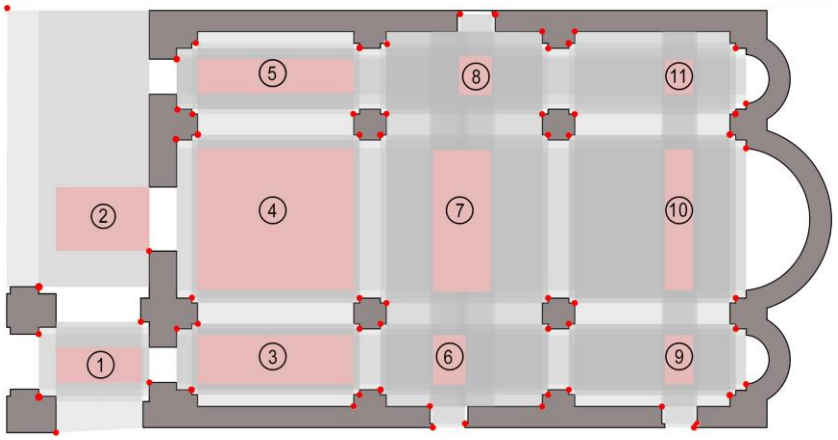

Fig. 109 Optimised visibility areas.

To confirm the comprehensive coverage of the entire church plan by the 11 designated areas, the UCL Depthmap software (Turner, 2007) was employed. This spatial network analysis tool is specifically designed for understanding social processes within a built environment. It operates at various scales, from architectural spaces to entire regions, assessing visual accessibility by constructing 'isovists' – regions visually accessible from specific locations (Casado and Sanchez, 2018).

By starting with the architectural space plan and fixing precise positions, the corresponding isovists represent the planar regions visible from those locations.
Fig. 110 demonstrates the usefulness of this tool in previewing and verifying the coverage of each of the calculated areas.

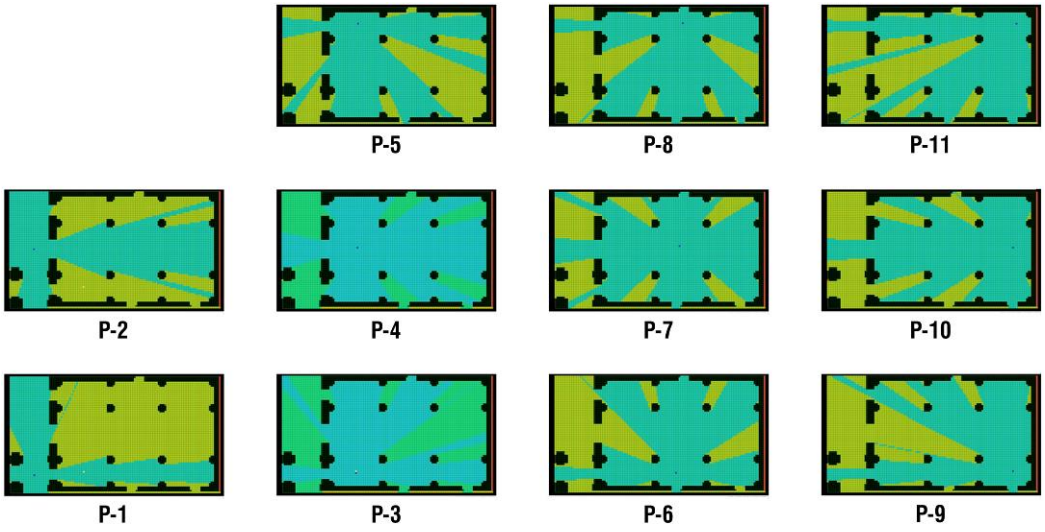

Fig. 110 Isovists generated for each of the 11 designated positions within the calculated visibility areas.

Additionally, the 11 calculated isovists have been overlaid to validate the coverage of the entire interior space. The image below illustrates the collective coverage achieved by the selected positions (See Fig. 111).

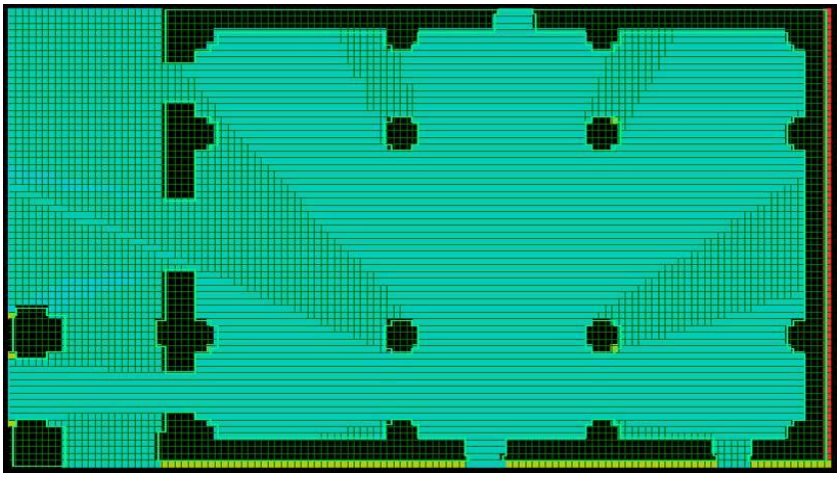

Fig. 111 Overlapping of the 11 isovists produced in UCL Depthmap.

Thus, it is inferred that these 11 positions would effectively cover the interior enclosure of the building. It is crucial to note that this is a theoretical approximation, and discrepancies may arise due to elements in height and objects not considered in the planimetry.

Furthermore, this deterministic method lacks consideration for variables such as working distance or the angle of incidence between the face and the laser ray. While this tool ensures theoretical space coverage, the expertise of the professional remains indispensable in determining the optimal point within each visibility area

ii. **Planning the Exterior Survey**

While the Art Gallery Problem provides a relevant framework for the task of planning for scanning, it is crucial to recognise that real-world scenarios involve constraints and situations not considered in theoretical models (Dehbi *et al.*, 2021). Therefore, the use of heuristic methods becomes essential for effectively addressing this problem in practical applications. These methods also enable the incorporation of TLS variables, such as working distance and the angle of incidence between the

instrument and the faces of the object. In this particular case, these variables are integrated into the genetic algorithm (GA).

Concerning the GA utilised in this study for analysing the exterior area of the church, it integrates the concept of *'survival of the fittest'* within sequence structures, employing a codified yet randomised exchange of information (Holland, 1992; Cabrera-Revuelta *et al.*, 2021).

Generally, GA commences with an initial set of potential solutions to a given problem, where each solution is denoted as an *'Individual',* collectively forming the *'Population'*, after the creation of an '*Initial Population'.* The operational environment for these individuals corresponds to the problem requiring resolution. Individuals will adapt to the environment with each successive generation. Each individual is assigned a code, analogous to the DNA of the individual, encapsulating all pertinent characteristics. These codes are associated with a value that quantifies the suitability of an individual as a solution to the problem, according to the *'Fitness Value',* determined by the *'Fitness Function'* (Cabrera-Revuelta, 2017).

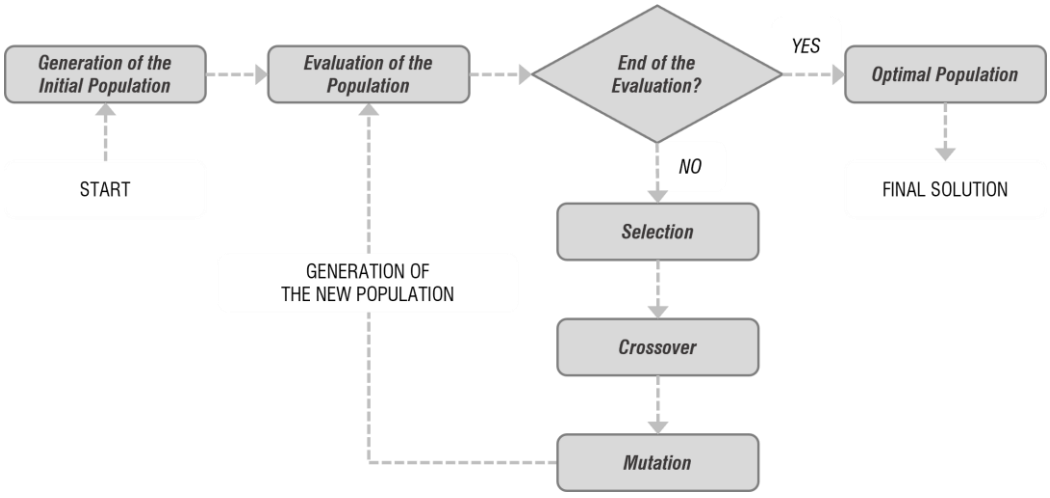

Fig. 112 Genetic Algorithm Workflow Diagram.

The stop criterion is defined to terminate the algorithm upon discovering an optimal solution. Until the stop criterion is met, the algorithm generates new pupolations through *'Selection', 'Crossover',* and '*Mutation*' operations (Majeed and Kumar, 2014). A workflow diagram illustrating the functioning of a GA is presented in Fig. 112.

In this work, a multi-agent model programmed in the NETLOGO environment was employed with the aim of maximising the monitored perimeter of a polygon using the minimum number of viewpoints from its exterior side. The main steps of the algorithm are described below:

- Draw or import the polygon to be monitored.
- Define the exterior area where potential positions can be situated.
- Specify the parameters of the TLS, including the working distance and angle of incidence.
- Initiate visibility areas: from each point along the perimeter, a vision area is launched based on the TLS parameters. Leveraging the principle of reciprocity of vision, the visible area for a point encompasses all the points capable of observing the initial point.
- Apply grayscale to the exterior area: lighter shades represent areas where a high number of visibility areas intersect, while darker shades indicate regions with fewer intersecting visibility areas.
- Implement the genetic algorithm, encompassing the following steps: a) Generate the initial population; b) Evaluate the initial population using the Fitness Function; c) Create a new population; d) Evaluate the new population; e) If the stop criterion is met, the algorithm halts; otherwise, proceed to step c.

- Validate the solution: upon completion of the genetic algorithm, it is imperative to confirm that the set of points is sufficient for monitoring the perimeter of the provided polygon.

In this algorithm, the *'Fitness Value' F(I_i)* of an individual, denoted as I_i, is derived by applying the *Fitness Function*. This function is specifically crafted to maximise the monitored perimeter of the polygon, minimise the required number of positions, and optimise the connectivity between positions. It is defined as a weighted sum of three parameters: a) *'Point of View Entropy' (Γ)*, quantifying the information provided by a potential solution; b) *Positioning Network Size (Φ)*, indicating the number of positions in a potential solution; c) *Connection between Positions (Δ)*, measuring the connectivity among positions within a potential solution.

This function is expressed in Equation [12]:

$$F(I_i) = \lambda_1 \Gamma(I_i) + \lambda_2 \Phi(I_i) + \lambda_3 \Delta(I_i) \quad \textbf{[12]}$$

Regarding the application of this tool to the analysed case study, NETLOGO allows to operates by generating the plan of the building from a .DXF file imported as a .CSV format file. The unit of measurement and the parameters of the TLS are then established. The tool provides a 2D space segmented into patches, and the resolution of these patches can be adjusted as needed.

Upon importing the plan, the tool autonomously identifies the perimeter of the polygon and defines the exterior area from which the perimeter needs to be monitored. The tool considers a working distance ranging from 30 to 100 meters and a minimum angle of incidence of 20° between the instrument and the walls to be recorded.

After establishing the primary parameters, the tool proceeds to analyse the entropy of each patch within the exterior area, reflecting the quality of a point of view in terms of the information it provides about the scene. This information is crucial for the *Fitness Function*, which evaluates the suitability of a potential solution to the problem.

The GA has successfully identified a total of 8 stations on the exterior side of the building. Fig. 113 illustrates the evolution of populations over more than 13,400 iterations. Notably, as the solution progressively adapts to the environment, increasing its *Fitness Value*, the number of positions oscillates until stabilising at 8.

In Fig. 114, the positions are highlighted with red dots. It's important to emphasise that this solution is theoretical, as the tool does not account for certain variables like the height of the building, environmental limitations, or the presence of obstacles.

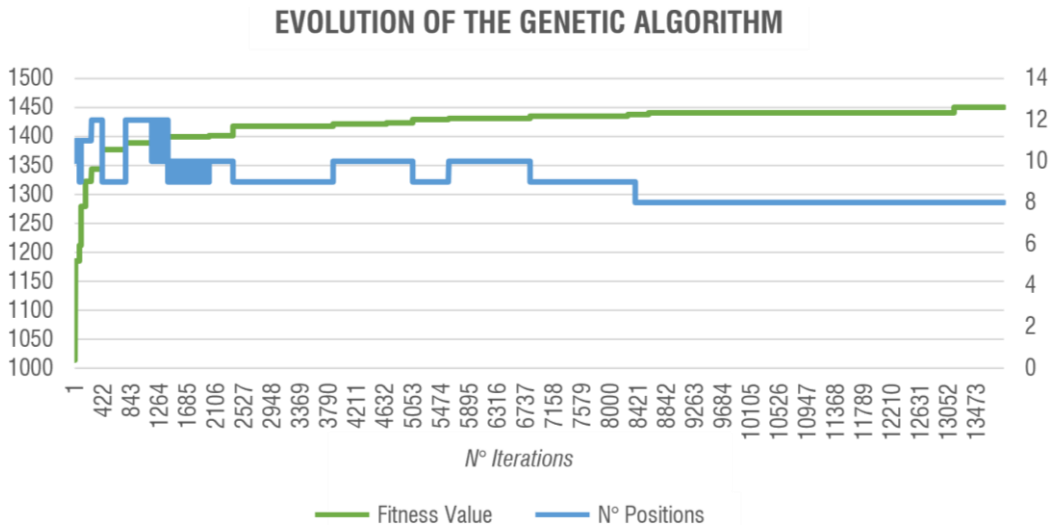

Fig. 113 Evolution of the Genetic Algorithm, depicting the rise in Fitness value in relation to the number of positions acquired.

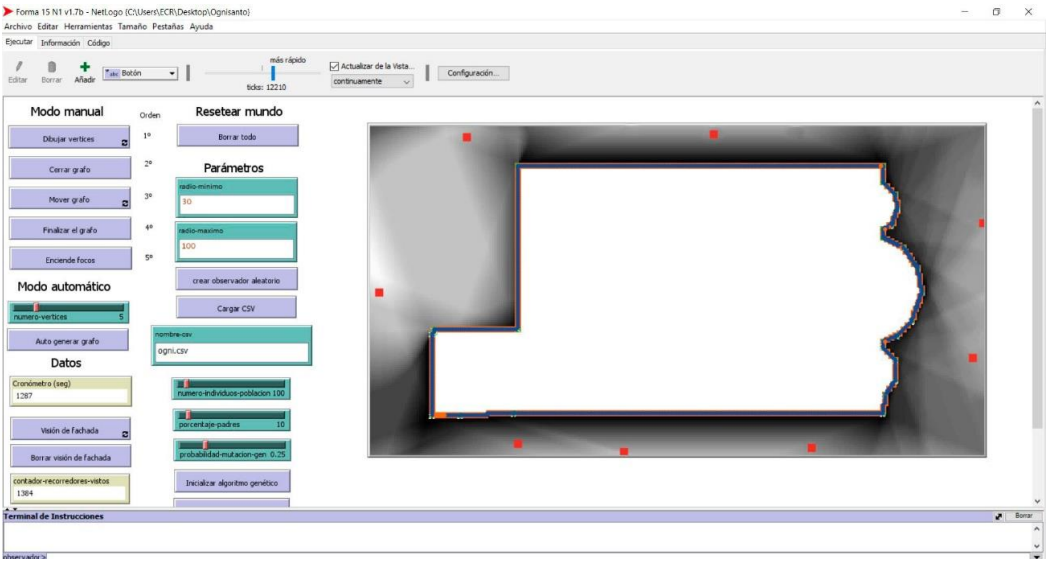

Fig. 114 Localisation of the 8 TLS positions (marked with red dots) identified through the Genetic Algorithm within the NETLOGO environment.

iii. **Data Acquisition**

Drawing upon optimisation methods for planning the church survey, a total of 19 TLS station locations are identified for effective data acquisition, with 11 positioned indoors and 8 outdoors. To ensure a satisfactory Level Of Completeness (LOC) and mitigate potential uncertainties that the Genetic Algorithm (GA) may not fully address, 7 additional strategically chosen stations were incorporated based on the operator's expertise.

These supplementary positions were thoughtfully selected to ensure connectivity between stations that might be mutually invisible. The overall execution involved 26 laser stationing positions, distributed as 14 for the exterior and 12 for the interior.

In Fig. 115, the positions of the TLS are depicted, with the predicted ones marked in green and the additional ones in yellow. It's noteworthy that the position of some of

the 19 initially calculated points has slightly adjusted, accounting for obstacles and ensuring connectivity between the interior and exterior areas.

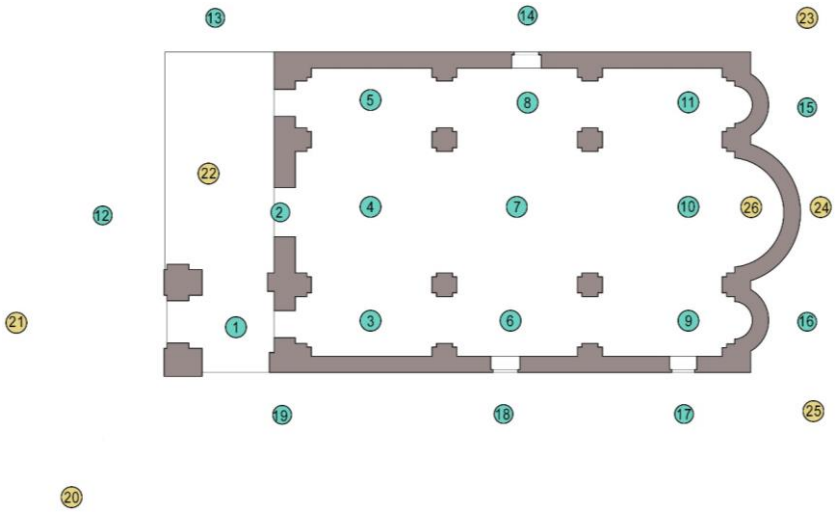

Fig. 115 Location of the 19 initially calculated stations (marked in green) and the 7 complementary ones (highlighted in yellow).

Point clouds were gathered both inside and outside the church using the CAM2®FARO Focus 3D 120 laser scanner. Outdoor scans, conducted within a 20-meter range, have a resolution of 28.2 Mpts and an acquisition resolution of 7.670 mm/10 m, lasting up to 6 minutes and 38 seconds. Indoor scans, executed at a 10-meter radius, possess an acquisition resolution of 12.272 mm/10 m and a resolution of 11 Mpts, with a scan time of 2 minutes and 57 seconds.

Depending on ambient light conditions, horizon-weighted metering near openings and balanced metering outside were employed to determine scanning exposure. An automatic sky filter was activated to remove points with very low reflectance values, streamlining subsequent processing.

For interior scans, only the inclinometer sensor was used to simplify and compensate for instrumental balance.

During external area acquisition, inclinometer, magnetometer sensors, GPS signals and also photogrammetry were utilised for metadata acquisition, aiding in subsequent processing and alignment (Fig. 116).

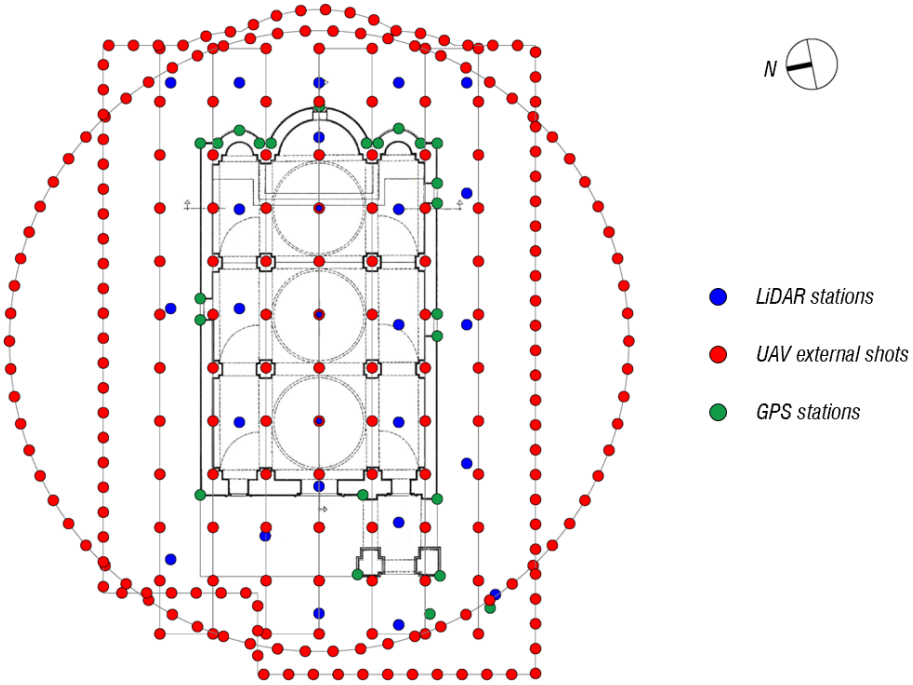

Fig. 116 Survey planning with LiDAR, UAV, and GPS equipment.

The photogrammetric survey was specifically conducted using a DJI Spark drone equipped with a 12 MPx camera, capturing a total of 240 shots. The flight plan involved a single-grid nadiral flight at a 45° angle in a circular path, and a 30° angle along the perimeter of the building. For georeferencing purposes, a topographic survey was performed utilising a Tersus Oscar GNSS receiver, measuring 24 ground control points (GCPs). Some of these points were positioned at targets associated with geographic coordinates in the WGS84 geodetic reference system (EPSG:4326), expressed in decimal degrees (latitude, longitude), with the addition of ellipsoidal height.

In this specific istance, the area, enclosed by a perimeter fence, proved to be sufficiently confined and secure for all laser survey and drone overflight operations. Safety and assessment procedures in compliance with Regulation (EU) No. 947/2019 and subsequent amendments were adhered to during these activities. This included searching for any Notice To AirMen (NOTAM) communications and consulting thematic geographic maps (see Fig. 117).

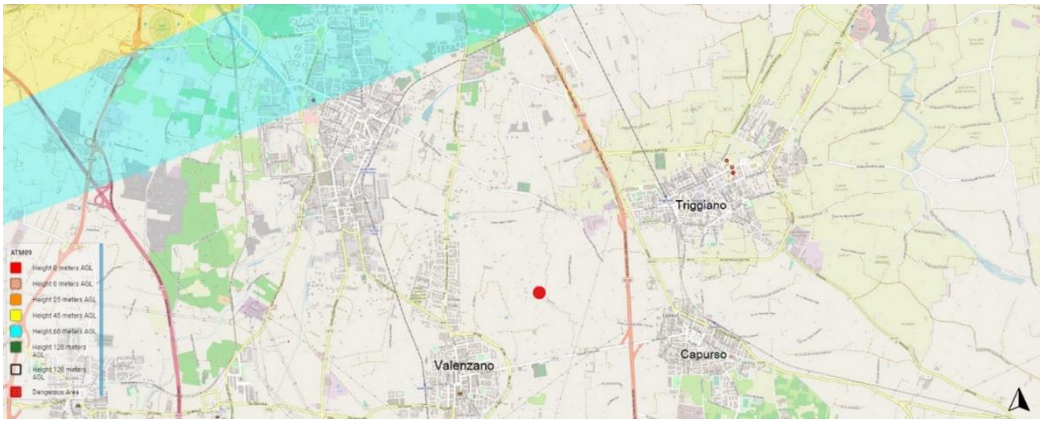

Fig. 117 Airspace map highlighting flight limitations.

4.5.3 Results

The LiDAR data processing was conducted using Autodesk Recap Pro® software. This involved the automated initial registration followed by a manual registration of aligned scan pairs through three homologous points.

The registration process was executed twice: initially, considering all 26 scans (R_26S), and subsequently focusing solely on the optimised subset of 19 scans (R_19S). Following this, an analysis was conducted to assess the feasibility of registration for both sets, taking into account processing time, file size, and the quality of registrations.

i. **Results of the TLS Data Registration**

The key outcomes for both scenarios (R_26S and R_19S) are presented inTab. 10. The optimised approach (R_19S) achieves a comprehensive registration of the geometry, leading to a 31% reduction in processing time and a 32% reduction in file size. The R_26S point cloud comprises 144 million points, while the R_19S point cloud comprises 119 million points. This indicates that the optimised process results in a 21% reduction in points.

Tab. 10 Results of point cloud Registration using two Planning Methods (R_19S - Optimised Method; R_26S - Addition of station points).

	R_26S	**R_19S**
Auto-registered groups	05	04
File .E57 weight (GB)	10.9	07.4
Number of points (millions)	144	119
Importation time (min)	84	55
Auto-registration time (min)	04	04
Index scan time (min)	18	15
Exportation time .E57 (min)	08	06
Total Process time (min)	127	88

Fig. 118 depicts the complete registrations of the perimeter for both projects.

Following the importation and registration of the scans, the alignment quality is described based on a report generated by the software, considering three parameters explained below. Firstly, the '*Overlap' (O)* represents the percentage of common features across the entire project. Secondly, the '*Balance' (B*) indicates the percentage of common features within the scan. Thirdly, the parameter '*Points (<6 mm)' (P)* signifies the percentage of overlapping points within 6 mm of the

corresponding feature in the project, aiming for a value higher than 90%. The data obtained for both registrations are presented in Tab. 11.

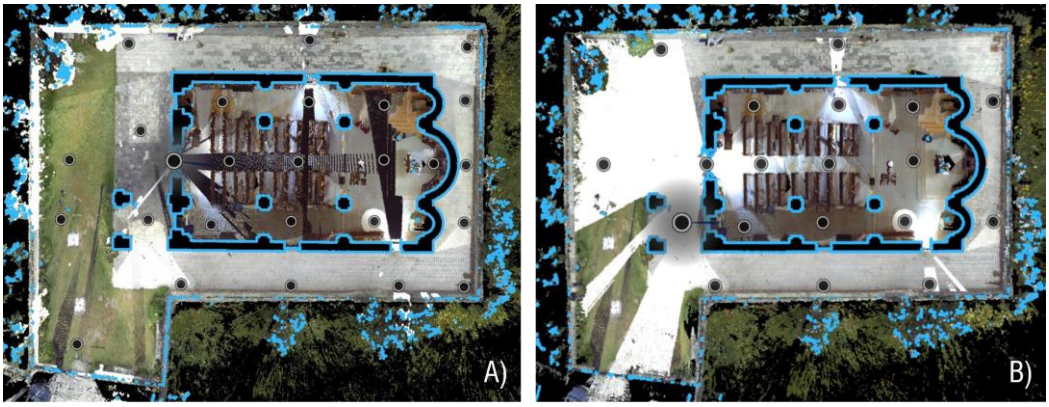

Fig. 118 Display of registered station points in Autodsk Recap: A) R_26 group; B) R_19 group.

Tab. 11 Results of point cloud Alignment using two Planning Methods (R_26S and R_19S).

	R_26S			***R_19S***		
Station	***O (%)***	***B (%)***	***P (%)***	***O (%)***	***B (%)***	***P (%)***
1	35.1	50.3	99.3	24.5	57.9	99.3
2	43.4	60.3	99.9	37.0	58.5	99.9
3	46.6	80.4	99.8	39.0	82.9	100
4	51.7	76.4	100	51.7	73.0	100
5	50.7	80.3	100	41.4	57.3	99.9
6	49.1	79.1	99.8	45.6	79.5	100
7	48.0	92.2	99.9	48.0	91.9	99.9
8	48.9	75.3	100	46.0	52.3	100
9	48.4	57.5	100	45.2	61.9	100
10	55.0	67.5	100	50.8	67.9	100
11	48.6	51.6	100	46.0	52.3	100
12	73.7	40.6	99.5	46.4	63.9	100
13	49.5	76.5	98.0	40.7	73.0	97.9
14	32.3	2.0	98.8	21.3	0.0	98.3
15	27.2	8.0	99.9	4.7	5.9	100

16	25.9	8.2	99.9	10.4	5.6	100
17	48.0	5.5	99.8	34.4	5.8	99.7
18	45.0	6.1	99.9	44.7	6.0	99.9
19	48.8	33.2	99.6	41.1	37.3	99.5
20	48.3	75.1	97.8			
21	65.7	24.2	99.2			
22	49.5	76.5	98.0			
23	35.9	31.1	99.5			
24	21.5	6.7	99.8			
25	46.6	34.5	99.9			
26	18.0	60.4	100			

The resulting point clouds from both sets were imported into the CloudCompare software (Girardeau-Montaut, 2020) to analyse geometric deviations between them.

The Cloud-to-Cloud Distance comparison (C2C) algorithm was employed to measure the disparity between the clouds. This tool calculates distances between two clouds by designating one as the reference and the other as the compared cloud. It measures the distance from a point in the compared cloud to the nearest point in the reference cloud, displaying the results on a scalar field's colour scale.

This method revealed negligible differences between the clouds, indicating similar quality with no significant losses from omitting complementary positions. Out of 143,951,541 points, 92% found corresponding points in the other cloud within a distance less than 5 mm.

Fig. 119a illustrates that 8% of points from R_26S do not find corresponding points in R_19S within 5 mm. Fig. 119b shows their superimposition, revealing effective coverage by the optimised process, attributing deviations to point cloud registration rather than data absence.

Additionally, Fig. 120 presents a histogram displaying the frequency of distances between points, with a notable concentration around 2 mm and a mean value of 2.98 mm.

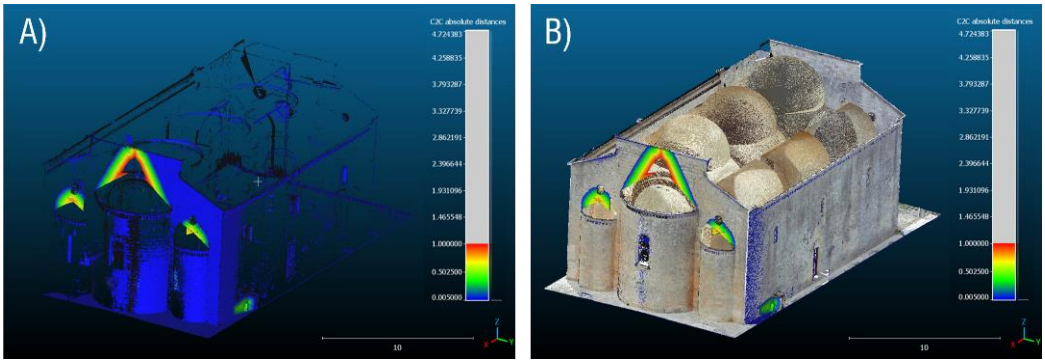

Fig. 119 A) 8% of points from R_26S without any corresponding points in R_19S within a distance less than 5 mm; B) Overlay of R_19S with this 8% of points.

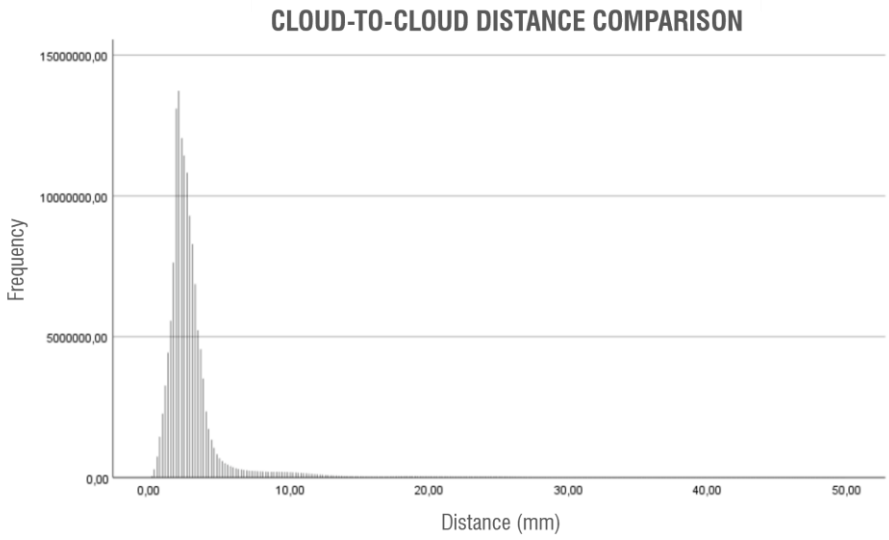

Fig. 120 Cloud-to-Cloud Distance Comparison between the two group of point clouds (R_19S and R_26S).

ii. **Results of the Data Integration**

Subsequently, utilising Agisoft Metashape Pro®, the photogrammetric data mentioned earlier underwent subsequent processing to scale and georeference the model within the WGS84 geodetic system (EPSG:4326) (Verdoscia *et al.*, 2023).
This was achieved by placing markers in accordance with points measured using the GPS receiver. The accuracy of the entire model's points averaged at 0.03 m, considering some Ground Control Points (GCPs) converted into Quality Control Points (QCPs).

Fig. 121 Georeferenced and integrated point cloud of the church.

Through targetless registration using three homologous points, the photogrammetric point cloud was later integrated with LiDAR data using Autodesk Recap Pro® software.

To position the church in EPSG:32633 – WGS 84/UTM zone 33N, geographic coordinates from GPS data were transformed into UTM projected coordinates. Georeferencing of the range/image-based data using GCPs as reference points was performed with the CloudCompare software. Fig. 121 displays the integrated and georeferenced point cloud.

4.5.4 Export and BIM Authoring Processes

Decimation, filtering, and point cloud segmentation procedures were implemented to optimise the entire processed data in one of the final processing stages.

To this purpose, utilising multi-RANSAC type algorithms in the Python language, automatic segmentation operations were conducted on the point cloud to recognise flat and curving walls, floors, and vaulted structures as references for adaptive parametric families used in model development (Fig. 122).

For flat elements, specific variables considered included the value of the maximum distance *(distance threshold)* between *inliers* and the ideal shape, the number of points sampled *(ransac_n)*, and the number of iterations *(num_iterations)*. Spherical ideal geometries (center and radius parameters) and cylindrical rotation surfaces (center, radius, and rotation axis *np.array (1,3)*) were employed for outliers found on vaulted structures and curving walls.

Subsequently, the segmented point clouds were imported into Autodesk Revit® modelling software for better management and visualisation, enhancing computational speed during the processing phase. System and in-place families were predominantly used for architectural and structural components. Customised loadable families (.rfa) were created using adaptable components, joined via splines or reference lines to define and fit the geometry of the vaulted structure to the point cloud, especially for reconstructing masonry vaults.

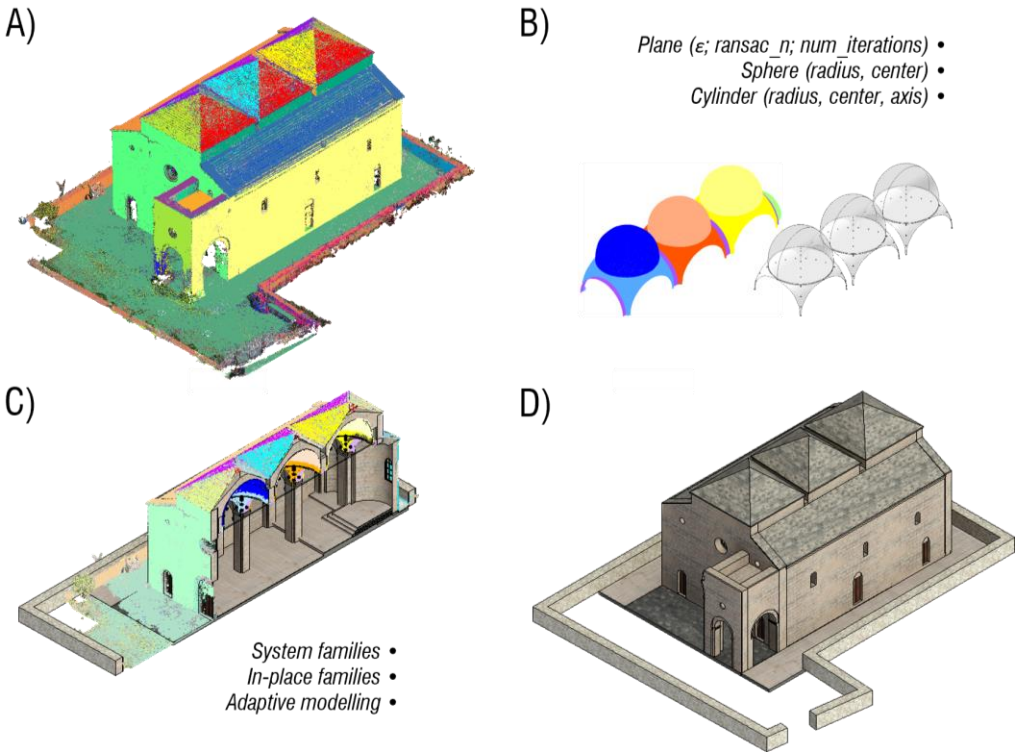

Fig. 122 Scan to BIM approach adopted: A) Multi-RANSAC automatic segmentation; B) Segmentation of the Vaulted Structures and Construction of the adaptive families; C) Integration of semantic segmentation in BIM Environment; D) Final BIM Authoring Model.

4.5.5 Closing Statements

While it is essential to begin digital data acquisition with a well-planned approach that incorporates the judgment and experience of the professional for on-site decisions, the presented work demonstrates promising results derived from the executed optimisation techniques.

The achievement of the Level of Completeness, obtained through a deterministic approach and particularly facilitated by triangulations, enabling visibility zones within the studied church, was further complemented by a meta-heuristic approach using the genetic algorithm to identify optimised survey points.

In particular, the shortcomings of the first method, such as the non-consideration of variables like the operational range of the laser scanner and the angle of incidence between the instrument and the surveyed object, were addressed by the second method. However, in the latter case, although the Fitness Function was designed to reward solutions minimising the number of positions and maximising the monitored perimeter, constraints such as obstacles around the building were not taken into account.

This work focused solely on the building's floor plan as input, neglecting height and treating the building as a two-dimensional element. Nevertheless, the registration of the entire geometry, consistent in height and covered by domes and vaults, was successfully achieved with an acceptable loss of information as the distance between the TLS scanner and the walls increased.

Given the diverse possibilities in the distribution, geometry, and external factors of buildings, it cannot be presumed that this method is universally applicable. However, it can be a valuable support during the survey planning phase, and it may be essential to develop a method capable of simultaneously considering both the exterior and interior of a building.

The enhancing of operational work timelines and processing/post-production methods allowed for the simultaneous fulfillment of the informational-geometric quality requirements of the survey and the pre-assigned safety standards, avoiding the recording of unnecessary information that typically causes delays during project execution.

Data integration, georeferencing, and automatic point cloud segmentation are additional operational aspects that achieved accurate geometric parameters of the building, providing valuable support for the creation of the as-built parametric model.

Nevertheless, limitations and challenges were encountered, primarily due to the lack of comprehensive software for model management, involving data conversion, import, and export, which can significantly impact project efficiency.

4.6 Point Cloud Semantic Segmentation and Classification with Random Forest Machine Learning Algorithm

The integration of automated point cloud segmentation and classification through various learning techniques signifies a noteworthy advancement in the current landscape of Artificial Intelligence (AI) and Heritage Building Information Modelling (HBIM) applications. These sophisticated methodologies introduce innovative approaches for the in-depth analysis of 3D data, particularly within the fields of architecture and engineering.

AI, specifically machine learning and deep learning, has transformed the handling and interpretation of extensive datasets. In the realm of point clouds, automatic segmentation identifies and segregates distinct components within a three-dimensional environment, including architectural elements and objects. This process is essential for enhancing the comprehensibility and usability of information collected from technologies like laser scanning and photogrammetry.

The integration of these techniques with HBIM (Bassir *et al.*, 2023) adds a layer of intelligence and contextualisation to geometric data. The automatic classification of point clouds enables the automatic assignment of semantic labels to different parts of the building (Grilli and Remondino, 2020; Croce, Caroti, De Luca, *et al.*, 2021), contributing to the development of more comprehensive and practical BIM models. Such a combination includes expediting and refining the modelling of existing buildings, facilitating a detailed assessment of structural conditions, and streamlining information management throughout the lifecycle of the structure.

This sets the stage for the work outlined below. The focus is on semantically segmenting the architectural elements of a renowned palace in Zaragoza, Spain. The objective is to classify the point cloud and break it down into its distinct components, laying the groundwork for expediting future processes in HBIM.

In this context, AI plays a crucial role through a machine learning algorithm developed in the Python environment. The algorithm undergoes testing on various combinations of geometric features that characterise the point cloud.

In this regard, the outcomes will be examined through analytical and visual comparisons, specifically focusing on the two floors within the inner courtyard of the building.

4.6.1 The Palace of the Counts of Sástago in Zaragoza (Spain)

The Palace of the Counts of Sástago in 16th-century Zaragoza, a symbol of the formidable influence of the III Count of Sástago, Don Artal de Alagón y Luna, has played a pivotal role in history. From hosting monarchs and serving as military headquarters to enduring the Siege of Zaragoza, the palace has a rich legacy. Damaged during the burning of the nearby convent of San Francisco, it has been repurposed over the years, housing the Captaincy General of Aragon and functioning as police headquarters.

Noteworthy for its eclecticist and neo-baroque charm, the palace features the renowned 'Casa Zorraquino' on the ground floor. Its brick façade reflects architectural norms shaped by the scarcity of stone in the region. The palace's interior boasts a grand Renaissance courtyard, entrance hall, noble stairs, and distinguished rooms, including the Throne Room. Despite limited public access, the palace houses a modernist library and hosts exhibitions, showcasing works by artists like Picasso, Dalí, and Manuel Viola, transforming it into a vibrant cultural hub within its historic walls.

Specifically, the architectural space of the inner courtyard (Fig. 123) is characterised by an elegant fusion of classical elements and typical Renaissance ornamental details. It features a symmetrical design with partially grooved columns and arches surrounding the central area. The columns, often adorned with sculpted motifs and floral details, support regular arches, creating a harmonious and refined atmosphere.
The courtyard facades may showcase decorative elements such as friezes, finely sculpted ionic capitals, and ornamental windows.

The judicious use of materials such as stone adds a timeless elegance to the courtyard evoking a sense of history and beauty.

Fig. 123 Inner courtyard of the Palace of the Counts of Sástago in Zaragoza, Spain.

4.6.2 Methodology

The adopted approach (Fig. 124) aims to automatically recognise recurring architectural elements in the point cloud, particularly pertaining to the inner courtyard of the building. These elements are then classified and cataloged within a Scan to BIM context, streamlining future modelling operations and optimising efficiency.

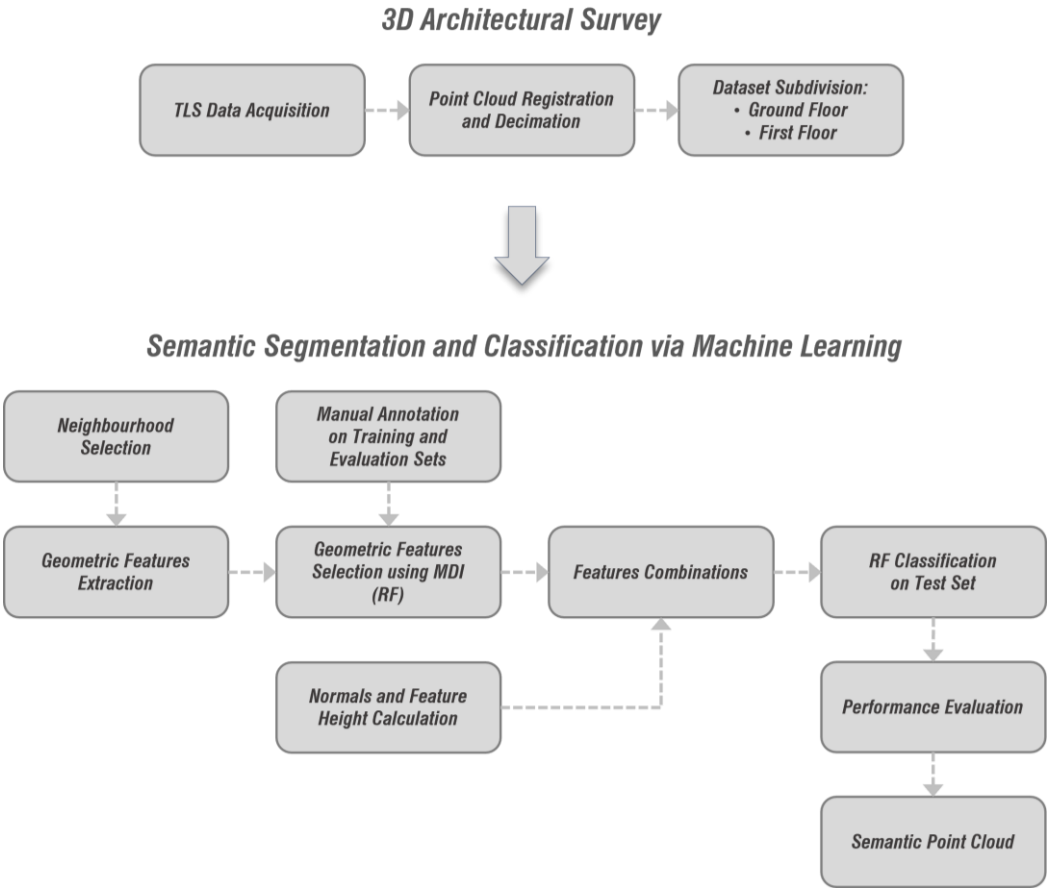

Fig. 124 Methodology Workflow.

Specifically, starting from a raw portion of point cloud data acquired through laser instrumentation, a processing procedure was applied.

This involved identifying the most relevant geometric features, which, combined with manual annotations, were used to train a Random Forest machine learning algorithm. The goal was to enable the algorithm to automatically classify the remaining point cloud.

The study area was divided into two subsets of data corresponding to the ground floor and the first floor. This division was based on different architectural components for each floor, aiming to facilitate the training process and prevent redundancy in error calculations.

i. **3D Architectural Survey**

The survey was conducted using the CAM2® FARO Focus M 70 laser scanner, with a Field of View of 300° vertical / 360° horizontal, a Ranging Error of ± 3 mm, and an Unambiguity Interval of 614m for up to 0.5 million points per second.

A total of 32 indoor scans were performed, comprising 21 scans on the ground floor and 11 on the first floor. The scans were carried out at a radius of 10 meters, featuring a Resolution of 11 million points, a Net Scan Duration of 5 minutes and 11 seconds, and a Scan Size of 5156*2134 points.

The point cloud was registered using Autodesk Recap software through an automated and manual registration process, the latter involving the identification of three corresponding points for pairs of scans.

The initial registration of 6 mm was subsequently refined. First, by employing a noise reduction process through the Statistical Outlier Removal (SOR) within the CloudCompare software, and then through subsampling at 2 cm intervals for better computational file weight management.

As a result, the entire dataset, spanning an area of approximately 12.20 m x 8.90 m, was divided into two groups: one related to the ground floor of the inner courtyard

and the other to the first floor (Fig. 125). Subsequent processing steps were then carried out concurrently for each floor.

Specifically, a portion of points was cropped for the Training phase, another for the Model Evaluation phase, and the remaining dataset for each floor was considered as the Test set for the final Classification.

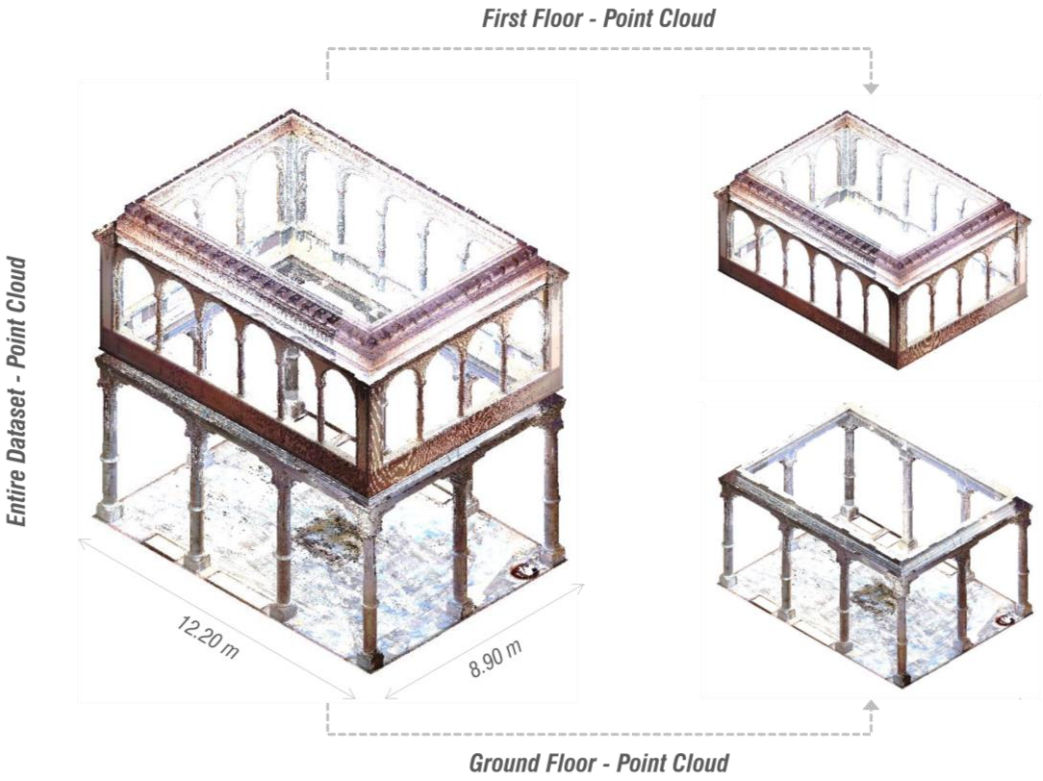

Fig. 125 Subdivision of the entire point cloud into two groups: Ground Floor and First Floor.

Tab. 12 provides a more detailed overview of the dataset.

Tab. 12 Full Dataset specification.

	N° points	Point spacing
Point cloud_Ground Floor	5,323,756	6 mm
Subsampled point cloud	427,068	2 cm
Training	53,713	2 cm
Evaluation	54,432	2 cm
Test	318,923	2 cm
Point cloud_First Floor	4,579,345	6 mm
Subsampled point cloud	440,695	2 cm
Training	56,032	2 cm
Evaluation	54,914	2 cm
Test	329,749	2 cm

ii. **Semantic Segmentation and Classification via Machine Learning**

The subsampled and optimised point cloud for each floor serves as input for the semantic segmentation work with Machine Learning. To achieve this, various phases are carried out, as mentioned in the previous workflow and outlined below:

- Neighbourhood Selection;
- Geometric Features Extraction;
- Manual Annotation on Training and Evaluation Sets;
- Geometric Features Selection using MDI (RF);
- Normals and Feature Height Calculation;

- Features Combinations;
- RF Classification on Test Set and Performance Evaluation;
- Annotated Point Cloud

Neighbourhood Selection

In detail, on the two subsets of point clouds, using CloudCompare software, a series of covariance features were extracted, mainly chosen on the basis of different local neighbourhood radii.

The 'Local Neighborhood Radius' refers to the extent of the surrounding area around each point in the point cloud that is taken into consideration during the extraction of geometric features (Weinmann, Jutzi and Mallet, 2013). This parameter establishes the maximum distance within which other nearby points are factored in when computing the geometric attributes of the central point.

The fundamental concept is that the geometric characteristics of a point in a point cloud are notably influenced by the neighboring points. By precisely adjusting the radius of the local neighborhood, one gains control over the spatial scope considered during the analysis of features associated with each point.

Hence, an approximately constant radius step, ranging from 10 to 20 cm, was established, covering the smallest element to be analysed up to values approaching one meter for larger architectural elements.

Geometric Features Extraction

'Covariance features' represent geometric characteristics extracted from the covariance matrix of a set of points in three-dimensional space, often referred to as the 3D structure tensor (Chehata, Guo and Mallet, 2009; Dahl, 2019; Rodríguez-Gonzálvez and Rodríguez-Martín, 2019). This structure tensor is computed based on the spatial information of points within a specific local neighborhood.

This computation enables the capture of geometric relationships among points, offering insights into the distribution and shape of the point cloud. Specifically, Covariance features are derived from the eigenvalues of the covariance matrix, providing meaningful information about the local geometry of the points.

From the Matrix of Points *(A)* [13], the Covariance Matrix *(Cov)* [14] for each of the *n* points in a point cloud with coordinates of *x, y, z* – where x_m, y_m, z_m are the centroid coordinates – is acquired. This covariance matrix reflects variance values along its principal diagonal. Using a statistical analysis known as 'Principal Component Analysis' (PCA), after applying the diagonalisation process to the covariance matrix, the eigenvectors (e_1, e_2, e_3) are obtained. This allows us to measure the local point variation set along the direction of the corresponding eigenvectors and reveals three eigenvalues $(\lambda 1, \lambda 2, \lambda 3)$ that help us understand the local geometry of the point cloud.

$$A=\begin{bmatrix} x_1-x_m & y_1-y_m & z_1-z_m \\ \vdots & \vdots & \vdots \\ x_n-x_m & y_n-y_m & z_n-z_m \end{bmatrix} \quad \textbf{[13]}$$

$$\mathrm{Cov}=\frac{1}{n}\,A^tA\begin{bmatrix} \sigma_{xx} & \sigma_{xy} & \sigma_{xz} \\ \sigma_{yx} & \sigma_{yy} & \sigma_{yz} \\ \sigma_{zx} & \sigma_{zy} & \sigma_{zz} \end{bmatrix} \quad \textbf{[14]}$$

The eigenvalues, which are sorted in descending order as $\lambda 1 \geq \lambda 2 \geq \lambda 3$, correspond to the major components of the spatial distribution of the points. The following 3D properties, which fall within the category of dimensional features are computed using these eigenvalues: Linearity [15], Planarity [16], and Sphericity [17].

These eigenvalues also serve as the basis for other measurements, including Omnivariance [18], Anisotropy [19], Eigenentropy [20], Sum of Eigenvalues [21], and Surface Variation [22], which is also referred to as the Change of Curvature. Additional features that can be extracted are Verticality [23], which is regarded as a 'Normal-based feature', and Height [24], which is considered as a 'Height-based feature'.

The kinds of features that can be extracted using the corresponding equations are listed in Tab. 13.

Tab. 13 Geometric Features specification.

Feature Typology	Name	Equation
Covariance	Linearity	$L_\lambda = \frac{\lambda_1 - \lambda_2}{\lambda_1}$ [15]
	Planarity	$P_\lambda = \frac{\lambda_2 - \lambda_3}{\lambda_1}$ [16]
	Sphericity	$S_\lambda = \frac{\lambda_3}{\lambda_1}$ [17]
	Omnivariance	$O_\lambda = \sqrt[3]{\lambda_1 \lambda_2 \lambda_3}$ [18]
	Anisotropy	$A_\lambda = \frac{\lambda_1 - \lambda_3}{\lambda_1}$ [19]

	Eigenentropy	$E_\lambda = -\sum_{i=1}^{3} \lambda_i \ln(\lambda_i)$ [20]
	Sum of Eigenvalues	$\Sigma_\lambda = \sum_{i=1}^{3} \lambda_i$ [21]
	Surface Variation	$C_\lambda = \frac{\lambda_3}{\Sigma_\lambda}$ [22]
Normal-based	Verticality	$V_\lambda = 1 - \lvert([0\ 0\ 1], e_3)\rvert$ [23]
Height-based	Height	Z Coordinate [24]

These features capture various aspects of the local geometry, allowing for a detailed analysis of the 3D point cloud. Adjusting the values of these features based on the radius influences the scale at which these geometric characteristics are evaluated within the point cloud.

In detail:

- Linearity: This feature measures how well the points in a local neighborhood align along a straight line. A higher value indicates a more linear arrangement, which could correspond to elongated structures or features in the point cloud.
- Planarity: It assesses the extent to which points lie on a plane. A higher value implies a more planar arrangement, indicating surfaces or areas with relatively flat geometry.

- Sphericity: It characterises how well points are distributed in a spherical manner. Higher sphericity suggests a more rounded or isotropic distribution, which could be relevant for spherical structures.
- Omnivariance: It represents the overall variance of the point distribution. It provides a comprehensive measure of the variability in different directions within the local neighborhood.
- Anisotropy: It measures the directional variability of the point distribution. A higher anisotropy value indicates a greater difference in spread along different directions, highlighting directional patterns in the point cloud.
- Eigenentropy: It measures the entropy or disorder based on the eigenvalues of the covariance matrix. Higher eigenentropy values indicate greater complexity and randomness in the point distribution.
- Sum of Eigenvalues: The sum of eigenvalues reflects the total variance within the local neighborhood. It gives an overall measure of how spread out the points are in the space.
- Surface Variation: Also kwons as Change of Curvature, it represents how much the surface curvature changes within the local neighborhood. Higher values suggest areas with more significant changes in surface shape.
- Verticality: It is a normal-based feature that characterises how vertical the local point distribution is. Higher values indicate a more vertical alignment of points, which could be relevant for identifying vertical structures.
- Height: It is a height-based feature that provides information about the overall height of the local point cloud. It could be useful for identifying elevated or depressed regions within the point cloud.

The graphics (Fig. 126 and Fig. 127) display examples of ‘ad hoc’ features, examples of features that will be further discussed in relation to ‘ad hoc’ features – named for their relation to the geometric dimensions (radius and diameter) of architectural elements.

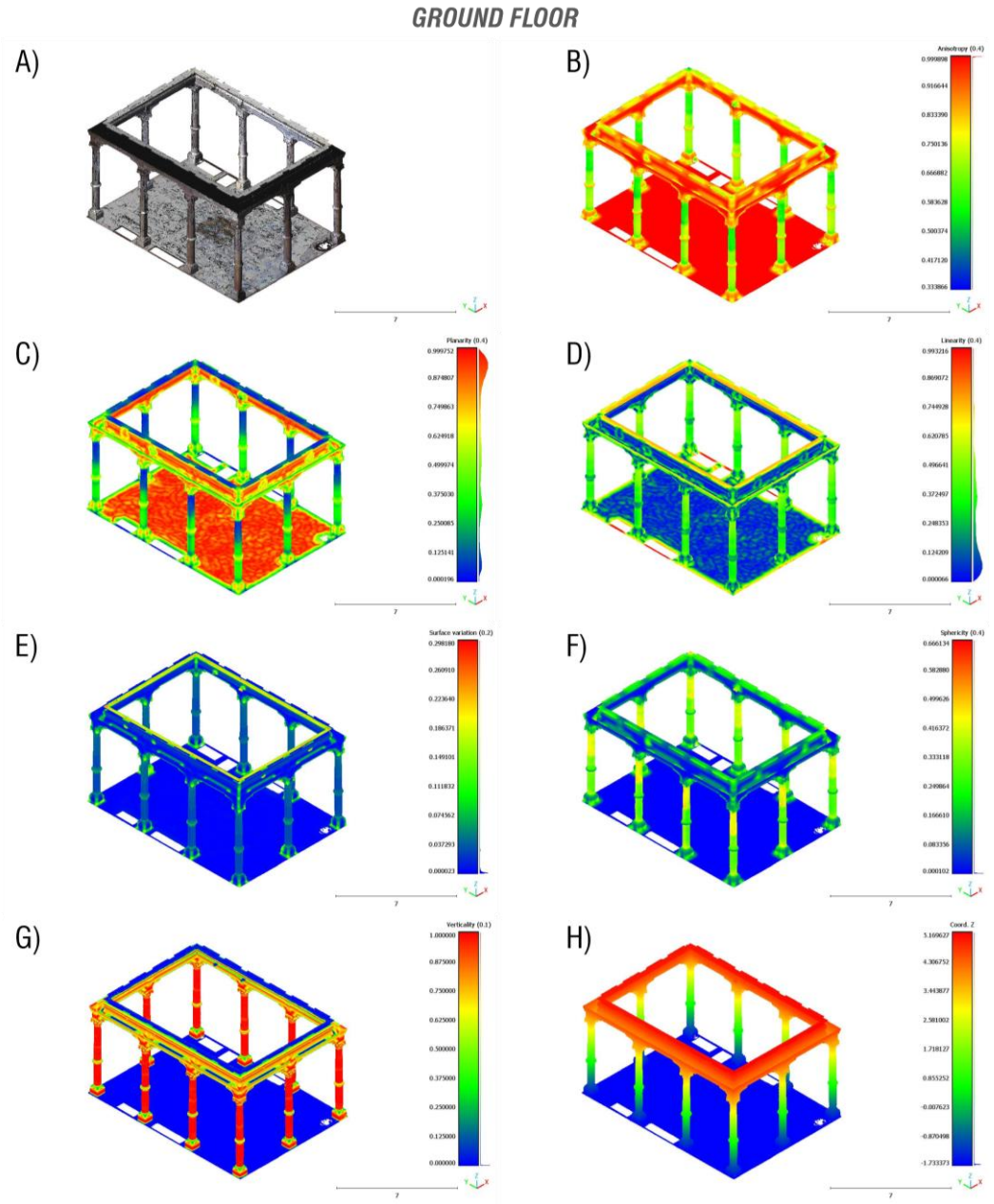

Fig. 126 Example of geometric features used for the training phase relating to the Ground Floor point cloud: A) Normals; B) Anisotropy; C) Planarity; D) Linearity; E) Surface Variation; F) Sphericity; G) Verticality; H) Z Coordinate.

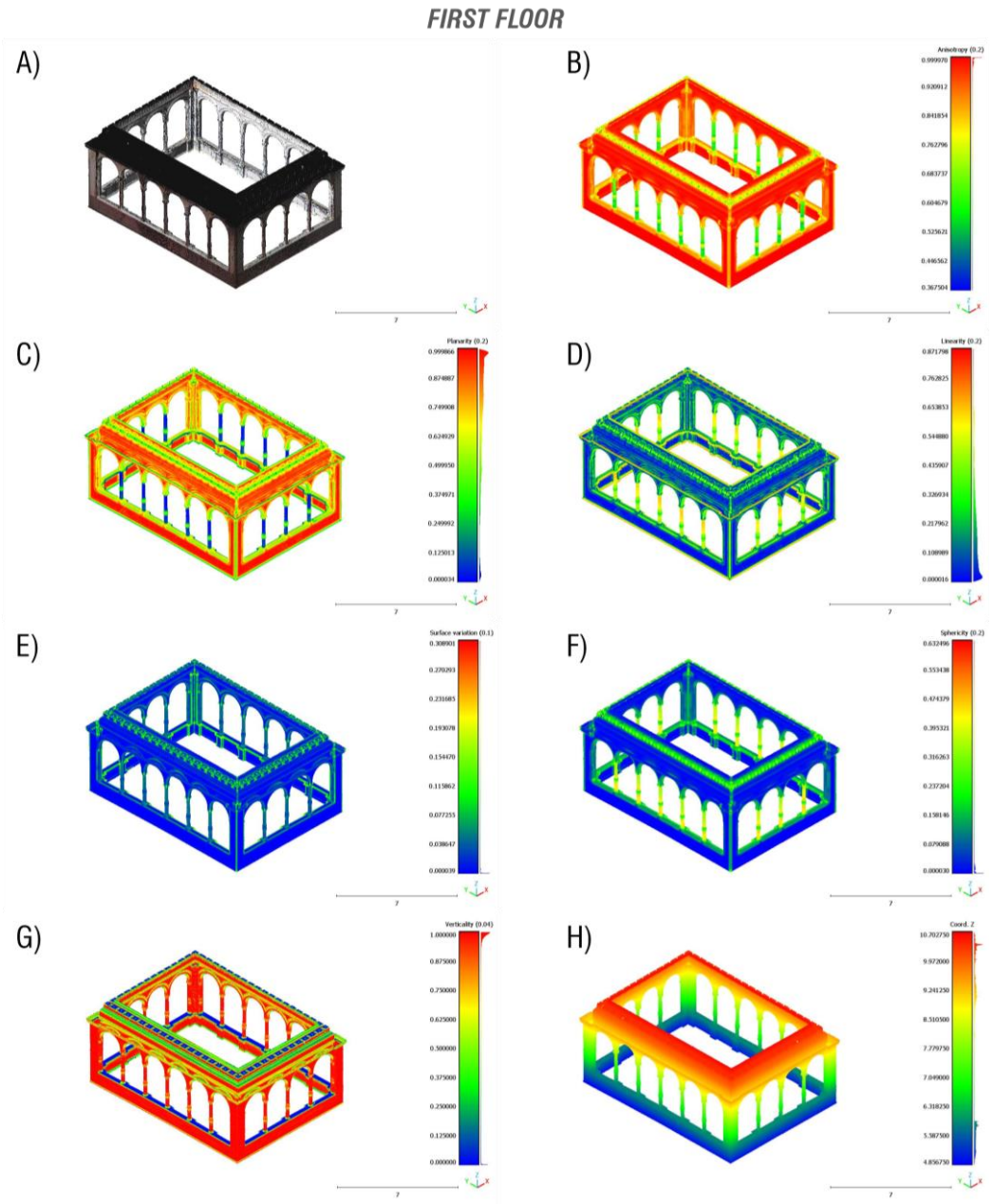

Fig. 127 Example of geometric features used for the training phase relating to the First Floor point cloud: A) Normals; B) Anisotropy; C) Planarity; D) Linearity; E) Surface Variation; F) Sphericity; G) Verticality; H) Z Coordinate.

In addition to these features, considering the calculation of Normals can be advantageous in the classification of complex scenes.

Normals in a point cloud consist of vectors perpendicular to the surface at each point, providing crucial insights into surface orientation. The normal can be described by a three-dimensional vector (N_x, N_y, N_z), where N_x is the component along the x-axis, N_y along the y-axis, and N_z along the z-axis. At this point, the decision was made to extract only the normal-based feature and the covariance features. After the previously mentioned best attributes are automatically selected by machine learning based on their value of relevance, the normals and height will be calculated. This will be used to test various feature combinations that could be used by the algorithm to automatically partition the test set.

Manual Annotation on Training and Evaluation Sets

To construct a Training and Evaluation set suitable for recognising architectural elements in the remaining portion of the point cloud, treated as the Test set, manual segmentation of point clouds for the ground floor and first floor was conducted. These training data, identified as classes, can be combined with selected geometric features, point coordinates, normals, and color properties (e.g., RGB scale). The point cloud was semantically segmented based on the classification of architectural elements according to the ontological taxonomy of the Art & Architecture Thesaurus© (AAT) by the Getty Research Institute (Getty, 2021), aligning with Information Standards in Practice (ISO and NISO) for thesaurus construction and, in this case, with classical architecture rules.

For the ground floor, the segmentation, from bottom to top, is as follows: Pavement, Base, Lower Shaft, Ring, Upper Shaft, Capital, Corbel, Architrave, Frieze, Cornice (Fig. 128)

For the first floor, on the other hand, it includes: Parapet, Base, Lower Shaft, Ring, Upper Shaft, Capital, Arch, Stringcourse, Cornice, Corner Column. Thus, each floor's ten classes were manually divided (Fig. 129).

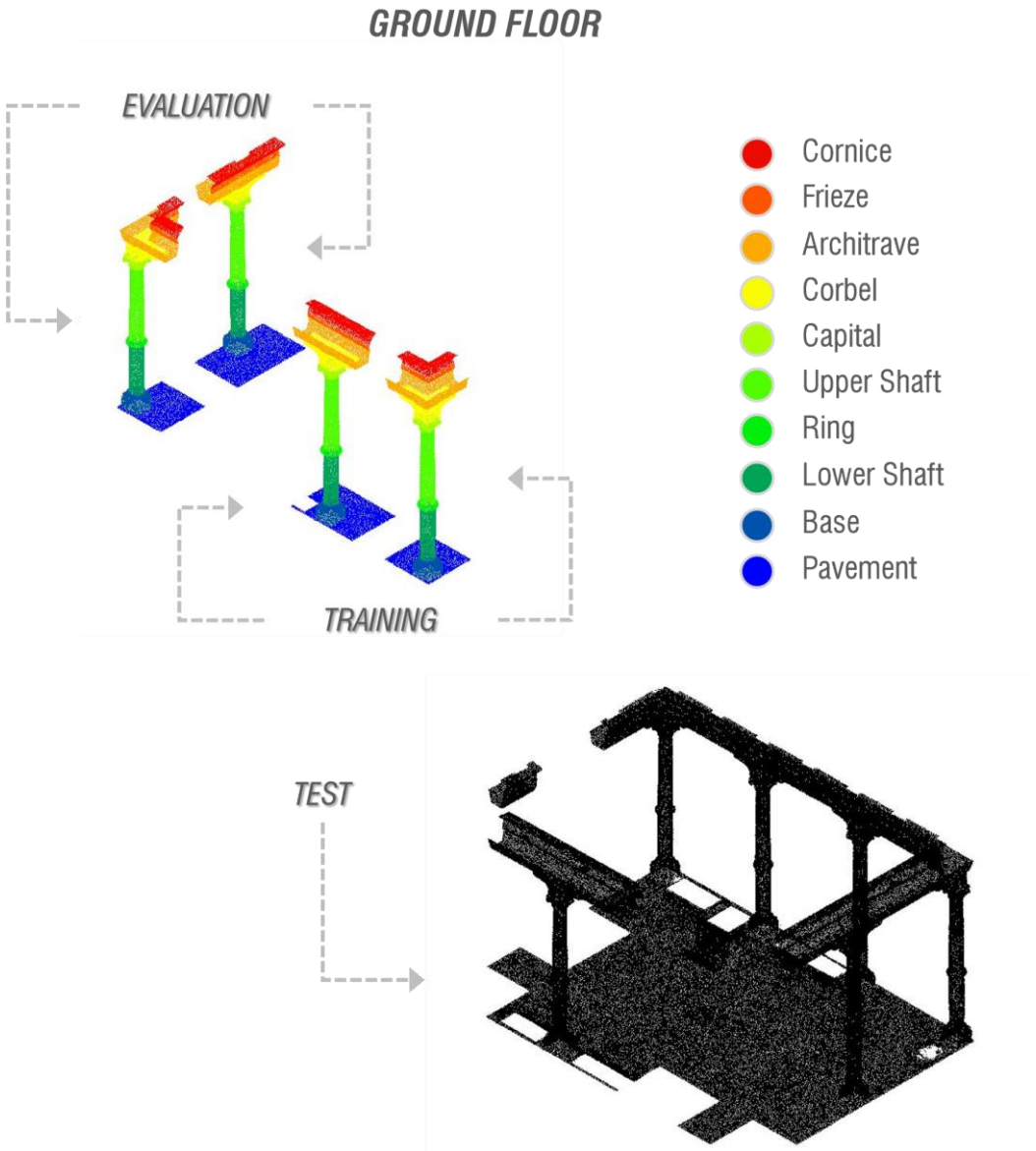

Fig. 128 Manual annotation on Training and Evaluation sets for the Ground Floor (on the top); Test set employed to use Machine Learning for automatic class identification (on the bottom).

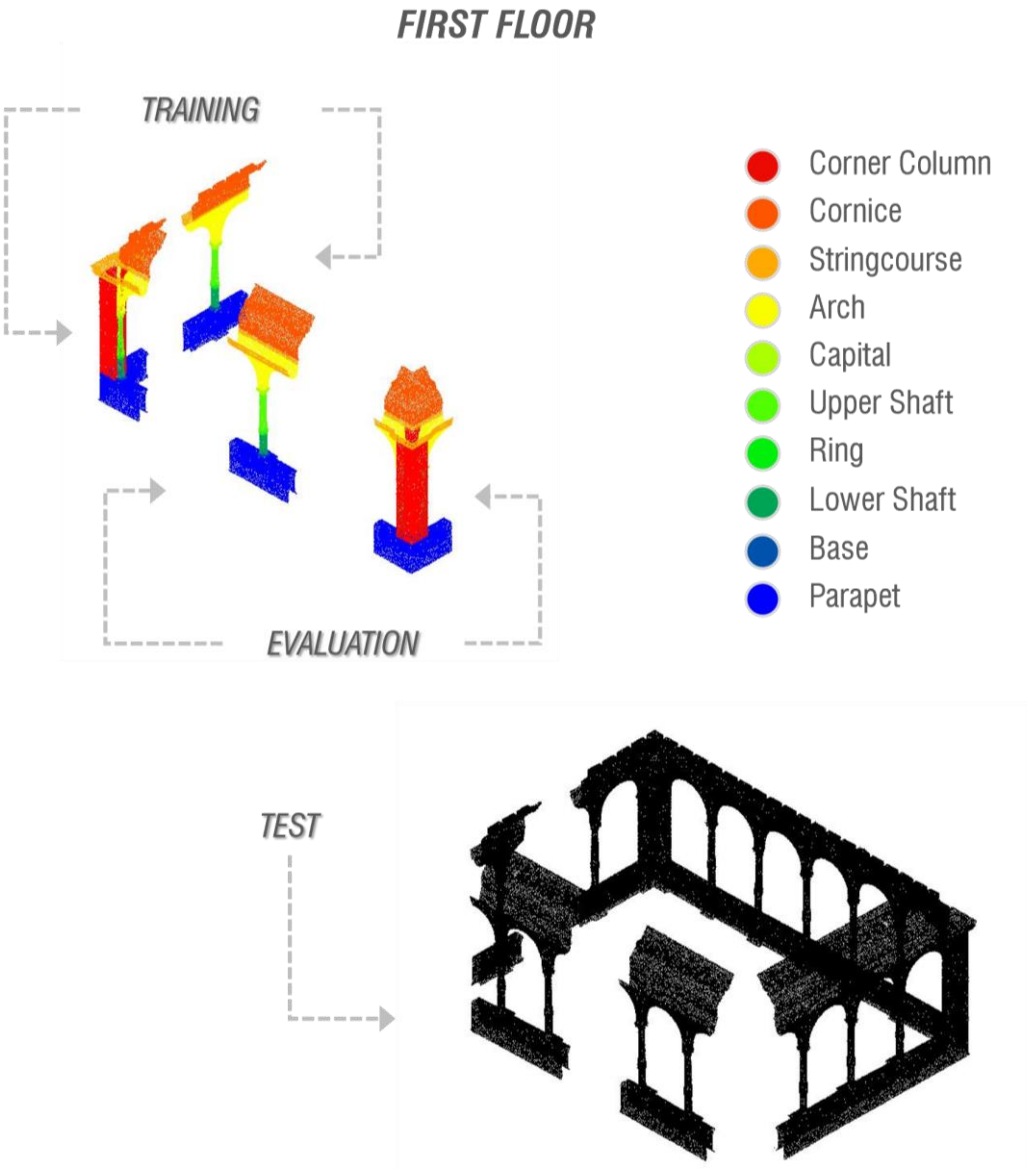

Fig. 129 Manual annotation on Training and Evaluation sets for the First Floor (on the top); Test set employed to use Machine Learning for automatic class identification (on the bottom).

Geometric Features Selection using MDI (RF)

To select the most relevant geometric features for training stage, a preliminary multiscale analysis of feature importance was conducted using the Random Forest machine learning algorithm in a Python environment (PyCharm). Initially, 63 features were originally extracted for the ground floor and 72 features for the first floor.

In detail, it was employed the 'Mean Decrease in Impurity' (MDI), that is a commonly used metric for feature importance in Random Forests (Scornet, 2021; Agarwal *et al.*, 2023). This metric assesses how each feature contributes to reducing impurity in the nodes of the forest's trees during the training process. A feature that effectively divides the data, leading to a significant reduction in impurity, is considered more important.

To obtain the feature importance ranking, several steps were executed:

- Data Preparation: The data was structured with features (independent variables) and class labels (dependent variable); The dataset was split into a training set and a test set.
- Random Forest Training: The scikit-learn library in Python was utilised to train the Random Forest model on the point cloud; During training, the model automatically calculates the importance of features.
- Extraction of Feature Importance: Post-training, the feature importance is obtained from the model. In this implementation, this was achieved using the feature_importances attribute.
- Creation of a Ranking: Features were organised to provide a visually intuitive understanding of their importance. The ranked features are depicted in Fig. 130 and Fig. 131, based on the local neighborhood radius on the x-axis and the normalised feature importance scores.

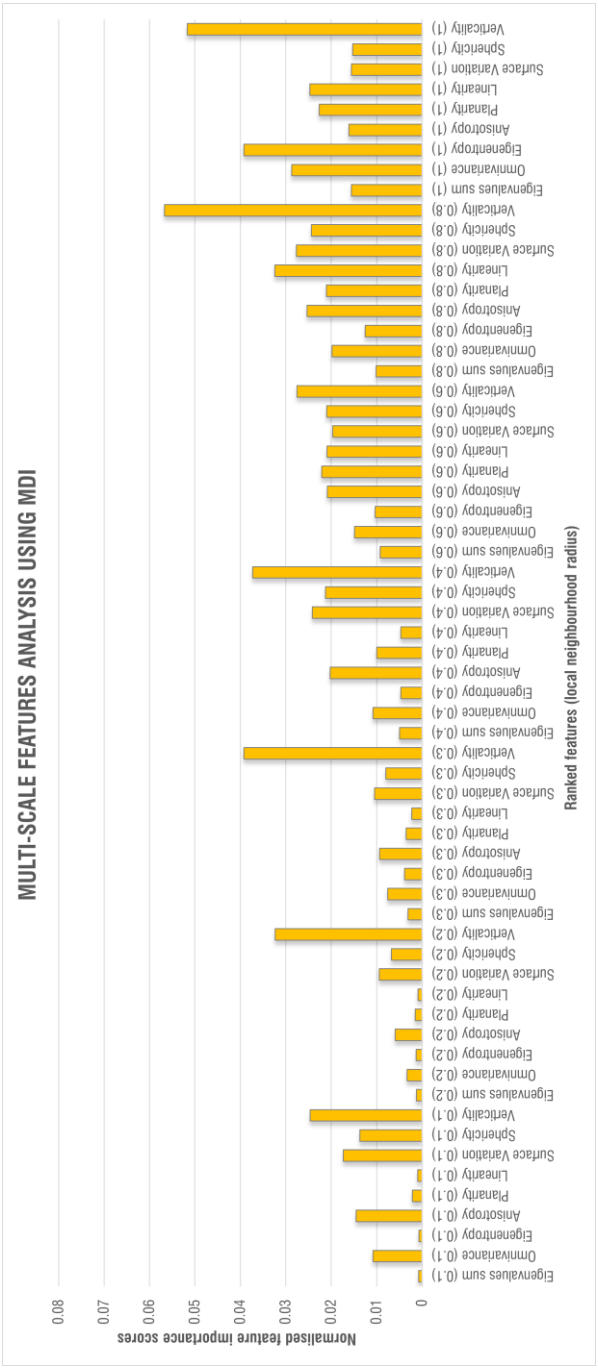

Fig. 130 Feature Importance Ranking for the Ground Floor obtained through Random Forest MDI Analysis.

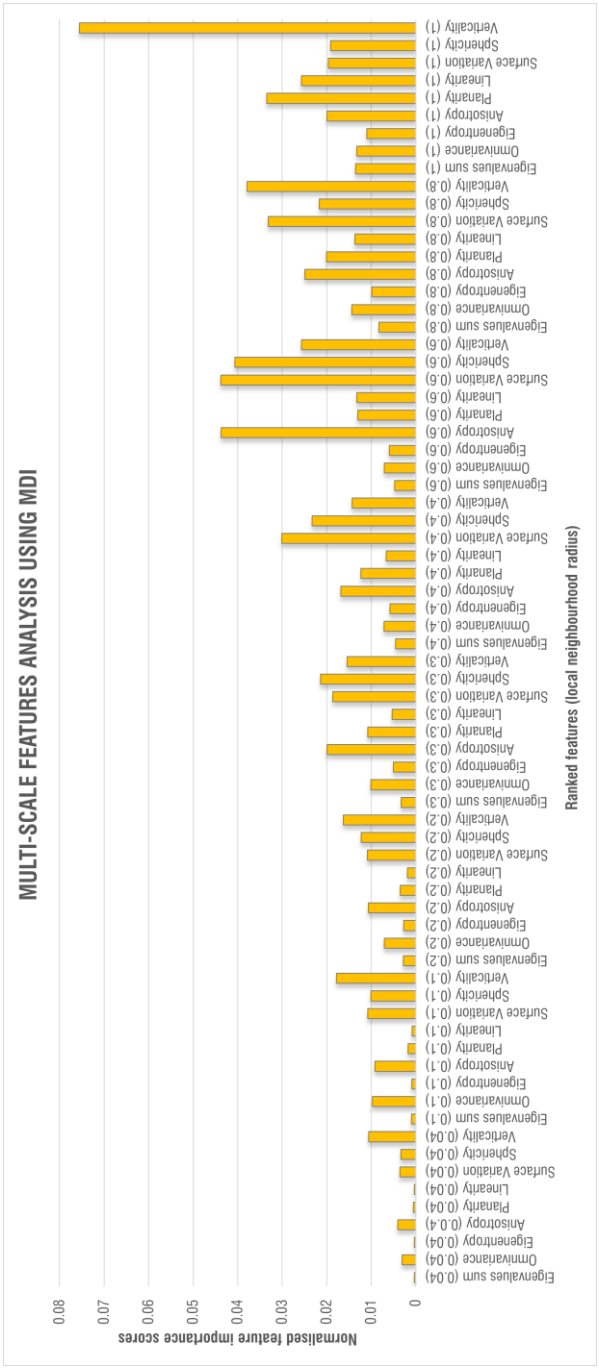

Fig. 131 Feature Importance Ranking for the First Floor obtained through Random Forest MDI Analysis.

At this stage, in an effort to optimise training time and assess the overall performance of the predictive model, the 15 most impactful features were carefully identified for the 63 features on the ground floor and the 72 features on the first floor, respectively.

Subsequently, employing an iterative process with the same methodology, an additional set of 6 features was selected to observe their impact on the model's behavior as the total number of features progressively decreased, aiming to mitigate overfitting errors.

Tab. 14 Feature Importance Scores of the 15 features for the Ground Floor and the First Floor.

Ground Floor		**First Floor**	
Feature (radius)	***Score***	***Feature (radius)***	***Score***
Verticality (0.8)	0.05674217	Verticality (1)	0.07552335
Verticality (1)	0.0516716	Surface Var. (0.6)	0.0438021
Verticality (0.3)	0.03921137	Anisotropy (0.6)	0.04372397
Eigenentropy (1)	0.03920605	Sphericity (0.6)	0.04066766
Verticality (0.4)	0.03728326	Verticality (0.8)	0.03792759
Linearity (0.8)	0.03241092	Planarity (1)	0.03345083
Verticality (0.2)	0.03235743	Surface Var. (0.8)	0.03309696
Omnivariance (1)	0.02869746	Surface Var. (0.4)	0.03010814
Surface Var. (0.8)	0.02767854	Linearity (1)	0.02567088

Verticality (0.6)	0.02750381	Verticality (0.6)	0.02564896
Anisotropy (0.8)	0.02535267	Anisotropy (0.8)	0.02492746
Linearity (1)	0.02473062	Sphericity (0.4)	0.0232871
Verticality (0.1)	0.02466849	Sphericity (0.8)	0.02164398
Sphericity (0.8)	0.02439382	Sphericity (0.3)	0.02137714
Surface Var. (0.4)	0.02417008	Planarity (0.8)	0.02003774

As shown in Tab. 14, in both floors, Verticality proves to be a significant feature, with 'Verticality (1)' playing a substantial role, especially on the first floor. Surface Variation and Anisotropy also hold importance on the first floor. Meanwhile, on the ground floor, additional features such as Omnivariance and Eigenentropy come to the forefront.

Tab. 15 Feature Importance Scores of the 6 features for the Ground Floor and the First Floor.

Ground Floor		**First Floor**	
Feature (radius)	***Score***	***Feature (radius)***	***Score***
Eigenentropy (1)	0.20324868	Verticality (1)	0.23757974
Verticality (0.8)	0.19481669	Planarity (1)	0.22981696
Verticality (1)	0.19275127	Surface Variation (0.6)	0.16260546

Linearity (0.8)	0.18289954	Verticality (0.8)	0.1468888
Verticality (0.4)	0.12677354	Sphericity (0.6)	0.11651344
Verticality (0.3)	0.09951028	Anisotropy (0.6)	0.10659559

In Tab. 15, it can be observed that in both floors, Verticality emerges as a significant feature, but other specific attributes also contribute significantly to the overall score, providing a distinctive profile for each floor.

Subsequently, a tailored selection of 6 'ad hoc' features was employed for each floor (as seen in Fig. 128 and Fig. 129Fig. 127), chosen based on their visual representation of individual architectural elements, closely aligning with manually labelled classes.

Specifically, for the ground floor, features such as Anisotropy, Planarity, Linearity, and Sphericity were meticulously chosen, each with a radius of 0.4 meters, mirroring the diameter of the column. Additionally, Surface Variation was selected with a radius of 0.2 meters, matching the column's radius, and Verticality with a radius of 0.1 meters, constituting half of the column's radius.

Regarding the first floor, the features chosen by the operator included Anisotropy, Planarity, Linearity, and Sphericity, each with a radius of 0.2 meters, corresponding to the column's diameter. Furthermore, Surface Variation was selected with a radius of 0.1 meters, equal to the column's radius, and Verticality with a radius of 0.04 meters, half of the column's radius.

On both floors, intentional exclusions were made, eliminating features like Omnivariance, Eigenentropy, and Sum of Eigenvalues. These features seemed, at least visually, to yield results that did not align with the expected outcomes, unlike the MDI method.

Normals and Feature Height Calculation

The integration of parameters such as Normals and Feature Height (Z Coordinate) alongside other geometric features can be considered advantageous for the segmentation and classification of point clouds. These additional pieces of information enrich the description of surface characteristics and enhance the model's ability to discriminate between different entities.

As previously mentioned, Normals represent the direction perpendicular to the surface at each point, providing valuable insights into the orientation of surfaces throughout the point cloud. This feature is crucial for understanding the detailed geometry of the surface and facilitates the segmentation of elements such as walls, floors, inclined structures, or other patterns that might be challenging to identify using spatial coordinates alone.

Simultaneously, the use of the Z coordinate proves equally valuable for exploring the three-dimensional structure of the environment. In particular, it enables the identification of variations in the arrangement of vertical spaces, providing a clear understanding of the overall building structure. This aspect is particularly useful for identifying significant details, such as the height difference between floors, balconies, or other elevated architectural features, contributing to a more accurate and detailed segmentation.

For these reasons, a decision was made to integrate these two parameters and assess their efficacy in both the training and classification processes.

Features Combinations

For each iteration with different features (63 - 15 - 6 - 6 specifically tailored for the ground floor and 72 - 15 - 6 - 6 specifically tailored for the first floor), three distinct combinations were executed, resulting in a total of 12 combinations per floor, as outlined below.

Ground Floor:

- 63 features; 63 features + Z Coordinate; 63 features + Z Coordinate + Normals
- 15 features; 15 features + Z Coordinate; 15 features + Z Coordinate + Normals
- 6 features; 6 features + Z Coordinate; 6 features + Z Coordinate + Normals
- 6 'ad hoc' features; 6 'ad hoc' features + Z Coordinate; 6 'ad hoc' features + Z Coordinate + Normals

First Floor:

- 72 features; 72 features + Z Coordinate; 72 features + Z Coordinate + Normals
- 15 features; 15 features + Z Coordinate; 15 features + Z Coordinate + Normals
- 6 features; 6 features + Z Coordinate; 6 features + Z Coordinate + Normals
- 6 'ad hoc' features; 6 'ad hoc' features + Z Coordinate; 6 'ad hoc' features + Z Coordinate + Normals

The 12 combinations were tested with the Random Forest algorithm and were compared in terms of weighted F1-score and according to model training time.

Specifically The weighted F1-score is a performance evaluation metric for a classification model that takes into account differences in the number of samples belonging to different classes, particularly useful when classes are imbalanced. The formula to calculate the weighted F1-score is as follows [25]:

$$F1_{weighted} = \frac{\sum_i w_i * F1_i}{\sum_i w_i}$$

[25]

Where:

$F1_i =$ F1-score for class i

$w_i =$ weight associated with class i

The summation is performed over all the classes. The F1-score for a single class is calculated using the standard F1-score formula [26]:

$$F1_i = \frac{2\ Precision_i * Recall_i}{Precision_i + Recall_i}$$

[26]

Where:

$Precision_i =$ precision for class i

$Recall_i =$ recall for class i

The weights w_i are calculated as the proportion of the number of samples in class i relative to the total number of samples.

Below, in Fig. 132 and Fig. 133, Tab. 16 and Tab. 17 the results of different combinations are displayed.

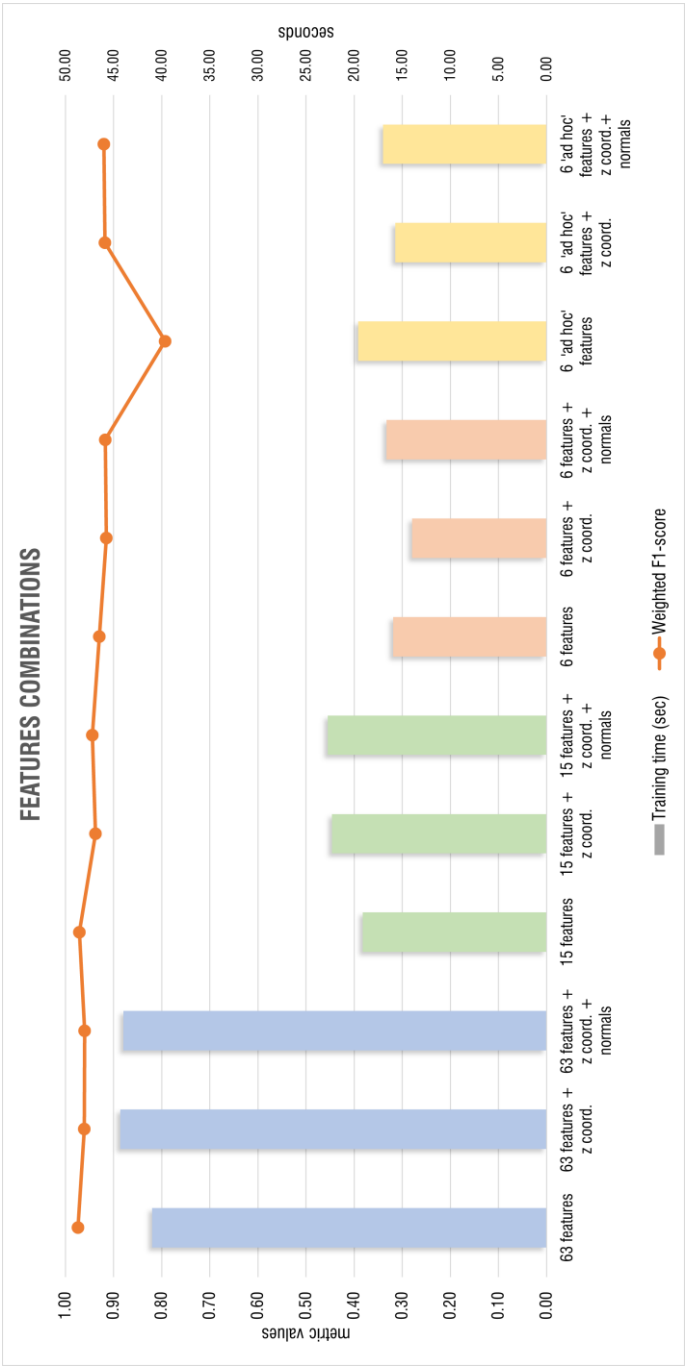

Fig. 132 Featuree Combinations for the Ground Floor compared by weighted F1 score and training time.

Tab. 16 Specification of Feautures Combinations for the Ground Floor.

Feature combinations	n-estimators	Training time (sec)	Weighted F1-score
63 features	200	40.9824	0.9736
63 features + z coord.	100	44.2787	0.9606
63 features + z coord. + normals	100	43.9770	0.9598
15 features	200	19.1061	0.9710
15 features + z coord.	200	22.3032	0.9373
15 features + z coord. + normals	50	22.7215	0.9439
6 features	200	15.9416	0.9296
6 features + z coord.	50	13.9675	0.9148
6 features + z coord. + normals	150	16.6206	0.9170
6 'ad hoc' features	200	19.5866	0.7930
6 'ad hoc' features + z coord.	200	15.7060	0.9180
6 'ad hoc' features + z coord. + normals	100	17.0059	0.9200

Furthermore, the hyperparameter that establishes the quantity of decision trees within the forest is referred to as the Number of Estimators'. Every decision tree adds to the final prediction, and the Random Forest model's performance and capacity for generalisation can be greatly impacted by the number of trees.

The results can be discussed for the specified four combinations:

a) 63 features; 63 features + z coord.; 63 features + z coord. + normals:

- For 63 features: The model with 63 features achieved a high weighted F1-score of 0.9736 with 200 estimators and a training time of 40.9824 seconds.

- For 63 features + z coord.: Adding the z coordinate slightly reduced the weighted F1-score to 0.9606 with 100 estimators, and the training time increased to 44.2787 seconds.
- For 63 features + z coord. + normals: Further adding normals led to a marginal decrease in the weighted F1-score to 0.9598 with 100 estimators, and the training time remained comparable at 43.9770 seconds.

b) 15 features; 15 features + z coord.; 15 features + z coord. + normals:

- For 15 features: The model with 15 features achieved a high weighted F1-score of 0.9710 with 200 estimators and a training time of 19.1061 seconds.
- For 15 features + z coord.: Adding the z coordinate led to a decrease in the weighted F1-score to 0.9373 with 200 estimators, and the training time increased to 22.3032 seconds.
- For 15 features + z coord. + normals: Further adding normals resulted in a slight increase in the weighted F1-score to 0.9439 with 50 estimators, and the training time remained similar at 22.7215 seconds.

c) 6 features; 6 features + z coord.; 6 features + z coord. + normals:

- For 6 features: The model with 6 features achieved a weighted F1-score of 0.9296 with 200 estimators and a training time of 15.9416 seconds.
- For 6 features + z coord.: Adding the z coordinate resulted in a decrease in the weighted F1-score to 0.9148 with 50 estimators, and the training time decreased to 13.9675 seconds.
- For 6 features + z coord. + normals: Further adding normals led to a slight increase in the weighted F1-score to 0.9170 with 150 estimators, and the training time increased to 16.6206 seconds.

d) 6 ‘ad hoc’ features; 6 ‘ad hoc’ features + z coord.; 6 ‘ad hoc’ features + z coord. + normals:

- For 6 ‘ad hoc’ features: The model achieved a weighted F1-score of 0.7930 with 200 estimators and a training time of 19.5866 seconds.
- For 6 ‘ad hoc’ features + z coord.: Adding the z coordinate resulted in a notable increase in the weighted F1-score to 0.9180 with 200 estimators, and the training time decreased to 15.7060 seconds.
- For 6 ‘ad hoc’ features + z coord. + normals: Further adding normals resulted in a slight increase in the weighted F1-score to 0.9200 with 100 estimators, and the training time remained comparable at 17.0059 seconds.

Considering only F1-score and overlooking the training time, which is relatively low across all configurations, the best performance for each of the four combinations is as follows:

a) The highest F1-score is achieved only with the 63 features combination, attaining a score of 0.9736.

b) Among the combinations with 15 features, the configuration with ‘15 features’ alone produces the highest F1-score, reaching 0.9710.

c) The combination ‘6 features’ yields the highest F1-score, with a value of 0.9296.

d) In the case of ‘6 ‘ad hoc’ features’, incorporating the z coordinate and the normals results in the best F1-score, with a score of 0.9200.

In light of this deduction, the optimal outcome for the ground floor emerges when all features are collectively considered. However, it is noteworthy that by reducing the number of features and incorporating ‘ad hoc’ features linked to the geometric dimensions of architectural elements, a highly satisfactory result is still achieved, as demonstrated in the subsequent figures.

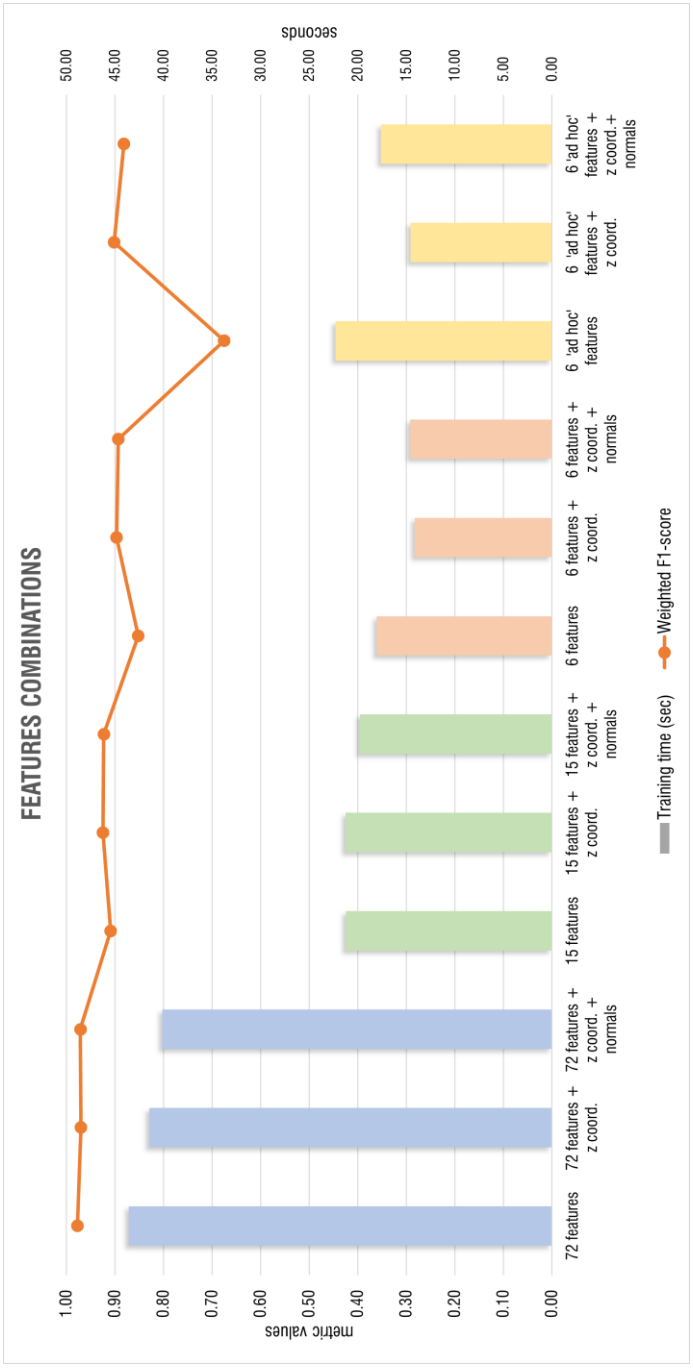

Fig. 133 Features Combinations for the First Floor compared by weighted F1 score and training time.

Tab. 17 Specification of Feautures Combinations for the First Floor.

Feature combinations	n-estimators	Training time (sec)	Weighted F1-score
72 features	100	43.5884	0.9772
72 features + z coord.	200	41.4688	0.9700
72 features + z coord. + normals	100	40.1178	0.9712
15 features	200	21.1950	0.9092
15 features + z coord.	200	21.2527	0.9248
15 features + z coord. + normals	100	19.7888	0.9230
6 features	200	18.0612	0.8521
6 features + z coord.	100	14.1282	0.8970
6 features + z coord. + normals	50	14.5784	0.8934
6 'ad hoc' features	200	22.2948	0.6749
6 'ad hoc' features + z coord.	200	14.5593	0.9018
6 'ad hoc' features + z coord. + normals	150	17.6194	0.8815

Concerning the outcomes for the specified feature combinations:

a) 72 features; 72 features + z coord.; 72 features + z coord. + normals:

- For 72 features: The model with 72 features achieved a high weighted F1-score of 0.9772 with 100 estimators and a training time of 43.5884 seconds.
- For 72 features + z coord.: Adding the z coordinate resulted in a slightly reduced F1-score of 0.9700 with 200 estimators, and the training time increased to 41.4688 seconds.
- For 72 features + z coord. + normals: Further adding normals led to a slightly increased F1-score of 0.9712 with 100 estimators, and the training time remained comparable at 40.1178 seconds.

b) 15 features; 15 features + z coord.; 15 features + z coord. + normals:

- For 15 features: The model with 15 features achieved a moderate weighted F1-score of 0.9092 with 200 estimators and a training time of 21.1950 seconds.
- For 15 features + z coord.: Adding the z coordinate resulted in an improved F1-score of 0.9248 with 200 estimators, and the training time remained similar at 21.2527 seconds.
- For 15 features + z coord. + normals: Further adding normals led to a slightly increased F1-score of 0.9230 with 100 estimators, and the training time decreased to 19.7888 seconds.

c) 6 features; 6 features + z coord.; 6 features + z coord. + normals:

- For 6 features: The model with 6 features achieved a moderate F1-score of 0.8521 with 200 estimators and a training time of 18.0612 seconds.
- For 6 features + z coord.: Adding the z coordinate resulted in an improved F1-score of 0.8970 with 100 estimators, and the training time decreased to 14.1282 seconds.
- For 6 features + z coord. + normals: Further adding normals led to a slightly decreased F1-score of 0.8934 with 50 estimators, and the training time remained comparable at 14.5784 seconds.

d) 6 'ad hoc' features; 6 'ad hoc' features + z coord.; 6 'ad hoc' features + z coord. + normals:

- For 6 'ad hoc' features: The model achieved a lower F1-score of 0.6749 with 200 estimators and a training time of 22.2948 seconds.
- For 6 'ad hoc' features + z coord.: Adding the z coordinate resulted in a significantly improved F1-score of 0.9018 with 200 estimators, and the training time decreased to 14.5593 seconds.

- For 6 ‘ad hoc’ features + z coord. + normals: Further adding normals led to a slightly decreased F1-score of 0.8815 with 150 estimators, and the training time increased to 17.6194 seconds.

In terms of F1-score, disregarding the training time, the best results for each of the four combinations are as follows:

a) The highest F1-score is achieved with the ‘72 features’ combination, attaining a score of 0.9772.

b) The best F1-score is obtained with the ‘15 features’ combination, reaching a score of 0.9248.

c) The highest F1-score is attained with the ‘6 features + z coord’. combination, with a score of 0.8970.

d) The best F1-score is obtained with the ‘6 ‘ad hoc’ features + z coord’. combination, achieving a score of 0.9018.

Once more, the outcomes seem encouraging for the first floor. The outcome that takes into account every possible feature combination is undoubtedly the greatest one, however when taking into account the ‘ad hoc’ features pertaining to the geometric dimensions of the architectural parts, the F1-score is extremely high.

4.6.3 Results

The following section presents the outcomes of machine learning classification, accompanied by evaluation metrics specifically chosen to serve the intended purpose.

RF Classification on Test Set and Performance Evaluation

For segmentation within the PyCharm environment, two main modules have been employed. The first module is dedicated to training a Random Forest model for the automatic segmentation of point clouds, while the second module is designed for classifying a point cloud using a pre-trained model.

In the training module, the code is structured in a modular manner to ensure a clear separation of functions. The 'load_features_and_class' function handles the loading of feature indices and class index from a specified text file. Similarly, the 'read_data' function is responsible for loading a labelled point cloud from a text file. The training phase of the model is managed by the 'train_model' function, which utilises a Random Forest classifier with specified parameters.

On the other hand, the classification module is designed to enable the classification of point clouds of the Test set using a pre-trained model. The 'load_features' function loads feature indices from a text file, while the 'read_model' function reads a Random Forest model from a binary .pkl file. The actual classification is performed by the main function, which loads features, the model, and the data to be classified. The classification results are then written to an output file.

To assess the performance of the machine learning model, the 'Cross-Validation' technique was employed. This approach was implemented to select the optimal hyperparameters (number of trees and maximum depth) for the Random Forest classifier. Specifically, the training set was partitioned into 5 folds, setting the number of folds in the cross-validation *(k=5)*. The decision not to reduce the number of folds was made to avoid the risk of overfitting during hyperparameter selection.

In this manner, the model was trained and evaluated five times, with each iteration using a different subset as the validation set and the remaining subsets for training.

This iterative process provided a more robust estimation of evaluation metrics, such as Precision, Recall, F1-Score, and Overall Accuracy. These metrics were associated

with confusion matrices, specifically for the four most promising combinations per plan, as illustrated in the subsequent figures. This correlation aids in enhancing the comprehension of the predictive capabilities of the model.

Specifically, for the confusion matrix (Tab. 18), the rows matrix display the actual (true) classes, manually annotated, while the columns display the predicted ones.

Tab. 18 Example of Confusion Matrix.

	Actual Values	
Predicted Values	TP	FP
	FN	TN

Where:

TP (True Positive): Instances correctly predicted as positive.

FP (False Positive): Instances incorrectly predicted as positive.

TN (True Negative): Instances correctly predicted as negative.

FN (False Negative): Instances incorrectly predicted as negative.

So, the metrics such as Precision [27], Recall [28], F1-Score [29], and Overall Accuracy [30] are calculated using values from the confusion matrix. Below are the formulas for each metric:

$$\text{Precision} = \frac{TP}{TP+FP} \quad [27]$$

$$\text{Recall} = \frac{TP}{TP+FN} \quad [28]$$

$$\text{F1-Score} = \frac{2\ \text{Precision}*\text{Recall}}{\text{Precision}+\text{Recall}} \quad [29]$$

$$\text{Overall Accuracy} = \frac{TP+TN}{TP+FP+TN+FN} \quad [30]$$

For each of the top four combinations per floor plan, the confusion matrices are displayed in the following images (for the ground floor, Fig. 134, and Fig. 135, and for the first floor, Fig. 136, and Fig. 137), accompanied by the metric results evaluating these matrices (for the ground floor, Tab. 19, Tab. 20, Tab. 21 and Tab. 22, and for the first floor, Tab. 23, Tab. 24, Tab. 25, and Tab. 26).

CLASS	Pavement	Base	Lower Shaft	Ring	Upper Shaft	Capital	Corbel	Architrave	Frieze	Cornice
Pavement	11354	61	0	0	0	0	0	1	0	0
Base	13	4409	21	0	0	0	15	16	0	0
Lower shaft	0	14	5846	24	395	0	0	0	0	0
Ring	0	0	0	1240	7	0	0	0	0	0
Upper shaft	0	0	0	19	10991	31	0	0	0	0
Capital	0	0	0	0	17	3522	23	0	0	0
Corbel	0	0	0	0	0	157	6871	70	0	0
Architrave	0	0	0	0	0	0	236	7746	55	0
Frieze	0	0	0	0	0	0	0	367	1570	21
Cornice	0	0	0	0	0	0	0	0	30	5731

63 Features_GROUND FLOOR

CLASS	Pavement	Base	Lower Shaft	Ring	Upper Shaft	Capital	Corbel	Architrave	Frieze	Cornice
Pavement	11376	40	0	0	0	0	0	0	0	0
Base	72	4380	19	0	0	2	1	0	0	0
Lower shaft	0	20	5828	16	401	14	0	0	0	0
Ring	0	0	0	1200	47	0	0	0	0	0
Upper shaft	0	0	0	23	10975	43	0	0	0	0
Capital	0	0	0	0	20	3474	68	0	0	0
Corbel	0	4	0	0	0	120	6836	138	0	0
Architrave	0	18	0	0	0	0	279	7553	187	0
Frieze	0	0	0	0	0	0	0	164	1757	37
Cornice	0	0	0	0	0	0	0	0	27	5734

15 Features_GROUND FLOOR

Fig. 134 Confusion Matrix for the Ground Floor with the best combinations: 63 Features and 15 Features.

CLASS (predicted \ actual)	Pavement	Base	Lower Shaft	Ring	Upper Shaft	Capital	Corbel	Architrave	Frieze	Cornice
Pavement	11385	31	0	0	0	0	0	0	0	0
Base	139	4197	7	0	0	31	15	62	0	23
Lower shaft	0	83	5021	0	1100	74	0	0	0	1
Ring	0	0	0	1018	229	0	0	0	0	0
Upper shaft	0	0	198	36	10750	57	0	0	0	0
Capital	0	37	0	0	27	3420	70	8	0	0
Corbel	0	41	1	0	0	289	6587	180	0	0
Architrave	0	22	0	0	0	2	421	7011	569	12
Frieze	0	0	0	0	0	0	0	303	1607	48
Cornice	0	2	0	0	0	0	0	15	143	5601

6 Features_GROUND FLOOR

CLASS (predicted \ actual)	Pavement	Base	Lower Shaft	Ring	Upper Shaft	Capital	Corbel	Architrave	Frieze	Cornice
Pavement	11387	29	0	0	0	0	0	0	0	0
Base	72	4395	7	0	0	0	0	0	0	0
Lower shaft	0	39	6240	0	0	0	0	0	0	0
Ring	0	0	47	1200	0	0	0	0	0	0
Upper shaft	0	0	0	38	11003	0	0	0	0	0
Capital	0	0	0	0	85	3477	0	0	0	0
Corbel	0	0	0	0	0	799	6270	29	0	0
Architrave	0	0	0	0	0	0	1822	6215	0	0
Frieze	0	0	0	0	0	0	0	1228	730	0
Cornice	0	0	0	0	0	0	0	0	693	5068

6 'ad hoc' Features + Z Coordinate + Normals_GROUND FLOOR

Fig. 135 Confusion Matrix for the Ground Floor with the best combinations: 6 Features and 6 'ad hoc' Features + Z Coordinate + Normals.

CLASS	Parapet	Base	Lower Shaft	Ring	Upper Shaft	Capital	Arch	Stringcourse	Cornice	Corner Column
Parapet	16013	1	0	0	0	0	59	3	0	74
Base	65	143	6	0	0	0	0	0	0	0
Lower shaft	0	21	1109	21	0	0	3	0	0	13
Ring	0	0	20	162	30	0	2	0	0	13
Upper shaft	0	0	0	25	2024	11	2	0	0	90
Capital	0	0	0	0	10	535	64	0	0	18
Arch	3	0	0	0	0	41	8176	78	0	24
Stringcourse	0	0	0	0	0	0	172	4076	37	26
Cornice	0	0	0	0	0	0	0	85	12127	0
Corner column	44	4	36	5	30	6	83	21	0	9289

72 Features_FIRST FLOOR

CLASS	Parapet	Base	Lower Shaft	Ring	Upper Shaft	Capital	Arch	Stringcourse	Cornice	Corner Column
Parapet	14618	551	351	0	0	0	40	0	0	590
Base	0	150	63	0	0	0	0	0	0	1
Lower shaft	0	32	1096	23	1	0	0	0	0	15
Ring	0	0	28	123	28	0	0	0	0	48
Upper shaft	0	0	0	18	1650	76	0	0	0	408
Capital	0	0	0	0	0	341	270	0	0	16
Arch	0	0	0	0	0	0	7492	807	0	23
Stringcourse	0	0	0	0	0	0	20	3996	290	5
Cornice	0	0	0	0	0	0	0	0	12212	0
Corner column	0	7	70	5	114	0	146	261	0	8915

15 Features + Z Coordinate_FIRST FLOOR

Fig. 136 Confusion Matrix for the First Floor with the best combinations: 72 Features and 15 Features + Z Coordinate.

CLASS	Parapet	Base	Lower Shaft	Ring	Upper Shaft	Capital	Arch	Stringcourse	Cornice	Corner Column
Parapet	13922	329	508	0	0	0	0	0	0	1391
Base	0	81	63	0	0	0	0	0	0	70
Lower shaft	0	17	1056	39	0	0	0	0	0	55
Ring	0	0	18	121	55	0	0	0	0	33
Upper shaft	0	0	0	3	1821	116	0	0	0	212
Capital	0	0	0	0	0	342	259	0	0	26
Arch	0	0	0	0	0	0	6963	1258	0	101
Stringcourse	0	0	0	0	0	0	42	3994	275	0
Cornice	0	0	0	0	0	0	0	0	12212	0
Corner column	0	0	70	31	209	63	299	292	0	8554

6 Features + Z Coordinate_FIRST FLOOR

CLASS	Parapet	Base	Lower Shaft	Ring	Upper Shaft	Capital	Arch	Stringcourse	Cornice	Corner Column
Parapet	14959	528	83	2	2	90	2	0	0	484
Base	0	138	68	0	0	0	0	0	0	8
Lower shaft	0	0	849	55	37	0	0	0	0	226
Ring	0	0	1	87	116	0	0	0	0	23
Upper shaft	0	0	0	0	1687	57	0	0	0	408
Capital	0	0	0	0	4	345	242	0	0	36
Arch	0	0	0	0	0	1	7151	713	0	457
Stringcourse	0	0	0	0	0	0	433	3470	341	67
Cornice	0	0	0	0	0	0	0	0	12212	0
Corner column	0	9	85	2	138	10	636	157	0	8481

6 'ad hoc' Features + Z Coordinate_FIRST FLOOR

Fig. 137 Confusion Matrix for the First Floor with the best combinations: 6 Features + Z Coordinate and 6 'ad hoc' Features + Z Coordinate.

Tab. 19 Performance Metrics with 63 Features (Ground Floor).

PERFORMANCE METRICS			
Precision	***Recall***	***F1-score***	
99.46	99.89	99.67	
98.55	98.33	98.44	
93.10	99.64	96.26	
99.44	96.65	98.02	
99.55	96.33	97.91	
98.88	94.93	96.86	
96.80	96.17	96.48	
96.38	94.46	95.41	
80.18	94.86	86.91	
99.48	99.63	99.56	
Simple Average			***Overall Accuracy***
96.18	***97.09***	***96.55***	***97.38***

Tab. 20 Performance Metrics with 15 Features (Ground Floor).

PERFORMANCE METRICS			
Precision	***Recall***	***F1-score***	
99.65	99.37	99.51	
97.90	98.16	98.03	
92.82	99.68	96.12	
96.23	96.85	96.54	
99.40	95.91	97.62	
97.53	95.10	96.30	
96.31	95.16	95.73	
93.98	96.16	95.05	
89.73	89.14	89.44	
99.53	99.36	99.45	
Simple Average			***Overall Accuracy***
96.31	***96.49***	***96.38***	***97.11***

Tab. 21 Performance Metrics with 6 Features (Ground Floor).

PERFORMANCE METRICS			
Precision	***Recall***	***F1-score***	
99.73	98.79	99.26	
93.81	95.11	94.45	
79.96	96.06	87.28	
81.64	96.58	88.48	
97.36	88.80	92.88	
96.01	88.30	92.00	
92.80	92.87	92.83	
87.23	92.51	89.79	
82.07	69.30	75.15	
97.22	98.52	97.87	
Simple Average			***Overall Accuracy***
90.78	***91.68***	***91.00***	***92.98***

Tab. 22 Performance Metrics with 6 'ad hoc' Features + Z Coordinate + Normals (Ground Floor).

PERFORMANCE METRICS			
Precision	***Recall***	***F1-score***	
99.75	99.37	99.56	
98.23	98.48	98.36	
99.38	99.14	99.26	
96.23	96.93	96.58	
99.66	99.23	99.44	
97.61	81.31	88.72	
88.33	77.48	82.55	
77.33	83.18	80.15	
37.28	51.30	43.18	
87.97	100.00	93.60	
Simple Average			***Overall Accuracy***
88.18	***88.64***	***88.14***	***91.97***

Tab. 23 Performance Metrics with 72 Features (First Floor).

PERFORMANCE METRICS			
Precision	***Recall***	***F1-score***	
99.15	99.31	99.23	
66.82	84.62	74.67	
95.03	94.71	94.87	
71.37	76.06	73.64	
94.05	96.66	95.34	
85.33	90.22	87.70	
98.25	95.50	96.85	
94.55	95.61	95.08	
99.30	99.70	99.50	
97.59	97.30	97.45	
Simple Average			***Overall Accuracy***
90.14	***92.97***	***91.43***	***97.73***

Tab. 24 Performance Metrics with 15 Features + Z Coordinate (First Floor).

PERFORMANCE METRICS			
Precision	***Recall***	***F1-score***	
90.51	100.00	95.02	
70.09	20.27	31.45	
93.92	68.16	78.99	
54.19	72.78	62.12	
76.67	92.02	83.65	
54.39	81.77	65.33	
90.03	94.03	91.98	
92.69	78.91	85.25	
100.00	97.68	98.83	
93.66	88.96	91.25	
Simple Average			***Overall Accuracy***
81.62	***79.46***	***78.39***	***92.15***

Tab. 25 Performance Metrics with 6 Features + Z Coordinate (First Floor).

PERFORMANCE METRICS			
Precision	***Recall***	***F1-score***	
86.20	100.00	92.59	
37.85	18.97	25.27	
90.49	61.57	73.28	
53.30	62.37	57.48	
84.62	87.34	85.96	
54.55	65.64	59.58	
83.67	92.07	87.67	
92.65	72.04	81.06	
100.00	97.80	98.89	
89.87	81.92	85.71	
Simple Average			***Overall Accuracy***
77.32	***73.97***	***74.75***	***89.37***

Tab. 26 Performance Metrics with 6 'ad hoc' Features + Z Coordinate (First Floor).

PERFORMANCE METRICS			
Precision	***Recall***	***F1-score***	
92.63	100.00	96.17	
64.49	20.44	31.05	
72.75	78.18	75.37	
38.33	59.59	46.65	
78.39	85.03	81.58	
55.02	68.59	61.06	
85.93	84.49	85.20	
80.49	79.95	80.22	
100.00	97.28	98.62	
89.10	83.23	86.07	
Simple Average			***Overall Accuracy***
75.71	***75.68***	***74.20***	***89.94***

On the Ground Floor, noteworthy results for Overall Accuracy are observed, particularly with the combination of 63 features, achieving an impressive 97.38. Following closely is the combination with only 15 features, displaying a commendable accuracy of 97.11, while the combination with 6 features reaches a respectable value of 92.98. The lowest but still acceptable accuracy is associated with the combination of 6 'ad hoc' features + Z Coordinate + Normals, yielding a score of 91.97.

Shifting focus to the First Floor, the highest accuracy is obtained with the combination of 72 features, reaching an outstanding 97.73. In contrast, a lower accuracy, at 92.15, is observed with the combination of 15 features + Z Coordinate. Subsequently, the combination of 6 'ad hoc' features + Z Coordinate achieves a value of 89.94, and finally, the lowest accuracy is attributed to the combination of 6 features + Z Coordinate, totaling 89.37.

Semantic Point Cloud

The subsequent figures depict the final point clouds ranked using Machine Learning, corresponding to the top four combinations for each respective floor (for the ground floor, Fig. 138, and Fig. 139, and for the first floor, Fig. 140, and Fig. 141).

All combinations applied to the two distinct floors yield highly significant results. While prioritising combinations with more features based on the confusion matrix results, an interesting observation emerges from a graphical perspective, suggesting a potential reversal of roles. Specifically, it becomes evident that 'ad hoc' features, when combined with the Z Coordinate and Normals, result in a nearly perfect semantic discretisation for components related to columns. In this configuration, the ring that divides the two parts of the shaft is accurately distinguished. However, some semantic confusion arises in the upper parts, where the architrave is occasionally mistaken for the corbel on the ground floor, and the arch is sometimes confused with the corner column on the first floor.

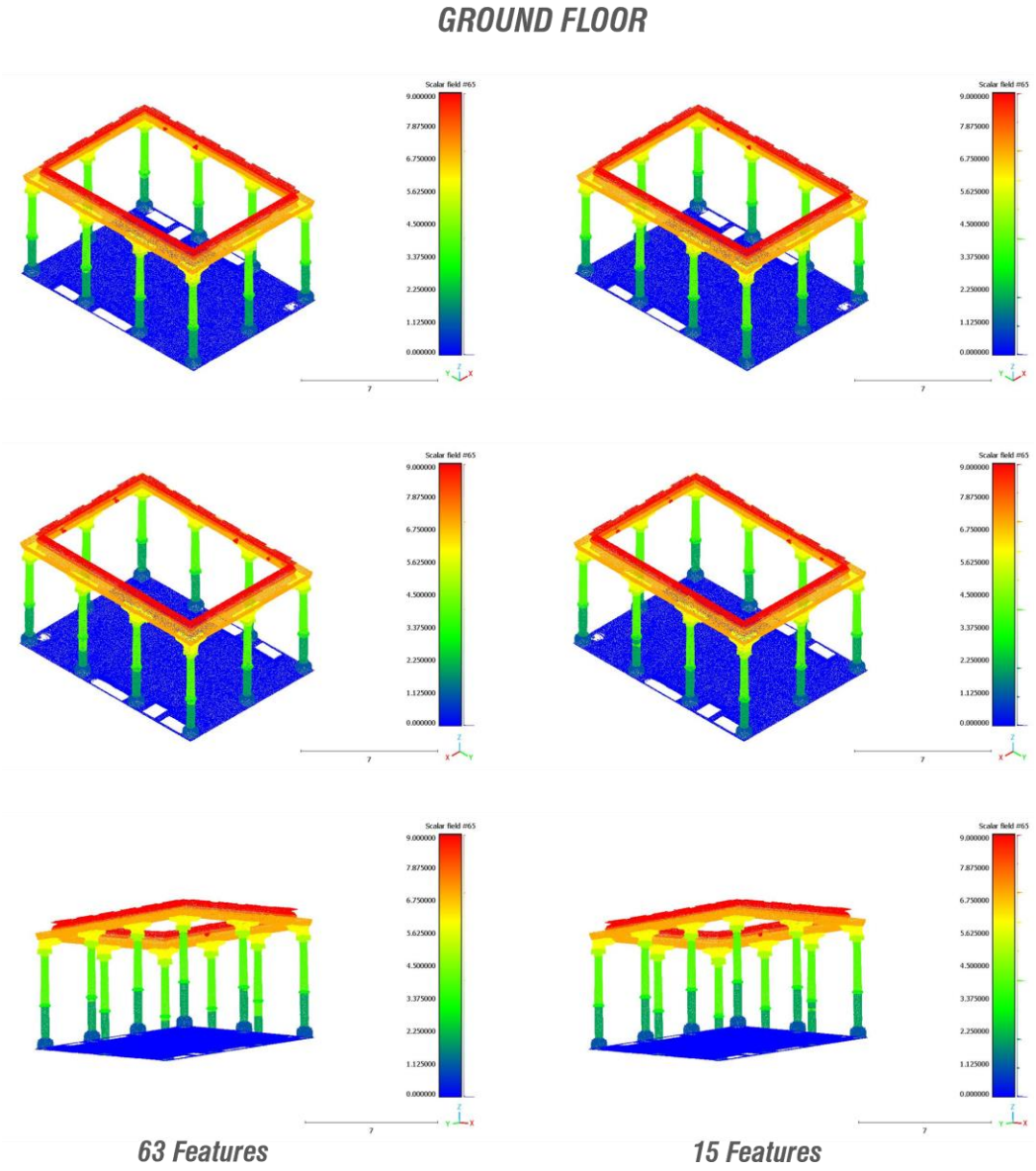

Fig. 138 Semantic Point cloud of the Ground Floor using 63 and 15 Features.

GROUND FLOOR

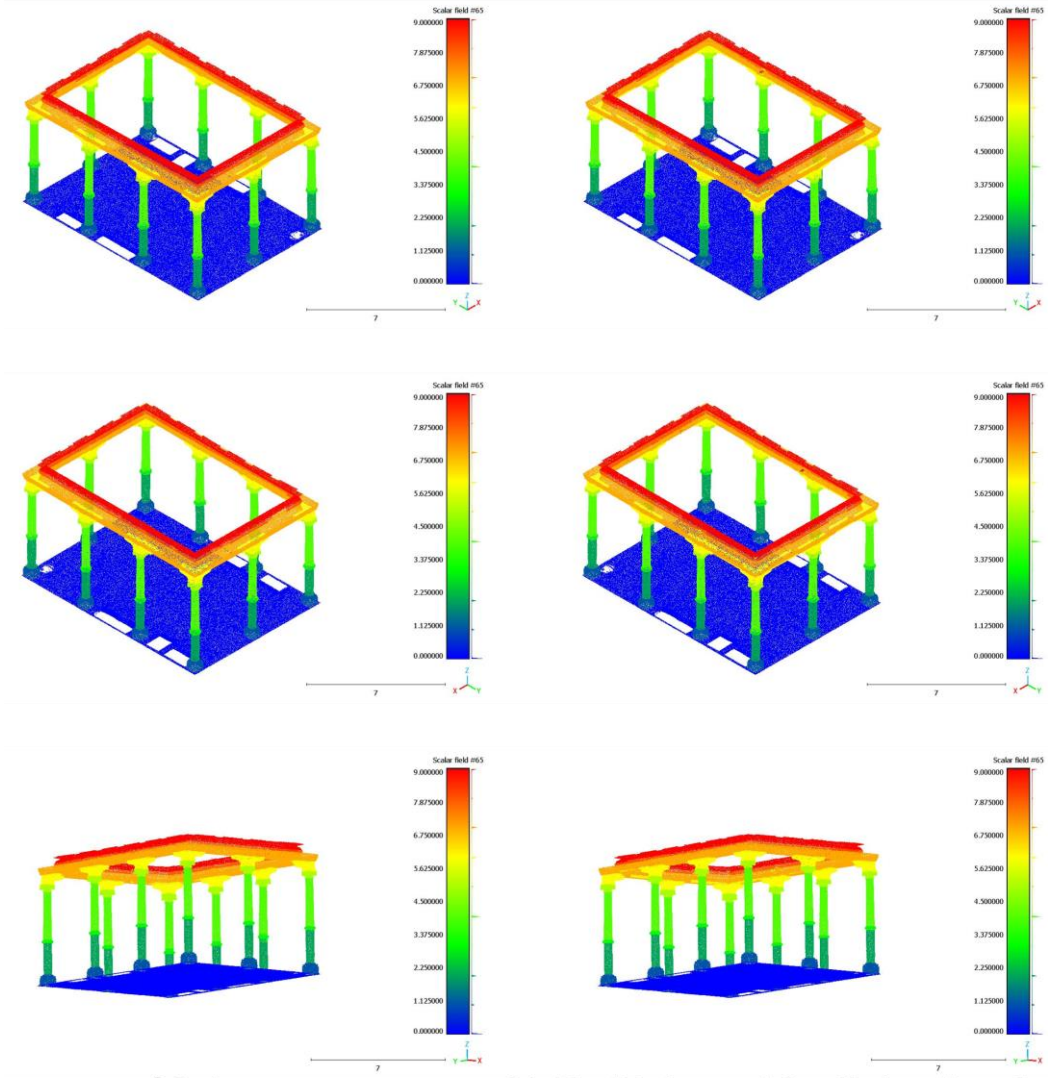

6 Features *6 'ad hoc' Features + Z Coordinate + Normals*

Fig. 139 Semantic Point cloud of the Ground Floor using 6 Features and 6 'ad hoc' Features + Z Coordinate + Normals.

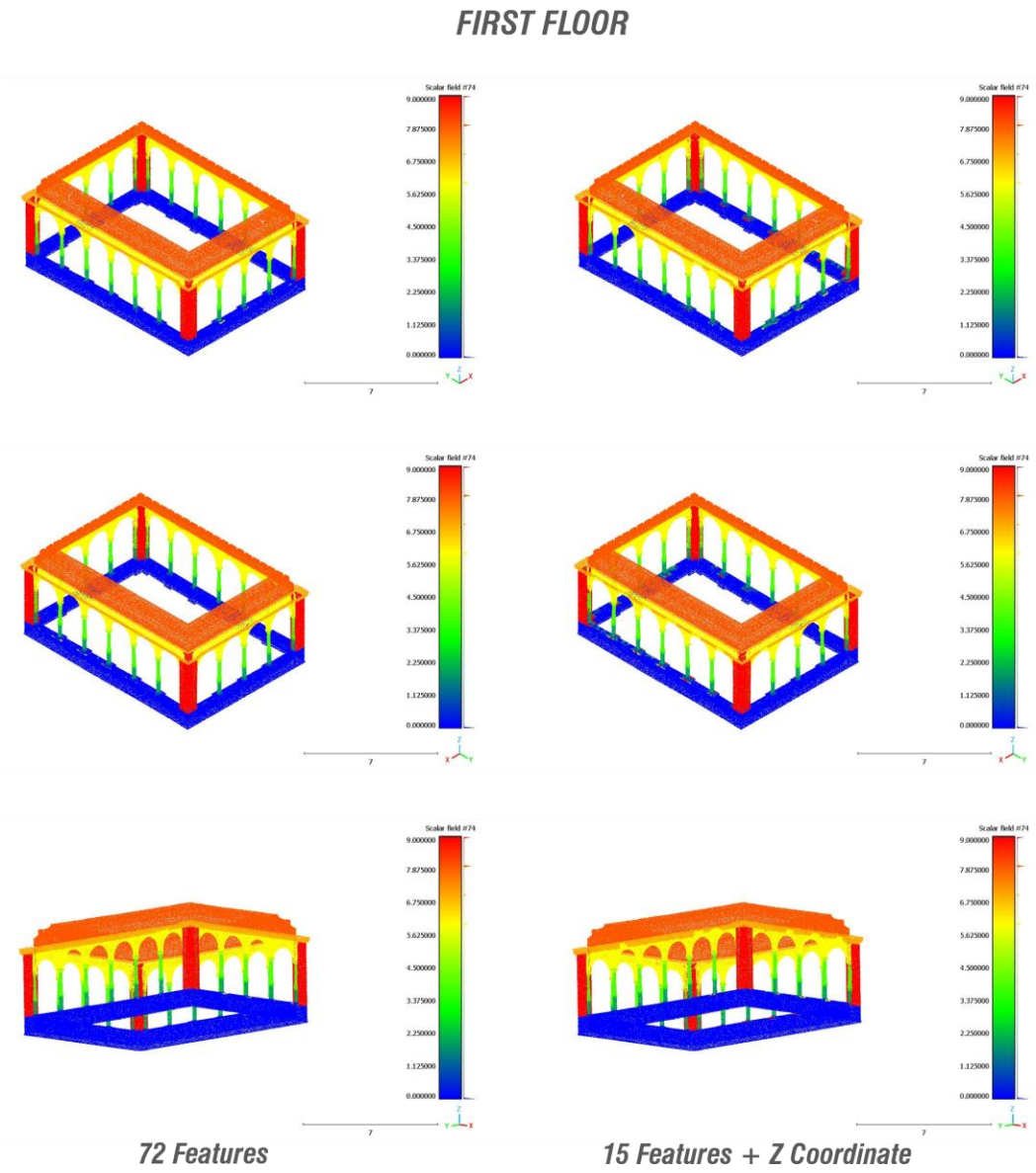

Fig. 140 Semantic Point cloud of the First Floor using 72 and 15 Features + Z Coordinate.

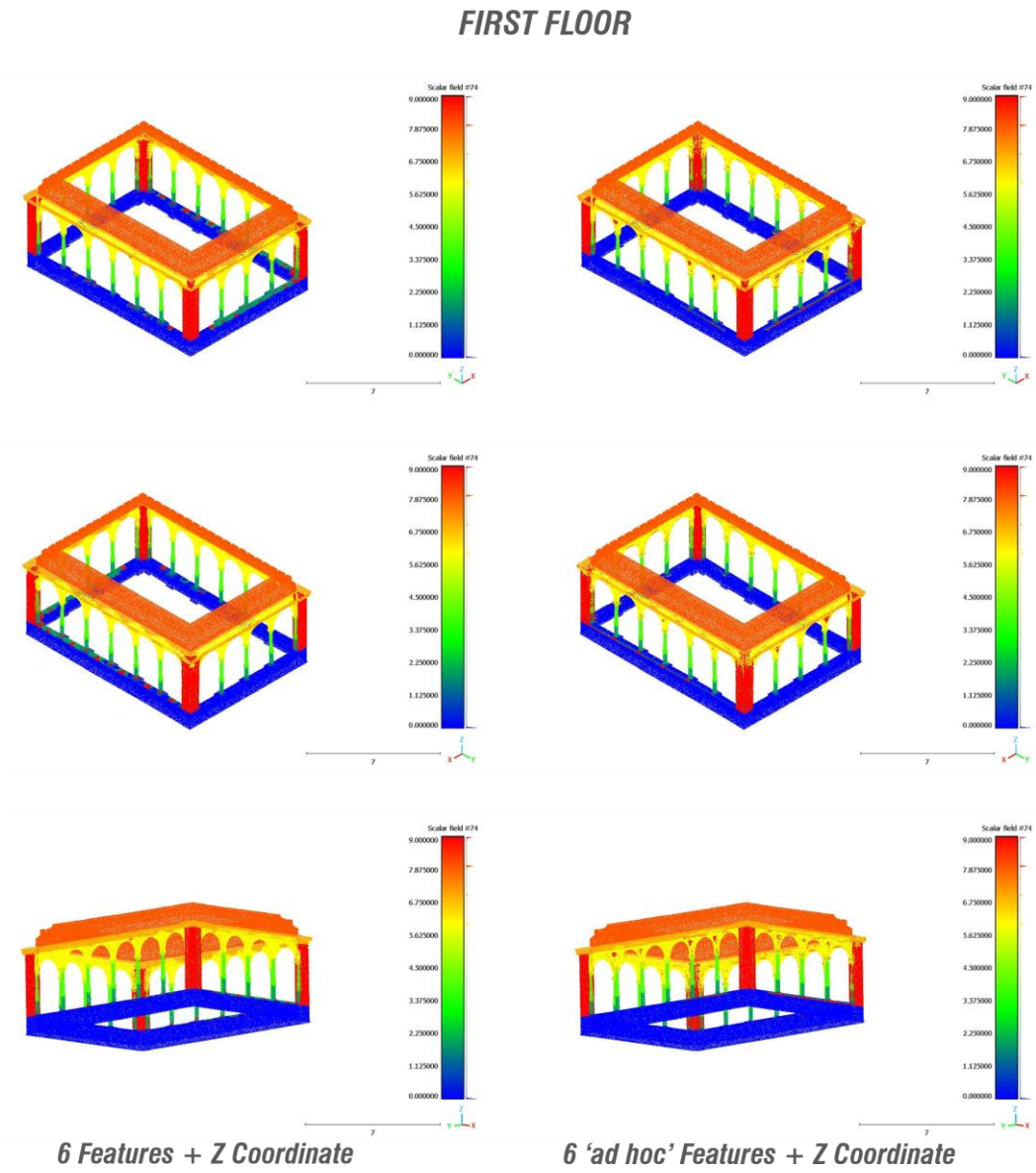

Fig. 141 Semantic Point cloud of the First Floor using 6 Features + Coordinate Z and 6 'ad hoc' Features + Z Coordinate.

Intermediate results are observed with combinations featuring 15 and 6 features, displaying a few semantic distinction errors primarily related to the lower shaft on the ground floor and the parapet and stringcourse on the first floor.

4.6.4 Ending Statements

The application of the Artificial Intelligence (AI) in the field of Architectural Heritage (AH), specifically concerning the automatic segmentation and classification of point clouds through Machine Learning, emerges as a revolutionary and promising approach for the preservation, analysis, and understanding of historical structures.

In the context of this study, outstanding results have been achieved in the detailed and precise representation of one of the significant palaces of the Renaissance in Saragozza.

The AI-based approach has enabled the differentiation of complex architectural and structural elements, facilitating the comprehension and digital documentation of details often overlooked by the human eye. Notably, processing times have been impressively optimised, as seen in the automatic classification of portions of point clouds used as test set, taking only a few seconds.

Despite the achieved successes, several significant challenges have been encountered, among which the need for an adequate and representative training dataset has emerged as a critical limitation. Manual point cloud segmentation undoubtedly consumes time, depending on the level of detail and precision of operations conducted by the operator, thereby influencing the outcome of the final classification.

The various combinations of geometric properties analysed in this study have allowed the highlighting of positive outcomes, even with a limited amount of training data, albeit requiring careful and logically rigorous selection. In this case, 'ad hoc' features were chosen based on the geometric dimensions of the architectural components intended for segmentation, yielding satisfactory results, though inferior to those obtained with combinations featuring more training data.

The in-depth segmentation analysis has been notably enhanced by incorporating normal coordinates and the Z-coordinate, which have significantly contributed to enhancing the effectiveness and accuracy of the process.

The automated process demonstrated is generalisable in the context of Architectural Heritage. However, it is crucial to emphasise that training data are specific to each analysed study, a gap that could be addressed by implementing more advanced models, integrating multi-sensor data, and exploring approaches based on Deep Learning to further enhance system performance. Therefore, the creation of more diversified and inclusive datasets will allow greater generalisation of models and the management of a broader range of historical contexts.

Innovation in this field holds the potential to open new perspectives for heritage preservation and enrich our understanding of architectural works that have shaped history, especially when integrated into a virtualisation context through HBIM. This undoubtedly serves as a point of reflection for future developments in this work, aiming to facilitate automation even in the operational phases of three-dimensional modelling.

CONCLUSIONS AND FUTURE DEVELOPMENTS

Throughout the extensive exploration conducted in this research, a diverse array of methodologies has been thoroughly examined, each uniquely applied to delve into the realm of advanced technologies in architectural design and surveying. The primary focus has been on the preservation of Architectural Heritage through the intricate process of digitisation. The indispensable role of a Scan to BIM protocol has been clearly identified as a critical component, crucial for elevating the precision in representing heritage in the digital landscape.

During the analysis of several case studies, unique challenges connected to the execution of integrated digital surveys have surfaced, with criteria and critical considerations that may vary based on metric and graphic requirements, as well as environmental factors. This has led to the definition of proven operational procedures, adhering to a standards-based approach, integrating parameters of quality and safety to ensure efficiency both in on-site execution and subsequent data processing. The avoidance of superfluous information, which could potentially lead to errors and result in significant time losses, has been a paramount consideration.

The pivotal integration between three-dimensional models and their corresponding databases has emerged as a fundamental aspect for the creation of comprehensive informational models. This approach not only facilitated the standardised organisation of information but also established a seamless interface with specific software tools, thereby allowing for the indexed structuring of informational resources. Operations involving programming language and data optimisation processes have been instrumental in augmenting process efficiency, thereby contributing significantly to the ongoing evolution of methodologies for assessing geometric accuracy.

An in-depth examination of automations and Artificial Intelligence algorithms has revealed groundbreaking perspectives. The focus has been on the analysis of data acquired through digital surveying, leading to novel applications such as monitoring

the physical-material obsolescence of buildings, graphical representation of heritage through BIM models, and the automated planning of digital surveying.
The incorporation of open-source algorithms and Machine Learning techniques has enriched the overall research framework, notably contributing to semantic segmentation and point cloud classification.

The outcomes obtained underscore the paramount importance of an integrated approach that seamlessly combines advanced technologies with specialised skills. This integration is crucial for optimising surveying methods and streamlining BIM-oriented operational processes. The challenges identified collectively lay a robust foundation for future research and developments in the expansive field of Architectural Heritage conservation, encompassing all conceivable facets of this multidimensional domain.

Most certainly, the extraordinary potential of Deep Learning in the analysis of point clouds, recently observed, could revolutionise the way experts automatically recognise and classify architectural elements within digital three-dimensional environments. A tempting idea is to create a large training dataset derived from a variety of case studies, thus enabling the adoption of a generalised methodology not bound to specific contexts but capable of extracting relevant information from each of them. This innovative approach could radically redefine information extraction from scanning data, perhaps facilitating the subsequent creation of detailed BIM models.

The outlook of automatically generating BIM models from raw data promises to significantly simplify modelling processes, minimising human intervention and accelerating project delivery times. This result would represent a genuine turning point in modelling practice, indicating a clear direction towards a future of greater efficiency and precision.

Naturally, to fully harness this potential, it will be essential to also develop standards for BIM data interoperability and ensure compatibility across different platforms and

software. This step is essential to promote more effective and seamless collaboration among stakeholders involved in Cultural/Architectural Heritage conservation projects and to ensure the success of large-scale implementations of these innovative methodologies.

Drawing on the insights derived from the provided results and simultaneously anticipating future developments, this research journey comes to a close, underscoring the need to perpetuate innovation and adaptability to emerging technologies, the latter aimed at fostering improved communication between manufacturing companies and designers. A synergy that contributes to the generation of industrial products within a digital framework that is simultaneously sustainable and forward-thinking.

ACKNOWLEDGEMENTS

I would like to express my heartfelt gratitude to all those who have played a significant role in the successful completion of my doctoral journey. Firstly, I extend my deepest thanks to my supervisor, Professor Cesare Verdoscia, for his unwavering guidance, support, and patience throughout these intensive years of research. His insightful advice and unwavering commitment to my academic growth have undeniably shaped the success of this work.

A sincere appreciation goes to my supervisor of the Universidad de Zaragoza, Professor Luis Agustín-Hernández, who, along with his exceptional team of researchers, warmly welcomed me during my research period abroad. Collaborating with them has profoundly enriched my studies, infusing a touch of *mudéjar* flair into our interactions, even turning a simple cup of Spanish coffee into a delightful experience.

I cannot overlook Engineer Riccardo Tavolare for our ongoing scientific discussions, which have evolved into a genuine friendship characterised by emotionally valuable exchanges and reflections. I also express my gratitude to Professor Elena Cabrera-Revuelta from the Universidad de Cádiz for her warmth, passion, and dedication to her research, which proved crucial for the development of a significant portion of mine.

Special thanks are extended to my colleagues of the MAULab, Antonella Musicco and Nicola Rossi, with whom I have shared not only intense work moments but also travels, aperitifs filled with *focaccia* and lunches with *peperone crusco.*

I appreciate other researchers I collaborated with over the years, particularly Professor Fabio Fatiguso and Professor Mariella De Fino, with whom I had the opportunity to cooperate for my first scientific publication, and other fellow doctoral candidates whom I had the chance to meet in person after a year of video calls due to the COVID period.

Of course, I extend my thanks to the coordinator of my PhD course, Professor Vito Iacobellis, for always being present for every need, along with the rest of the technical and administrative staff.

My profound gratitude goes to my family and my old and new friends for their constant encouragement and the invaluable support they have offered, as always, and especially throughout these three years.

BIBLIOGRAPHY

Abgaz, Y. *et al.* (2021) 'A Methodology for Semantic Enrichment of Cultural Heritage Images Using Artificial Intelligence Technologies', *Technologies. J Imaging*, 7(8). doi: 10.3390/jimaging7080121.

Abreu, N. *et al.* (2023) 'Procedural Point Cloud Modelling in Scan-to-BIM and Scan-vs-BIM Applications: A Review', *ISPRS International Journal of Geo-Information*, 12(7). doi: 10.3390/ijgi12070260.

Adami, A. *et al.* (2019) 'Ultra light UAV systems for the metrical documentation of Cultural Heritage: applications for architecture and archaeology', in *International Archives of the Photogrammetry, Remote Sensing and Spatial Information Sciences - ISPRS Archives*, pp. 15–21. doi: 10.5194/isprs-archives-XLII-2-W17-15-2019.

Adán, A., Quintana, B. and Prieto, S. A. (2019) 'Autonomous mobile scanning systems for the digitization of buildings: A review', *Remote Sensing*, 11(3). doi: 10.3390/rs11030306.

Adekunle, S. A., Aigbavboa, C. and Ejohwomu, O. A. (2022) 'SCAN TO BIM: a systematic literature review network analysis', *IOP Conference Series: Materials Science and Engineering*, 1218(1), p. 012057. doi: 10.1088/1757-899x/1218/1/012057.

Agarwal, A. *et al.* (2023) 'MDI+: A Flexible Random Forest-Based Feature Importance Framework', pp. 1–83. Available at: http://arxiv.org/abs/2307.01932.

Agisoft (2020) 'Agisoft Metashape User Manual', p. 160. Available at: https://www.agisoft.com/pdf/metashape-pro_1_5_en.pdf.

Agustín-Hernández, L. *et al.* (2021) 'From tls point cloud data to geometrical genesis determination of ribbed masonry vaults', *International Archives of the Photogrammetry, Remote Sensing and Spatial Information Sciences - ISPRS Archives*, 46(M-1–2021), pp. 9–16. doi: 10.5194/isprs-Archives-XLVI-M-1-2021-9-2021.

Agustín-Hernández, L., Fernández-Morales, A. and Quintilla-Castán, M. (2018) 'Digital graphic inventory of the architectural heritage', in *XVII Congreso Internacional de Expresión Gráfica Arquitectónica*.

Agustín-Hernández, L. and Quintilla-Castán, M. (2019) 'Virtual Reconstruction in BIM Technology and Digital Inventories of Heritage', *International Archives of the Photogrammetry, Remote Sensing and Spatial Information Sciences - ISPRS Archives*, 42(2/W15), pp. 25–31. doi: 10.5194/isprs-archives-XLII-2-W15-25-2019.

Agustín-Hernández, L., Sancho-Mir, M. and Fernández-Morales, A. (2016) 'Sobre la didáctica de BIM en el currículo del arquitecto: Un caso de estudio', in *EUBIM 2016 - BIM International Conference*, pp. 92–101.

Agustín-Hernández, L., Sancho-Mir, M. and Fernández-Morales, A. (2023) 'Layout and Geometry in the Medieval Ribbed Vault With Brick Ribs in Aragon', *EGA Revista de Expresion Grafica Arquitectonica*, 28(47), pp. 96–109. doi: 10.4995/ega.2023.19387.

Aicardi, I. *et al.* (2018) 'Recent trends in cultural heritage 3D survey: The photogrammetric computer vision approach', *Journal of Cultural Heritage*, 32, pp. 257–266. doi: 10.1016/j.culher.2017.11.006.

Akca, D. (2003) 'Full Automatic Registration of Laser Scanner Point Clouds', *Optical 3-D Measurement Techniques VI*, 1, pp. 330–337.

Akca, D. *et al.* (2006) 'Recording and modeling of cultural heritage objects with coded structured light projection systems', *2nd International Conference on Remote Sensing in Archaeology*, (March 2015), pp. 375–382.

Akca, D. (2010) 'Co-registration of Surfaces by 3D Least Squares Matching', *Photogrammetric Engineering and Remote Sensing*, 76(3), pp. 307–318. doi: 10.14358/PERS.76.3.307.

Alexander, D. (1983) 'The Limitations of Traditional Surveying Techniques in a Forested Environment', *Journal of Field Archaeology*, 10(2), pp. 177–186. doi: https://doi.org/10.2307/529608.

Ali, K. N., Alhajlah, H. H. and Kassem, M. A. (2022) 'Collaboration and Risk in Building Information Modelling (BIM): A Systematic Literature Review', *Buildings*, 12(571). doi: 10.3390/buildings12050571.

Alshawabkeh, Y. *et al.* (2020) 'Heritage documentation using laser scanner and photogrammetry. The case study of Qasr Al-Abidit, Jordan', *Digital Applications in*

Archaeology and Cultural Heritage, 16(December 2019), p. e00133. doi: 10.1016/j.daach.2019.e00133.

Alshawabkeh, Y., Baik, A. and Miky, Y. (2021) 'Integration of laser scanner and photogrammetry for heritage BIM enhancement', *ISPRS International Journal of Geo-Information*, 10(5). doi: 10.3390/ijgi10050316.

Altuntas, C., Karabork, H. and Tusat, E. (2014) 'Georeferencing of ground-based LIDAR data using continuously operating reference stations', *Optical Engineering*, 53(11), p. 114110. doi: 10.1117/1.oe.53.11.114110.

Alzara, M. *et al.* (2023) 'Dynamo script and a BIM-based process for measuring embodied carbon in buildings during the design phase', *International Journal of Low-Carbon Technologies*, 18(June), pp. 943–955. doi: 10.1093/ijlct/ctad053.

Amicis, R. *et al.* (2010) *Geomatics and Geoinformatics for the Digital 3D Documentation, Fruition and Valorization of Cultural Heritage*.

Andrews, P., Zaihrayeu, I. and Pane, J. (2012) 'A classification of semantic annotation systems', *Semantic Web*, 3(3), pp. 223–248. doi: 10.3233/SW-2011-0056.

Angjeliu, G., Cardani, G. and Coronelli, D. (2019) 'A parametric model for ribbed masonry vaults', *Automation in Construction*, 105(January), p. 102785. doi: 10.1016/j.autcon.2019.03.006.

Anil, E. B. *et al.* (2013) 'Deviation analysis method for the assessment of the quality of the as-is Building Information Models generated from point cloud data', *Automation in Construction*, 35, pp. 507–516. doi: 10.1016/j.autcon.2013.06.003.

Antón, D. *et al.* (2018) 'Accuracy evaluation of the semi-automatic 3D modeling for historical building information models', *International Journal of Architectural Heritage*, 12(5), pp. 790–805. doi: 10.1080/15583058.2017.1415391.

Appel, K., Haken, W. and Koch, J. (1977) 'Every planar map is four colorable part II: Reducibility', *Illinois Journal of Mathematics*, 21(3), pp. 491–567. doi: 10.1215/ijm/1256049012.

Arganda-Carreras, I. *et al.* (2017) 'Trainable Weka Segmentation: A machine learning tool for microscopy pixel classification', *Bioinformatics*, 33(15), pp. 2424–2426. doi:

10.1093/bioinformatics/btx180.

Aryan, A., Bosché, F. and Tang, P. (2021) 'Planning for terrestrial laser scanning in construction: A review', *Automation in Construction*, 125, pp. 1–14. doi: 10.1016/j.autcon.2021.103551.

Atasoy, G. *et al.* (2010) 'Visualizing laser scanner data for bridge inspection', *2010 - 27th International Symposium on Automation and Robotics in Construction, ISARC 2010*, 2010-Janua(Isarc), pp. 390–399. doi: 10.22260/isarc2010/0042.

Aterini, B. and Giuricin, S. (2020) 'The Integrated survey for the recovery of the former Hospital / Monastery of San Pietro in Luco di Mugello', *SCIRES-IT - SCIentific RESearch and Information Technology*, 10(2), pp. 99–116. doi: 10.2423/i22394303v10n2p99.

Avis, D. and Toussaint, G. T. (1981) 'An Optimal Algorithm for Determining the Visibility of a Polygon from an Edge', *IEEE Transactions on Computers*, C–30(12), pp. 910–914.

Badenko, V. *et al.* (2019) 'Scan-to-bim methodology adapted for different application', *International Archives of the Photogrammetry, Remote Sensing and Spatial Information Sciences - ISPRS Archives*, 42(5/W2), pp. 1–7. doi: 10.5194/isprs-archives-XLII-5-W2-1-2019.

Bagnolo, V., Argiolas, R. and Vanini, C. (2022) 'Algorithmic Modelling as a Key Tool for Ribbed Vault Geometry', *Nexus Network Journal*, 24(1), pp. 147–166. doi: 10.1007/s00004-021-00570-z.

Baik, A., Boehm, J. and Abaikkauedusa, U. K. (2017) 'HIJAZI ARCHITECTURAL OBJECT LIBRARY Dept . of Geomatic Engineering , University College London , Gower Street , London , WC1E 6BT Dept . of Geomatic Engineering , University College London , Gower Street , London , WC1E 6BT UK –', XLII(March), pp. 1–3. doi: 10.5194/isprs-archives-XLII-2-W3-55-2017.

Bakirman, T. *et al.* (2020) 'Implementation of ultra-light UAV systems for cultural heritage documentation', *Journal of Cultural Heritage*, 44, pp. 174–184. doi: 10.1016/j.culher.2020.01.006.

Ballard, D. H. (1981) 'Readings in Computer Vision: Issues, Problems, Principles, and

Paradigms', *Pattern Recoqnition*, 13(2), pp. 111–122. Available at: https://pdfs.semanticscholar.org/2c8c/97918a24c26da7c949a7d6aaf3201d9d9cf9.pdf%0Ahttp://dl.acm.org/citation.cfm?id=33517.33574.

Balzani, M., Maietti, F. and Mugayar Kühl, B. (2017) 'Point cloud analysis for conservation and enhancement of modernist architecture', *International Archives of the Photogrammetry, Remote Sensing and Spatial Information Sciences - ISPRS Archives*, 42(2/W3), pp. 71–77. doi: 10.5194/isprs-archives-XLII-2-W3-71-2017.

Banfi, F. (2020) 'HBIM, 3D drawing and virtual reality for archaeological sites and ancient ruins', *Virtual Archaeology Review*, 11(23), pp. 16–33. doi: 10.4995/var.2020.12416.

Bassir, D. *et al.* (2023) 'Application of artificial intelligence and machine learning for BIM: review', *International Journal for Simulation and Multidisciplinary Design Optimization*, 14(5), pp. 1–8. doi: https://doi.org/10.1051/smdo/2023005.

Battini, C. (2012) *Rilievo digitale e restituzione: concetti base ed esempi*. Alinea.

Battini, C. *et al.* (2024) 'Automatic generation of synthetic heritage point clouds: Analysis and segmentation based on shape grammar for historical vaults', *Journal of Cultural Heritage*, 66, pp. 37–47. doi: 10.1016/j.culher.2023.10.003.

Battini, C. and Sorge, E. (2016) 'Dynamic Management of Survey Data and Archaeological Excavation. the Case Study of the Amphitheatre of Volterra', *SCIentific RESearch and Information Technology*, 6(2), pp. 119–132. doi: 10.2423/i22394303v6n2p119.

Bedford, J. (2017) 'Photogrammetric Applications for Cultural Heritage. Guidance for Good Practice', *Historic England*, pp. 1–124.

Bellekens, B., Spruyt, V. and Weyn, M. (2014) 'A Survey of Rigid 3D Pointcloud Registration Algorithms', *AMBIENT 2014, The Fourth International Conference on Ambient Computing, Applications, Services and Technologies. 2014.*, pp. 8–13.

Beraldin, J.-A. (2004) 'Integration of laser scanning and close-range photogrammetry. The last decade and beyond', in *Proceedings of the XXth ISPRS Congress, Commission VII*.

Bernardini, F. *et al.* (1999) 'The Ball-Pivoting Algorithm for Surface Reconstruction',

IEEE Transactions on Visualization and Computer Graphics, 5(4), pp. 349–359. doi: 10.1109/2945.817351.

Besl, P. J. and McKay, N. D. (1992) 'A Method for Registration of 3-D Shapes', *IEEE Transactions on Pattern Analysis and Machine Intelligence*, 14(2), pp. 239–256. doi: 10.1109/34.121791.

Bhanu, B. *et al.* (1986) 'Range Data Processing: Representation of Surfaces By Edges'., *Proceedings - International Conference on Pattern Recognition*, pp. 236–238.

Biegelbauer, G., Vincze, M. and Wohlkinger, W. (2010) 'Model-based 3D object detection', *Machine Vision and Applications*, 21, pp. 497–516. doi: https://doi.org/10.1007/s00138-008-0178-3.

BIMForum and American Institute of Architects (2023) 'Level of Development (LOD) Specification. Part I: Draft for Public Comment'. Available at: www.bimforum.org/lod 2023.

Biosca, J. M. and Lerma, J. L. (2008) 'Unsupervised robust planar segmentation of terrestrial laser scanner point clouds based on fuzzy clustering methods', *ISPRS Journal of Photogrammetry and Remote Sensing*, 63(1), pp. 84–98. doi: 10.1016/j.isprsjprs.2007.07.010.

Biswas, H. K., Bosché, F. and Sun, M. (2015) 'Planning for scanning using building information models: A novel approach with occlusion handling', *32nd International Symposium on Automation and Robotics in Construction and Mining: Connected to the Future, Proceedings*, pp. 1–8. doi: 10.22260/isarc2015/0047.

Blaise, J.-Y., Florenzano, M. and De Luca, L. (2004) 'Architectural Surveying : From a point-cloud to a 3D model, benefits of using theoretical models stemming from the history of representation', *Electronic Imaging & the Visual Arts*.

Boehler, W. and Heinz, G. (1999) 'Documentation, Surveying, Photogrammetry', in *Proceedings of CIPA Symposium 17*. Olinda (Brazil).

Bonacini, E. (2015) 'A pilot project with Google Indoor Street View: a 360° tour of "Paolo Orsi" Museum (Syracuse, Italy)', *SCIRES-IT - SCIentific RESearch and Information Technology*, 5(2), pp. 151–168. doi: 10.2423/i22394303v5n2p151.

Bosché, F. *et al.* (2015) 'The value of integrating Scan-to-BIM and Scan-vs-BIM techniques for construction monitoring using laser scanning and BIM: The case of cylindrical MEP components', *Automation in Construction*, 49, pp. 201–213. doi: 10.1016/j.autcon.2014.05.014.

Bosco, A. *et al.* (2019) 'A BIM Approach for the Analysis of an Archaeological Monument', *ISPRS Annals of the Photogrammetry, Remote Sensing and Spatial Information Sciences*, 42(2/W9), pp. 165–172. doi: 10.5194/isprs-archives-XLII-2-W9-165-2019.

Breiman, L. (2001) 'Random Forests', in *Machine Learning*. Springer Nature, pp. 5–32.

Brodu, N. and Lague, D. (2012) '3D terrestrial lidar data classification of complex natural scenes using a multi-scale dimensionality criterion: Applications in geomorphology', *ISPRS Journal of Photogrammetry and Remote Sensing*, 68(1), pp. 121–134. doi: 10.1016/j.isprsjprs.2012.01.006.

Bruno, S. *et al.* (2019) 'Gestione Integrata di Informazioni Computazionali nell'Approccio Historic Building Information Modelling', in *VII Convegno Internazionale ReUSO Matera 23-26 Ottobre 2019*, pp. 1–12.

Bruno, S. *et al.* (2020) 'Rule-based inferencing diagnosis in hbim', *Archeologia e Calcolatori*, 312, pp. 269–280. doi: 10.19282/ac.31.2.2020.25.

Brusaporci, S., Maiezza, P. and Tata, A. (2018) 'A framework for Architectural Heritage HBIM semantization and development', *International Archives of the Photogrammetry, Remote Sensing and Spatial Information Sciences - ISPRS Archives*, 42(2), pp. 179–184. doi: 10.5194/isprs-archives-XLII-2-179-2018.

Brusaporci, S. and Trizio, I. (2013) 'La "Carta di Londra" e il patrimonio architettonico: riflessioni circa una possibile implementazione', *SCIRES-IT - SCIentific RESearch and Information Technology*, 3(2), pp. 55–68. doi: 10.2423/i22394303v3n2p55.

Bryan, P. *et al.* (2009) *Metric Survey Specifications for Cultural Heritage*. DGO-Digi, *Historic England*. DGO-Digi. Edited by D. Andrews. Swindon: Liverpool University Press, Historic England. doi: 10.2307/j.ctvxbphrz.

BSI (2013) 'BSI Standard PAS: 1192-2', *BSI Standards Publication*, (1), pp. 1–68.

Buldo, M. *et al.* (2023) 'A Scan-to-BIM workflow proposal for Cultural Heritage. Automatic point cloud segmentation and parametric-adaptive modelling of vaulted systems', *The International Archives of the Photogrammetry, Remote Sensing and Spatial Information Sciences - ISPRS Archives*, XLVIII(M–2), pp. 333–340. doi: 10.5194/isprs-archives-XLVIII-M-2-2023-333-2023.

Cabo, C., Ordóñez, C. and Argüelles-Fraga, R. (2017) 'An algorithm for optimizing terrestrial laser scanning in tunnels', *Automation in Construction*, 83, pp. 163–168. doi: 10.1016/j.autcon.2017.08.028.

Cabrera-Revuelta, E. (2017) *Optimización en el posicionamiento para la realización de un levantamiento arquitectónico*. Available at: https://idus.us.es/handle/11441/63989.

Cabrera-Revuelta, E. *et al.* (2021) 'Optimization of laser scanner positioning networks for architectural surveys through the design of genetic algorithms', *Measurement: Journal of the International Measurement Confederation*, 174. doi: 10.1016/j.measurement.2020.108898.

Cabrera-Revuelta, E. *et al.* (2024) 'Planning for terrestrial laser scanning: Methods for optimal sets of locations in architectural sites', *Journal of Building Engineering*, 85. doi: 10.1016/j.jobe.2024.108599.

Cabrera-Revuelta, E., Chávez de Diego, M. J. and Márquez-Pérez, A. (2018) 'The Fortress Problem in Terms of the Number of Reflex and Convex Vertices. A 3D objects scanning application', *Electronic Notes in Discrete Mathematics*, 68, pp. 173–178. doi: 10.1016/j.endm.2018.06.030.

Camiña, J. *et al.* (2022) 'Analysis of a SLAM-Based Laser Scanner for the 3D Digitalization of Underground Heritage Structures. A Case Study in the Wineries of Baltanas (Palencia, Spain)', in *The Future of Heritage Science and Technologies: ICT and Digital Heritage*. Springer, Cham. doi: https://doi.org/10.1007/978-3-031-20302-2_4.

Capone, M. and Lanzara, E. (2019) 'Scan-to-BIM vs 3D Ideal Model HBIM: Parametric Tools to Study Domes Geometry', *ISPRS Annals of the Photogrammetry, Remote Sensing and Spatial Information Sciences*, 42(2/W9), pp. 219–226. doi:

10.5194/isprs-archives-XLII-2-W9-219-2019.

Capparelli, F. and Camiz, A. (2019) 'Bim Documentation for Architecture and Archeology: the Shipwreck Museum in the Kyrenia Castle, Cyprus', in, pp. 333–342.

Casado, A. E. and Sanchez, J. M. D. (2018) 'Modelling in Science Education and Learning', in, pp. 39–57.

Chehata, N., Guo, L. and Mallet, C. (2009) 'Airborne LiDAR feature selection for urban classification using random forests', *International Archives of Photogrammetry, Remote Sensing and Spatial Information Sciences*, 38. doi: 10.13203/j.whugis20130206.

Chen, D. *et al.* (2014) 'A methodology for automated segmentation and reconstruction of urban 3-D buildings from ALS point clouds', *IEEE Journal of Selected Topics in Applied Earth Observations and Remote Sensing*, 7(10), pp. 4199–4217. doi: 10.1109/JSTARS.2014.2349003.

Cheng, D. *et al.* (2021) 'PCA-based denoising algorithm for outdoor lidar point cloud data', *Sensors*, 21(11). doi: 10.3390/s21113703.

Chesnokov, N. (2018) 'The Art Gallery Problem: An Overview and Extension to Chromatic Coloring and Mobile Guards', pp. 1–13. Available at: https://api.semanticscholar.org/CorpusID:209683690.

Chien, S. *et al.* (2017) 'Implementation of Cloud BIM-based Platform Towards High-performance Building Services', *Procedia Environmental Sciences*, 38, pp. 436–444. doi: 10.1016/j.proenv.2017.03.129.

Chirisa, I. (2020) 'Scope for Virtual Tourism in the Times of COVID-19 in Select African Destinations', *Journal of Social Sciences*, 64(1–3), pp. 0–13. doi: 10.31901/24566756.2020/64.1-3.2266.

Chvátal, V. (1975) 'A combinatorial theorem in plane geometry', *Journal of Combinatorial Theory, Series B*, 18(1), pp. 39–41. doi: 10.1016/0095-8956(75)90061-1.

Croce, P. *et al.* (2022) 'Parametric HBIM Procedure for the Structural Evaluation of Heritage Masonry Buildings', *Buildings*, 12(194). doi: https://doi.org/10.3390/buildings12020194.

Croce, V., Bevilacqua, M. G., *et al.* (2021) 'Connecting geometry and semantics via artificial intelligence: From 3D classification of heritage data to H-BIM representations', *International Archives of the Photogrammetry, Remote Sensing and Spatial Information Sciences - ISPRS Archives*, 43(B2-2021), pp. 145–152. doi: 10.5194/isprs-archives-XLIII-B2-2021-145-2021.

Croce, V., Caroti, G., Piemonte, A., *et al.* (2021) 'From survey to semantic representation for Cultural Heritage: The 3D modelling of recurring architectural elements', *Acta IMEKO*, 10(1), pp. 98–108. doi: 10.21014/ACTA_IMEKO.V10I1.842.

Croce, V., Caroti, G., De Luca, L., *et al.* (2021) 'From the semantic point cloud to heritage-building information modeling: A semiautomatic approach exploiting machine learning', *Remote Sensing*, 13(3), pp. 1–34. doi: 10.3390/rs13030461.

Croce, V., Caroti, G., *et al.* (2023) 'Neural radiance fields (nerf): Review and potential applications to digital cultural heritage', *International Archives of the Photogrammetry, Remote Sensing and Spatial Information Sciences - ISPRS Archives*, 48(M-2–2023), pp. 453–460. doi: 10.5194/isprs-Archives-XLVIII-M-2-2023-453-2023.

Croce, V., Manuel, A., *et al.* (2023) 'Semi-automatic classification of digital heritage on the Aïoli open source 2D/3D annotation platform via machine learning and deep learning', *Journal of Cultural Heritage*, 62, pp. 187–197. doi: 10.1016/j.culher.2023.05.017.

Croce, V., Caroti, G. and Piemonte, A. (2021) 'Propagation of semantic information between orthophoto and 3D replica: a H-BIM system for the north transept of Pisa Cathedral', *Geomatics, Natural Hazards and Risk*, 12(1), pp. 2225–2252. doi: 10.1080/19475705.2021.1960432.

Dahl, V. A. (2019) 'Structure Tensor. Computation, Visualization, and Application', in *Quantitative Analysis of Tomographic Volumes*, pp. 1–14. Available at: https://people.compute.dtu.dk/vand/notes/ST_intro.pdf.

Daniels, J. *et al.* (2007) 'Robust smooth feature extraction from point clouds', *Proceedings - IEEE International Conference on Shape Modeling and Applications 2007, SMI'07*, pp. 123–133. doi: 10.1109/SMI.2007.32.

Deb, S. K. and Nafi, S. M. (2021) 'Impact of COVID-19 pandemic on tourism: Recovery proposal for future tourism', *Geojournal of Tourism and Geosites*, 33(4),

pp. 1486–1492. doi: 10.30892/gtg.334spl06-597.

Dehbi, Y. *et al.* (2021) 'Optimal scan planning with enforced network connectivity for the acquisition of three-dimensional indoor models', *ISPRS Journal of Photogrammetry and Remote Sensing*, 180(August), pp. 103–116. doi: 10.1016/j.isprsjprs.2021.07.013.

Diara, F. and Rinaudo, F. (2020) 'Building Archaeology Documentation and Analysis through Open Source HBIM Solutions via NURBS Modelling', *International Archives of the Photogrammetry, Remote Sensing and Spatial Information Sciences - ISPRS Archives*, 43(B2), pp. 1381–1388. doi: 10.5194/isprs-archives-XLIII-B2-2020-1381-2020.

DJI (2020) *DJIFlightPlanner*. Available at: https://www.djiflightplanner.com/ (Accessed: 30 January 2024).

Dore, C. and Murphy, M. (2013) 'Semi-automatic techniques for as-built BIM façade modeling of historic buildings', in *2013 Digital Heritage International Congress (DigitalHeritage)*, pp. 473–480. doi: 10.1109/DigitalHeritage.2013.6743786.

Dung, H. T. N. and Lee, S. (2015) 'Outlier removal based on boundary order and shade information in structured light 3D camera', *Proceedings of the 2015 7th IEEE International Conference on Cybernetics and Intelligent Systems, CIS 2015 and Robotics, Automation and Mechatronics, RAM 2015*, pp. 124–129. doi: 10.1109/ICCIS.2015.7274608.

Eastman, C. M. C. *et al.* (2011) *BIM Handbook: A Guide to Building Information Modeling for Owners, Managers, Designers, Engineers and Contractors*. 2nd Ed. New Jersey: John Wiley & Sons, Inc.

Edl, M., Mizerák, M. and Trojan, J. (2018) '3D Laser Scanners: History and Applications', *Acta Simulatio*, 4(4), pp. 1–5. doi: 10.22306/asim.v4i4.54.

Eggert, D. W., Fitzgibbon, A. W. and Fisher, R. B. (1998) 'Simultaneous Registration of Multiple Range Views for Use in Reverse Engineering of CAD Models', *Computer Vision and Image Understanding*, 69(3), pp. 253–272. doi: 10.1006/cviu.1998.0667.

El-Din Fawzy, H. (2019) '3D laser scanning and close-range photogrammetry for buildings documentation: A hybrid technique towards a better accuracy', *Alexandria*

Engineering Journal, 58(4), pp. 1191–1204. doi: 10.1016/j.aej.2019.10.003.

Ente Italiano di Normazione (UNI) (2006) *UNI 11182:2006 Cultural Heritage - Natural and artificial stone - Description of the alteration - Terminology and Definition*.

Ente Italiano di Normazione (UNI) (2017) *UNI 11337-4:2017 Edilizia e opere di ingegneria civile - Gestione digitale dei processi informativi delle costruzioni - Parte 4: Evoluzione e sviluppo informativo di modelli, elaborati e oggetti*.

Fan, L. and Atkinson, P. M. (2019) 'An iterative coarse-to-fine sub-sampling method for density reduction of terrain point clouds', *Remote Sensing*, 11(8). doi: 10.3390/rs11080936.

Fatiguso, F. and Buldo, M. (2020) 'Complesso della SS. Trinità di Venosa (PZ)', in De Fino, M. and Fatiguso, F. (eds) *La diagnostica per gli edifici storici: Metodi non distruttivi e tecnologie innovative per la valutazione e il controllo. Collana Architettura sostenibile/culture costruttive per il recupero sostenibile*. Monfalcone (GO), Italy: EdicomEdizioni, pp. 169–180.

Fernández Álvarez, P. *et al.* (2008) 'Laser scan planning based on visibility analysis and space partitioning techniques', *International Journal of Advanced Manufacturing Technology*, 39(7–8), pp. 699–715. doi: doi:10.1007/s00170-007-1248-9.

Filin, S. (2001) 'Surface clustering from airborne laser scanning data', *International Archives of Photogrammetry Remote Sensing and Spatial Information Sciences*, 34, pp. 119–124. Available at: http://campus.ewi.tudelft.nl/live/binaries/2faaf567-465a-48c7-b204-4944195b6b6c/doc/paper120GrazFilin.pdf.

De Fino, M., Galantucci, R. A. and Fatiguso, F. (2019) 'Remote diagnosis and control of the heritage Architecture by photorealistic digital environments and models', *SCIRES-IT - SCIentific RESearch and Information Technology*, 9(2), pp. 1–16. doi: 10.2423/I22394303V9N2P1.

De Fino, M., Galantucci, R. A. and Fatiguso, F. (2023) 'Condition Assessment of Heritage Buildings via Photogrammetry: A Scoping Review from the Perspective of Decision Makers', *Heritage*, 6(11), pp. 7031–7067. doi: 10.3390/heritage6110367.

Fiorillo, F. *et al.* (2015) '3d Surveying and modelling of the Archaeological Area of Paestum, Italy', *Virtual Archaeology Review*, 4(8), p. 55. doi:

10.4995/var.2013.4306.

Fiorucci, M. *et al.* (2020) 'Machine Learning for Cultural Heritage: A Survey', *Pattern Recognition Letters*, 133, pp. 102–108. doi: 10.1016/j.patrec.2020.02.017.

Fischler, M. A. and Bolles, R. C. (1981) 'Random sample consensus: A Paradigm for Model Fitting with Applications to Image Analysis and Automated Cartography', *Communications of the ACM*, 24(6), pp. 381–395. doi: 10.1145/358669.358692.

Florio, R., Catuogno, R. and Della Corte, T. (2019) 'The interaction of knowledge as though field experimentation of the integrated survey. The case of sacristy of Francesco Solimena in the church of san Paolo Maggiore in Naples', *SCIRES-IT - SCIentific RESearch and Information Technology*, 9(2), pp. 69–84. doi: 10.2423/i22394303v9n2p69.

Folinas, S. and Metaxas, T. (2020) 'Tourism: the Great Patient of Coronavirus Covid-2019', *International Journal of Advanced Research*, 08(04), pp. 365–375. doi: 10.21474/ijar01/10788.

Frey, J. (2019) *Evaluating close range remote sensing techniques for the retention of biodiversity-related forest structures*. doi: 10.6094/UNIFR/151315.

Frías, E. *et al.* (2022) 'Optimal scan planning for surveying large sites with static and mobile mapping systems', *ISPRS Journal of Photogrammetry and Remote Sensing*, 192, pp. 13–32. doi: 10.1016/j.isprsjprs.2022.07.025.

García-Gago, J. *et al.* (2014) 'A photogrammetric and computer vision-based approach for automated 3D architectural modeling and its typological analysis', *Remote Sensing*, 6(6), pp. 5671–5691. doi: 10.3390/rs6065671.

Garland, M. and Heckbert, P. S. (1997) 'Surface simplification using quadric error metrics', *Proceedings of the 24th Annual Conference on Computer Graphics and Interactive Techniques, SIGGRAPH 1997*, pp. 209–216. doi: 10.1145/258734.258849.

Gelfand, N. and Guibas, L. J. (2004) 'Shape segmentation using local slippage analysis', *ACM International Conference Proceeding Series*, 71, pp. 214–223. doi: 10.1145/1057432.1057461.

Getty, J. P. (2021) *Art & Architecture Thesaurus® Online*. Available at:

https://www.getty.edu/research/tools/vocabularies/aat/ (Accessed: 24 October 2023).

Girardeau-Montaut, D. (2020) *CloudCompare (version 2.12.0) [GPL software]*. Available at: http://www.cloudcompare.org/.

Di Giulio, R. *et al.* (2017) 'Integrated data capturing requirements for 3D semantic modelling of Cultural Heritage: The Inception protocol', *International Archives of the Photogrammetry, Remote Sensing and Spatial Information Sciences - ISPRS Archives*, 42(2W3), pp. 251–257. doi: 10.5194/isprs-archives-XLII-2-W3-251-2017.

Godager, B. *et al.* (2022) 'Towards an Improved Framework for Enterprise Bim: the Role of ISO 19650', *Journal of Information Technology in Construction*, 27(June), pp. 1075–1103. doi: 10.36680/j.itcon.2022.053.

Golovinskiy, A. and Funkhouser, T. (2009) 'Min-cut based segmentation of point clouds', *2009 IEEE 12th International Conference on Computer Vision Workshops, ICCV Workshops 2009*, pp. 39–46. doi: 10.1109/ICCVW.2009.5457721.

Gonizzi Barsanti, S., Guidi, G. and De Luca, L. (2017a) 'Segmentation of 3D Models for Cultural Heritage Structrual Analysis - Some critial issues', *ISPRS Annals of the Photogrammetry, Remote Sensing and Spatial Information Sciences*, 4(2W2), pp. 115–122. doi: 10.5194/isprs-annals-IV-2-W2-115-2017.

Gonizzi Barsanti, S., Guidi, G. and De Luca, L. (2017b) 'Segmentation of 3D models for Cultural Heritage structural analysis - Some critical issues', *ISPRS Annals of the Photogrammetry, Remote Sensing and Spatial Information Sciences*, 4(2W2), pp. 115–122. doi: 10.5194/isprs-annals-IV-2-W2-115-2017.

Grilli, E. *et al.* (2018) 'From 2D to 3D supervised segmentation and classification for cultural heritage applications', *International Archives of the Photogrammetry, Remote Sensing and Spatial Information Sciences - ISPRS Archives*, 42(2), pp. 399–406. doi: 10.5194/isprs-archives-XLII-2-399-2018.

Grilli, E., Menna, F. and Remondino, F. (2017) 'A review of point clouds segmentation and classification algorithms', *International Archives of the Photogrammetry, Remote Sensing and Spatial Information Sciences - ISPRS Archives*, 42(2W3), pp. 339–344. doi: 10.5194/isprs-archives-XLII-2-W3-339-2017.

Grilli, E. and Remondino, F. (2019) 'Classification of 3D digital heritage', *Remote Sensing*, 11(7), pp. 1–23. doi: 10.3390/RS11070847.

Grilli, E. and Remondino, F. (2020) 'Machine Learning generalisation across different 3D Architectural Heritage', *ISPRS International Journal of Geo-Information*, 9(6). doi: 10.3390/ijgi9060379.

Gros, A. *et al.* (2023) 'Faceting the post-disaster built heritage reconstruction process within the digital twin framework for Notre-Dame de Paris', *Scientific Reports*, 13(1), pp. 1–12. doi: 10.1038/s41598-023-32504-9.

Haddad, N. A. (2011) 'From ground surveying to 3D laser scanner: A review of techniques used for spatial documentation of historic sites', *Journal of King Saud University - Engineering Sciences*, 23(2), pp. 109–118. doi: 10.1016/j.jksues.2011.03.001.

Har'el, Z. (1995) 'Curvature of Curves and Surfaces–a Parabolic Approach', *Department of Mathematics, Technion–Israel Institute of Technology*, pp. 1–14.

Hassan, A. T. and Fritsch, D. (2019) 'Integration of Laser Scanning and Photogrammetry in 3D/4D Cultural Heritage Preservation - A Review', *International Journal of Applied Science and Technology*, 9(December), pp. 76–91. doi: 10.30845/ijast.v9n4p9.

Herban, S. *et al.* (2022) 'Use of Low-Cost Spherical Cameras for the Digitisation of Cultural Heritage Structures into 3D Point Clouds', *Journal of Imaging*, 8(1). doi: 10.3390/JIMAGING8010013.

Hichri, N., Stefani, C., De Luca, L., Veron, P., *et al.* (2013) 'From point cloud to BIM: a survey of existing approaches', *The nternational Archives of the Photogrammetry, Remote Sensing and Spatial Information Sciences*, XL(5/W2), pp. 343–348. doi: https://doi.org/10.5194/isprsarchives-XL-5-W2-343-2013, 2013.

Hichri, N., Stefani, C., De Luca, L. and Veron, P. (2013) 'Review of the "As-Built Bim" Approaches', *The International Archives of the Photogrammetry, Remote Sensing and Spatial Information Sciences*, XL(5/W1), pp. 107–112. doi: 10.5194/isprsarchives-xl-5-w1-107-2013.

HistAntArtSI Site (2019) *histantartsi.eu*. Available at:

http://db.histantartsi.eu/web/rest/Opera di Arte/460 (Accessed: 9 January 2022).

Holland, J. (1992) *Adaptation in Natural and Artificial Systems. An Introductory Analysis with Applications to Biology, Control, and Artificial Intelligence*. Massachusetts: The Mit Press.

Horaud, R. *et al.* (2016) 'An overview of depth cameras and range scanners based on time-of-flight technologies', *Machine Vision and Applications*, 27(7), pp. 1005–1020. doi: 10.1007/s00138-016-0784-4.

Hu, M. *et al.* (2021) 'A novel lidar signal denoising method based on convolutional autoencoding deep learning neural network', *Atmosphere*, 12(11). doi: 10.3390/atmos12111403.

Huang, H., Zhang, C. and Hammad, A. (2021) 'Effective Scanning Range Estimation for Using TLS in Construction Projects', *Journal of Construction Engineering and Management*, 147(9). doi: 10.1061/(asce)co.1943-7862.0002127.

Huber, D. (2011) 'The ASTM E57 file format for 3D imaging data exchange', in *Proceedings of SPIE - The International Society for Optical Engineering*. doi: 10.1117/12.876555.

ICOMOS, I. S. C. for S. (2008) *Illustrated Glossary on Stone Deterioration Patterns: Monuments and Sites*. Available at: http://www.international.icomos.org/home.htm.

International Organization for Standardization (ISO) (2018) *ISO 19650 – Part 1: Concepts and principles*.

Italian Ministry of Culture (MiC) (2004) 'Codice dei Beni Culturali e del Paesaggio - Legge n. 42 del 2004'.

Italian Ministry of Labour and Social Policies (MLPS) (2008) 'Testo Unico sulla Salute e Sicurezza sul Lavoro - Decreto Legislativo 9 aprile 2008, n. 81'.

Italian President of the Republic (2001) 'Testo Unico delle Disposizioni Legislative e Regolamentari in Materia Edilizia - Decreto del Presidente della Repubblica 6 giugno 2001, n. 380'.

Jagannathan, A. and Miller, E. L. (2007) 'Three-dimensional surface mesh segmentation using curvedness-based region growing approach', *IEEE Transactions*

on Pattern Analysis and Machine Intelligence, 29(12), pp. 2195–2204. doi: 10.1109/TPAMI.2007.1125.

Janković, R. (2020) 'Machine Learning Models for Cultural Heritage Image classification: Comparison Based on Attribute Selection', *Information*, 11(1). doi: 10.3390/info11010012.

Jeevitha, K. *et al.* (2020) 'A Review on various segmentation techniques in Image Processing', 7(4), pp. 1342–1348.

Jeong, W. S. and Kim, K. H. (2016) 'A performance evaluation of the BIM-based object-oriented physical modeling technique for building thermal simulations: A comparative case study', *Sustainability (Switzerland)*, 8(7). doi: 10.3390/su8070648.

Jia, F. and Lichti, D. D. (2022) 'A Practical Algorithm for the Viewpoint Planning of Terrestrial Laser Scanners', *Geomatics*, 2(2), pp. 181–196. doi: 10.3390/geomatics2020011.

Jo, T. (2021) *Machine Learning Foundations. Supervised, Unsupervised, and Advanced Learning*. Springer Cham. doi: https://doi.org/10.1007/978-3-030-65900-4.

Jung, J., Stachniss, C. and Kim, C. (2017) 'Automatic room segmentation of 3D laser data using morphological processing', *ISPRS International Journal of Geo-Information*, 6(7). doi: 10.3390/ijgi6070206.

Kang, Z. *et al.* (2009) 'Automatic Registration of Terrestrial Laser Scanning Point Clouds using Panoramic Reflectance Images', *Sensors*, 9(4), pp. 2621–2646. doi: 10.3390/s90402621.

Keitaanniemi, A. *et al.* (2021) 'The combined use of slam laser scanning and tls for the 3d indoor mapping', *Buildings*, 11(9), pp. 1–18. doi: 10.3390/buildings11090386.

Khalsa, S. J. S. *et al.* (2022) *A Review of Options for Storage and Access of Point Cloud Data in the Cloud*. doi: https://doi.org/10.5067/DOC/ESO/ESCO-PUB003VERSION1.

Khohar, H. A. *et al.* (2021) 'Assessment Strategies to Evaluate Building Information Modeling Capabilities of Organizations', *IOP Conference Series: Earth and*

Environmental Science, 641(012012). doi: 10.1088/1755-1315/641/1/012012.

Koch, T., Körner, M. and Fraundorfer, F. (2019) 'Automatic and semantically-aware 3D UAV flight planning for image-based 3D reconstruction', *Remote Sensing*, 11(13), pp. 1–29. doi: 10.3390/rs11131550.

Kutlu, H. *et al.* (2023) 'AI Based Image Segmentation of Cultural Heritage Objects used for Multi-View Stereo 3D Reconstructions', in *GCH 2023 - Eurographics Workshop on Graphics and Cultural Heritage*, pp. 75–79. doi: 10.2312/gch.20231160.

Kyriazis, I., Fudos, I. and Palios, L. (2007) 'Detecting features from sliced point clouds', *GRAPP 2007 - 2nd International Conference on Computer Graphics Theory and Applications, Proceedings*, GM(R/-), pp. 188–192. doi: 10.5220/0002082701880192.

de Lachenal, L. (1998) 'L'Incompiuta di Venosa. Un'abbaziale fra propaganda e reimpiego', *Mélanges de l'Ecole française de Rome. Moyen-Age, Temps modernes*, 110(1), pp. 299–315. doi: 10.3406/mefr.1998.3628.

Lanzara, E., Samper, A. and Herrera, B. (2019) 'Point Cloud Segmentation and Filtering to Verifiy the Geometric Genesis of Simple and Composed Vaults', *International Archives of the Photogrammetry, Remote Sensing and Spatial Information Sciences - ISPRS Archives*, 42(2/W15), pp. 645–652. doi: 10.5194/isprs-archives-XLII-2-W15-645-2019.

Laviano, R. and Summa, V. (1999) 'Incompiuta di Venosa (Potenza): Mineralogy, petrography and geochemistry of the building stone', *Mineralogica et Petrographica Acta*, 42, pp. 211–222.

Lavoué, G., Dupont, F. and Baskurt, A. (2005) 'A new CAD mesh segmentation method, based on curvature tensor analysis', *CAD Computer Aided Design*, 37(10), pp. 975–987. doi: 10.1016/j.cad.2004.09.001.

Lerones, P. M. *et al.* (2016) 'Moisture detection in heritage buildings by 3D laser scanning', *Studies in Conservation*, 61(August), pp. 46–54. doi: 10.1179/2047058415Y.0000000017.

Li, S.-D. and Xu, Z.-D. (2022) 'System Configuration Design of BIM Object-Oriented

Database for Civil Engineering', *Journal of Construction Engineering and Management*, 148(12). doi: https://doi.org/10.1061/(ASCE)CO.1943-7862.0002389.

Liang, H. *et al.* (2018) 'The integration of terrestrial laser scanning and terrestrial and unmanned aerial vehicle digital photogrammetry for the documentation of Chinese classical gardens – A case study of Huanxiu Shanzhuang, Suzhou, China', *Journal of Cultural Heritage*, 33, pp. 222–230. doi: 10.1016/j.culher.2018.03.004.

Litchi (2020) *Litchi*. Available at: https://flylitchi.com/ (Accessed: 30 January 2024).

Liu, J. *et al.* (2023) 'Comparative Analysis of Point Clouds acquired from a TLS Survey and a 3D Virtual Tour for HBIM Development', *International Archives of the Photogrammetry, Remote Sensing and Spatial Information Sciences - ISPRS Archives*, 48(M-2–2023), pp. 959–968. doi: 10.5194/isprs-Archives-XLVIII-M-2-2023-959-2023.

Liu, Junshan *et al.* (2023) 'Static Terrestrial Laser Scanning (TLS) for Heritage Building Information Modeling (HBIM): A Systematic Review', *Virtual Worlds*, 2(2), pp. 90–114. doi: 10.3390/virtualworlds2020006.

Liu, Y. and Xiong, Y. (2008) 'Automatic segmentation of unorganized noisy point clouds based on the Gaussian map', *CAD Computer Aided Design*, 40(5), pp. 576–594. doi: 10.1016/j.cad.2008.02.004.

Llamas, J. *et al.* (2016) *Applying Deep Learning Techniques to Cultural Heritage Images Within the INCEPTION Project*. doi: 10.1007/978-3-319-48974-2_4.

López, A. *et al.* (2023) 'Metaheuristics for the optimization of Terrestrial LiDAR set-up', *Automation in Construction*, 146(104675). doi: 10.1016/j.autcon.2022.104675.

López, F. J. *et al.* (2017) 'A Framework for Using Point Cloud Data of Heritage Buildings Toward Geometry Modeling in A BIM Context: A Case Study on Santa Maria La Real De Mave Church', *International Journal of Architectural Heritage*, 11(7), pp. 965–986. doi: 10.1080/15583058.2017.1325541.

De Luca, L., Veron, P. and Florenzano, M. (2006) 'Reverse engineering of architectural buildings based on a hybrid modeling approach', *Computers and Graphics (Pergamon)*, 30(2), pp. 160–176. doi: 10.1016/j.cag.2006.01.020.

Luh, L. C. *et al.* (2014) 'High resolution survey for topographic surveying', *IOP*

Conference Series: Earth and Environmental Science, 18(1), pp. 6–12. doi: 10.1088/1755-1315/18/1/012067.

Luo, X., Wang, X. and Tan, X. (2019) 'Semantically Enriched Presentation for Cultural Heritage Image: A POI-Based Perspective', in *2019 ACM/IEEE Joint Conference on Digital Libraries (JCDL)*. Champaign, IL, USA, pp. 410–411. doi: doi: 10.1109/JCDL.2019.00094.

Macher, H., Landes, T. and Grussenmeyer, P. (2015) 'Point clouds segmentation as base for as-built BIM creation', *ISPRS Annals of the Photogrammetry, Remote Sensing and Spatial Information Sciences*, 2(5W3), pp. 191–197. doi: 10.5194/isprsannals-II-5-W3-191-2015.

MacQueen, J. (1967) 'Some methods for classification and analysis of multivariate observations', in *5th Berkeley symposium on mathematical statistics and probability*, pp. 281–297. doi: 10.1007/s11665-016-2173-6.

Mader, D. *et al.* (2016) 'Potential of UAV-Based laser scanner and multispectral camera data in building inspection', *International Archives of the Photogrammetry, Remote Sensing and Spatial Information Sciences - ISPRS Archives*, XLI-B1, pp. 1135–1142. doi: 10.5194/isprsarchives-XLI-B1-1135-2016.

Mahmud, M. *et al.* (2011) '3D part inspection path planning of a laser scanner with control on the uncertainty', *CAD Computer Aided Design*, 43(4), pp. 345–355. doi: 10.1016/j.cad.2010.12.014.

Maiezza, P. (2019) 'As-Built Reliability in Architectural HBIM Modeling', *ISPRS Annals of the Photogrammetry, Remote Sensing and Spatial Information Sciences*, 42(2/W9), pp. 461–466. doi: 10.5194/isprs-archives-XLII-2-W9-461-2019.

Majeed, P. G. and Kumar, S. (2014) 'Genetic Algorithms in Intrusion Detection Systems: A Survey', *International Journal of Innovation and Applied Studies*, 5(3), pp. 233–240. Available at: http://www.issr-journals.org/ijias/.

Malinverni, E. S. *et al.* (2017) 'Documentation & detection of colour changes of bas relieves using close range photogrammetry', *International Archives of the Photogrammetry, Remote Sensing and Spatial Information Sciences - ISPRS Archives*, 42(5W1), pp. 203–210. doi: 10.5194/isprs-Archives-XLII-5-W1-203-2017.

Malinverni, E. S. *et al.* (2019) 'Deep Learning for Semantic Segmentation of 3D Point Cloud', *International Archives of the Photogrammetry, Remote Sensing and Spatial Information Sciences - ISPRS Archives*, 42(2/W15), pp. 735–742. doi: 10.5194/isprs-archives-XLII-2-W15-735-2019.

Matrone, F., Lingua, A. M., *et al.* (2020) 'A Benchmark for Large-Scale Heritage Point Cloud Semantic Segmention', *International Archives of the Photogrammetry, Remote Sensing and Spatial Information Sciences - ISPRS Archives*, 43(B2), pp. 1419–1426. doi: 10.5194/isprs-archives-XLIII-B2-2020-1419-2020.

Matrone, F., Grilli, E., *et al.* (2020) 'Comparing machine and deep learning methods for large 3D heritage semantic segmentation', *ISPRS International Journal of Geo-Information*, 9(535). doi: 10.3390/ijgi9090535.

Matrone, F. *et al.* (2023) 'Explaining AI: Understanding Deep Learning Models for Heritage Point Clouds', *ISPRS Annals of the Photogrammetry, Remote Sensing and Spatial Information Sciences*, 10(M-1–2023), pp. 207–214. doi: 10.5194/isprs-annals-X-M-1-2023-207-2023.

Maturana, D. and Scherer, S. (2015) 'VoxNet: A 3D Convolutional Neural Network for Real-Time Object Recognition', in *IEEE/RSJ International Conference on Intelligent Robots and Systems (IROS)*. Hamburg, Germany. Available at: http://www.thepositiveencourager.global/the-mentoring-approach/.

Mazzacca, G. *et al.* (2023) 'Nerf for heritage 3d reconstruction', *International Archives of the Photogrammetry, Remote Sensing and Spatial Information Sciences - ISPRS Archives*, 48(M-2–2023), pp. 1051–1058. doi: 10.5194/isprs-Archives-XLVIII-M-2-2023-1051-2023.

Meroño, J. E. *et al.* (2015) 'Recognition of materials and damage on historical buildings using digital image classification', *South African Journal of Science*, 111(1–2), pp. 1–9. doi: 10.17159/sajs.2015/20140001.

Mesároš, P., Smetanková, J. and Mandičák, T. (2019) 'The Fifth Dimension of BIM - Implementation Survey', *IOP Conference Series: Earth and Environmental Science*, 222(1). doi: 10.1088/1755-1315/222/1/012003.

Messaoudi, T. *et al.* (2018) 'An ontological model for the reality-based 3D annotation of heritage building conservation state', *Journal of Cultural Heritage*, 29(July), pp.

100–112. doi: 10.1016/j.culher.2017.05.017.

Meyer, B. J. and Drummond, T. (2017) 'Improved semantic segmentation for robotic applications with hierarchical conditional random fields', in *2017 IEEE International Conference on Robotics and Automation (ICRA)*, pp. 5258–5265. doi: 10.1109/ICRA.2017.7989617.

Mirarchi, C. *et al.* (2020) *Structuring general information specifications for contracts in accordance with the UNI 11337:2017 standard*, *Research for Development*. Springer International Publishing. doi: 10.1007/978-3-030-33570-0_10.

Monterroso-Checa, A. and Gasparini, M. (2016) 'Aerial Archaeology and Photogrammetric Surveys along the roman way from Corduba to Emerita. Digitalizing the ager Cordubensis and the ager Mellariensis', *SCIRES-IT - SCIentific RESearch and Information Technology*, 6(2), pp. 175–188. doi: 10.2423/i22394303v6n2p175.

Morsi, D. M. A. *et al.* (2022) 'BIM-based life cycle assessment for different structural system scenarios of a residential building', *Ain Shams Engineering Journal*, 13(101802). doi: 10.1016/j.asej.2022.101802.

Moyano, J. *et al.* (2021) 'Semantic interpretation of architectural and archaeological geometries: Point cloud segmentation for HBIM parameterisation', *Automation in Construction*, 130(August). doi: 10.1016/j.autcon.2021.103856.

Mugner, E. and Seube, N. (2019) 'Denoising of 3D point clouds', *International Archives of the Photogrammetry, Remote Sensing and Spatial Information Sciences - ISPRS Archives*, 42(2/W17), pp. 217–224. doi: 10.5194/isprs-archives-XLII-2-W17-217-2019.

Muralikrishnan, B. (2021) 'Performance evaluation of terrestrial laser scanners - A review', *Measurement Science and Technology*, 32(7), pp. 1–68. doi: 10.1088/1361-6501/abdae3.

Murphy, M., McGovern, E. and Pavia, S. (2009) 'Historic building information modelling (HBIM)', *Structural Survey*, 27(4), pp. 311–327. doi: https://doi.org/10.1108/02630800910985108.

Musicco, A. *et al.* (2021) 'Automatic Point Cloud Segmentation for the Detection of Alterations on Historical Buildings Through an Unsupervised and Clustering-Based

Machine Learning Approach', in *ISPRS Annals of the Photogrammetry, Remote Sensing and Spatial Information Sciences*, pp. 129–136. doi: 10.5194/isprs-annals-v-2-2021-129-2021.

Musicco, A., Rossi, N. and Verdoscia, C. (2023) 'Accuracy evaluation of smartphone-based videogrammetry for cultural heritage documentation process', *International Archives of the Photogrammetry, Remote Sensing and Spatial Information Sciences - ISPRS Archives*, 48(M-2–2023), pp. 1119–1126. doi: 10.5194/isprs-Archives-XLVIII-M-2-2023-1119-2023.

Nazeri, B. and Crawford, M. (2021) 'Detection of outliers in lidar data acquired by multiple platforms over sorghum and maize', *Remote Sensing*, 13(21). doi: 10.3390/rs13214445.

Negendahl, K. (2015) 'Building performance simulation in the early design stage: An introduction to integrated dynamic models', *Automation in Construction*, 54, pp. 39–53. doi: 10.1016/j.autcon.2015.03.002.

Ng, R. T. and Han, J. (1994) 'Efficient and Effective Clustering Data Mining Methods for Spatial', in *In Proceedings of the 20th International Conference on Very Large Data Bases, (VLDB)*, pp. 144–155.

Nguyen, A. and Le, B. (2013) '3D Point Cloud Segmentation: A survey', in *6th IEEE Conference on Robotic, Automation and Mechatronics (RAM)*, pp. 225–230. doi: doi: 10.1109/RAM.2013.6758588.

Nguyen, T. D. and Adhikari, S. (2023) 'The Role of BIM in Integrating Digital Twin in Building Construction: A Literature Review', *Sustainability (Switzerland)*, 15(13), pp. 1–26. doi: 10.3390/su151310462.

Oh, S. *et al.* (2021) 'Building component detection on unstructured 3d indoor point clouds using ransac-based region growing', *Remote Sensing*, 13(2), pp. 1–20. doi: 10.3390/rs13020161.

Oreni, D. *et al.* (2013) 'Hbim for conservation and management of built heritage: Towards a library of vaults and wooden bean floors', *ISPRS Annals of the Photogrammetry, Remote Sensing and Spatial Information Sciences*, 2(5/W1), pp. 215–221. doi: 10.5194/isprsannals-II-5-W1-215-2013.

Osman, A., Wahab, N. A. and Ismail, M. H. (2009) 'Development and Evaluation of an Interactive 360 Virtual Tour for Tourist Destinations', *Journal of Information Technology Impact*, 9(3), pp. 173–182. Available at: http://scholar.google.com/scholar?hl=en&btnG=Search&q=intitle:Development+and+Evaluation+of+an+Interactive+360+°+Virtual+Tour+for+Tourist+Destinations#0.

Palomba, D. *et al.* (2019) 'Multi-scalar surveys for complex architectures', *International Archives of the Photogrammetry, Remote Sensing and Spatial Information Sciences - ISPRS Archives*, 42(2/W18), pp. 151–158. doi: 10.5194/isprs-archives-XLII-2-W18-151-2019.

Pellegri, G. (2015) 'Survey and Drawing Representation of Architecture and Environment: Different Teaching Approach for Architects and Engineers', *Procedia - Social and Behavioral Sciences*, 174, pp. 4090–4095. doi: 10.1016/j.sbspro.2015.01.1159.

Pellis, E. *et al.* (2022) '2D to 3D Label Propagation for the Semantic Segmentation of Heritage Building Point Clouds', *International Archives of the Photogrammetry, Remote Sensing and Spatial Information Sciences - ISPRS Archives*, 43(B2-2022), pp. 861–867. doi: 10.5194/isprs-archives-XLIII-B2-2022-861-2022.

Pellis, E. *et al.* (2023) 'Synthetic data generation and testing for the semantic segmentation of heritage buildings', *International Archives of the Photogrammetry, Remote Sensing and Spatial Information Sciences - ISPRS Archives*, 48(M-2–2023), pp. 1189–1196. doi: 10.5194/isprs-Archives-XLVIII-M-2-2023-1189-2023.

Piaseckienė, G. (2022) 'Dimensions of Bim in Literature: Review and Analysis', *Science - Future of Lithuania*, 14, pp. 1–11. doi: 10.3846/mla.2022.16071.

Pierdicca, R. *et al.* (2020) 'Point cloud semantic segmentation using a deep learning framework for cultural heritage', *Remote Sensing*, 12(6). doi: 10.3390/rs12061005.

Pierdicca, R. *et al.* (2023) 'Challenging architectures: An integrated and multipurpose survey for the complete mapping of the emir palace in kogon (uzbekistan)', *International Archives of the Photogrammetry, Remote Sensing and Spatial Information Sciences - ISPRS Archives*, 48(M-2–2023), pp. 1225–1232. doi: 10.5194/isprs-Archives-XLVIII-M-2-2023-1225-2023.

Pinti, L., Codinhoto, R. and Bonelli, S. (2022) 'A Review of Building Information Modelling (BIM) for Facility Management (FM): Implementation in Public Organisations', *Applied Sciences*, 12(3). doi: 10.3390/app12031540.

Pocobelli, D. P. *et al.* (2018) 'BIM for heritage science: a review', *Heritage Science*, 6(1), pp. 23–26. doi: 10.1186/s40494-018-0191-4.

Potthast, C. and Sukhatme, G. S. (2014) 'A probabilistic framework for next best view estimation in a cluttered environment', *Journal of Visual Communication and Image Representation*, 25(1), pp. 148–164. doi: 10.1016/j.jvcir.2013.07.006.

Poux, F. and Billen, R. (2019) 'Voxel-based 3D Point Cloud Semantic Segmentation: Unsupervised geometric and relationship featuring vs deep learning methods', *ISPRS International Journal of Geo-Information*, 8(5). doi: 10.3390/ijgi8050213.

Del Pozo, S. *et al.* (2017) 'Multispectral imaging in cultural heritage conservation', *International Archives of the Photogrammetry, Remote Sensing and Spatial Information Sciences - ISPRS Archives*, 42(2W5), pp. 155–162. doi: 10.5194/isprs-archives-XLII-2-W5-155-2017.

Pritchard, D. *et al.* (2022) *Study on quality in 3D digitisation of tangible Cultural Heritage: mapping parameters, formats, standards, benchmarks, methodologies, and guidelines. VIGIE 2020 Final Study Report*. Publications Office of the European Union. doi: 10.2759/471776.

Puma, P. (2016) 'Editorial. Landscape & Archaeology', *SCIRES-IT - SCIentific RESearch and Information Technology*, 6(2), pp. 1–6. doi: 10.2423/i22394303v6n2p1.

Qiu, Q. *et al.* (2022) 'An adaptive down-sampling method of laser scan data for scan-to-BIM', *Automation in Construction*, 135(March). doi: 10.1016/j.autcon.2022.104135.

Quattrini, R. *et al.* (2015) 'From tls to hbim. high quality semantically-aware 3d modeling of complex architecture', *International Archives of the Photogrammetry, Remote Sensing and Spatial Information Sciences - ISPRS Archives*, 40(5W4), pp. 367–374. doi: 10.5194/isprsarchives-XL-5-W4-367-2015.

Quattrini, R. *et al.* (2023) 'Knowledge-based modelling for automatizing hbim

objects.The vaulted ceilings of palazzo ducale in urbino', *International Archives of the Photogrammetry, Remote Sensing and Spatial Information Sciences - ISPRS Archives*, 48(M-2–2023), pp. 1271–1278. doi: 10.5194/isprs-Archives-XLVIII-M-2-2023-1271-2023.

Rabbani, T., van den Heuvel, F. A. and Vosselman, G. (2006) 'Segmentation of point clouds using smoothness constraint', *International archives of photogrammetry, remote sensing and spatial information sciences*, 36(5), pp. 248–253.

Rabbani, T., van den Wildenberg, F. and Vosselman, G. (2006) 'Segmentation of point clouds using smoothness constraint', *International archives of photogrammetry, remote sensing and spatial information sciences*, 36(5), pp. 248–253.

Radanovic, M., Khoshelham, K. and Fraser, C. (2020) 'Geometric accuracy and semantic richness in heritage BIM: A review', *Digital Applications in Archaeology and Cultural Heritage*, 19(October 2021). doi: 10.1016/j.daach.2020.e00166.

Raju, A. and Khandakar, H. M. (2022) 'Potentiality of high-resolution topographic survey using unmanned aerial vehicle in Bangladesh', *Remote Sensing Applications: Society and Environment*, 26. doi: https://doi.org/10.1016/j.rsase.2022.100729.

RecorDIM, T. G. 16 (2007) *International Heritage Documentation Standards*, *Heritage Documentation Standards*.

Remondino, F. (2011) 'Heritage Recording and 3D Modeling with Photogrammetry and 3D Scanning', *Remote Sensing*, 3(6), pp. 1104–1138. doi: 10.3390/rs3061104.

Rifandi, R., Ningtyas, Y. D. W. K. and Assagaf, S. F. (2013) 'An Insight About GPS', in *Utrecht University Summer School 2013*, pp. 1–12. doi: 10.13140/RG.2.2.34893.13285.

Risbøl, O. and Gustavsen, L. (2018) 'LiDAR from drones employed for mapping archaeology – Potential, benefits and challenges', *Archaeological Prospection*, 25(4), pp. 329–338. doi: 10.1002/arp.1712.

Rocha *et al.* (2020) 'A Scan-to-BIM Methodology Applied to Heritage Buildings', *Heritage*, 3(1), pp. 47–67. doi: 10.3390/heritage3010004.

Rodríguez-Gonzálvez, P. *et al.* (2019) 'Diachronic reconstruction and visualization of lost cultural heritage sites', *ISPRS International Journal of Geo-Information*, 8(2), pp.

1–25. doi: 10.3390/ijgi8020061.

Rodríguez-Gonzálvez, P. and Rodríguez-Martín, M. (2019) 'Weld Bead Detection Based on 3D Geometric Features and Machine Learning Approaches', *IEEE Access*, 7, pp. 14714–14727. doi: 10.1109/ACCESS.2019.2891367.

Rondelet, G. (1832) *Trattato teorico e pratico dell'arte di edificare*. Mantova: Negretto Editore.

Rougeron, G., Garrec, J. Le and Andriot, C. (2022) 'Optimal positioning of terrestrial LiDAR scanner stations in complex 3D environments with a multiobjective optimization method based on GPU simulations', *ISPRS Journal of Photogrammetry and Remote Sensing*, 193, pp. 60–76. doi: 10.1016/j.isprsjprs.2022.08.023.

Russo, M. *et al.* (2021) 'Machine Learning for Cultural Heritage Classification', *Representation Challenges. Augmented Reality and Artificial Intelligence in Cultural Heritage and Innovative Design Domain*, pp. 209–214. doi: 10.3280/oa-686.33.

Russo, M. and Manferdini, A. M. (2014) 'Integration of image and range-based techniques for surveying complex architectures', *ISPRS Annals of the Photogrammetry, Remote Sensing and Spatial Information Sciences*, 2(5), pp. 305–312. doi: 10.5194/isprsannals-II-5-305-2014.

Russo, M., Remondino, F. and Guidi, G. (2011) 'Principali tecniche e strumenti per il rilievo tridimensionale in ambito archeologico'., *Archeologia e Calcolatori*, (22), pp. 169–198.

Rusu, R. B. *et al.* (2008) 'Towards 3D Point cloud based object maps for household environments', *Robotics and Autonomous Systems*, 56(11), pp. 927–941. doi: 10.1016/j.robot.2008.08.005.

Saccardi, U. (2004) 'Applicazioni della geometria descrittiva', in. Firenze: LEF, pp. 427–468.

Samberg, A. (2007) 'An Implementation of the ASPRS LAS Standard', *IAPRS*, XXXVI(W52), pp. 363–372. Available at: http://www.isprs.org/proceedings/XXXVI/3-W52/Final_papers/Samberg_2007.pdf.

Sanchirico, S. (2016) 'FORMA URBIS - Anno XXI, n. 6, Maggio 2016 - Il museo nazionale romano alle Terme di Diocleziano. Romarchè 2016', *Forma Urbis - Itinerari*

nascosti di Roma Antica.

Santagati, C. (2005) '3D laser scanner aimed to architectural heritage survey: From the point's cloud to the geometrical genesis determination', *2005 Virtual Reconstruction and Visualization of Complex Architectures, 3D-ARCH 2005*, 36(5/W17).

Sappa, A. D. and Devy, M. (2001) 'Fast range image segmentation by an edge detection strategy', *Proceedings of International Conference on 3-D Digital Imaging and Modeling, 3DIM*, pp. 292–299. doi: 10.1109/IM.2001.924460.

Saygi, G. and Remondino, F. (2013) 'Management of Architectural Heritage Information in BIM and GIS: State-of-the-Art and Future Perspectives', *International Journal of Heritage in the Digital Era*, 2(4), pp. 695–713. doi: 10.1260/2047-4970.2.4.695.

Schindelin, J. *et al.* (2012) 'Fiji: An open-source platform for biological-image analysis', *Nature Methods*, 9(7), pp. 676–682. doi: 10.1038/nmeth.2019.

Schlarp, J., Csencsics, E. and Schitter, G. (2020) 'Optical Scanning of a Laser Triangulation Sensor for 3-D Imaging', *IEEE Transactions on Instrumentation and Measurement*, 69(6), pp. 3606–3613. doi: 10.1109/TIM.2019.2933343.

Schnabel, R., Degener, P. and Klein, R. (2009) 'Completion and reconstruction with primitive shapes', *Computer Graphics Forum*, 28(2), pp. 503–512. doi: 10.1111/j.1467-8659.2009.01389.x.

Schnabel, R., Wahl, R. and Klein, R. (2007) 'Efficient RANSAC for point-cloud shape detection', *Computer Graphics Forum*, 26(2), pp. 214–226. doi: 10.1111/j.1467-8659.2007.01016.x.

Scianna, A., Serlorenzi, M. and Gristina, S. (2015) 'Sperimentazione di tecniche BIM sull'archeologia romana: il caso delle strutture rinvenute all'interno della cripta della Chiesa dei SS: Sergio e Bacco in Roma', in *Archeologia e calcolatori*, pp. 199–212.

Scornet, E. (2021) 'Trees , forests , and impurity-based variable importance', pp. 1–40. Available at: https://hal.science/hal-02436169v3.

Scott, W. R. (2009) 'Model-based view planning', *Machine Vision and Applications*, 20, pp. 47–69. doi: https://doi.org/10.1007/s00138-007-0110-2.

Serna, A. *et al.* (2014) 'Paris-rue-madame database: A 3D mobile laser scanner dataset for benchmarking urban detection, segmentation and classification methods', in *ICPRAM 2014 - Proceedings of the 3rd International Conference on Pattern Recognition Applications and Methods*, pp. 819–824. doi: 10.5220/0004934808190824.

Sevgen, E. and Abdikan, S. (2023) 'Classification of Large-Scale Mobile Laser Scanning Data in Urban Area with LightGBM', *Remote Sensing*, 15(15), pp. 1–19. doi: 10.3390/rs15153787.

Seyis, S. and Cekin, E. (2020) 'BIM Execution Plan based on BS EN ISO 19650 - 1 and BS EN ISO 19650 - 2 Standards', (November). Available at: https://www.researchgate.net/publication/347518863_BIM_Execution_Plan_based_on_BS_EN_ISO_19650-1_and_BS_EN_ISO_19650-2_Standards.

Sim, J. Y., Lee, S. U. and Kim, C. S. (2005) 'Construction of regular 3d point clouds using octree partitioning and resampling', in *Proceedings - IEEE International Symposium on Circuits and Systems*, pp. 956–959. doi: 10.1109/ISCAS.2005.1464748.

Son, S., Park, H. and Lee, K. H. (2002) 'Automated laser scanning system for reverse engineering and inspection', *International Journal of Machine Tools & Manufacture*, 42, pp. 889–897. doi: 10.1201/9780203741771.

Di Stefano, F. *et al.* (2021) 'Mobile 3D scan LiDAR: a literature review', *Geomatics, Natural Hazards and Risk*, 12(1), pp. 2387–2429. doi: 10.1080/19475705.2021.1964617.

Storeide, M. S. B. *et al.* (2023) 'Standardization of digitized heritage: a review of implementations of 3D in cultural heritage', *Heritage Science*, 11(1), pp. 1–22. doi: 10.1186/s40494-023-01079-z.

Strecha, C., Küng, O. and Fua, P. (2012) 'Automatic Mapping from Ultra-Light UAV Imagery', in *EuroCOW 2012 Conference*, pp. 2–5.

Strom, J., Richardson, A. and Olson, E. (2010) 'Graph-based segmentation for colored 3D laser point clouds', *IEEE/RSJ 2010 International Conference on Intelligent Robots and Systems, IROS 2010 - Conference Proceedings*, pp. 2131–2136. doi: 10.1109/IROS.2010.5650459.

Stylianidis, E. (2019) 'CIPA - Heritage Documentation: 50 Years: Looking Backwards', *The International Archives of the Photogrammetry, Remote Sensing and Spatial Information Sciences*, XLII-2/W14, pp. 1–130. doi: 10.5194/isprs-archives-xlii-2-w14-1-2019.

Sun, J., Zhang, Z. and Zhang, J. (2021) 'Reconstructing Normal Section Profiles of 3-D Revolving Structures via Pose-Unconstrained Multiline Structured-Light Vision', *IEEE Transactions on Instrumentation and Measurement*, 70, pp. 1–12. doi: doi: 10.1109/TIM.2020.3024339.

Sun, Z. and Zhang, Y. (2019) 'Accuracy evaluation of videogrammetry using a low-cost spherical camera for narrow architectural heritage: An observational study with variable baselines and blur filters', *Sensors (Switzerland)*, 19(3). doi: 10.3390/s19030496.

Tan, P. (2020) 'Image-Based Modeling', in *Computer Vision: A Reference Guide*. Cham: Springer International Publishing, pp. 1–4. doi: 10.1007/978-3-030-03243-2_11-1.

Tarsha-Kurdi, F., Landes, T. and Grussenmeyer, P. (2007) 'Hough-transform and extended ransac algorithms for automatic detection of 3d building roof planes from lidar data', 36, pp. 407–412.

Tatoglu, A. and Pochiraju, K. (2012) 'Point cloud segmentation with LIDAR reflection intensity behavior', *Proceedings - IEEE International Conference on Robotics and Automation*, pp. 786–790. doi: 10.1109/ICRA.2012.6225224.

Tavolare, R. *et al.* (2023) 'A point cloud classification method for the ScanToBIM process in Architectural Heritage', *DISEGNARECON*, 16(30). doi: 10.20365/disegnarecon.30.2023.20.

Tavolare, R., Buldo, M. and Verdoscia, C. (2023) 'Automated Processes for Preparing a Point Cloud Within the Scan-To-BIM Methodology', in Bienvenido-Bárcena, R. et al. (eds) *32 INGEGRAF International Conference*. Puerto Real, Cádiz (Spain): University of Cádiz, pp. 104–105.

Templin, T., Brzezinski, G. and Rawa, M. (2019) 'Visualization of Spatiooral Building Changes Using 3D Web GIS', *IOP Conference Series: Earth and Environmental Science*, 221(1). doi: 10.1088/1755-1315/221/1/012084.

Teppati Losè, L. *et al.* (2022) 'Apple LiDAR Sensor for 3D Surveying: Tests and Results in the Cultural Heritage Domain', *Remote Sensing*, 14(17). doi: 10.3390/rs14174157.

Teruggi, S. *et al.* (2020) 'A Hierarchical Machine Learning Approach for Multi-Level and Multi-Resolution 3D Point Cloud Classification', *Remote Sensing*, 12(16). doi: 10.3390/RS12162598.

Tomasello, N., Cascone, S. M. and Russo, G. (2018) 'BIM for archaeological heritage : the case study of the Terme Romane dell ' Indirizzo of Catania', in, pp. 1–13.

Turkan, Y. *et al.* (2013) 'Tracking secondary and temporary concrete construction objects using 3D imaging technologies', *Computing in Civil Engineering - Proceedings of the 2013 ASCE International Workshop on Computing in Civil Engineering*, pp. 749–756. doi: 10.1061/9780784413029.094.

Turner, A. (2007) 'UCL Depthmap 7: From Isovist Analysis to Generic Spatial Network Analysis', *New Developments in Space Syntax Software*, pp. 43–51. Available at: http://www.vr.ucl.ac.uk/events/syntaxsoftware07/ndsss07-turner.html.

Vatan, M., Selbesoglu, M. . and Bayram, B. (2009) 'The use of 3D laser scanning technology in preservation of historical structures', *Wiadomosci Konserwatorskie*, 44, pp. 659–669.

Verdoscia, C. *et al.* (2020) '4D-HBIM for the conservation and valorization of Cultural Heritage', *World Heritage and Contamination*, pp. 1000–1008.

Verdoscia, C., Musicco, A., Tavolare, R., *et al.* (2021a) 'Evaluation of the geometric reliability in the Scan to BIM process, the case study of Santa Croce monastery', in Gambardella, C. (ed.) *World Heritage and Design for Health. XIX International Forum Le Vie dei Mercanti*. Roma, Italy: Gangemi Editore SpA International, pp. 650–657.

Verdoscia, C., Musicco, A., Tavolare, R., *et al.* (2021b) 'Evaluation of the geometric reliability in the Scan to BIM process: the case study of Santa Croce monastery', *Abitare la Terra/Dwelling on Earth, Quaderni n.6*. Edited by P. Portoghesi and C. Gambardella, pp. 54–55.

Verdoscia, C., Musicco, A., Buldo, M., *et al.* (2021) 'La documentazione digitale del

patrimonio costruito attraverso l'A-BIM. Il caso studio delle Terme di Diocleziano, Roma/The Digital Documentation of Cultural Heritage through A-BIM. The Case Study of the Baths of Diocletian, Rome', in Arena, A. et al. (eds) *Connecting. Drawing for weaving relationship. Languages Distances Technologies. Proceedings of the 42th International Conference of Representation Disciplines Teachers Congress of Unione Italiana per il Disegno*. Milano, Italy: FrancoAngeli, pp. 2686–2703. doi: 10.3280/oa-693.152.

Verdoscia, C., Buldo, M., Tavolare, R., *et al.* (2022) 'Integrated 3D survey techniques for historical architecture. The Church of S. Maria Veterana in Triggiano (Italy)', in Gambardella, C. (ed.) *World Heritage and Ecological Transition. XX International Forum Le Vie dei Mercanti*. Roma, Italy: Gangemi Editore SpA International, pp. 425–433.

Verdoscia, C., Buldo, M., Musicco, A., *et al.* (2022a) 'Integrated Architectural Survey Techniques for the Cultural Heritage Preservation and Enhancement in the Covid-Era. The Case Study of Venosa's Most Holy Trinity Complex, Italy', in Ródenas-López, M. A., Calvo-López, J., and Salcedo-Galera, M. (eds) *Architectural Graphics. EGA 2022. Springer Series in Design and Innovation*. Cham: Springer, pp. 188–198. doi: 10.1007/978-3-031-04632-2_20.

Verdoscia, C., Buldo, M., Musicco, A., *et al.* (2022b) 'Technological Paradigms for Cultural Heritage. A Scan To BIM Methodology for the Description of Historical Architecture', in Bienvenido-Huertas, D. and Moyano-Campos, J. (eds) *New Technologies in Building and Construction. Lecture Notes in Civil Engineering*. Singapore: Springer, pp. 187–205. doi: 10.1007/978-981-19-1894-0_11.

Verdoscia, C. *et al.* (2023) 'Sensor Data Fusion per i processi Scan to BIM. La Chiesa Ognissanti di Valenzano, Bari/Sensor Data Fusion for Scan to BIM Processes. The All Saints' Church in Valenzano, Bari', in Cannella, M., Garozzo, A., and Morena, S. (eds) *Transitions. Proceedings of the 44th International Conference of Representation Disciplines Teachers Congress of Unione Italiana per il Disegno*. Milano, Italy: FrancoAngeli, pp. 3260–3277. doi: 10.3280/oa-1016-c466.

Verdoscia, C., Musicco, A. and Tavolare, R. (2019) '3D Data Acquisition and Visualisation for implementing Cognitive Systems. The School Building "F. Corridoni" in the old town of Bari', in *XVII International Forum World Heritage and Legacy*. Capri.

Vieira, M. and Shimada, K. (2005) 'Surface mesh segmentation and smooth surface

extraction through region growing', *Computer Aided Geometric Design*, 22(8), pp. 771–792. doi: 10.1016/j.cagd.2005.03.006.

Voinea, G. and Girbacia, F. (2019) *VR Technologies in Cultural Heritage*. doi: 10.1007/978-3-030-05819-7.

Vorobel, R. *et al.* (2021) 'Segmentation of rust defects on painted steel surfaces by intelligent image analysis', *Automation in Construction*, 123(October 2020), p. 103515. doi: 10.1016/j.autcon.2020.103515.

Vosselman, G. and Dijkman, S. (2001) '3D building model reconstruction from point clouds and ground plans', *International Archives of Photogrammetry and Remote Sensing*, XXXIV(3/W4), pp. 22–24.

Wackrow, R. and Chandler, J. H. (2011) 'Minimising systematic error surfaces in digital elevation models using oblique convergent imagery', *The Photogrammetric Record*, 26. doi: 10.1111/j.1477-9730.2011.00623.x.

Wang, F. *et al.* (2022) 'Automated UAV path-planning for high-quality photogrammetric 3D bridge reconstruction', *Structure and Infrastructure Engineering*, pp. 1–20. doi: 10.1080/15732479.2022.2152840.

Wang, L., Zhang, Y. and Wang, J. (2017) 'Map-Based Localization Method for Autonomous Vehicles Using 3D-LIDAR', *IFAC-PapersOnLine*, 50(1), pp. 276–281. doi: 10.1016/j.ifacol.2017.08.046.

Wang, S. *et al.* (2022) 'A new point cloud simplification method with feature and integrity preservation by partition strategy', *Measurement: Journal of the International Measurement Confederation*, 197(December 2021), p. 111173. doi: 10.1016/j.measurement.2022.111173.

Wang, X. *et al.* (2020) 'The evolution of LiDAR and its application in high precision measurement', *IOP Conference Series: Earth and Environmental Science*, 502(1). doi: 10.1088/1755-1315/502/1/012008.

Wang, X. *et al.* (2021) 'Multi-view stereo in the Deep Learning Era: A comprehensive review', *Displays*, 70(102102). doi: https://doi.org/10.1016/j.displa.2021.102102.

Wang, Y., Zhu, J. and Wei, B. (2022) 'Domestic and International Mainstream BIM Software Application and Comparison Study', *Journal of Physics: Conference Series*,

2185(1). doi: 10.1088/1742-6596/2185/1/012088.

Wang, Z. and Jin Liu (2020) 'A Seven-Dimensional Building Information Model for the Improvement of Construction Efficiency', *Advances in Civil Engineering*, 2020. doi: https://doi.org/10.1155/2020/8842475 Research.

Wani, M. A. and Arabnia, H. R. (2003) 'Parallel edge-region-based segmentation algorithm targeted at reconfigurable MultiRing network', *Journal of Supercomputing*, 25(1), pp. 43–62. doi: 10.1023/A:1022804606389.

Weinmann, M., Jutzi, B. and Mallet, C. (2013) 'Feature relevance assessment for the semantic interpretation of 3D point cloud data', *ISPRS Annals of the Photogrammetry, Remote Sensing and Spatial Information Sciences*, 2(5W2), pp. 313–318. doi: 10.5194/isprsannals-II-5-W2-313-2013.

Willis, M. *et al.* (2016) 'Archeological 3D Mapping: The Structure from Motion Revolution', *Journal of Texas Archaeology and History*, 3, pp. 1–36. doi: 10.21112/ita.2016.1.110.

Xiao, J. *et al.* (2013) 'Three-dimensional point cloud plane segmentation in both structured and unstructured environments', *Robotics and Autonomous Systems*, 61(12), pp. 1641–1652. doi: 10.1016/j.robot.2013.07.001.

Xie, Y., Tian, J. and Zhu, X. X. (2020) 'Linking Points with Labels in 3D: A Review of Point Cloud Semantic Segmentation', *IEEE Geoscience and Remote Sensing Magazine*, 8(4), pp. 38–59. doi: 10.1109/MGRS.2019.2937630.

Xu, S., Vosselman, G. and Oude Elberink, S. (2014) 'Multiple-entity based classification of airborne laser scanning data in urban areas', *ISPRS Journal of Photogrammetry and Remote Sensing*, 88, pp. 1–15. doi: 10.1016/j.isprsjprs.2013.11.008.

Yahya, Z. *et al.* (2017) 'A Concave Hull Based Algorithm for Object Shape Reconstruction', *International Journal of Information Technology and Computer Science*, 9(3), pp. 1–9. doi: 10.5815/ijitcs.2017.03.01.

Yamauchi, H. *et al.* (2005) 'Feature sensitive mesh segmentation with mean shift', *Proceedings - International Conference on Shape Modeling and Applications, SMI'05*, 2005, pp. 236–243. doi: 10.1109/SMI.2005.21.

Yan, Z. *et al.* (2019) 'A Concave Hull Methodology for Calculating the Crown Volume of Individual Trees Based on Vehicle-Borne LiDAR Data', *Remote Sensing*, 11(6). doi: 10.3390/rs11060623.

Yang, S., Hou, M. and Li, S. (2023) 'Three-Dimensional Point Cloud Semantic Segmentation for Cultural Heritage: A Comprehensive Review', *Remote Sensing*, 15(3), pp. 1–25. doi: 10.3390/rs15030548.

Yang, S., Xu, S. and Huang, W. (2022) '3D Point Cloud for Cultural Heritage: A Scientometric Survey', *Remote Sensing*, 14(5542), pp. 1–25. doi: 10.3390/rs14215542.

Yang, X. *et al.* (2015) 'Feature-preserving simplification of point cloud by using clustering approach based on mean curvature', *The Society for Art and Science*, 14(4), pp. 117–128.

Zaccaria, C. (1983) *Le volte in muratura. Genesi geometrica e rappresentazione grafica.* Bari: Adriatica Editrice.

Zhang, R. *et al.* (2023) 'Deep-Learning-Based Point Cloud Semantic Segmentation: A Survey', *Electronics*, 12(17). doi: 10.3390/electronics12173642.

Zhang, S. *et al.* (2013) 'Building Information Modeling (BIM) and Safety: Automatic Safety Checking of Construction Models and Schedules', *Automation in Construction*, 29, pp. 183–195. doi: 10.1016/j.autcon.2012.05.006.

Zhang, Z. (1994) 'Iterative point matching for registration of free-form curves and surfaces', *International Journal of Computer Vision*, 13(2), pp. 119–152. doi: 10.1007/BF01427149.

Zhao, J. *et al.* (2023) 'A Review of Point Cloud Segmentation of Architectural Cultural Heritage', *ISPRS Annals of the Photogrammetry, Remote Sensing and Spatial Information Sciences*, X-1/W1-202(September), pp. 247–254. doi: 10.5194/isprs-annals-x-1-w1-2023-247-2023.

LIST OF ABBREVIATIONS

2D: Two-dimensional

3D: Three-dimensional (and so on according to the number of dimensions)

AAT: Art & Architecture Thesaurus

ABIM: Archaeological Building Information Modelling

AEC: Architectural, Engineering, and Construction

AGP: Art Gallery Problem

AH: Architectural Heritage

AI: Artificial Intelligence

ALS: Airborne Laser Scanner

ANN: Artificial Neural Network

ASO: Homogeneous Spatial Scope

ASTM International: American Society for Testing and Materials International

BDS: Building Description System

BIM: Building Information Modelling

BPA: Ball-Pivoting Algorithm

BRep: Boundary Representation

CAD: Computer Aided Design

CANUPO: CAractérisation de NUages de Points

C2C: Cloud-to-Cloud Distance

CCD: Charged Coupled Device

CH: Cultural Heritage

CIE: Commission Internationale de l'Eclairage

CIPA: International Committee for Documentation of Cultural Heritage or or International Committee for Documentation of Cultural Heritage

cm: centimetre

CMOS: Complementary Metal Oxide Semiconductor

CRP: Close-Range Photogrammetry

DGCNN: Dynamic Graph Convolutional Neural Network

DL: Deep Learning

EPSG: European Petroleum Survey Group

ESCO: ESDIS Standards Coordination Office

ESDIS: Earth Science Data and Information System

FF: First Floor

FN: False Negative

FOV: Field of View

FP (1): False Positive

FP (2): Fortress Problem

FRF: Fast Random Forest

GA: Genetic Algorithm

GCP: Ground Control Point

GF: Ground Floor

GIS: Geographic Information System

GLONASS: Globalnaya Navigazionnaya Sputnikovaya Sistema

GNSS: Global Navigation Satellite System

GOAL: Graphical Methods, Optimization and Learning Research Group

GP-GPU: General Purpose Computing on Graphics Processing Unit

GPS: Global Positioning System

GRAPHyC: Grupo de Representación Arquitectónica del Patrimonio Histórico y Contemporáneo

GSA: General Service Administration

GSD: Ground Sample Distance

HBIM: Heritage/Historic Building Information Modelling

HC: Hierarchical Clustering

HFS: Homogeneous Functional Scope

HSS: Homogeneous Spatial Scope

HT: Hough Transformation

IAI: International Alliance for Interoperability

ICOMOS: International Council on Monuments and Sites

ICP: Iterative Closest Point

IFC: Industry Foundation Class

IMU: Inertial Measurement Unit

ISO: International Organization for Standardization

ISPRS: International Society of Photogrammetry and Remote Sensing

KMC: K-Means Clustering

KNN: K-Nearest Neighbours

LiDAR: Light Detection and Ranging

LOA: Level of Accuracy

LOC: Level of Surface Completeness or Level of Surface Coverage

LOD: Level of Detail, Development or Density

LOG: Level of Geometry

LOI: Level of Information

LOIN: Level of Information Need

LRV: Light Reflectance Value

LUT: Look-Up Table

MAULab: Architectural and Urban Modelling Laboratory

MDI: Mean Decrease in Impurity

MiBACT: Ministry of Cultural Heritage and Activities and Tourism of Italy

MiC: Italian Ministry of Culture

ML: Machine Learning

MLPS: Italian Ministry of Labour and Social Policies

MLS: Mobile Laser Scanner

m: metre

mm: millimetre

Mpt: Megapoint

NAS: Network-Attached Storage

NBV: Next Best View

NeRF: Neural Radiance Field

NISO: National Information Standards Organization

NOHD: Nominal Ocular Hazard Distance

NURBS: Non-Uniform Rational B-Splines

NOTAM: Notice To AirMen

ODBC: Open DataBase Connectivity

OP: Overlooking Probability

OTS: Optical Triangulation Scanner

P4S: Planning for Scanning

PC: Point Cloud

PCA: Principal Component Analysis

PSS: Phase Shift Scanner

QCP: Quality Control Point

RANSAC: Random Sample Consensus

RGB: Red, Green, Blue

RF: Random Forest

ROI: Region of Interest

SfM: Structure from Motion

SLS: Structured Light Scanner

SOR: Statistical Outlier Removal

SVM: Support Vector Machine

TLS: Terrestrial Laser Scanner

TN: True Negative

TNT: Triangulated Irregular Network

ToFS: Time of Light Scanner

TP: True Positive

TS: Triangulation Scanner

TST: Total Theodolite Station

UAV: Unmanned Aerial Vehicle

UNESCO: United Nations Educational, Scientific and Cultural Organization

UNI: Ente Italiano di Normazione

VPL: Visual Programming Language

VR: Virtual Reality

WEKA: Waikato Environment for Knowledge Analysis

XML: eXtensible Markup Language

XSD: XML Schema Definition

LIST OF FIGURES

LIST OF TABLES

EUROPEAN CURRICULUM VITAE FORMAT

PERSONAL INFORMATION

Name	**BULDO Michele**
Address	18 Zoccolanti St., 85029, Venosa (PZ), Italia
Telephone	+39 3270846997
E-mail	michelebuldomb@gmail.com - michele.buldo@poliba.it
Certified e-mail	michele.buldo@ingpec.eu
Nationality	Italian
Date of birth	09/08/1989

EMPLOYMENT IN THE ACADEMIC FIELD

June 2023 – March 2024	**Coordination Service of the Informative Tutoring and Orientation/Accommodation Activities**, at the Politecnico di Bari
October/December 2022 – December 2023/January 2024	**Visiting PhD Student** at the Universidad de Zaragoza - Escuela de Ingeniería y Arquitectura, Departamento de Arquitectura
A.Y. 2023/2024 – 2022/2023	**Collaborator in supplementary Teaching Activities for the course of 'Drawing Theories and Methods'** (Prof. Cesare Verdoscia, Bachelor's Degree in Building Engineering), at the Politecnico di Bari
June 2023	**Scientific and organisational Secretariat of the 'Colloqui.AT.e 2023' Conference,** at the Ar.Tec. (Società Scientifica di Architettura Tecnica)

A.Y. 2020/2021 – 2021/2022	**Collaborator in supplementary Teaching Activities for the course of 'Design, Survey and Modelling of Built Structures,'** (Prof. Arch. Cesare Verdoscia, Bachelor's Degree in Building Engineering), at the Politecnico di Bari
A.Y 2020/2021 – 2021/2022	**Internal Tutor for PoliBa Transversal Skills and Orientation Courses (PCTO)**, at the Politecnico di Bari

WORK EXPERIENCE

July/August 2020	**Technical Collaborator** – **3D Survey Specialist** in collaboration with the Municipality of Venosa (Italy) and Eng. Pietro Grimaldi (COIFA - Comitato Internazionale di Fotogrammetria Architettonica)
September 2019/March 2020	**Technical Collaborator** – **BIM Specialist** at the architectural firm of Arch. Antonio Caldarulo, Bari (Italy)
October 2016/January 2017	**Technical Collaborator - BIM Specialist and Rendering** Specialist, at the architectural firm of Arch. Giuseppina De Fronzo, Bari (Italy)

EDUCATION AND TRAINING

November 2020 – January 2024	**PhD in 'Risk and Environmental, Territorial and Building Development' – XXXVI cycle**. SDS: Drawing (ICAR-17) – EQF Level 8, at the Politecnico di Bari Thesis Title: 'Scan-to-BIM for Architectural Heritage enhancement and preservation. Leading techniques and advanced automation processes'
27/09/2023	**BIM Expert 11337-7 UNI/PdR 78:2020** in accordance with UNI 11337-7 and UNI/PdR 78:2020 – 'BIM Specialist – discipline Architecture,' (registration no: 23-02239), at the ICMQ S.p.A.
21/06/2021	**Teacher Training Course - 24 CFU** (M.D. 616/17), at the Università degli Studi eCampus, Novedrate (Italy)

12/04/2021	**Professional Engineer Licensure** (Section A, Civil and Environmental Sector – registration no. 11920), at the Order of Engineers of the Province of Bari (OIBA)
04/09/2020	**APR Pilot Certificate A1-A3** (Non-Critical Operations), issued by Italian Civil Aviation Authority (ENAC) and European Aviation Safety Agency (EASA)
04/04/2020	**Master's Degree in Building Systems Engineering**, class LM-24 (M.D. 270/04) – EQF Level 7, at the Politecnico di Bari Mark: 110/110 with thesis dissertation recognised as being of 'particular merit' Thesis Title: 'Innovative techniques of integrated architectural survey and Supervised Machine Learning for the knowledge of Cultural Heritage. The Abbey Complex of the Most Holy Trinity in Venosa (PZ)'
21/04/2017	**Bachelor's Degree in Building Engineering**, class L-23 (M.D. 270/04) – EQF Level 6, at the Politecnico di Bari Thesis Title: 'Study of IBM methodologies for processing complex point clouds: the monastery of Virgin Mary of Graces, Venosa'
19/09/2008	**Humanistic High School Diploma** – EQF Level 5, at the Liceo Classico 'Quinto Orazio Flacco', Venosa (Italy)

PERSONAL SKILLS AND COMPETENCES

MOTHER TONGUE	Italian
OTHER LANGUAGES	English – C1 Level B2 Level Certificate, at the Trinity College London (issued on 22/05/2007) Spanish – B1 Level French – B1 Level

SOCIAL SKILLS AND COMPETENCES	Excellent ability to work and interact as part of a team, skills acquired in university, and during work experience.
ORGANISATIONAL SKILLS AND COMPETENCES	Perfectly able to organise a job with precision, quality and on time. Excellent project and team management skills and excellent ability to interact positively and fruitfully with colleagues. Skills acquired by character and throughout his academic career.
TECHNIQUE SKILLS AND COMPETENCES	Excellent knowledge of CAD-BIM-SfM software (Autodesk Autocad, Autodesk Revit, Graphisoft Archicad, Cinema 4D, Agisoft Metashape, CloudCompare, MeshLab, Autodesk Recap, Faro Scene, Pix4D, Litchi). Excellent knowledge in the use of LiDAR technology (Faro Focus M 70, Faro Focus 3D 120, Faro Arm Quantum S), and image-based surveying techniques from UAV systems (DJI Phantom 4 Pro, DJI Phantom 3 Pro, DJI Spark quadricopters) and digital SLR cameras. Excellent knowledge of office suite (Microsoft Office, word processor, spreadsheet, presentation software), photo-editing software (Adobe Photoshop, Adobe InDesign, Adobe Illustrator), software for geographical analysis (QGIS), programming languages (Python, R, Matlab).
PATENTS	Driving Licence (category B)
SCIENTIFIC PUBLICATIONS	
• ANVUR's A-class Journal (Area 08)	Buldo, M., Agustín-Hernández, L., Verdoscia, C., & Tavolare, R. (2023). A Scan-to-BIM workflow proposal for Cultural Heritage. Automatic point cloud segmentation and parametric-adaptive modelling of vaulted systems. *The International Archives of the Photogrammetry, Remote Sensing and Spatial Information Sciences - ISPRS Archives*, *XLVIII*(M–2), 333–340. https://doi.org/10.5194/isprs-archives-XLVIII-M-2-2023-333-2023 Verdoscia, C., Buldo, M., Tavolare, R., & Musicco, A. (2022). Automatic model-based segmentation for the Scan-to-BIM process applied to Cultural Heritage. A study focused on masonry vaults. In P. Portoghesi & C. Gambardella (Eds.), *Abitare la Terra/Dwelling on Earth, Quaderni n.7-8*, 24–27.

Gangemi Editore SpA International, Roma. ISBN13: 9788849245318, ISBN10: 1592-860822002

Verdoscia, C., Musicco, A., Tavolare, R., & Buldo, M. (2021). Evaluation of the geometric reliability in the Scan to BIM process: the case study of Santa Croce monastery. In P. Portoghesi & C. Gambardella (Eds.), *Abitare la Terra/Dwelling on Earth, Quaderni n.6*, 54–55. Gangemi Editore SpA International, Roma. ISBN13: 9788849241020, ISBN10: 1592-860820006

• ANVUR's Scientific Journal (Area 08)

Cabrera-Revuelta, E., Tavolare, R., Buldo, M., & Verdoscia, C. (2024). Planning for terrestrial laser scanning: Methods for optimal sets of locations in architectural sites. *Journal of Building Engineering*, *85*. https://doi.org/10.1016/j.jobe.2024.108599

Tavolare, R., Cabrera-Revuelta, E., Verdoscia, C., & Buldo, M. (2023). A point cloud classification method for the ScanTo-BIM process in Architectural Heritage. *DISEGNARECON*, *16*(30). https://doi.org/10.20365/disegnarecon.30.2023.20. ISSN: 1828-5961

• Book Chapter

Verdoscia, C., Buldo, M., Musicco, A., & Tavolare, R. (2022). Technological Paradigms for Cultural Heritage. A Scan To BIM Methodology for the Description of Historical Architecture. In D. Bienvenido-Huertas & J. Moyano-Campos (Eds.), *New Technologies in Building and Construction. Lecture Notes in Civil Engineering* (Vol. 258, pp. 187–205). Springer, Singapore. https://doi.org/10.1007/978-981-19-1894-0_11. ISBN: 978-981-19-1893-3

Fatiguso, F., Buldo, M., (2020), Complesso della SS. Trinità di Venosa (PZ), In M. De Fino & F. Fatiguso (Eds.), *La diagnostica per gli edifici storici. Metodi non distruttivi e tecnologie innovative per la valutazione e il controllo* (Collana architettura sostenibile/culture costruttive per il costruire sostenibile, pp. 169-180). EdicomEdizioni, Monfalcone. ISBN: 978-88-96386-92-7

• Conference Proceedings (Paper)

Tavolare, R., Buldo, M., & Verdoscia, C. (2024). Automated Processes for Preparing a Point Cloud Within the Scan-To-BIM Methodology. In C. Manchado-del Val, M. Suffo-Pino, R.

Miralbes-Buil, D. Moreno-Sánchez, & D. Moreno-Nieto (Eds.), *Advances in Design Engineering IV. INGEGRAF 2023. Lecture Notes in Mechanical Engineering* (pp. 44–55). Springer, Cham. https://doi.org/10.1007/978-3-031-51623-8_5. ISBN: 978-3-031-51622-1

Verdoscia, C., Buldo, M., Tavolare, R., Cabrera-Revuelta, E., & Musicco, A. (2023). Sensor Data Fusion per i processi Scan to BIM. La Chiesa Ognissanti di Valenzano, Bari/Sensor Data Fusion for Scan to BIM Processes. The All Saints' Church in Valenzano, Bari. In M. Cannella, A. Garozzo, & S. Morena (Eds.), *Transizioni. Atti del 44° Convegno Internazionale dei Docenti delle Discipline della Rappresentazione/Transitions. Proceedings of the 44th International Conference of Representation Disciplines Teachers Congress of Unione Italiana per il Disegno* (pp. 3260–3277). FrancoAngeli, Milano.
https://doi.org/10.3280/oa-1016-c466. ISBN: 978-88-35-15511-9

Verdoscia, C., Buldo, M., Tavolare, R., & Musicco, A. (2022). Integrated 3D survey techniques for historical architecture. The Church of S. Maria Veterana in Triggiano (Italy). In C. Gambardella (Ed.), *World Heritage and Ecological Transition. XX International Forum Le Vie dei Mercanti* (pp. 425–433). Gangemi Editore SpA International, Roma. ISBN: 978-88-492-4530-1

Verdoscia, C., Buldo, M., Musicco, A., & Tavolare, R. (2022). Integrated Architectural Survey Techniques for the Cultural Heritage Preservation and Enhancement in the Covid-Era. The Case Study of Venosa's Most Holy Trinity Complex, Italy. In M. A. Ródenas-López, J. Calvo-López, & M. Salcedo-Galera (Eds.), *Architectural Graphics. EGA 2022. Springer Series in Design and Innovation* (Vol. 21, pp. 188–198). Springer, Cham. https://doi.org/10.1007/978-3-031-04632-2_20. ISBN: 978-3-031-04631-5

Verdoscia, C., Musicco, A., Buldo, M., Tavolare, R., & Pepe, N. (2021). La documentazione digitale del patrimonio costruito attraverso l'A-BIM. Il caso studio delle Terme di Diocleziano, Roma/The Digital Documentation of Cultural Heritage through A-BIM. The Case Study of the Baths of Diocletian,

Rome. In A. Arena, M. Arena, D. Mediati, & P. Raffa (Eds.), *Connettere. Un disegno per annodare e tessere. Linguaggi Distanze Tecnologie. Atti del 42° Convegno Internazionale dei Docenti delle Discipline della Rappresentazione/Connecting. Drawing for weaving relationship. Languages Distances Technologies. Proceedings of the 42th International Conference of Representation Disciplines Teachers Congress of Unione Italiana per il Disegno* (pp. 2686–2703). FrancoAngeli, Milano. https://doi.org/10.3280/oa-693.152. ISBN: 978-88-35-12589-1

Verdoscia, C., Musicco, A., Tavolare, R., & Buldo, M. (2021). Evaluation of the geometric reliability in the Scan to BIM process, the case study of Santa Croce monastery. In C. Gambardella (Ed.), *World Heritage and Design for Health. XIX International Forum Le Vie dei Mercanti* (pp. 650–657). Gangemi Editore SpA International, Roma. ISBN: 978-88-492-4089-4

• Conference Proceedings (Abstract)

Tavolare, R., Buldo, M., & Verdoscia, C. (2023). Automated Processes for Preparing a Point Cloud Within the Scan-To-BIM Methodology. In R. Bienvenido-Bárcena, E. Cabrera-Revuelta, P. Camacho-Magriñán, S. de la Rosa-Silva, I. del Sol-Illana, R. Gómez-Cabrera, D. Moreno-Nieto, D. Moreno-Sánchez, M. Ángel Pardo-Vicente, P. Pavón-Domínguez, L. Rodríguez-Parada, P. Ruiz-Villalobos, M. Suffo-Pino, & A. Pliar Valerga-Puerta (Eds.), *32 INGEGRAF International Conference* (pp. 104–105). University of Cádiz. ISBN: 978-84-09-52380-1

Verdoscia, C., Buldo, M., Tavolare, R., & Musicco, A. (2022). Integrated 3D survey techniques for historical architecture. The Church of S. Maria Veterana in Triggiano (Italy). In C. Gambardella (Ed.), *World Heritage and Ecological Transition. XX International Forum Le Vie dei Mercanti* (p. 81). Gangemi Editore SpA International, Roma. ISBN: 978-88-492-4529-5

Verdoscia, C., Buldo, M., Musicco, A., & Tavolare, R. (2022). Tecniche di rilievo architettonico integrato per la conservazione e la valorizzazione dei Beni Culturali. Il caso di studio del Complesso abbaziale della SS. Trinità di Venosa, Italia. *MÁS ALLÁ DE LAS LÍNEAS. La Gráfica y Sus Usos. XIX Congreso Expresión Gráfica Arquitectónica (EGA)* (pp. 539–542). Universidad Politécnica de Cartagena, Cartagena. https://doi.org/10.31428/10317/11207. ISBN: 978-84-17853-51-8

Verdoscia, C., Musicco, A., Tavolare, R., & Buldo, M. (2021). Geometric reliability evaluation in Scan to BIM process, the case study of Santa Croce monastery. In C. Gambardella (Ed.), *World Heritage and Design for Health. XIX International Forum Le Vie dei Mercanti* (p. 112). Gangemi Editore SpA International, Roma. ISBN: 978-88-492-4088-7

Bari, 12/04/2024

The declarant

(full and legible signature)